NEW 1,3,4-THIADIAZOLE DERIVATIVES AND INVESTIGATION OF THEIR BIOLOGICAL ACTIVITIES

Master's Degree Thesis

Amal Abdulsamad Naji Farhan AL-SHARABI

Eskişehir 2022

NEW 1,3,4-THIADIAZOLE DERIVATIVES AND INVESTIGATION OF THEIR BIOLOGICAL ACTIVITIES

Amal Abdulsamad Naji Farhan AL-SHARABI

MASTER'S DEGREE THESIS

Department of Pharmaceutical Chemistry

Supervisor: Prof. Dr. Leyla YURTTAŞ

Eskişehir

Anadolu University

Graduate School of Health Sciences

June 2022

FINAL APPROVAL FOR THESIS

This thesis titled “New 1,3,4-Thiadiazole Derivatives and Investigation of Their Biological Activities” has been prepared and submitted by Amal Abdulsamad Naji Farhan AL-SHARABI in partial fulfillment of the requirements in “Anadolu University Directive on Graduate Education and Examination” for the Degree of Master of Science in Pharmaceutical Chemistry Department has been examined and approved on 28/06/2022.

Committee Members		**Signature**
Member (Supervisor)	: Prof. Dr. Leyla YURTTAŞ	……
Member	: Prof. Dr. Ahmet Çağrı KARABURUN	……
Member	: Assoc. Prof. Dr. Murat DURAN	……

Prof. Dr. Gülşen Akalın ÇİFTÇİ
Director
Graduate School of Health Sciences

ÖZET

Yeni 1,3,4-Tiyadiazol Türevleri ve Biyolojik Aktivitelerinin Araştırılması

Amal Abdulsamad Naji Farhan AL-SHARABI
Farmasötik Kimya Anabilim Dalı
Anadolu Üniversitesi, Sağlık Bilimleri Enstitüsü, Haziran 2022
Danışman: Prof. Dr. Leyla YURTTAŞ

Alzheimer hastalığı (AH), yaşlılar arasında en sık görülen demans türü olan çok faktörlü bir nörolojik bozukluktur. AH'nın patofizyolojisini açıklamak için çeşitli patojenik süreçler önerilmiş olsa da, kesin nedeni uzmanlar için bir gizem olmaya devam etmektedir. Hastalığın karmaşık patolojik süreci nedeniyle, tek hedefli terapiler ve kombinasyon terapileri dahil olmak üzere mevcut geleneksel tedaviler, hastalığın tedavisi veya ilerlemesini yavaşlatmak için yetersiz kabul edilmektedir. Araştırmacılar, aynı anda birden fazla bölgede hareket edebilen yeni çok hedefli ligandların (MTL) geliştirilmesine giderek daha fazla odaklanmaktadır. Bu çalışmada, 1,3,4-tiyadiazol heterosiklik halkasının ve trisiklik hidrokarbon adamantanın karakteristik özellikleri kullanarak, on sekiz yeni türev sentezlenmiştir. Sentezlenen tüm bileşiklerin kimyasal yapıları IR, ^{1}H-NMR, ^{13}C-NMR ve yüksek çözünürlüklü kütle spektroskopisi (HR-MS) ile aydınlatılmıştır. Bu türevler, AH'deki patojenik yolaklarla ilişkili olan asetilkolinesteraz (AChE), butirilkolinesteraz (BChE) ve monoamin oksidazlara (MAO-A ve MAO-B) karşı *in vitro* aktiviteleri açısından araştırılmıştır. Aktivite sonuçlarına göre **3a**, **3b**, **3d**, **4a** ve **4b** bileşikleri AChE'ye karşı iyi dercede inhibisyon aktivitesi göstermiştir. Bileşikler **3a**, **4a** ve **4b**, MAO-B'ye karşı inhibe edici aktivite gösterirken, bileşiklerin hiçbiri BChE ve MAO-A'ya karşı belirgin bir inhibisyon sergileyememişlerdir. Bu aktif bileşikler arasında, **3a**, **4a** ve **4b**'nin ikili inhibisyon aktiviteye sahip olduğu ve aralarından bileşik **4a**'nın en umut verici ikili inhibitör molekül olduğu tespit edilmiştir. En aktif bileşikler için moleküler docking, enzimin aktif bölgesi ile bağlanma etkileşimlerini araştırmak için hem AChE hem de *h*MAO-B kristal yapıları üzerinde çalışmalar gerçekleştirilmiştir.

Anahtar Sözcükler: Alzheimer hastalığı, 1,3,4-Tiyadiazol, Adamantan, Asetilkolinesteraz ihibitörü, Monoamin oksidaz-B inhibitörü.

ABSTRACT

New 1,3,4-Thiadiazole Derivatives and Investigation of Their Biological Activities

Amal Abdulsamad Naji Farhan AL-SHARABI

Department of Pharmaceutical Chemistry

Anadolu University, Graduate School of Health Sciences, June 2022

Supervisor: Prof. Dr. Leyla YURTTAŞ

Alzheimer's disease (AD) is a multifactorial neurological disorder that is the most common form of dementia among the elderly. While various pathogenic processes have been proposed to explain the pathophysiology of Alzheimer's disease, the exact cause remains a mystery to scientists. Because of the disease's complex pathological process, current conventional treatments including mono-targeted therapies and combination therapies are considered insufficient to cure or slow the progression of the disease. As a result, researchers are increasingly concentrating on the development of novel multi-targeted drugs (MTDs) that can act on several targets at the same time. In this thesis, the characteristic features of the 1,3,4-thiadiazole heterocyclic ring and the tricyclic hydrocarbon adamantane were used to design and synthesize novel derivatives. The chemical structures of all synthesized compounds were elucidated by using IR, ^{1}H-NMR, ^{13}C-NMR, and High-resolution mass spectrometry (HR-MS). These derivatives were investigated for their *in vitro* activity against acetylcholinesterase (AChE), butyrylcholinesterase (BChE) and monoamine oxidases (MAO-A and MAO-B) which have been linked to pathogenic pathways in AD. According to the activity results, compounds **3a, 3b, 3d, 4a** and **4b** showed remarkable inhibition activity against AChE. Compounds **3a**, **4a** and **4b** showed inhibition activity against MAO-B while none of the compounds showed inhibition activity against BChE and MAO-A. Among these active compounds, **3a**, **4a** and **4b** showed dual inhibition activity, however compound **4a** was the most promising dual inhibitor candidate. Additionally, Molecular docking studies for the most active compounds were performed on both AChE and *h*MAO-B crystal structures to investigate the binding interactions with the enzyme's active site.

Keywords: Alzheimer’s disease, 1,3,4-Thiadiazole, Adamantane, Acetylcholinesterase inhibitor, Monoamine oxidase-B inhibitor.

28/06/2022

STATEMENT OF COMPLIANCE WITH ETHICAL PRINCIPLES AND RULES

I hereby truthfully declare that this thesis is an original work prepared by me; that I have behaved in accordance with the scientific ethical principles and rules throughout the stages of preparation, data collection, analysis and presentation of my work; that I have cited the sources of all the data and information that could be obtained within the scope of this study, and included these sources in the references section; and that this study has been scanned for plagiarism with “scientific plagiarism detection program” used by Anadolu University, and that “it does not have any plagiarism” whatsoever. I also declare that, if a case contrary to my declaration is detected in my work at any time, I hereby express my consent to all the ethical and legal consequences that are involved.

Amal Abdulsamad Naji Farhan AL-SHARABI

ACKNOWLEDGEMENT

First and foremost, I want to express my heartfelt thankfulness to ALLAH for giving me tremendous blessings and chances throughout my life.

I also owe a lot of appreciation to many people who supported my efforts on this work. My sincere thanks go to my supervisor Prof. Dr. Leyla YURTTAŞ for her valuable directions, patience and cooperation which enabled me to deliver this study work in its current form.

I appreciate the efforts of my colleague M.Pharm. Asaf Evrim EVREN who has been extremely helpful at different stages of this work.

I extend my thanks to my labmates Sam DAWBAA and Demokrat NUHA who were always ready to help me with any questions that I had.

Special gratitude to Sana SAFFOUR, with whom I experienced most of the master journey and who has been a supportive friend.

Many thanks to Assoc. Prof. Dr. Begüm Nurpelin SAĞLIK for carrying out the biological evaluation studies, Dr. Serkan LEVENT and Mrs. Betül AYDIN for performing the chemical analysis measurements. I'm also grateful to the DOPNA laboratory and AÜ-BİBAM laboratory, where the chemical analysis was performed.

I would like also to thank the Turkish Scholarship Committee for giving me the chance for being one of its holders.

Last, but not least, my warm and heartfelt thanks go to my family for their unconditional and loving support. Thank you all for the strength you gave me. Your prayers for me have kept me going thus far.

TABLE OF CONTENTS

LIST OF TABLES

Page

LIST OF FIGURES

Page

LIST OF ABBREVIATIONS

^{13}C NMR	: Carbon-13 nuclear magnetic resonance
^{1}H NMR	: Proton nuclear magnetic resonance
2D	: Two-dimensional
3D	: Three-dimensional
ACh	: Acetylcholine
AChE	: Acetylcholinesterase
ACN	: Acetonitrile
AD	: Alzheimer's disease
ADME	: Absorption, distribution, metabolism and excretion
APOE-e4	: Apolipoprotein E-e4
APP	: Amyloid precursor protein
Ar H-bond	: Aromatic hydrogen bond
ATC	: Acetylcholine iodide
ATR	: Attenuated total reflection
Aβ	: Amyloid-beta
BBB	: Blood-brain barrier
BChE	: Butyrylcholinesterase
br-s	: Broad singlet
BTC	: Butyrylcholine iodide
CAS	: Catalytic active site
$CDCl_3$	: Deuterated chloroform
ChEI	: Cholinesterase inhibitors

ChEs : Cholinesterases

CNS : Central nervous system

Cpd. : Compound

d : Doublet

DLS : Drug-likeness score

DMF : *N*,*N*-Dimethylformamide

DMSO : Dimethyl sulfoxide

DMSO-d_6 : Deuterated dimethyl sulfoxide

DTNB : 5,5-Dithiobis(2-nitrobenzoic acid)

ESI^+ : Electrospray ionization- positive ion mode

FAD : Flavin adenine dinucleotide

FDA : Food and drug administration

GIA : Gastrointestinal absorption

h : Human

HBA : Hydrogen bond acceptors

HBD : Hydrogen bond donors

HR-MS : High-resolution mass spectrometry

IC_{50} : The half-maximal inhibitory

IR : Infra-red

IT : Ion trap

IUPAC : International Union of Pure and Applied Chemistry

J : Coupling constant

LCMS : Liquid chromatography-mass spectrometry

Log P : Octanol/water partition coefficient

Log S	: Aqueous solubility
LR	: Lawesson’s reagent
m	: Multiplet
M.P.	: Melting point
m/z	: mass/charge
MAO	: Monoamine oxidase
MTD	: Multi-target drug
MV	: Molecular volume
MW	Molecular weight
NFT	: Neurofibrillary tangles
NMDA	: *N*-Methyl-D-aspartate
No. V	: Number of Violations (Lipinski’s rule)
PAS	: Peripheral anionic site
PNS	: Peripheral nervous system
ppm	: Part per million
PS-1	: Presenilin-1
PS-2	: Presenilin-2
q	: Quartet
ROS	: Reactive oxygen species
RT	: Room temperature
SD	: Standard deviation
SPs	: Senile plaques
t	: Triplet
TEA	: Triethylamine

THF	: Tetrahydrofuran
TLC	: Thin layer chromatography
TMS	: Tetramethylsilane
TOF	: Time of flight
UV	: Ultraviolet light

1. INTRODUCTION

Dementia is a general term used to describe a group of cognitive, functional, and behavioral symptoms characterized mainly by memory loss, difficulties in thinking, learning and language, social withdrawal and significant changes in mood and behavior. Dementia's negative impacts on the physical, psychological, social and economic aspects of patients also extend to affect their caregivers and society. According to the World Alzheimer Report published in 2021, dementia is now the seventh leading cause of death worldwide with over 55 million cases that are expected to increase to 78 million by 2030. Dementia appears in numerous forms such as vascular dementia, frontotemporal dementia and Lewy body dementia; however, Alzheimer's disease (AD) has been the most prevalent form, contributing to about 60-80% of all cases.[1, 2].

AD is an irreversible progressive neurodegenerative brain disorder mainly affecting elderly people. Most patients with AD are of 65 age and over and this highlights the fact that increasing age is considered the greatest risk factor for developing AD. Other risk factors include family history, female gender, serious head injury, cardiovascular diseases, diabetes mellitus, high cholesterol levels, low physical, social and mental activity, obesity, smoking, excessive alcohol intake and unhealthy diets. Besides that, the existence of apolipoprotein E-e4 (APOE-e4) genes increases the risk to develop late-onset AD. However, less than 1% of cases are classified as inherited early-onset AD, with patients developing symptoms between the ages of 30 and 65 due to a rare mutation in amyloid precursor protein (APP) or the subcomponents of γ-secretase presenilin-1(PS-1) or presenilin-2 (PS-2) proteins [3].

AD is a complex multifactorial disorder represented by several brain change markers including cerebral cortical atrophy, neuronal loss, extraneuronal deposition of senile plaques (SPs) with a central core of amyloid-beta (Aβ) aggregates, intraneuronal deposition of neurofibrillary tangles (NFT), overactivation of monoamine oxidase (MAOs), activation of *N*-methyl-D-aspartate (NMDA) receptors, dysregulation of metal ions, oxidative stress, neuroinflammation as well as disruption of neurotransmitters systems, more prominently cholinergic depletion [4].

While the exact cause of AD is still a mystery to scientists, several hypotheses have been proposed as possible pathophysiological mechanisms (**Figure 1.1**). Among them, the amyloid cascade hypothesis has suggested that the extracellular buildup of the insoluble neurotoxic Aβ peptide fragments at synapses in the brain is the primary cause

of initiating AD. Aβ peptide is produced from the proteolysis of the single-domain transmembrane protein APP by β-secretase and γ secretase, respectively. These Aβ fragments are finally aggregated into β sheets to form senile plaques (SPs) that are responsible for initiating a cascade of secondary pathological events in AD including hyperphosphorylation of tau protein and formation of NFT, oxidative stress, abnormal calcium homeostasis and inflammation. All these events eventually cause apoptosis, which leads to the death of neuronal cells and the depletion of neurotransmitters. A second hypothesis has suggested that tau protein, which normally supports the cytoskeleton of neurons by binding and maintaining microtubules, undergoes hyperphosphorylation during AD and clumps into insoluble intraneuronal NFT, causing microtubules to become unstable and blocking communication between neurons, which leads eventually to neurons death [4-7]. The third is the cholinergic theory, which has been the subject of several drug development studies, including some that have already been approved. This hypothesis suggested that the cognitive decline in AD patients is linked to irreversible damage to the central nervous system's cholinergic pathways leading to a decreased level of acetylcholine (ACh) neurotransmitter which plays a major role in numerous physiological functions in the brain for instance learning, attention, memory, stress and sleep [5]. Additionally, monoamine oxidase (MAO) enzymes were also found to affect the progress of AD, especially the MAO-B isoform. The overexpression of these enzymes in AD patients, hence their oxidative deamination of monoamine neurotransmitters leads to a significant generation of neurotoxic by-products such as hydrogen peroxides and consequently reactive oxygen species (ROS) which further cause and exaggerate many pathological mechanisms in AD including the oxidative stress, neuroinflammation, Aβ deposition, neuronal damage and death [6, 7].

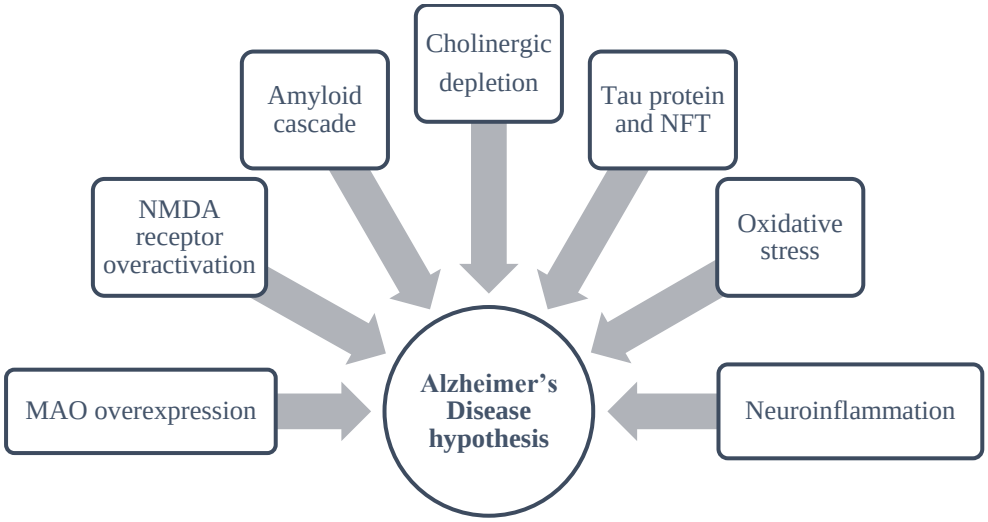

Figure 1.1. *Proposed hypothesis for the pathophysiological mechanisms in AD*

So far, clinically Food and Drug Administration (FDA) authorized drugs for AD (**Figure 1.2**) mainly work as cholinesterase enzyme inhibitors (ChEIs) in the brain in accordance with the cholinergic hypothesis. These anticholinesterase drugs include tacrine, donepezil, rivastigmine and galantamine, however tacrine is no longer available in markets due to its hepatotoxicity and other side effects [8, 9]. Another FDA-approved drug for AD is memantine which acts as an antagonist for NMDA receptors that are overactivated by the action of the excitatory neurotransmitter glutamate which has an abnormally high concentration in the brain of AD patients leading to high calcium ion Ca^{+2} concentration at synapses that can activate multiple enzymes, disrupt cellular functions, and ultimately causes cells death [10, 11]. The last recently approved drug for AD is aducanumab which acts as an anti-amyloid monoclonal antibody [12]. However, none of the approved drugs provide a radical treatment for AD. They only help to alleviate the symptoms of AD to a certain extent. As a result, the focus of AD has shifted from conventional mono-target therapy and combinational therapy toward the development of multi-target drugs (MTDs) with safer side effects profiles [13, 14].

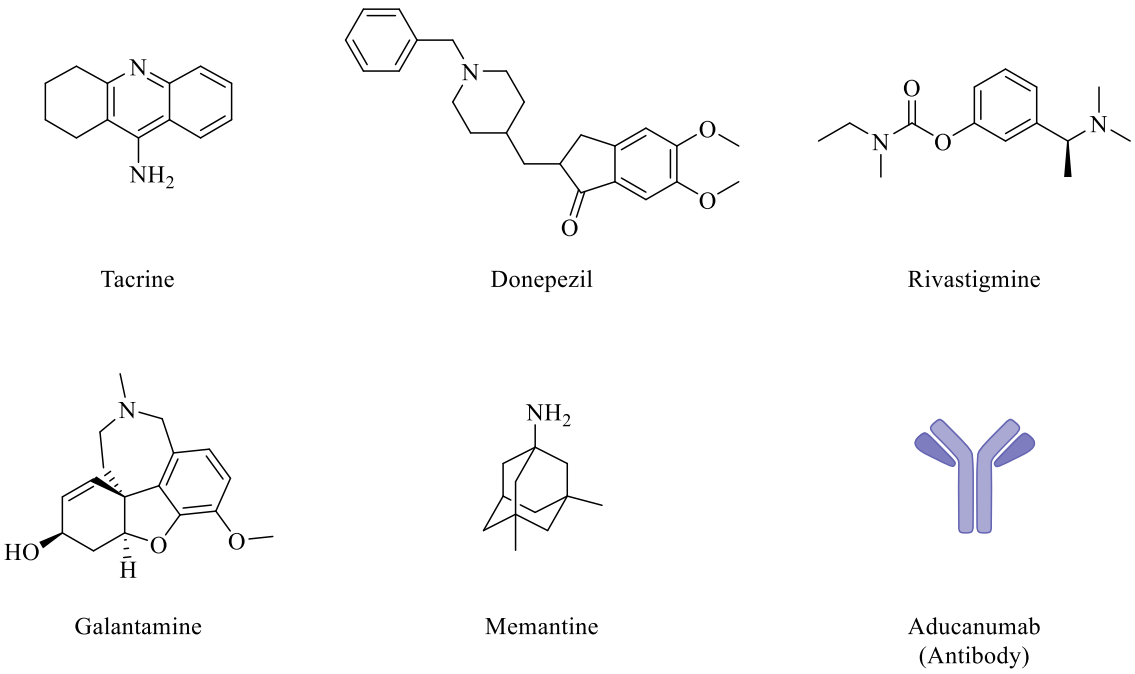

Figure 1.2. *FDA approved drugs for AD*

Cholinesterases (ChEs) are a group of enzymes that hydrolyze ACh into choline and acetic acid in the central and peripheral nervous system (CNS and PNS), thus inhibiting this normal degradation and consequently increasing the concentration of ACh at synapses leads to improvement in the cholinergic transmission in AD patients. Both acetylcholinesterase (AChE) and butyrylcholinesterase (BChE) are types of cholinesterase found in human brains with more than 50 % amino acids homology leading to similar tertiary structures. However, their affinity for substrates, distribution within the body, and catalytic activity are different [15].

AChEs which were given this name after their endogenous substrate ACh are mainly found in the CNS and erythrocytes whereas BChEs which have no known endogenous substrate and are named after the exogenous substrate butyrylcholine are found mainly in blood plasma. In terms of their substrate affinity, AChE has a stronger affinity for ACh than BChE, whereas BChE preferentially hydrolyzes high molecular weight esters. The amount of AChE in the brain drops as AD progresses, whereas the amount of BChE increases which indicates that BChE can compensate for the absence of AChE. As a result, developing BChE selective inhibitors can be beneficial in the late stages of AD [16].

MAOs are mitochondrial enzymes that are involved in the oxidative deamination of intrinsic and extrinsic amines utilizing flavin adenine dinucleotide (FAD) in both CNS and PNS. Both MAO-A and MAO-B are forms of this enzyme with nearly 70 % amino acid sequence homology, however they crystallize as monomers and dimers, respectively. Additionally, they have different tissue distribution with MAO-A is mainly found in the heart, intestines and placenta whereas MAO-B is mainly found in brain glial cells, liver cells and platelets. Both forms have different substrate selectivity as the larger substrates including serotonin, noradrenaline, and adrenaline are preferentially degraded by MAO-A while the smaller ones including phenethylamine and benzylamine are preferentially degraded by MAO-B. Tyramine and dopamine are degraded by both forms non-selectively [17]. For AD patients, inhibiting MAOs that contribute to the progression of the disease has been considered a potential treatment for AD due to the neuroprotective effect that mainly includes reduced neurotoxic chemical production and improved neurotransmission [18].

Many heterocyclic systems have been included in the structures of many active compounds, for example, three out of four ChEI drugs approved for the treatment of AD contain a heterocyclic system, encouraging medicinal chemists to further investigate their potential activities [19, 20]. Among these heterocyclic systems is the five-membered 1,3,4-thiadiazole ring. The wide pharmacological activities, the enhanced lipophilicity, hence bioavailability and blood-brain barrier (BBB) permeability due to ring's mesoionic nature and the presence of the lipophilic sulfur atom are all features making 1,3,4-thiadiazole a promising nucleus for the design and development of novel drugs [21]. Additionally, five-membered heterocyclic rings such as 1,3,4-thiadiazole can be utilized as a bio-isostere to replace ester groups, resulting in more metabolically stable cholinomimetic substrates [22].

On the other hand, adamantane is also a promising hydrocarbon with a tricyclic cage structure and unique properties that provide additional benefits to compounds containing it. Among these interesting features, is the increasing lipophilicity of adamantane-containing compounds, hence enhanced pharmacokinetic profile. This property is of great importance for drugs to cross biological membranes, especially CNS drugs which need to be transported to the site of action through BBB [23]. Adamantane moiety could also enhance the affinity toward targets through the formation of more hydrophobic interactions or through providing a rigid spatial arrangement of the ligand's

pharmacophore [24]. Additionally, the rigid bulk nature of this moiety can protect nearby functional groups from metabolic degradation, thus enhancing stability and duration of action [25].

By considering all of these findings, derivatives of *N*-(5-(adamantan-1-yl)-1,3,4-thiadiazol-2-yl)-2-substituted-acetamide **(3a-3j)** and *N*-(5-(adamantan-1-yl)-1,3,4-thiadiazol-2-yl)-2-substituted-propanamide **(4a-4g)** as shown in **Table 1.1** and **Table 1.2**, respectively were synthesized within the scope of this master thesis and their structures were elucidated by using IR, ^{1}H-NMR, ^{13}C-NMR, and HR-MS. The *in vitro* inhibition activity of these derivatives against AChE, BChE, MAO-A and MAO-B were examined with the goal of developing safe and effective MTDs for AD. Molecular docking studies for the most potent compounds were conducted in addition to the *in-silico* prediction of pharmacokinetic profile.

Table 1.1. *Synthesized targeted compounds* ***(3a-3j)***

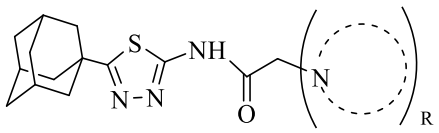

(3a-3j)

Compound	R
3a	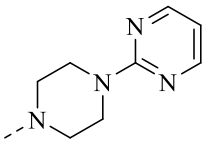
3b	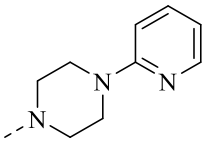
3c	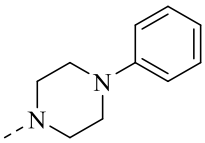
3d	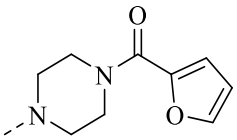
3e	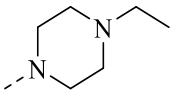
3f	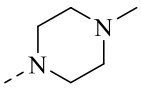
3g	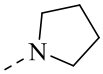
3h	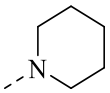
3i	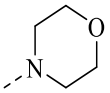
3j	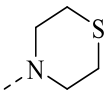

Table 1.2. *Synthesized targeted compounds* ***(4a-4g)***

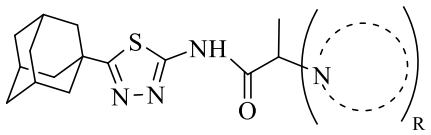

(4a-4g)

Compound	R
4a	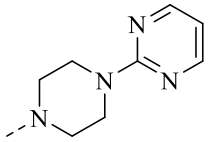
4b	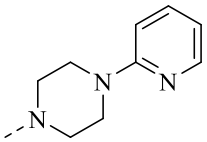
4c	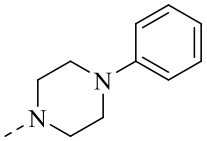
4d	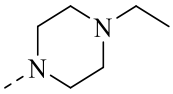
4e	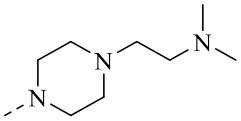
4f	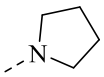
4g	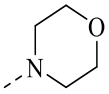

2. LITERATURE REVIEW

2.1. 1,3,4-Thiadiazole

2.1.1. Chemistry

Thiadiazole is a heterocyclic five-membered ring system comprising two nitrogen atoms, one sulfur atom, and two carbon atoms. It acts as a hydrogen binding domain and two-electron donor system. It exists in nature as four isomers: 1,2,3-thiadiazole, 1,2,4-thiadiazole, 1,2,5-thiadiazole, and 1,3,4-thiadiazole, with the numbering starting at the sulfur atom (**Figure 2.1**) [26].

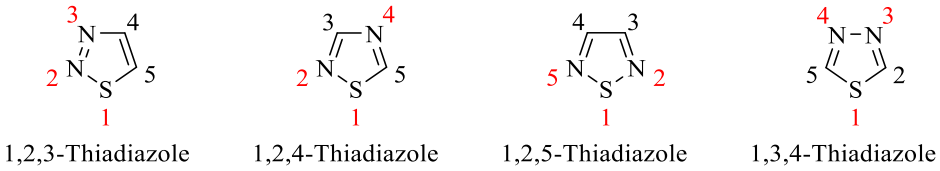

Figure 2.1. *Isomers of thiadiazole*

The origin of 1,3,4-thiadiazole chemistry which is the most investigated isomer can be traced back to the late nineteenth century, following the discovery of phenylhydrazine and hydrazine by Emil Fischer and Th. Curtius, respectively. Emil Fischer was the first to describe 1,3,4-thiadiazole in 1882, however, it was not until 1890 that Freund and Kuh established the real properties of the ring system. After that, Busch and his colleagues attributed much to the rapid growth in this field during the first decade of the twentieth century [27].

1,3,4-Thiadiazole can be found either as aromatic derivatives including the parent 1,3,4-thiadiazole (**Figure 2.2-a**), 1,3,4-thiadiazolium cation (**Figure 2.2-b**) and mesoionic systems which are five-membered heterocyclic rings with conjugated π and p electrons and separate areas of negative and positive charges (**Figure 2.2-c**) or as non-aromatic derivatives including 1,3,4-thiadiazolines (**Figure 2.2-d** and **Figure 2.2-e**), tetrahydro-1,3,4-thiadiazolidine (**Figure 2.2-f**) and tautomeric compounds (**Figure 2.2-g**) [28].

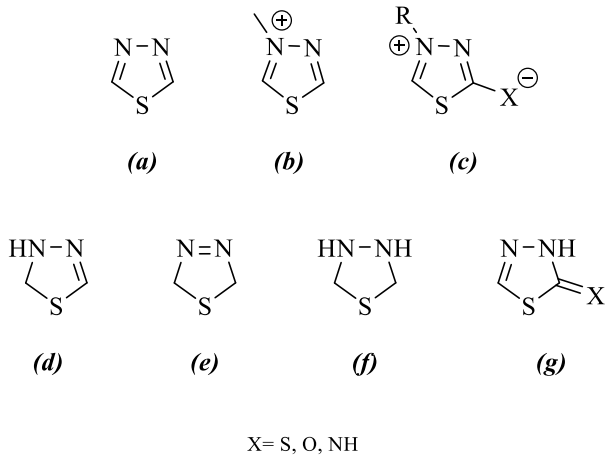

Figure 2.2. *Different forms of 1,3,4-thiadiazole*

The melting point of unsubstituted 1,3,4-thiadiazole is 43 ˚C, whereas 2-amino-l,3,4-thiadiazole is 193 ˚C. In addition, 1,3,4-thiadiazoles are generally soluble in water, however, their solubility in water decreases as the size of substituents at positions 2 and 5 increases [29].

Because of the inductive effect of the sulfur atom, 1,3,4-thiadiazole acts as a weak base. In acids, it is relatively stable, but in bases, it is readily cleaved. Additionally, 1,3,4-thiadiazoles containing mercapto, hydroxyl and amino substituents at positions 2 or 5 are found to have tautomers as shown in **Figure 2.3** [30]. Nitrogen atoms of the ring skeleton at positions 3 and 4 can be attacked by electrophiles. On the other hand, due to the electron-withdrawing impact of nitrogen atoms, carbon atoms in the ring are electron deficient which makes them generally inert to electrophiles but prone to nucleophilic substitution. Generally, different substituents at C_2 and C_5 determine the reactivity of the ring [31].

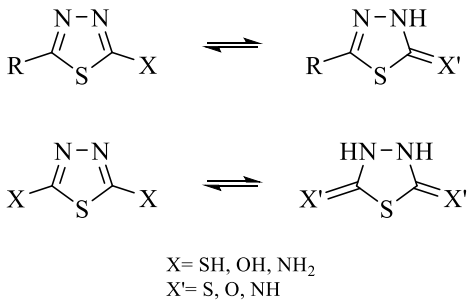

Figure 2.3. *Tautomerism of 1,3,4-thiadiazole*

2.1.2. Synthesis

Goerdeler *et al.* synthesized the parent unsubstituted 1,3,4-thiadiazole for the first time in 1956 [32], however several procedures for synthesizing substituted 1,3,4-thiadiazole had been reported earlier in the literature, each with distinct starting materials, conditions, and number of formed bonds. Most of these cyclization methods depend on the presence of the fundamental structural unit (C-N-N-C-S). Thus, reactants with either sulfur source or carbon source or carbon-sulfur source are chosen to complete the missing fragments of the basic unit as summarized in **Figure 2.4**. This is in addition to the synthesis by ring transformation.

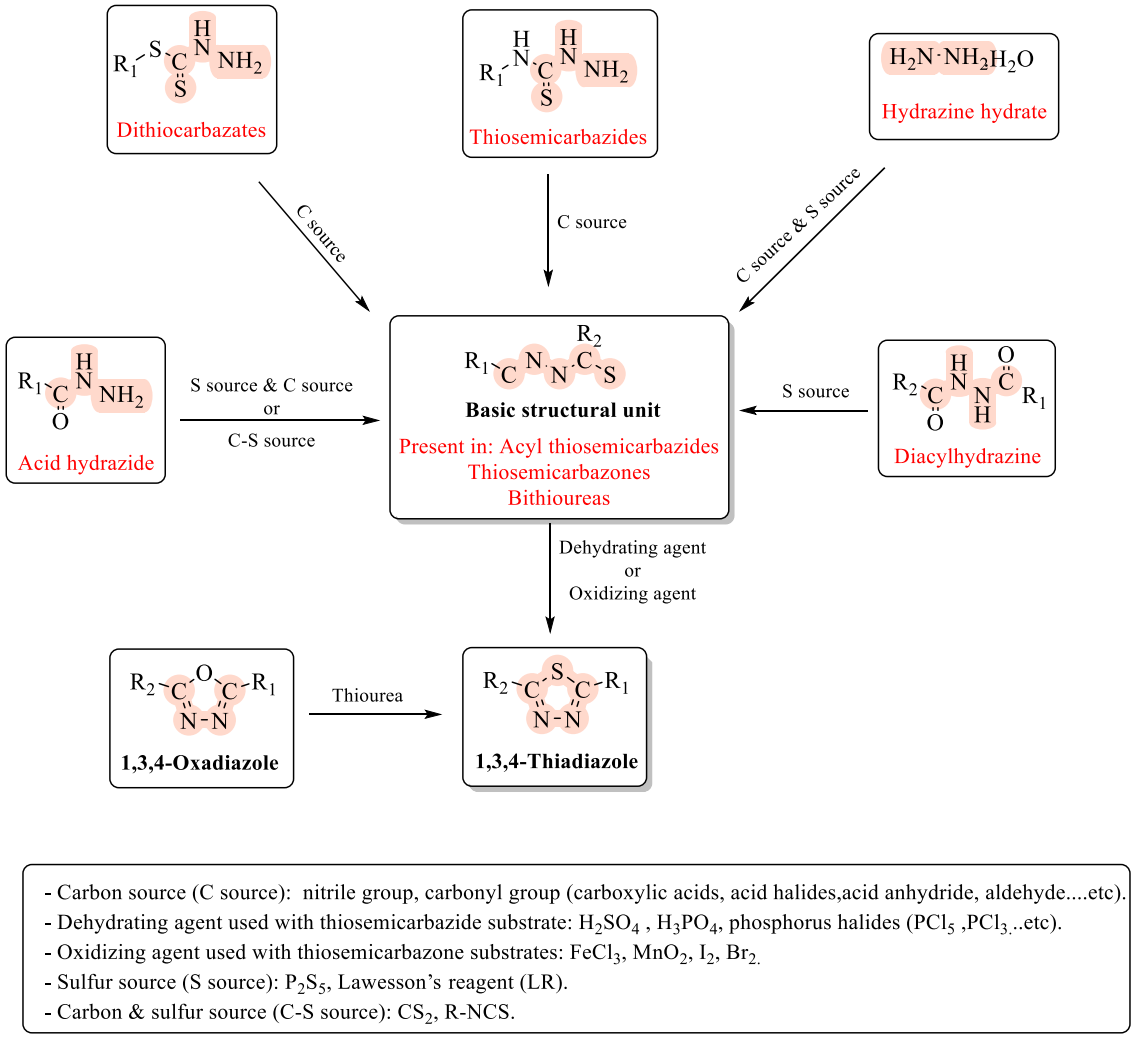

Figure 2.4. *General methods for cyclization reactions of 1,3,4-thiadiazole*

2.1.2.1. Formation of one bond

2,5-Diamino-1,3,4-thiadiazole was synthesized starting from dithiobiurea which was treated with 3% hydrogen peroxide as an oxidizing agent in water by Fromm *et al.* (1923) (**Figure 2.5**) [33].

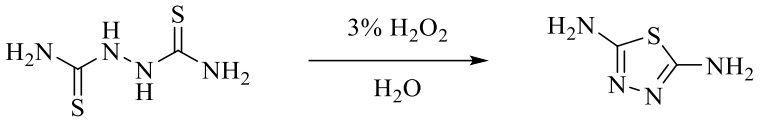

Figure 2.5. *Synthesis of 2,5-diamino-1,3,4-thiadiazole from dithiobiurea by using 3% H_2O_2*

Young and Wood (1955) synthesized 2-substituted-5-alkylmercapto-1,3,4-thiadiazole compounds by the cyclization of different 3-acyldithiocarbazates with acidic reagents including H_2SO_4, H_3PO_4 and ρ-toluenesulfonic acid (**Figure 2.6**) [34].

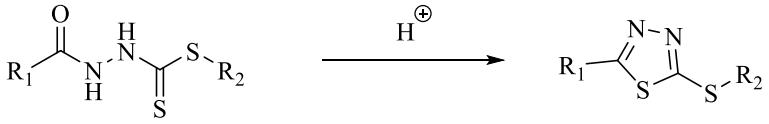

Figure 2.6. *Synthesis of 2-substituted-5-alkylmercapto-1,3,4-thiadiazole from acylated dithiocarbazate by using acidic reagents*

Foroumadi *et al.* (2003) used ammonium ferric sulfate $NH_4Fe(SO_4)_2$. dodecahydrate to oxidatively cyclize 5-nitrothiophene-2-carboxaldehyde thiosemicarbazone into 2-amino-5-(5-nitro-2-thienyl)-1,3,4-thiadiazole (**Figure 2.7**) [35].

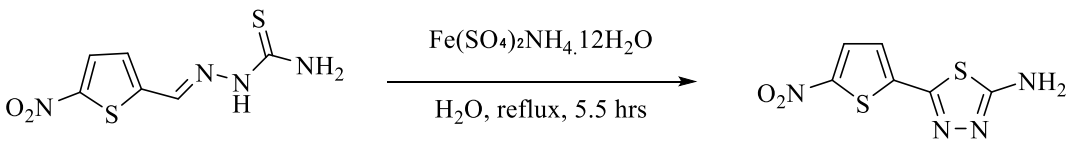

Figure 2.7. *Synthesis of 2-amino-5-(5-nitro-2-thienyl)-1,3,4-thiadiazole by oxidative cyclization of thiosemicarbazone by using $NH_4Fe(SO_4)_2$*

2.1.2.2. Formation of two bonds

Acylation-dehydration of thiosemicarbazide is considered one of the most common methods to synthesize 2-amino-5-substituted 1,3,4-thiadiazole in which an acylating agent- such as carboxylic acids, acid halides and acid anhydride- is used first to give acyl thiosemicarbazide that is further treated with a dehydrating agent such as sulphuric acid H_2SO_4, hydrochloric acid HCl, phosphoric acid H_3PO_4, phosphorus pentachloride PCl_5 and phosphorus oxychloride PCl_3. This method was first reported by E. Hoggarth (1949) to synthesize 2-amino-5-substituted phenyl -1,3,4-thiadiazoles by using benzoyl chloride as the acylating agent and phosphoric acid H_3PO_4 as the dehydrating agent (**Figure 2.8**) [36].

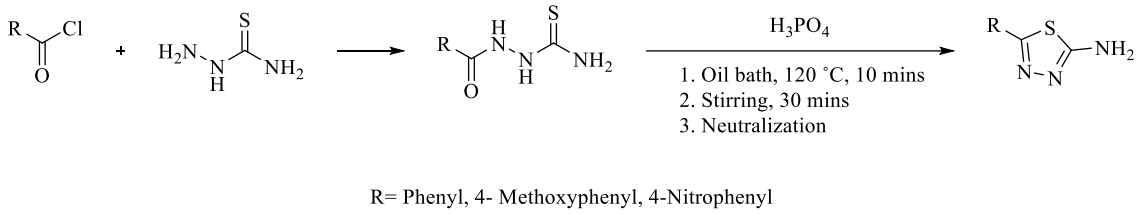

Figure 2.8. *Synthesis of 2-amino-5-substituted 1,3,4-thiadiazole from thiosemicarbazide and benzoyl chloride derivatives by using phosphoric acid*

Whitehead and Traverso (1955) reported the use of orthoesters including triethyl orthoformate, triethyl orthoacetate and triethyl orthopropionate as the cyclizing agents with aryl/alkyl thiosemicarbazides to give 2-substituted amino-1,3,4-thiadiazole, 2-substituted amino-5-methyl-1,3,4-thiadiazole and 2-substituted amino-5-ethyl-1,3,4-thiadiazole, respectively (**Figure 2.9**) [37].

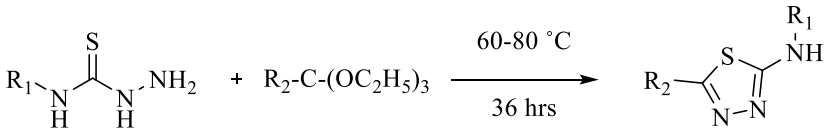

Figure 2.9. *Synthesis of 2-substituted amino-1,3,4-thiadiazole by using orthoesters*

Kurzer (1961) used aminoguanidine as a starting material and treated it with sodium (thiobenzoylthio)acetate as the thioacylating agent to give *N*-(thiobenzamido)guanidine which was cyclized into 2-amino-5-phenyl-l,3,4-thiadiazole by treating with hot HCl or into 2-acetylamino-5-phenyl-l,3,4-thiadiazole by treating with acetic anhydride (**Figure 2.10**) [38].

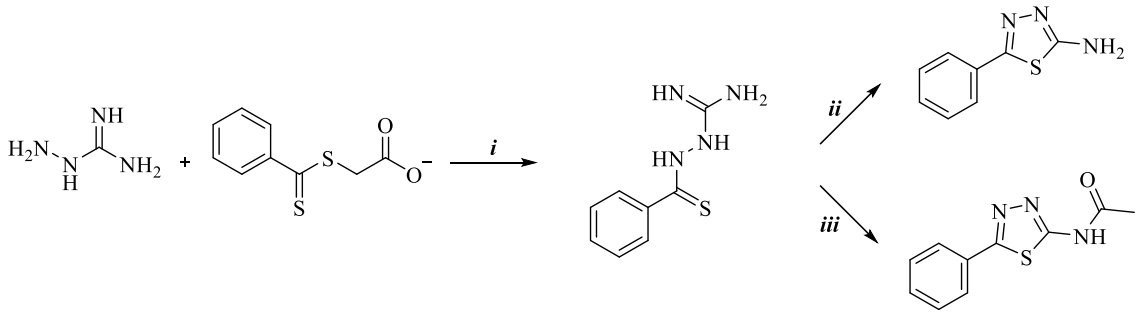

i: H_2O, 3N NaOH, R.T, ***ii:*** 3N HCl, reflux, 15 mins, ***iii:*** acetic anhydride, 100 ˚C, 1hr

Figure 2.10. *Synthesis of 2-amino/2-acetylamino-5-phenyl-l,3,4-thiadiazole from aminoguanidine and (thiobenzoylthio)acetate*

Grigat and Puetter (1965) reported the reaction of thiobenzhydrazide with aryl cyanate to produce 2-amino-5-phenyl-l,3,4-thiadiazole as shown in **Figure 2.11**. Aryl cyanate is used as cyclizing agent, carbon source and amino group source [39].

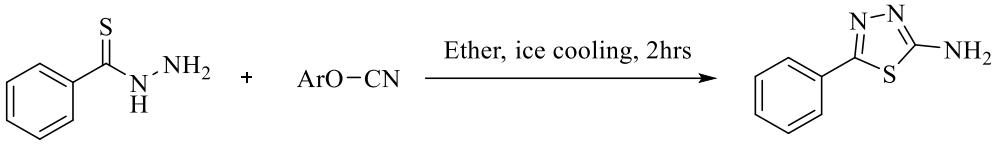

Figure 2.11. *Synthesis of 2-amino-5-phenyl-l,3,4-thiadiazole from thiobenzhydrazide and aryl cyanate*

The synthesis of a series of 5-substituted-2-amino-1,3,4-thiadiazole derivatives was reported by Tsuji and Keiko (1982). Different carboxylic acids were heated at 70 ˚C for 10 hours with thiosemicarbazide in a 1:5 mixture of phosphorus pentaoxide P_2O_5: methane sulfonic acid MsOH followed by neutralization with aqueous ammonia (**Figure 2.12**) [40].

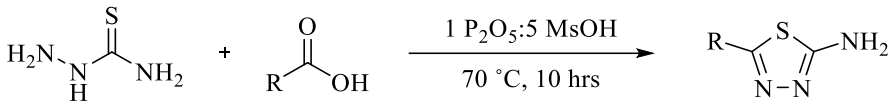

R= CH_3, C_6H_5, ρ-ClC_6H_4, ρ-$NO_2C_6H_4$,

Figure 2.12. *Synthesis of 5-substituted-2-amino-1,3,4-thiadiazole from carboxylic acids and thiosemicarbazide by using 1 P_2O_5:5 MsOH*

Thomsen *et al.* (1983) reported the synthesis of 5-phenyl-1,3,4-thiadiazole-2(3*H*)-thione from *N*-benzoyl-*N'*-ethoxycarbonyl hydrazine using Lawesson's reagent (LR) as thionating agent in xylene (**Figure 2.13**) [41].

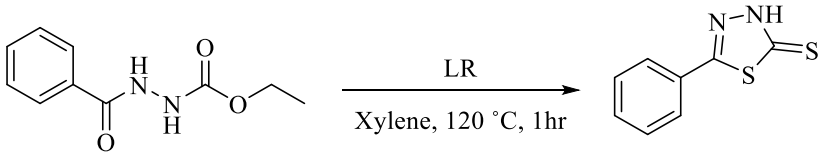

Figure 2.13. *Synthesis of 5-phenyl-1,3,4-thiadiazole-2(3H)-thione from acylated carbazate by using LR*

Using aldehydes as the starting materials Chapleo *et al.* (1986) cyclized 2-aryl-5-amino-l,3,4-thiadiazoles as part of their work [42]. Aldehydes were first treated with thiosemicarbazides to give thiosemicarbazones followed by oxidative cyclization using $FeCl_3$ as illustrated in **Figure 2.14**.

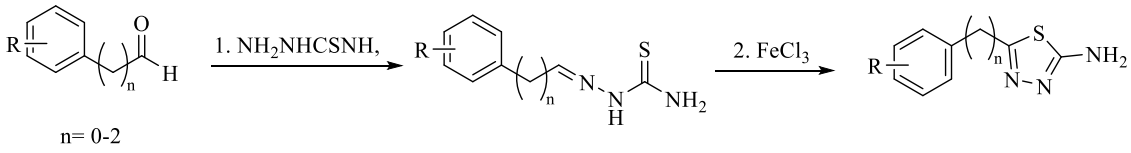

Figure 2.14. *Synthesis of 2-aryl-5-amino -l,3,4-thiadiazoles by oxidative cyclization of thiosemicarbazone by using $FeCl_3$*

Cho and Kim (1993) described the cyclization of 5-amino-3*H*-1,3,4-thiadiazole-2-thione starting from thiosemicarbazide which was refluxed with CS_2 in KOH/ethanol for 6 hours as shown in **Figure 2.15** [43].

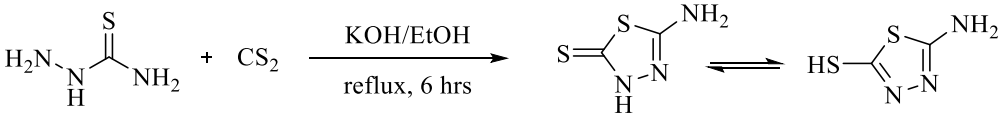

Figure 2.15. *Synthesis of 5-amino-3H-1,3,4-thiadiazole-2-thione from thiosemicarbazide and CS_2 under basic conditions*

Kiryanov *et al.* (2001) used LR as a thionating agent to cyclize *N,N'*-diacyl hydrazine into 1,3,4-thiadiazole with a yield of 91% utilizing microwave irradiation in solvent-free conditions (**Figure 2.16**) [44].

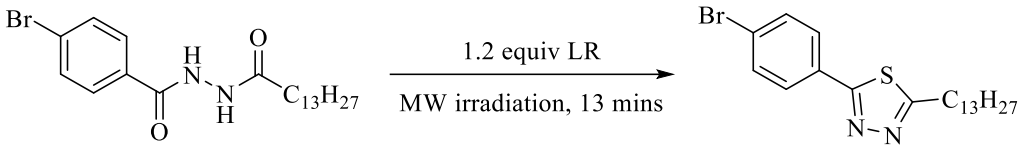

Figure 2.16. *Synthesis of 2,5-disubstituted-1,3,4-thiadiazole from N, N'-diacyl hydrazine by using LR*

An oxidative cyclization method using I_2 was reported by Niu *et al.* (2004) to obtain 2-amino-1,3,4-thiadiazole derivatives starting from aldehydes that were condensed with thiosemicarbazide to produce thiosemicarbazone derivatives which were further heated to reflux after treated with I_2 in 1,4-dioxane and potassium carbonate (**Figure 2.17**) [45].

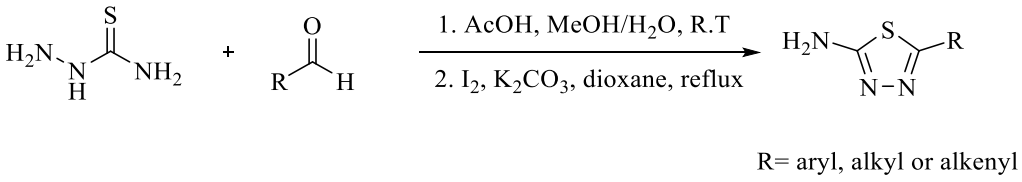

Figure 2.17. *Synthesis of 2-amino-1,3,4-thiadiazole derivatives by oxidative cyclization of thiosemicarbazone by using I_2*

The dehydrating cyclization of 5-substituted-2-amino-1,3,4-thiadiazole using different carboxylic acids and thiosemicarbazide in the presence of $POCl_3$ and H_2O as illustrated in **Figure 2.18** was reported by Jakovljevic *et al.* (2019) [46].

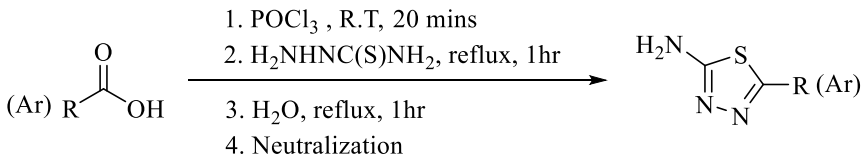

Figure 2.18. *Synthesis of 5-substituted-2-amino-1,3,4-thiadiazole from carboxylic acids and thiosemicarbazide by using $POCl_3$ and H_2O*

A series of 2-amino-1,3,4-thiadiazole derivatives were synthesized from isothiocyanates and different hydrazides in TEA, Dry THF, *p*-tosyl chloride (*P*-TsCl) and *N*-methyl-2- pyrrolidone (NMP) by Chandra Sekhar *et al.* (2019) by using two-steps conventional method and one-pot microwave-assisted method with 66-87% of yield (**Figure 2.19**) [47].

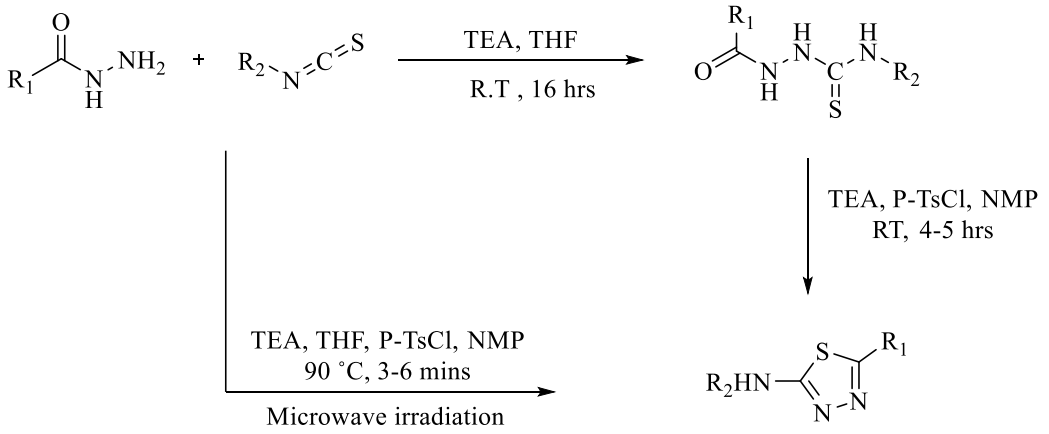

Figure 2.19. *Synthesis of 2-amino-5-substituted-1,3,4-thiadiazole from isothiocyanates and hydrazides*

Starting from nitriles, Xue *et al.* (2020) synthesized 5-substituted-2-amino-1,3,4-thiadiazole as intermediate derivatives in their work. Mixtures of different nitriles were refluxed for 6 hours with thiosemicarbazide in trifluoroacetic acid TFA, followed by neutralization with aqueous ammonia (**Figure 2.20**) [48].

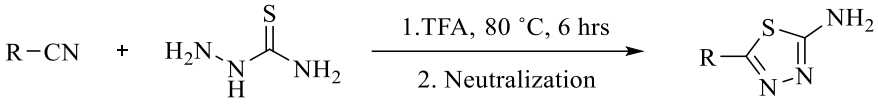

Figure 2.20. *Synthesis of 5-substituted-2-amino-1,3,4-thiadiazole from nitriles and thiosemicarbazide by using TFA*

2.1.2.3. Formation of three bonds

Mazzone *et al.* (1984) reported the synthesis of 2-pyridyl/quinolyl-5-aryl-1,3,4-thiadiazole by reacting aroylhydrazines with methyl pyridines/methyl quinolines at 180 ˚C for 12 hours in the presence of sulfur. However, the corresponding symmetrical diaryl-1,3,4- thiadiazoles and 2-pyridyl/quinolyl-5-aryl-1,3,4-oxadiazoles were also formed as by-products (**Figure 2.21**) [49].

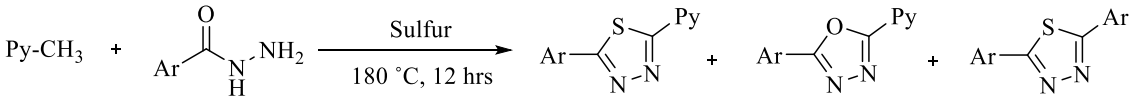

Figure 2.21. *Synthesis of 2-pyridyl/quinolyl-5-aryl-1,3,4-thiadiazole from methyl pyridines/methyl quinolines and aroylhydrazines in the presence of sulfur*

2.1.2.4. Formation of four bonds

Aldehyde, hydrazine, and sulfur were reacted in ethanol for 12 hours at 150 ˚C using a steel autoclave to give symmetrically 2,5-diaryl-1,3,4-thiadiazoles by Mazzone *et al.* (1982) [50]. However, Lebrini *et al.* (2004) reported the same synthetic method by using microwave irradiation that shortens the duration of reaction to 1 hour with a good yield of the symmetrically 2,5-diaryl-1,3,4-thiadiazoles [51] as shown in **Figure 2.22**.

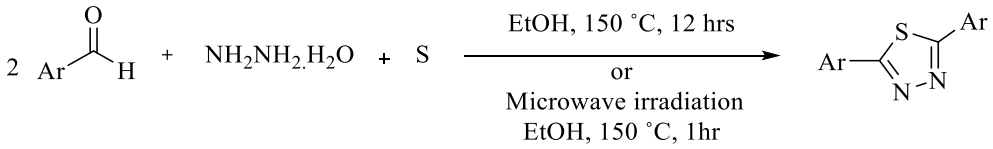

Figure 2.22. *Synthesis of symmetrical 2,5-diaryl-1,3,4-thiadiazole from aldehyde, hydrazine, and sulfur in EtOH*

2.1.2.5. Formation by ring transformation

Linganna and Lokanatha Rai (1998) reported the synthesis of 2,5-diaryl-1,3,4-thiadiazole by ring transformation of 2,5-diaryl-1,3,4-oxadiazole using thiourea in tetrahydrofuran THF as shown in **Figure 2.23** [52].

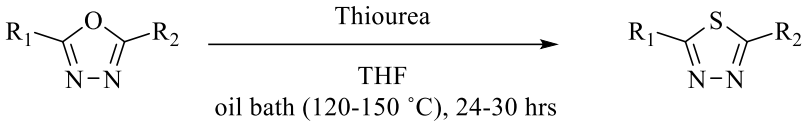

Figure 2.23. *Synthesis of 2,5-diaryl-1,3,4-thiadiazole from 2,5-diaryl-1,3,4-oxadiazole by using thiourea*

2.1.3. Pharmacological profile

The 1,3,4-thiadiazole heterocyclic system has a wide spectrum of biological functions due to its -N=C-S- group. It is also considered a bio-isostere of pyridazine, thiazole, and oxadiazole [53] which contributes further to its wide activities that include antimicrobial, carbonic anhydrase inhibition, antioxidant, anti-inflammatory, anti-depressant and antidiabetic activity [54-57], as well as anticancer [58] and anticonvulsant activity [59].

Many drugs incorporating the 1,3,4- thiadiazole moiety are currently available in the market (**Figure 2.24**) including the antiparasitic megazole, the carbonic anhydrase inhibitor diuretics acetazolamide and methazolamide and the antibacterial cefazolin sodium and cefazedone [60, 61].

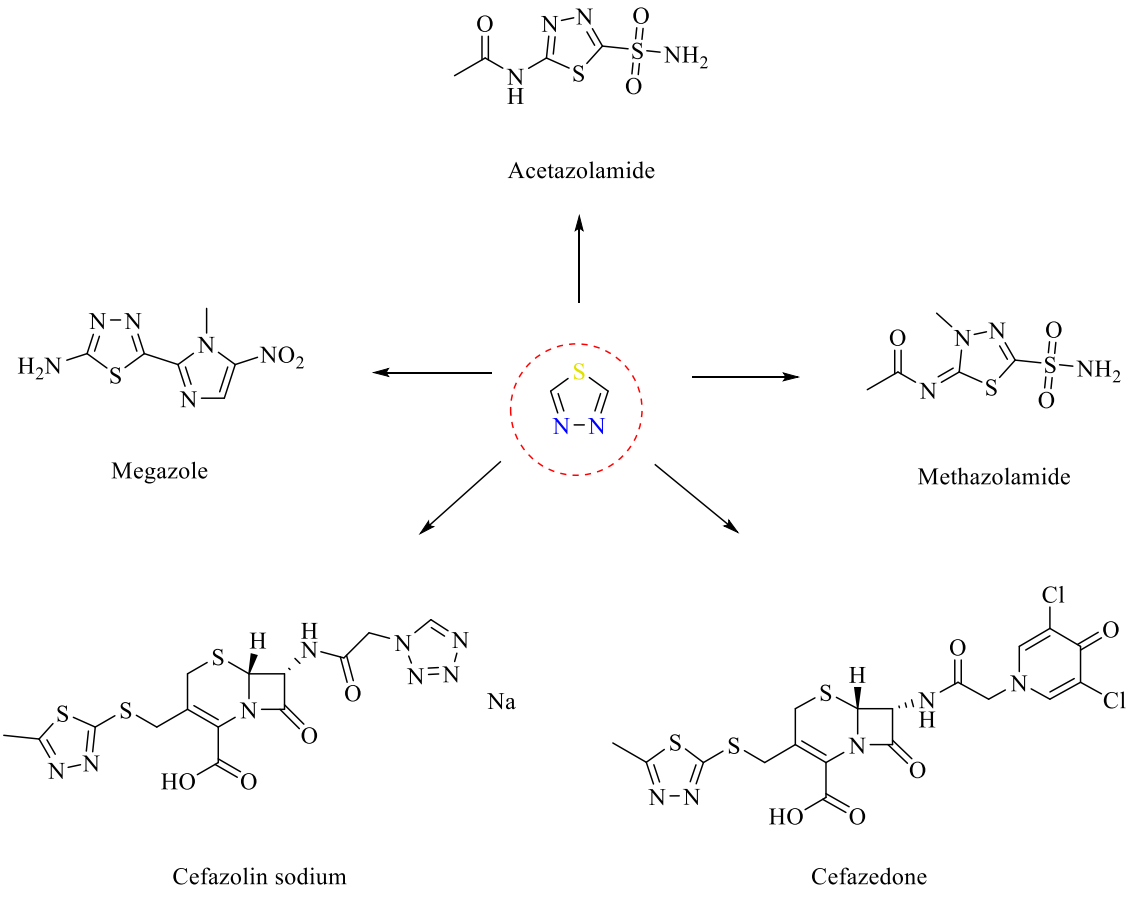

Figure 2.24. *Clinically available drugs containing 1,3,4-thiadiazole scaffold*

2.1.3.1. Literature review of 1,3,4-thiadiazole derivatives with anticholinesterase inhibition activity

Gupta and Misra (1980) synthesized 1,3,4-thiadiazole substituted quinazoline derivatives and test their *in vitro* inhibition activities against AChE. It was noticed that derivatives with 6,8-dibromo substituents were more potent than those with only 6-bromo containing substituents. Among synthesized derivatives, compound shown in **Figure 2.25** was the most active with 36.843 inhibition % at 6.6 x 10^{-5} M and IC_{50} of 8.95x 10^{-5} in comparison to IC_{50} of 1.96 x 10^{-7} M for the reference neostigmine [62].

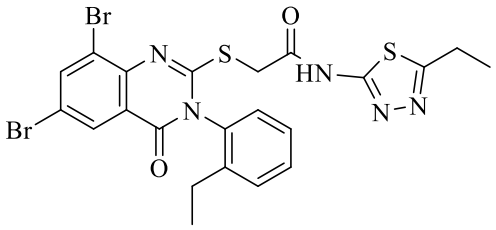

Figure 2.25. *2-((6,8-Dibromo-3-(2-ethylphenyl)-4-oxo-3,4-dihydroquinazolin-2-yl)thio)-N-(5-ethyl-1,3,4-thiadiazol-2-yl)acetamide*

Altintop *et al.* (2012) synthesized derivatives of 2-(5-Amino/Methyl-1,3,4-thiadiazol-2-yl)thio-*N*-(6-substituted-benzothiazol-2-yl)- acetamide and investigated their AChE and BChE inhibition activity [63]. Cholinesterase inhibitory activity was observed in derivatives having 5-amino-1,3,4-thiadiazole moiety, among which compound shown in **Figure 2.26** was the most active one with a cytotoxic value below its therapeutic effective dose (66 ± 0.71 mg/ml).

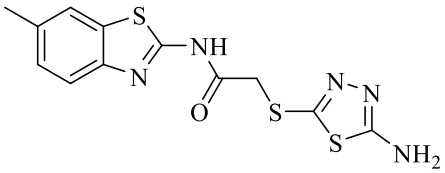

Figure 2.26. *2-(5-Amino-1,3,4-thiadiazol-2-yl)thio-N-(6-methylbenzothiazol-2-yl)acetamide*

Derivatives of *N*,5-Substituted diphenyl-1,3,4-thiadiazole-2-amine were synthesized and screened for cholinesterase inhibitory activity by Khan *et al.* (2012). Compound with *meta*-chlorophenyl at the fifth carbon atom of 1,3,4-thiadiazole as shown in **Figure 2.27** has the maximum acetylcholinesterase inhibition activity among other

1,3,4-thiadiazole derivatives with 0.351 ± 0.013 μM IC_{50} compared to 0.021± 0.004 μM IC_{50} of donepezil [64].

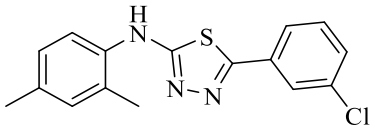

Figure 2.27. *5-(3-Chlorophenyl)-N-(2,4-dimethylphenyl)1,3,4-thiadiazol-2-amine*

Skrzypek *et al.* (2013) synthesized and evaluated twenty-one 2,5-substituted-1,3,4-thiadiazole derivatives which have the general structure as shown in **Figure 2.28** for anticholinesterase activity [65]. Most of the compounds showed considerable inhibition activity with IC_{50} of 0.06 to 128.42 μM against AChE and IC_{50} of 0.29 to >500 μM against BChE compared to donepezil which has IC_{50} of 0.02 μM and 7.52 μM against AChE and BChE, respectively. Moreover, all compounds except one derivative were stronger against AChE than BChE and one of them showed three times more selectivity toward AChE than donepezil.

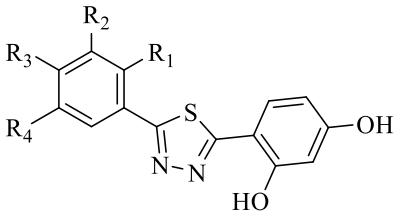

Figure 2.28. *4-(5-(2,3,4,5-Substituted phenyl)-1,3,4-thiadiazol-2-yl)benzene-1,3-diol derivatives*

Skrzypek *et al.* (2013) reported the synthesis and cholinesterase inhibitory activity of other 1,3,4-thiadiazole derivatives. Majority of the compounds significantly inhibited AChE and BChE, however, one derivative that is illustrated in **Figure 2.29** was the most potent AChE inhibitor among others with 947- times more activity against AChE than BChE making it a good candidate for selective inhibition [66].

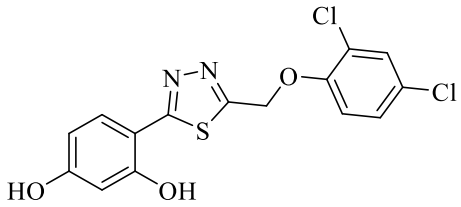

Figure 2.29. *4-(5-((2,4-Dichlorophenoxy)methyl)-1,3,4-thiadiazol-2-yl)benzene-1,3-diol*

Another study was reported by Altintop *et al.* (2014) in which *N'*-benzylidene-2-[[5-(phenylamino)-1,3,4-thiadiazol-2- yl]thio]acetohydrazide derivatives as shown in **Figure 2.30** were tested against AChE and BChE [67]. The most effective AChE inhibitors were those with *m*-methyl and *m*-methoxy substituents with 49.79 ± 3.08 and 42.39 ± 3.19 % of inhibition, respectively at a concentration of 80 μg/ml. However, the one with *m*-methoxy substituent was less toxic, thus it is considered the most promising AChE inhibitor. In addition, the compound with *m*-fluoro substituent had the highest anti-BChE activity with a % inhibition of 35.15 ± 2.21.

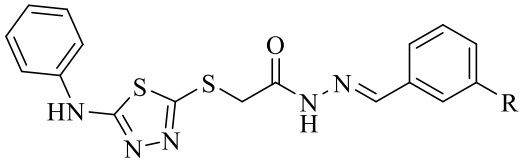

Figure 2.30. *N'-Benzylidene-2-[[5-(phenylamino)-1,3,4-thiadiazol-2- yl]thio]acetohydrazide derivatives, R= CH_3, OCH_3 for the most potent AChEI, R=F for the most potent BChEI*

Xue *et al.* (2014) synthesized and evaluated the AChE inhibitory activity of 5-substituted-1,3,4-thiadiazol-2-yl urea derivatives [68]. Many of them have good AChE inhibition activity, however, 1-(5-(4-methoxyphenyl)-1,3,4-thiadiazol-2-yl)-3-(pyridine-3-yl) urea as seen in **Figure 2.31** was the most active derivative with IC_{50}=1.17 μM that is equivalent to the inhibition activity of the reference drug galanthamine IC_{50}=1.07 μM.

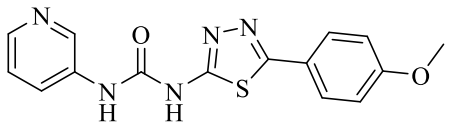

Figure 2.31. *1-(5-(4-Methoxyphenyl)-1,3,4-thiadiazol-2-yl)-3-(pyridine-3-yl) urea*

Liu *et al.* (2017) evaluated the AChE inhibitory activity of glycosyl-containing 1,2,4-triazolo[3,4-b][1,3,4]thiadiazole derivatives [69]. It was found that six out of eight derivatives have over 90 % inhibition and the one containing phenyl substituent at the third position as shown in **Figure 2.32** was the most potent against AChE with inhibition % of 97.55 at 50 μg/ml and IC_{50} value of 2.464 ± 0.522 μM.

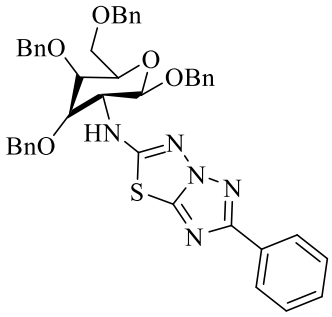

Figure 2.32. *3-Phenyl-6-(1,3,4,6-tetra-O-benzyl-2-deoxy-β-d-glucopyranose-2- yl)-[1,2,4]triazolo[3,4-b][1,3,4]thiadiazole*

Uraz *et al.* (2017) synthesized 2-methyl-3-4-[5-(substituted amino)-1,3,4-thiadiazol-2- yl]phenylquinazolin-4(3*H*)-one as shown in **Figure 2.33** and evaluated them as AChE inhibitors [70]. Compounds that are with ethylamino and cyclohexylamino substituents were the most active with inhibition % of 27.10 ± 2.51 and 25.84 ± 0.59, respectively at 1 mM concentration.

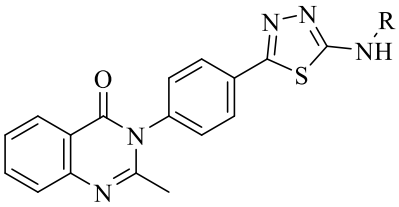

Figure 2.33. *2-Methyl-3-{4-[5-(substitutedamino)-1,3,4-thiadiazol-2-yl]phenyl}quinazolin-4(3H)-one.(R= C_2H_5, C_6H_{11} for the most active compounds)*

Ujan *et al.* (2019) investigated the acetylcholinesterase inhibitory activity of hybridized market-available drugs having a carboxylic acid group and 1,3,4-thiadiazole [71]. Compounds showed AChE inhibition activity in the nanomolar ring, however, the most active derivative as shown in **Figure 2.34** had an IC_{50} value of 18.1 nM which was

better than the reference neostigmine methyl sulfate which had an IC_{50} value of 2186.5 nM.

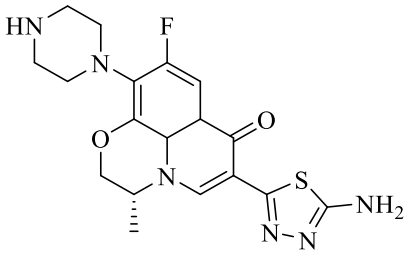

Figure 2.34. *(R)-6-(5-Amino-1,3,4-thiadiazol-2-yl)-9-fluoro-3-methyl-10-(piperazin-1-yl)-2H-[1,4]oxazino[2,3,4-ij]quinolin7(3H)-one*

Sağlik and Çevik (2019) reported the acetyl anticholinesterase activity of eight 1,3,4-thiadiazole-piperazine derivatives [72]. The most active one among compounds as shown in **Figure 2.35** has an inhibition % of 37.51±0.76 at a concentration of 10^{-3} M.

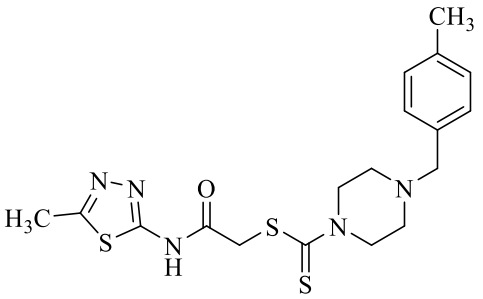

Figure 2.35. *2-((5-Methyl-1,3,4-thiadiazol-2-yl)amino)-2-oxoethyl 4-(4-methylbenzyl)piperazine-1-carbodithioate*

Derivatives of acridine having 1,3,4-thiadiazole ring structure as shown in **Figure 2.36** were synthesized and investigated for their cholinesterase inhibitory effect by Lotfi *et al.* (2020) [73]. All derivatives showed significant inhibition effects toward both AChE and BChE with more selectivity toward AChE. Two derivatives coded as **4i** (IC_{50} = 0.002 μM) and **4d** (IC_{50} =0.006 μM) were the most potent against AChE with respective 8- and 2.6-folds better activity than the reference compound tacrine (IC_{50} = 0.016 μM), they were also the most active inhibitors against BChE. Both compounds **4i** and **4d** have lower hepatotoxicity than tacrine. Also, two other derivatives coded as **4j** (IC_{50} =0.018 μM) and **4k** (IC_{50} =0.017 μM) demonstrated AChE inhibitory efficacy comparable to tacrine.

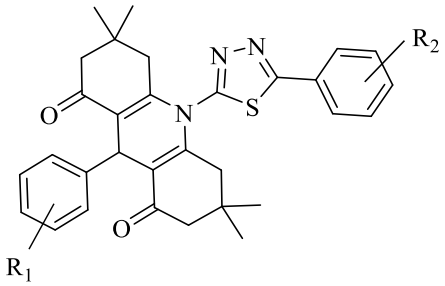

Figure 2.36. *Acridine-1,3,4-thiadiazole derivatives. (R_1= 2,4-diCl, R_2=4-Cl for 4d, R_1, R_2=4-NO_2 for 4i, R_1=H, R_2= 3-NO_2 for 4j, R_1= 3-OCH_3, R_2=3-Cl for 4k)*

Skrzypek *et al.* (2020) worked on the anticholinesterase activity of novel 1,3,4-thiadiazole-resorcinol conjugates [74]. Most compounds had moderate to high inhibitory activity, especially toward AChE, however, alkylamine and halogenophenylamine derivatives were the most promising ones. The butylamine derivative shown in **Figure 2.37** was the most potent one against both AChE and BChE with IC_{50} of 0.029 ± 0.005 μM and 1.731 ± 0.013 μM, respectively.

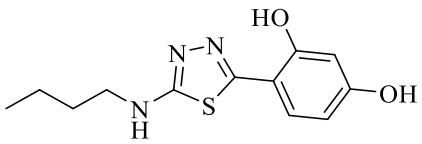

Figure 2.37. *4-(5-(Butylamino)-1,3,4-thiadiazol-2- yl)benzene-1,3-diol*

The acetylcholinesterase inhibition activity of coumarin-1,3,4-thiadiazole hybrids and their corresponding Cu(II) and Zn(II) complexes was reported by Karcz *et al.* (2021). All compounds were moderately active, however, derivatives with an amido substituent and its corresponding Cu(II) and Zn(II) complexes as shown in **Figure 2.38** were the most potent ones among others with IC_{50} of 0.181 μM, 0.174 μM and 0.184 μM, respectively [75].

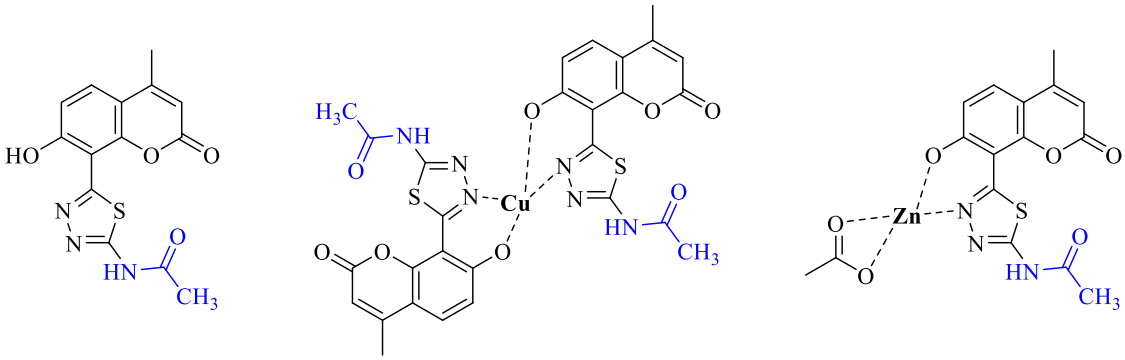

Figure 2.38. *Coumarin-1,3,4-thiadiazole derivatives hybrids and their Cu(II) and Zn(II) complexes*

2.1.3.2. Literature review of 1,3,4-thiadiazole derivatives with monoamine oxidase inhibition activity

Abdelhafez *et al.* (2012) reported the synthesis of 4-methyl and 3,4-dimethyl-7-oxycoumarin derivatives containing different five-membered heterocyclic rings. All compounds showed significant potency and selectivity toward *h*MAO-A at subnanomolar concentrations while their activity against *h*MAO-B were more than that of selegiline at submicromolar concentrations. Remarkably, among other heterocyclic rings the derivative which contains diethylaminoethylthio-1,3,4- thiadiazole (**Figure 2.39**) was the most active one with K_i values of 5.18 pM and 0.496 μM against *h*MAO-A and *h*MAO-B, respectively [76].

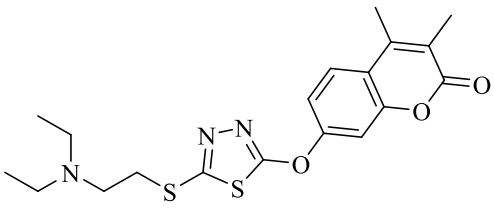

Figure 2.39. *7-[(5-[(2-(Diethylamino)ethyl)thio]-1,3,4-thiadiazol-2-yl)oxy]-3,4-dimethyl-2H-chromen-2-one*

Wang *et al.* (2019) reported novel C_7-substituted coumarin derivatives. Those with the 1,3,4-thiadiazole ring at C_7 were within this series as shown in **Figure 2.40**. However, the compound with two additional methyl groups at C_7 and C_8 of coumarin was the most potent *h*MAO-A inhibitor with an IC_{50} value of 0.019 μM while the one with a propyl

group at C_4 of coumarin was the most potent *h*MAO-B inhibitor with IC_{50} value of 0.01 μM [77].

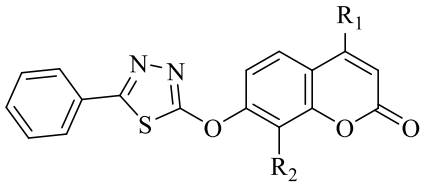

R_1=H, R_2= $(CH_2)_2CH_3$ for the most active *h*MAO-B inhibitor
R_1, R_2= CH_3 for the most active *h*MAO-A inhibitor

Figure 2.40. *Novel C_7-substituted coumarin derivatives*

Sağlık *et al.* (2020) reported the synthesis and MAO inhibitory activity of novel 1,3,4-thiadiazole derivatives with different alkyl/arylamine substituents. All compounds displayed more efficacy against *h*MAO-A than *h*MAO-B with IC_{50} values that were lower than the standard drug moclobemide (IC_{50} = 4.664 μM) for most of the compounds, however the derivative seen in **Figure 2.41** was the most potent MAO-A inhibitor with IC_{50} = 0.060 μM [78].

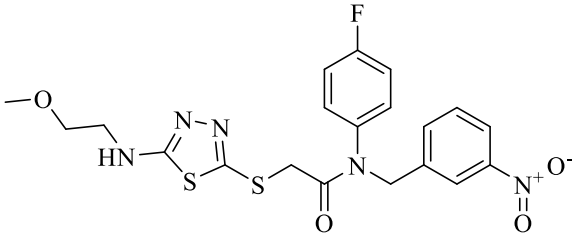

Figure 2.41. *N-(4-Fluorophenyl)-2-[(5-((methoxyethyl)amino)-1,3,4-thiadiazol-2-yl)thio]-N-(3-nitrobenzyl)acetamide*

Bekircan *et al.* (2021) reported the synthesis and inhibition activity against MAOs of 3,5-diphenyl-1,2,4-triazole substituted [1,2,4]triazolo[3,4-b] [1,3,4]thiadiazole derivatives [79]. All compounds showed inhibitory effect on both *h*MAO-A and *h*MAO-B to some extent, however they were more selective toward *h*-MAO-B. Among these compounds, [1,2,4]triazolo[3,4-b] [1,3,4]thiadiazole-6-amine derivatives with Cl, Br, F and CF_3 groups at C_4 of phenyl (**Figure 2.42**) displayed the most potent inhibition effect toward *h*MAO-B with IC_{50} values in the range of 2.51-3.55 μM.

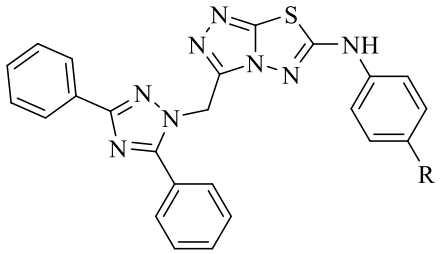

Figure 2.42. *[1,2,4]Triazolo[3,4-b] [1,3,4]thiadiazole-6-amine derivatives*

2.2. Adamantane

2.2.1. Chemistry

Adamantane is the common name for a cage-like, rigid, and unstrained symmetrical three-fused chair conformation of cyclohexanes (**Figure 2.43**) with the chemical formula of $C_{10}H_{16}$. Tricyclo[3.3.1.1^{3,7}]decane is the systematic name for adamantane according to the International Union of Pure and Applied Chemistry (IUPAC). It has a white crystalline appearance with a camphor-like odor. Its structure is characterized by atypical physiochemical properties including a high melting point of 269 ˚C which is considered unusual for a hydrocarbon, ease of sublimation and good solubility in organic solvents but not in water [80, 81].

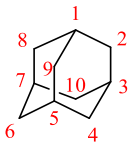

Figure 2.43. *Structure of adamantane*

Adamantane was first presented in 1924 as tricyclic decaterpene by H. Decker [82]. In 1933, it was isolated from petroleum using fractional distillation by Landa and given the name adamantane from the Greek word “ adamantinos” which refers to the diamond-like structure [83]. The first successful synthesis of adamantane was reported in 1941 by Prelog [84, 85]. However, Schleyer introduced a more convenient method to synthesize adamantane in 1956 via Lewis-acid induced rearrangement of $C_{10}H_{16}$ precursor tetrahydodicyclopentadiene [86].

2.2.2. Pharmacological profile

The first detected activity for adamantane was the antiviral activity of amantadine (1-aminoadamantane) in the 1960s, however, adamantane derivatives were also found to have other pharmacological activities with many clinical available drugs containing this moiety in their scaffold (**Figure 2.44**) including the previously mentioned amantadine as antiviral and antiparkinsonian agent, rimantadine, tromantadine and adapromine as antiviral agents, memantine as NMDA receptor antagonist in AD, saxagliptin and vildagliptin as antidiabetic II agents and adapalene as acne vulgaris treatment [87-89].

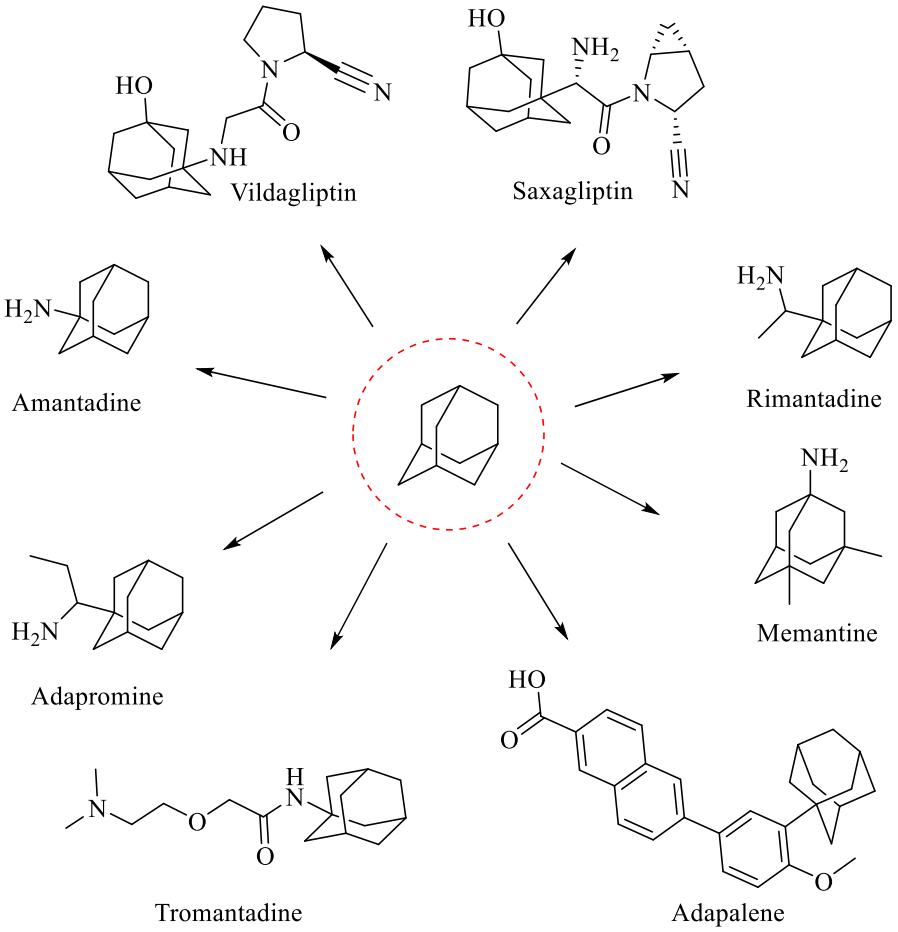

Figure 2.44. *Clinically available drugs containing adamantane scaffold*

2.2.2.1. Literature review of adamantane derivatives with anticholinesterase inhibition activity

The synthesis and BChE inhibitory activity of adamantane-substituted guanylhydrazones derivatives by determining the enzyme-inhibitor dissociation constants K_i for the catalytic and peripheral active sites were reported by Šekutor *et al.* (2012). Both derivatives 2-(*N*-guanidino)iminoadamantane hydrochloride and 2,4-bis(*N*,*N'*-guanidino)iminoadamantane dihydrochloride as shown in **Figure 2.45-a** and **b**, respectively, were the best BChE inhibitors with five times decreased affinity for the peripheral active site [90].

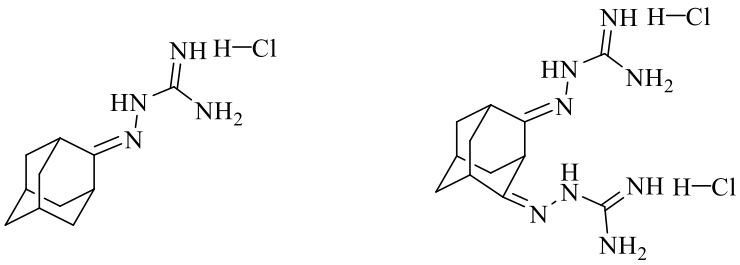

Figure 2.45. *Adamantane-substituted guanylhydrazones derivatives*

Simoni *et al.* (2012) reported the synthesis of linked galantamine-memantine derivatives and evaluated them as multitarget ligands for AD [91]. The synthesized hybrids displayed significant AChE inhibition activity with IC_{50} = 0.52 nM for the most active one shown in **Figure 2.46**.

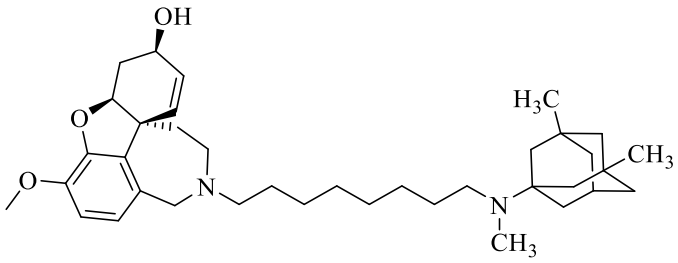

Figure 2.46. *Galantamine-memantine linked derivatives*

AL-Aboudi *et al.* (2015) synthesized and tested twenty-eight hydrazide hybrids of adamantane for anticholinesterase activity [92]. All derivatives were inactive against

AChE except for adamantane-1-carboxylic acid hydrazide (**Figure 2.47-a**) which was a moderate AChE inhibitor. In contrast, several derivatives were more active toward BChE with two derivatives that are methyl adamantane-1-carboxylate (**Figure 2.47-b**) and *N*-4-hydroxybenzylidene-1-adamantylcarbohydrazide (**Figure 2.47-c**) were the most potent BChE inhibitors with nearly similar IC_{50} of 8.65 μM and 8.80 μM, respectively.

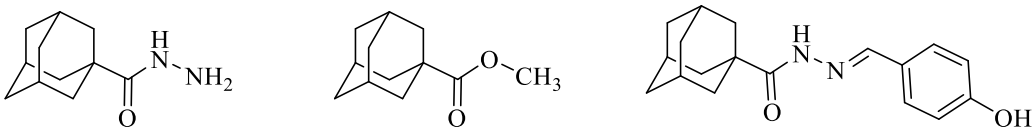

(a) **(b)** **(c)**

Figure 2.47. *Hydrazide-adamantane hybrids*

Gazova *et al.* (2016) reported the synthesis of 7-methoxytacrine-adamantylamine heterodimers and tested their multitargeted activity for AD. All the tested compounds were more effective against AChE and BChE than the used reference 7-methoxytacrine with micromolar and submicromolar inhibition concentrations. Among derivatives, the compound with five carbon spacer and thiourea as shown in **Figure 2.48** was the most potent against both AChE and BChE with IC_{50} values of 0.47 μM and 0.11 μM, respectively [93].

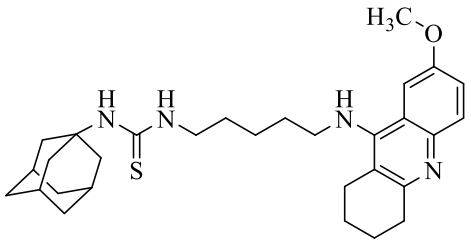

Figure 2.48. *7-Methoxytacrine-adamantylamine heterodimer*

Kwong *et al.* (2017) synthesized and tested eighteen adamantyl-based ester compounds for anticholinesterase activity [94]. Among synthesized compounds, the one with 2,4-dichlorophenyl substituent was the most active AChE inhibitor while the one with 3-methoxyphenyl moiety was the most active BChE inhibitor as shown in **Figure 2.49**.

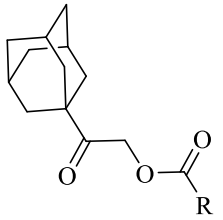

Figure 2.49. *Adamantyl-based ester derivatives. (R=2,4-dichlorophenyl for the most active AChEI, R= 3-methoxyphenyl for the most active BChEI)*

Ocheretniuk *et al.* (2017) investigated the cholinesterase inhibition effect of adamantyl-containing 5-substituted *N*-benzyl and *N*-phenacylthiazolium salts. Compounds were more selective toward BChE with micromolar inhibition concentrations compared to their effect on AChE. Derivative shown in **Figure 2.50** was the most potent against BChE with IC_{50} = 0.42 μM [95].

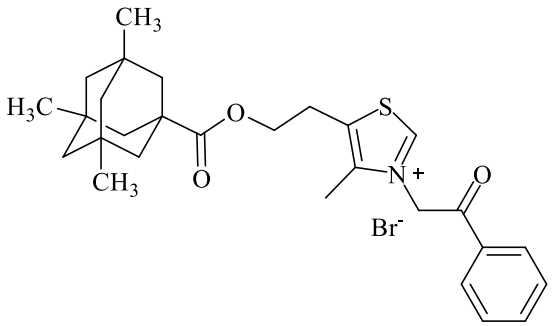

Figure 2.50. *4-Methyl-3-(2-oxo-2-phenylethyl)-5-{2-[(3,5,7- trimethyl-1-adamantyl)carbonyloxy]ethyl}-1,3- thiazolium bromide*

Bachurin *et al.* (2017) investigated a series of carbazoles/tetrahydrocarbazoles and aminoadamantane conjugates as multifunctional ligands for AD [96]. Tested compounds were selective toward BChE and blocked them in micromolar concentrations, however they were weak AChE inhibitors. The derivative with 6-fluorotetrahydrocarbazole and 3,5-dimethyladamantane moieties as shown in **Figure 2.51** was the most potent against BChE with IC_{50} = 5.43 μM.

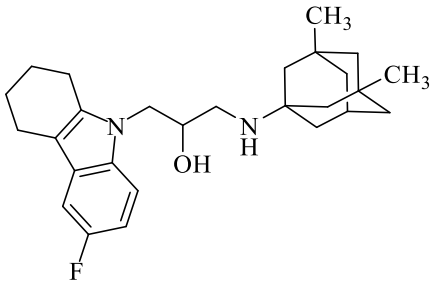

Figure 2.51. *Tetrahydrocarbazoles-aminoadamantane conjugate*

Aminoadamantane-carbazole conjugates linked by different spacers were investigated as multitarget agents for AD by Makhaeva *et al.* (2018). All synthesized compounds were weak inhibitors for AChE. In contrast, their BChE inhibition depends on the spacer structure. With an IC_{50} of 0.74 μM, the one containing the flexible spacer ethylene as shown in **Figure 2.52** was the most potent against BChE [97].

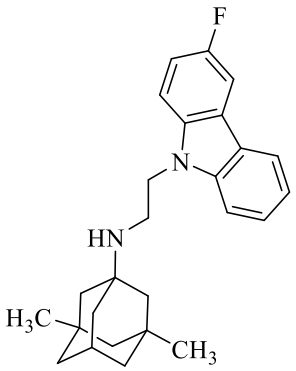

Figure 2.52. *N-(2-(6-fluoro-9H-carbazol-9-yl)ethyl)-3,5-dimethyladamantan-1-amine*

Perez-Areales *et al.* (2019) synthesized derivatives of benzohomoadamantane-chlorotacrine hybrids as shown in **Figure 2.53** and evaluated them as multitarget agents for AD [98]. They showed nanomolar to submicromolar inhibition against *h*AChE and *h*BChE, however, all hybrids were 6-44 times more potent against *h*AChE than the used reference 6-Chlorotacrine. In contrast, some hybrids were more potent against *h*BChE with IC_{50} = 0.02 μM for the most potent one compared to IC_{50} = 0.5 μM for 6-chlorotacrine.

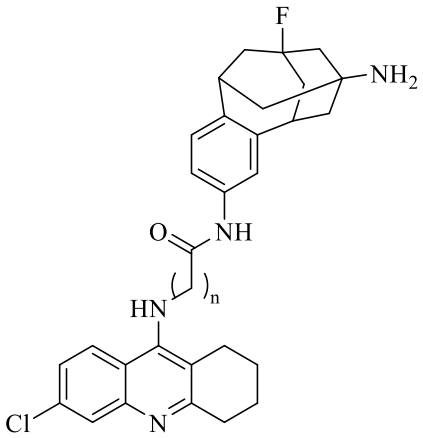

Figure 2.53. *Benzohomoadamantane- chlorotacrine hybrid derivatives (n=3 for the most potent hAChEI, n=4 for the most potent hBChEI)*

In a study conducted by Bosak et al (2019), 4-aminoquinolines derivatives were synthesized and investigated as *h*AChE and *h*BChE. However, the derivative with adamantyl group substituent as seen in **Figure 2.54** was one of the derivatives with the highest affinity for both *h*AChE and *h*BChE with K_i values = 0.77 μM and 3.2 μM, respectively indicating that bulkiness and lipophilicity play important roles in providing high anticholinesterase activity [99].

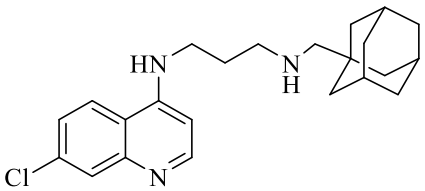

Figure 2.54. *N-(3-{[(adamantan-1-yl)methyl]amino}propyl)-7-chloroquinolin-4-amine*

A series of aminoadamantane and γ-carboline conjugates were synthesized and evaluated as multifunctional ligands for AD by Bachurin *et al.* (2021). Compounds showed inhibition activity against both AChE and BChE, however their ability to inhibit BChE is much stronger with two among them coded as **4a** and **4c** as shown in **Figure 2.55** were the most active BChE inhibitors with IC_{50} = 0.666 μM and IC_{50} = 0.729 μM, respectively. The structure of the spacer was observed to affect the inhibitory activity, with conjugates containing an ethylene spacer being substantial BChE inhibitors, moderate AChE inhibitors, and interacted with AChE's catalytic and peripheral anionic sites, thus they can inhibit AChE-induced β-amyloid aggregation [100].

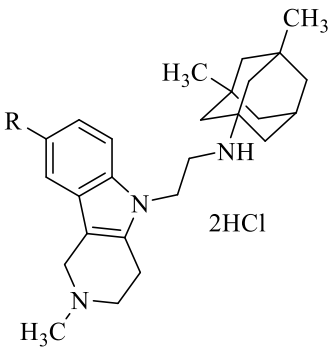

Figure 2.55. *Aminoadamantane and γ-carboline derivatives (R=H for **4a**, R=F for **4c**)*

2.2.2.2. Literature review of adamantane derivatives with monoamine oxidase inhibition activity

Zindo *et al.* (2014) synthesized polycyclic propargylamine and acetylene derivatives and tested their multitargeted neuroprotective activities including their activity against MAO-B. Amantadine-propargylamine hybrids were among the synthesized compounds with *N*,*N*-dipropargyl-adamantan-1-amine (**Figure 2.56-a**) and *N*-propargyl-*N*-benzyl-adamantan-1-amine (**Figure 2.56-b**) showed 14 and 20.13 inhibition % against MAO-B at 300 μM, respectively [101].

(a) **(b)**

Figure 2.56. *Amantadine-propargylamine hybrids*

3. MATERIALS

3.1. Chemicals

1- Ethylpiperazine	: Sigma-Aldrich, Germany
1- Methylpiperazine	: Sigma-Aldrich, Germany
1- Phenylpiperazine	: Acros Organics, USA
1-(2-Dimethylamino)ethylpiperazine	: Acros Organics, USA
1-(2-Furoyl)piperazine	: Sigma-Aldrich, Germany
1-(2-Pyridyl)piperazine	: Sigma-Aldrich, Germany
1-(2-Pyrimidyl)piperazine	: Sigma-Aldrich, Germany
1-Adamantane carboxylic acid	: Sigma-Aldrich, Germany
2-Chloropropionyl chloride	: Merck, Germany
5,5-Dithiobis(2-nitrobenzoic acid) (DTNB)	: Sigma-Aldrich, Germany
Acetonitrile	: Sigma-Aldrich, Germany
Acetylthiocholine iodide (ATC)	: Fluka, Germany
AChE-E.C.3.1.1.7, electric eel	: Sigma-Aldrich, Germany
Ampliflu™ Red (10-Acetyl-3,7-dihydroxyphenoxazine)	: Sigma-Aldrich, Germany
BChE-E.C. 3.1.1.8, equine serum	: Sigma-Aldrich, Germany
Butyrylthiocholine iodide (BTC)	: Fluka, Germany
Chloroacetyl chloride	: Merck, Germany
Deuterated chloroform ($CDCl_3$)	: Merck, Germany
Deuterated dimethyl sulfoxide (DMSO-d_6)	: Merck, Germany
Dimethylsulfoxide (DMSO)	: Merck, Germany
Donepezil	: Sigma-Aldrich, Germany
Ethanol	: Merck, Germany

Ethyl acetate	: Merck, Germany
Gelatin	: Merck, Germany
*h*MAO-A	: Sigma-Aldrich, Germany
*h*MAO-B	: Sigma-Aldrich, Germany
Horseradish peroxidase	: Sigma-Aldrich, Germany
Hydrogen peroxide (H_2O_2)	: Sigma-Aldrich, Germany
Methanol	: Sigma-Aldrich, Germany
Moclobemide	: Sigma-Aldrich, Germany
Morpholine	: Merck, Germany
N,*N*-Dimethylformamide (DMF)	: Sigma-Aldrich, Germany
Petroleum ether	: Sigma-Aldrich, Germany
Phosphoryl chloride	: Merck, Germany
Piperidine	: Sigma-Aldrich, Germany
Potassium carbonate (K_2CO_3)	: Sigma-Aldrich, Germany
Potassium dihydrogen phosphate	: Merck, Germany
Potassium hydroxide (KOH)	: Sigma-Aldrich, Germany
Pyrrolidine	: Merck, Germany
Selegiline	: Sigma-Aldrich, Germany
Silica gel 60 F_{254} aluminum sheets	: Merck, Germany
Sodium bicarbonate ($NaHCO_3$)	: Merck, Germany
Sodium hydroxide (NaOH)	: Sigma-Aldrich, Germany
Tacrine	: Sigma-Aldrich, Germany
Tetrahydrofuran (THF)	: Sigma-Aldrich, Germany
Thiomorpholine	: Acros Organics, USA
Thiosemicarbazide	: Sigma-Aldrich, Germany

Triethylamine	: Sigma-Aldrich, Germany
Tyramine hydrochloride	: Sigma-Aldrich, Germany

3.2. Instruments and Tools

Electronic balance	: Shimadzu, Libror EB-330 HU, Japan
Incubator	: Heraeus, Germany
Infrared spectrophotometer	: Shimadzu-IR Affinity-1S, Japan
Magnetic stirrer hotplate	: Heidolph, MR 3003, Germany
Mass spectrophotometer	: Shimadzu, LCMS-IT-TOF, Japan
Melting point system	: Mettler Toledo-MP90 Melting Point System, USA
Microplate Reader	: BioTek-Synergy H1, USA
Nuclear magnetic resonance spectrometry	: Bruker, UltraShield 300 MHz, USA
Robotic pipetting table	: Biotek Precision XS robotic, USA
Sterile cabinet	: Class II TypeA2 (CHC-222A2-60), : South Korea
Ultraviolet lamp	: Camag, Switzerland
Vortex	: Wisemix, Korea

4. METHODOLOGY

4.1. Synthetic Methods

4.1.1. Method A: Synthesis of 5-(adamantan-1-yl)-1,3,4-thiadiazol-2-amine (1)

To a round bottom flask, equimolar amounts of 1-adamantane carboxylic acid (61.03 mmol, 11g) and thiosemicarbazide (61.03mmol, 5.56g) were first refluxed at 75-80 ˚C in phosphoryl chloride $POCl_3$ (40 ml) for half an hour. After cooling the reaction mixture in an ice bath, cold distilled water (31 ml) was added cautiously drop by drop and left for 15 minutes. Then, the reaction mixture was further refluxed for 4-5 hours. The mixture was cooled before being poured into iced water and neutralized with 2N NaOH until a pH of nearly 8 was reached (**Figure 4.1**). The precipitated product was filtered and recrystallized from ethanol [46, 102, 103].

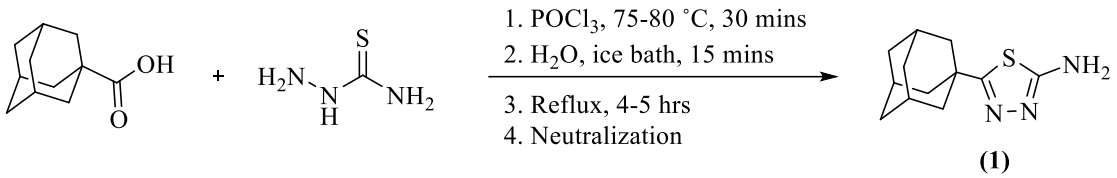

Figure 4.1. *Synthesis of 5-(adamantan-1-yl)-1,3,4-thiadiazol-2-amine (Method A)*

4.1.2. Method B: Synthesis of *N*-(5-(adamantan-1-yl)-1,3,4-thiadiazol-2-yl)-2-chloroacetamide (2a)

Solution of chloroacetyl chloride in THF (30.6 mmol, 2.4 ml) was added drop by drop to a stirred solution of 5-(adamantan-1-yl)-1,3,4-thiadiazol-2-amine **(1)** (25.49 mmol, 6g) and TEA as a catalyst (30.6 mmol, 4.3 ml) in THF for 3-4 hours at 0-5 C˚ (**Figure 4.2**). The solvent THF was evaporated after the reaction was completed, and the residue was washed with water. The product was filtered and recrystallized from ethanol.

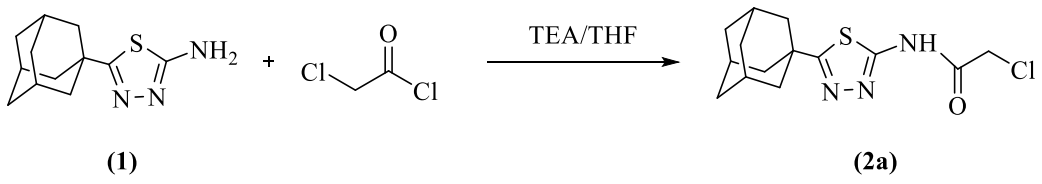

Figure 4.2. *Synthesis of N-(5-(adamantan-1-yl)-1,3,4-thiadiazol-2-yl)-2-chloroacetamide (Method B)*

4.1.3. Method C: Synthesis of *N*-(5-(adamantan-1-yl)-1,3,4-thiadiazol-2-yl)-2-chloropropanamide (2b)

Solution of 2-chloropropionyl chloride (30.6 mmol, 2.9 ml) in THF was added drop by drop to a stirred solution of 5-(adamantan-1-yl)-1,3,4-thiadiazol-2-amine **(1)** (25.49 mmol, 6g) and TEA as a catalyst (30.6 mmol, 4.3 ml) in THF for 3-4 hours at 0-5 ˚C (**Figure 4.3**). The solvent THF was evaporated after the reaction was completed, and the residue was washed with water. The product was filtered and recrystallized from ethanol.

(1) **(2b)**

Figure 4.3. *Synthesis of N-(5-(adamantan-1-yl)-1,3,4-thiadiazol-2-yl)-2-chloropropanamide (Method C)*

4.1.4. Method D: Synthesis of *N*-(5-(adamantan-1-yl)-1,3,4-thiadiazol-2-yl)-2-substituted-acetamide derivatives (3a-3j)

Equimolar amounts of an appropriate cyclic secondary amine (1.28 mmol) and *N*-(5-(adamantan-1-yl)-1,3,4-thiadiazol-2-yl)-2-chloroacetamide **(2a)** (1.28 mmol, 0.4g) were reacted in THF as solvent and TEA (1.54 mmol, 0.21 ml) as catalyst at room temperature (R.T) for 12-24 hours (**Figure 4.4**). The reaction was controlled by using TLC and THF was evaporated after the reaction was completed. Solid residues were washed with water, filtered, and recrystallized from ethanol.

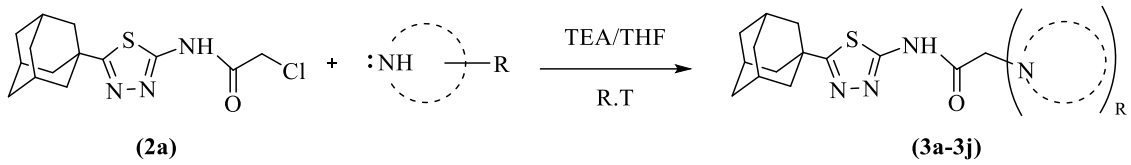

(2a) **(3a-3j)**

Figure 4.4. *Synthesis of N-(5-(adamantan-1-yl)-1,3,4-thiadiazol-2-yl)-2-substituted-acetamide derivatives (Method D)*

4.1.5. Method E: Synthesis of *N*-(5-(adamantan-1-yl)-1,3,4-thiadiazol-2-yl)-2-substituted-propanamide derivatives (4a-4g)

Equimolar amounts of an appropriate cyclic secondary amine (1.23 mmole) and *N*-(5-(adamantan-1-yl)-1,3,4-thiadiazol-2-yl)-2-chloropropanamide **(2b)** (1.23 mmole, 0.4g) were refluxed in ACN as solvent and K_2CO_3 (2.46 mmol, 0.34 g) as catalyst for 12-24 hours (**Figure 4.5**). The reaction was controlled by using TLC and ACN was evaporated after the reaction was completed. Solid residues were washed with water, filtered, and recrystallized from ethanol while liquid residue was extracted using ethyl acetate.

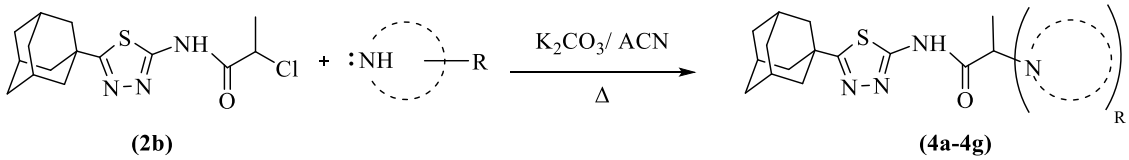

Figure 4.5. *Synthesis of N-(5-(adamantan-1-yl)-1,3,4-thiadiazol-2-yl)-2-substituted-propanamide derivatives (Method E)*

4.2. Thin Layer Chromatography (TLC) Studies

All the synthetic reactions within this thesis were monitored using TLC techniques. Aluminum sheets covered with silica gel 60 F_{254} were used as the stationary phase while ethanol, mixtures of petroleum ether and ethyl acetate in ratios of 1:1 and 3:1 were used as the mobile phase from the more polar to the less polar, respectively. Samples from the reaction medium that were taken at a certain time interval and from the corresponding starting materials were diluted in ethanol or DMF, spotted using capillary tubes onto one end of the plaque and placed vertically into a closed chamber containing the appropriate mobile phase. Ultraviolet light (UV) at 254 nm and 366 nm was used to visualize TLC plates. Based on their polarity, sample components migrate over different distances, resulting in separated spots and different retention factors R_f, allowing for reaction control.

4.3. Melting Points Determination

Melting points of the synthesized final products and intermediate products were measured by using the Mettler Toledo-MP90 Melting Point System. Small amounts of

the synthesized compounds were filled into capillary tubes which were sealed at one end by burning and placed in the chambers of the device. The melting points were determined after the process was completed by watching the recorded videos taken from the device.

4.4. Chemical Spectral Analysis

4.4.1. Infra-red spectrometry (IR)

IR spectra of the final synthesized compounds were recorded using the Shimadzu-IR Affinity-IS instrument. Spectra were obtained by applying compounds into the attenuated total reflection (ATR) chamber. The spectra were plotted as wave number cm^{-1} against transmittance % and peaks were detected automatically.

4.4.2. Proton nuclear magnetic resonance spectrometry (^{1}H-NMR)

The ^{1}H-NMR spectra of the solution of the final synthesized compounds (10 µg) dissolved in 0.5 ml of either DMSO-d_6 or $CDCl_3$ were recorded using Bruker 300 MHz and 400 MHz NMR spectrometers with tetramethylsilane (TMS) as the internal standard.

4.4.3. Carbon nuclear magnetic resonance spectrometry (^{13}C-NMR)

The ^{13}C-NMR spectra of the solution of the final synthesized compounds (10 µg) dissolved in 0.5 ml of either DMSO-d_6 or $CDCl_3$ were recorded using Bruker 75 MHz and 100 MHz NMR spectrometers with tetramethylsilane (TMS) as the internal standard.

4.4.4. High resolution- mass spectrometry (HR-MS)

Mass spectra were recorded by injecting the solution of the final synthesized compounds dissolved in acetonitrile or methanol into liquid chromatography attached to a hybrid ion-trap and time-of-flight mass spectrometry LCMS-IT-TOF (Shimadzu, Kyoto, Japan) device by using the electrospray ionization- positive ion mode technique (ESI+).

4.5. Determination of Cholinesterase Inhibitory Activity

The anticholinesterase activity of synthesized compounds against the AChE enzyme (E.C.3.1.1.7, electric eel) and the BChE enzyme (BChE-E.C.3.1.1.8, horse serum) was determined *in vitro* by using modified Ellman's method [104]. A BioTek-

Synergy H1 Microplate Reader was used to perform the spectrophotometric readings. A Biotek Precision XS robotic system was used in pipetting processes. All the prepared solutions were kept at -20 ˚C and delivered to R.T before the experiment.

4.5.1. Preparation of cholinesterase enzyme solution

The lyophilized AChE and BChE enzymes were dissolved separately in 1% gelatin solution to prepare 500 U/ml enzyme solutions, then 5 U/ml stock enzyme solutions were prepared by diluting 1 ml of the 500 U/ml solutions to 100 ml in water. After that, just before being used in the test, 2.5 U/ml enzyme solutions were prepared by diluting 0.7 ml of the 5 U/ml stock solutions to 1.4 ml in water.

4.5.2. Preparation of (0.075 M) substrates solution

Separate solutions of acetylthiocholine iodide (ATC) and butyrylthiocholine iodide (BTC) which are substrates for AChE and BChE, respectively were prepared by dissolving 0.217 g of ATC and 0.237 g of BTC in water and then filling the final volume up to 10 ml with water.

4.5.3. Preparation of (0.01 M) 5,5-dithiobis (2-nitrobenzoic acid) (DTNB) solution

DTNB was used as the chromogenic reagent that is responsible to produce yellow color upon reaction with thiocholines produced from substrates hydrolysis by cholinesterase enzymes. A solution at a concentration of 0.01 M was made by dissolving 0.396 g of DTNB in water, then 0.15 g of $NaHCO_3$ was added, and the final volume was filled up to 100 ml with water.

4.5.4. Preparation of phosphate buffer solution (pH = 8.0)

The buffer solution was prepared by dissolving 13.61 g of potassium dihydrogen phosphate (KH_2PO_4) in 1 L of water and adjusting its pH to 8.0 ± 0.1 using 0.1 N potassium hydroxide solution.

4.5.5. Preparation of inhibitor solutions

Solutions of the synthesized compounds (**3a**-**3j** and **4a**-**4g**), donepezil and tacrine as the reference drugs against AChE and BChE, respectively were made at initial

concentrations of 10^{-3} and 10^{-4} M in a 2 % dimethylsulfoxide DMSO aqueous solution. Solutions for donepezil, tacrine and the synthesized compounds which displayed more than 50% inhibitory activity at both initial concentrations were further prepared at lower diluted concentrations ranging from 10^{-5} M to 10^{-9} M.

4.5.6. AChE and BChE enzymatic inhibition assay

For each of the synthesized compounds and the reference drugs, phosphate buffer (140 µL/well), AChE or BChE enzyme solution (20 µL/well), inhibitor solution at the initial concentrations of 10^{-3} and 10^{-4} (20 µL/well), DTNB solution (20 µL/well) and lastly ATC or BTC solution ((10 µL/well) were all added in 96-well plates, mixed, and incubated at 25 ˚C for 15 mins. Then, absorbance measurements of the yellow-colored chromophore were recorded twice at 412 nm over 5 mins intervals. The process was also applied for a blank sample without inhibitor and substrate solution and for a negative control sample without inhibitor solution. The same procedure was repeated for 10^{-5} to 10^{-9} M diluted concentrations of the reference drugs and the synthesized compounds which displayed more than 50% inhibitory activity at the initial concentrations. The process was carried out four times for blank, control and inhibitor solutions at all concentrations.

After determining the differences between the two absorbance measurements, the inhibition % was determined by applying the following equation,

$$\frac{[(A(C)-A(B))-(A(I)-A(B))]}{(A\,(C)-A(B))}\ x\ 100 \qquad (4.1)$$

where B: blank, C: control, A(B): difference in absorbance readings of the blank sample, A(C): difference in absorbance readings of the control sample and A(I): difference in absorbance readings of the inhibitor sample.

The IC_{50} values were determined using a dose-response curve generated by plotting the inhibition % versus the log concentration by using the GraphPad 'PRISM' software (version 5.0). The data were presented as mean ± standard deviation (SD).

4.6. Determination of Monoamine Oxidase Inhibitory Activity

An *in vitro* Ampliflu™ Red-based fluorimetric method was used to evaluate the MAO inhibitory activity of the synthesized compounds against both *h*MAO-A and

*h*MAO-B. [17]. A Biotek Precision XS robotic system was used in pipetting processes. A BioTek-Synergy H1 microplate reader was utilized to monitor the produced fluorescence (excitation/ emission: 535/587 nm) with the fluorescence rising linearly for 30 minutes.

4.6.1. Preparation of MAO enzymes solutions

Enzyme solutions of recombinant *h*MAO-A and recombinant *h*MAO-B were prepared by first dissolving in phosphate buffer solution, then final volumes were set to 10 ml to get concentrations of 0.5 U/ml and 0.64 U/ml, respectively.

4.6.2. Preparation of working solution

Horseradish peroxidase (200 U/ml, 100 µl), the fluorescence reagent Ampliflu™ Red (20 mM, 200 µl) and the substrate tyramine (100 mM, 200 µl) were prepared separately by first being dissolved in phosphate buffer solution, and then the volume was set to 10 ml.

4.6.3. Preparation of inhibitor solutions

Solutions of the synthesized compounds (**3a**-**3j** and **4a**-**4g**), moclobemide and selegiline as the reference drugs against MAO-A and MAO-B, respectively were prepared at initial concentrations of 10^{-3} and 10^{-4} M in a 2 % dimethylsulfoxide DMSO aqueous solution. Further diluted solutions at lower concentrations from 10^{-5} M to 10^{-9} M were prepared for moclobemide, selegiline and the synthesized compounds which showed over 50% inhibitory activity at both initial concentrations.

4.6.4. MAO-A and MAO-B enzymatic inhibition assay

The assay detects hydrogen peroxides generated by *h*MAO-A and *h*MAO-B during the oxidation of the substrate tyramine, which react with the non-fluorescent Ampliflu™ Red agent in the availability of horseradish peroxidase to produce the fluorescent resorufin, which is then measured. The test was conducted in two steps. In the first step, a black flat-bottomed 96-well micro test plate was filled with solutions of either *h*MAO-A or *h*MAO-B (100 µL/well) and inhibitor at the initial concentrations of 10^{-3} and 10^{-4} (20 µL/well) and incubated at 37 ˚C for 30 mins. The working solution (100 µL/well) was

then added to initiate the reaction and the mixture was incubated at 37 ˚C for another 30 minutes, with the level of fluorescent resorufin measured at 5-minute intervals on the fluorescence (Ex/Em: 535/587 nm). Negative control measurements were conducted by changing the inhibitor solution with 2% DMSO (20 µL) whereas the possible inhibitory effect of each inhibitor on horseradish peroxidase was assessed by changing enzyme solutions with 3% H_2O_2 solution (20 mM 100 µL/well). The ability of the inhibitors to affect the fluorescence produced in the reaction medium due to non-enzymatic inhibition was assessed by using samples containing only working and inhibitor solutions. The background activity was evaluated using a blank sample comprising all components except the *h*MAO isoforms which were changed with phosphate buffer (100 µL /well). These background activity values were then subtracted to calculate the specific fluorescence emission value for each compound that is needed to get the results as % inhibition by using the equation below,

$$\frac{(FC_{t2} - FC_{t1}) - (FI_{t2} - FI_{t1})}{FC_{t2} - FC_{t1}} \; x \; 100 \qquad (4.2)$$

where FC_{t2}: fluorescence of the control sample measured at t_2 time, FC_{t1}: fluorescence of the control sample measured at t_1 time, FI_{t2}: fluorescence of an inhibitor sample measured at t_2 time, FI_{t1}: fluorescence of an inhibitor sample measured at t_1 time.

In the second step, the same procedure was applied for 10^{-5} to 10^{-9} M diluted concentrations of standard drugs and synthesized compounds which showed over 50% inhibition at the initial concentrations. The whole process was carried out four times for blank, control and all concentrations of inhibitors. The IC_{50} values were determined using a dose-response curve generated by plotting the inhibition % versus the log concentration by using the GraphPad 'PRISM' software (version 5.0). The data were presented as mean ± standard deviation (SD).

4.7. Molecular Docking

Molecular docking simulations were carried out for the most active AChE inhibitors (**4a**, **4b** and **3a)** and for the most active *h*MAO-B inhibitor (**4a**) to visualize the binding interactions by using the *in-silico* Schrödinger Maestro interface [105]. The Protein Data Bank server (www.rcsb.org) was used to get the X-ray crystal structures of *h*AChE (PDB ID: *4EY7*) and *h*MAO-B (PDB ID: *2V5Z*). The enzyme structure was then prepared for docking by applying the Protein Preparation Wizard protocol of the Schrödinger Suite

2020. Ligands were then prepared using the LigPrep module [106] to accurately designate the atom types and the protonation states at pH 7.4±1.0. Hydrogen atoms were inserted into the structures, and bond orders were determined. The Glide module [107] was used to generate the grid, and docking simulations were performed in standard precision docking mode.

4.8. Prediction of the Pharmacokinetic Profile

Several *in silico* approaches are available nowadays to examine compounds' physiochemical properties which give an early prediction of their absorption, distribution, metabolism, and elimination properties (ADME), hence their pharmacokinetic profile. The *in silico* theoretical calculation of ADME parameters including molecular weight (MW), the number of hydrogen bond acceptors (HBA) and donors (HBD), aqueous solubility (Log S) using the ESOL model [108]**,** octanol/water partition coefficient (MLog P), absorption from the gastrointestinal tract (GIA), in addition to the number of violations of Lipinski's rule (No.V) were estimated for donepezil and selegiline as the reference drugs and the synthesized effective compounds **3a**, **3b**, **3d**, **4a** and **4b** using SwissADME software [109, 110]. Additionally, blood-brain barrier scores (BBB scores) and drug-likeness score values (DLS) were calculated using Molsoft software [111].

5. RESULTS AND DISCUSSION

5.1. Synthesis of the Targeted Compounds

5.1.1. Synthesis of 5-(adamantan-1-yl)-1,3,4-thiadiazol-2-amine (1)

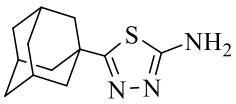

Figure 5.1. *Molecular structure of compound **(1)***

It was synthesized according to method A. Yield: 85 %. Physical appearance: white powder. Experimental m.p.: 223-224 ˚C. Literature m.p.: 200-203 ˚C [112].

5.1.2. Synthesis of *N*-(5-(adamantan-1-yl)-1,3,4-thiadiazol-2-yl)-2-chloroacetamide (2a)

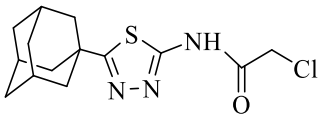

Figure 5.2. *Molecular structure of compound **(2a)***

It was synthesized according to method B. Yield: 78 %. Physical appearance: white powder. Experimental m.p.: 184-185 ˚C. Literature m.p.: 179-180 ˚C [113].

5.1.3. Synthesis of *N*-(5-(adamantan-1-yl)-1,3,4-thiadiazol-2-yl)-2-chloropropanamide (2b)

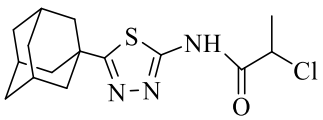

Figure 5.3. *Molecular structure of compound **(2b)***

It was synthesized according to method C. Yield: 73 %. Physical appearance: white powder. Experimental m.p.: 231-232 ˚C.

5.1.4. Synthesis of *N*-(5-(adamantan-1-yl)-1,3,4-thiadiazol-2-yl)-2-substituted-acetamide derivatives (3a-3j)

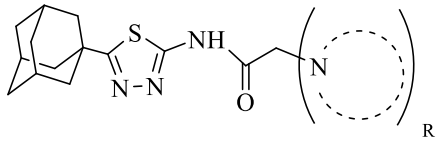

Figure 5.4. *General molecular structure of derivatives (**3a-3j**)*

5.1.4.1. N-(5-(Adamantan-1-yl)-1,3,4-thiadiazol-2-yl)-2-(4-(pyrimidin-2-yl)piperazin-1-yl)acetamide (3a)

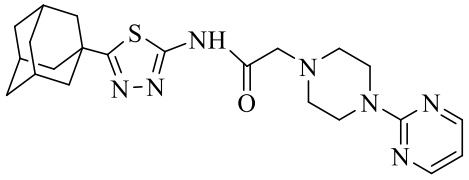

Figure 5.5. *Molecular structure of compound* ***(3a)***

It was synthesized according to method D. Yield: 96 %. Physical appearance: light creamy powder. Experimental m.p.: 195-196 ˚C.

IR (ATR) υ_{max} (cm^{-1}): 3153 (N-H stretching), 3030 (Aromatic sp^2 C-H stretching), 2926-2818 (sp^3 C-H stretching), 1695 (C=O stretching), 1583-1446 (aromatic C=C and C=N stretching), 1253 (C-N stretching).

^{1}H-NMR (300 MHz) (DMSO-*d*$_6$) δ (ppm): 1.73 (6H, s, adamantane-H), 1.99 (6H, s, adamantane-H), 2.04 (3H, s, adamantane-H), 2.55 (4H, t, *J*= 4.74 Hz, piperazine's $H_{2,6}$), 3.36 (2H, s, CO-$\underline{CH_2}$), 3.75 (4H, t, *J*= 4.56 Hz, piperazine's $H_{3,5}$), 6.60 (1H, t, *J*= 7.74 Hz, pyrimidine's H_5), 8.34 (2H, d, *J*= 4.72 Hz, pyrimidine's $H_{4,6}$), 12.21 (1H, br-s, $\underline{N\text{-}H}$).

^{13}C-NMR (75 MHz) (DMSO-*d*$_6$) δ (ppm): 28.29 (adamantane), 36.28 (adamantane), 37.66 (adamantane), 43.12 (adamantane), 43.66 (piperazine), 52.63 (piperazine), 60.47 (CO-$\underline{CH_2}$-), 110.55 (pyrimidine's C_5), 157.68 (thiadiazole), 158.37 (pyrimidyl's $C_{4,6}$), 161.6 (pyrimidine's C_2), 168.87 (thiadiazole), 174.11 (CO).

HRMS (ESI) (m/z) $[M+1]^+$: for $C_{22}H_{29}N_7OS$ calculated: 440.2227; found: 440.2209.

DOPNALAB

	Item	Value
	Acquired Date&Time	9.06.2022 13:34:46
	Acquired by	System Administrator
	Filename	C:\Users\dopnalab\Desktop\MASAÜSTÜ\LEYLA YURTDAŞ\AYL-A-B\AYL-A1.1.ispd
	Spectrum name	AYL-A1.1
	Sample name	AYL-A1
	Sample ID	
	Option	
	Comment	
	No. of Scans	15
	Resolution	4 [cm-1]
	Apodization	Happ-Genzel

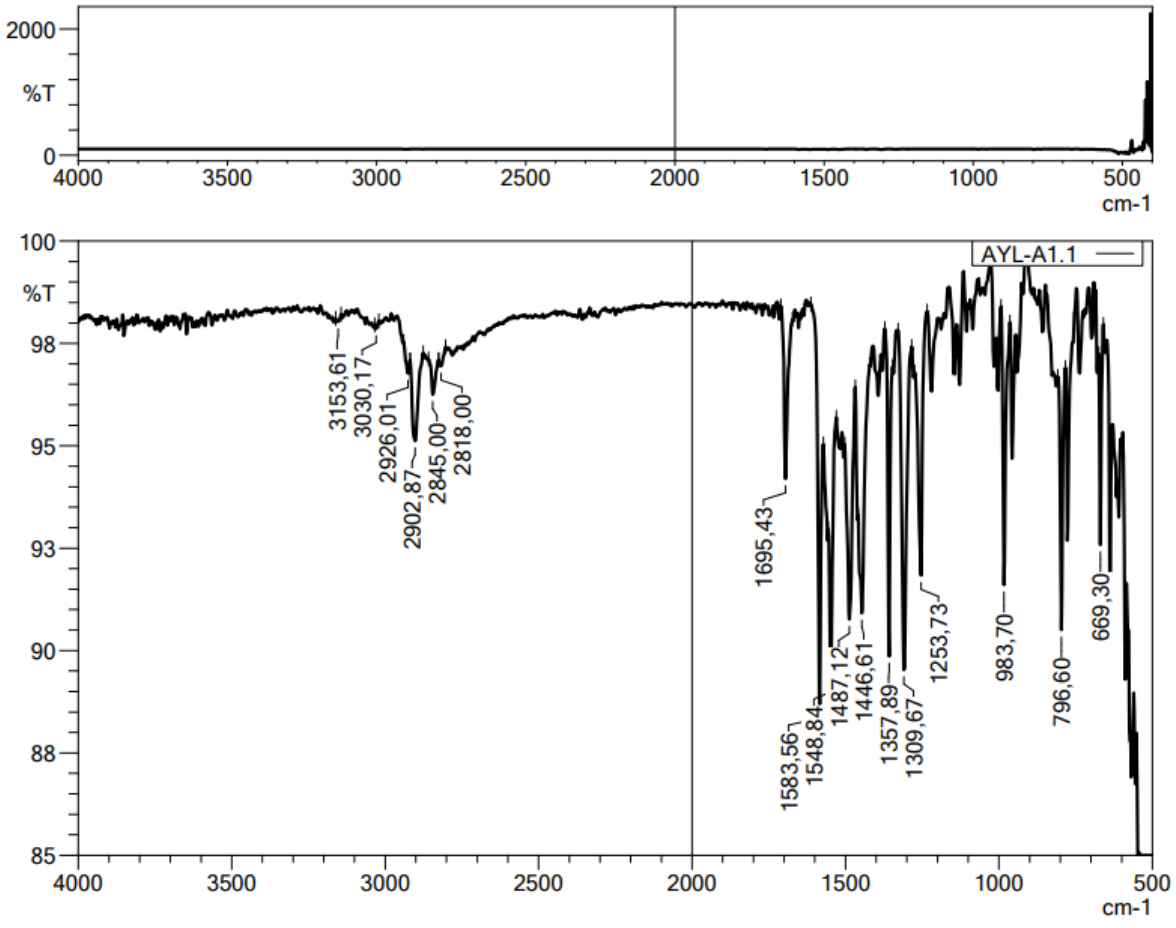

Figure 5.6. *IR spectrum of compound* ***3a***

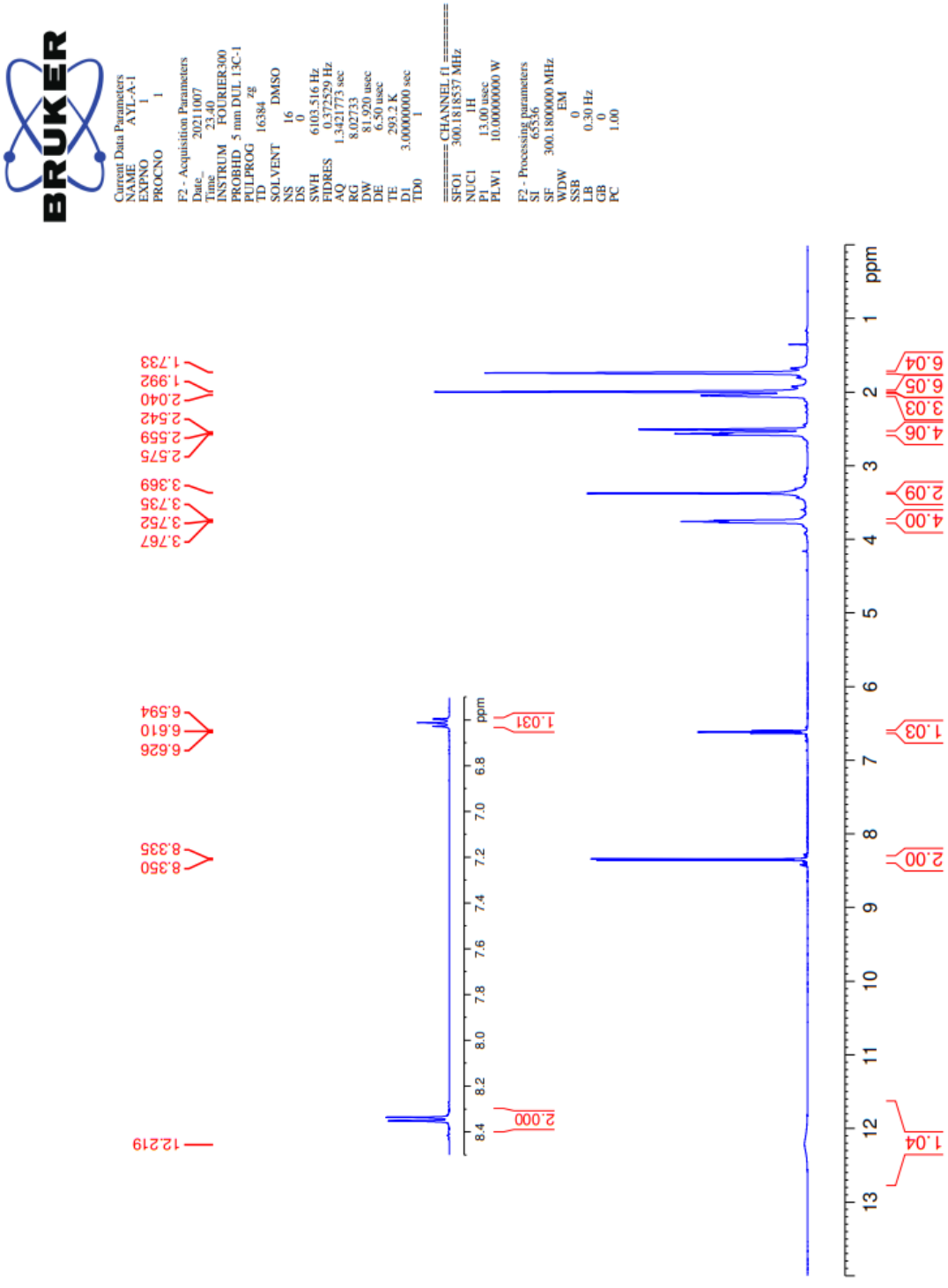

Figure 5.7. *^{1}H-NMR spectrum of compound **3a***

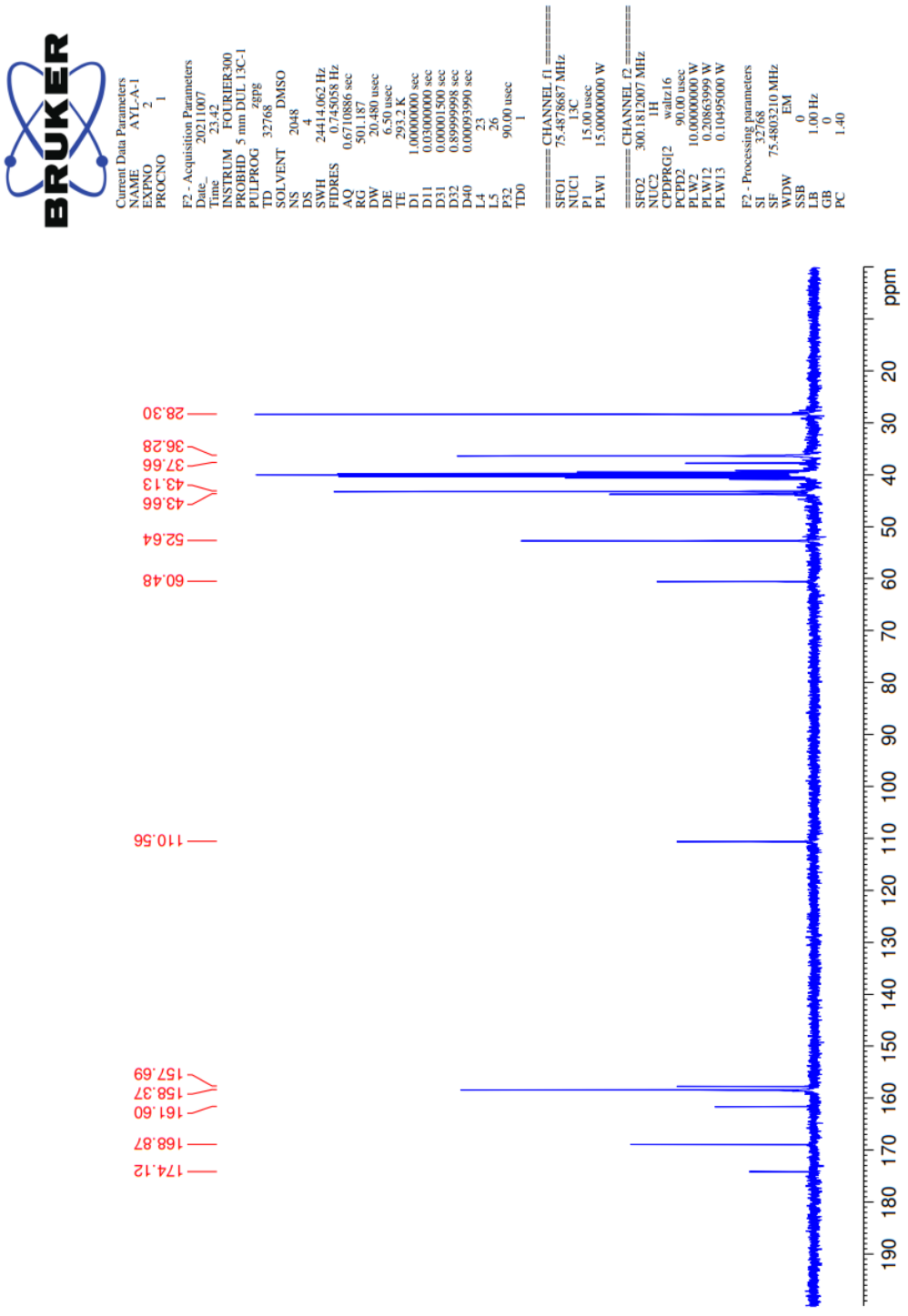

Figure 5.8. *[13]C-NMR spectrum of compound **3a***

Elmt	Val.	Min	Max	Elmt	Val.	Min	Max	Elmt	Val.	Min	Max	Elmt	Val.	Min	Max	Use Adduct
H	1	10	40	O	2	0	4	S	2	1	1	Ru	2	0	0	H
C	4	9	40	F	1	0	0	Cl	1	0	1	Pd	2	0	0	
N	3	2	10	P	3	0	0	Br	1	0	0	I	3	0	0	

Error Margin (ppm): 5
HC Ratio: unlimited
Max Isotopes: 3
MSn Iso RI (%): 10.00

DBE Range: 5.0 - 25.0
Apply N Rule: yes
Isotope RI (%): 1.00
MSn Logic Mode: AND

Electron Ions: both
Use MSn Info: yes
Isotope Res: 9000
Max Results: 150

Event#: 1 MS(E+) Ret. Time : 4.493 -> 4.493 Scan# : 675 -> 675

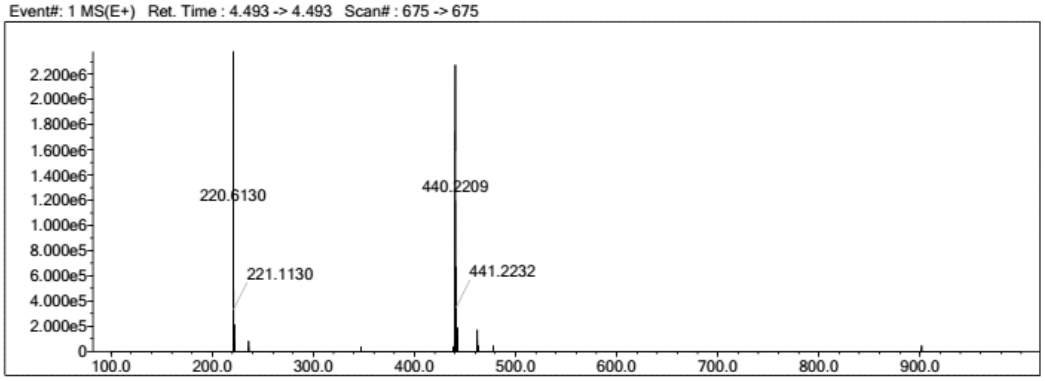

Measured region for 440.2209 m/z

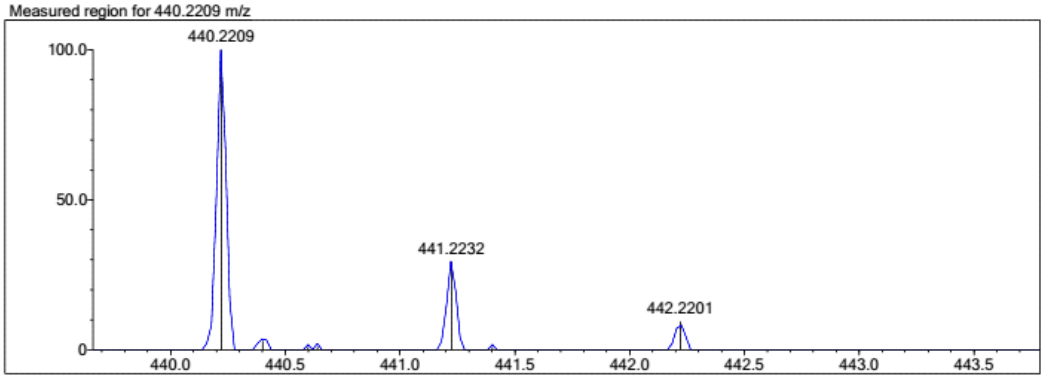

C22 H29 N7 O S [M+H]+ : Predicted region for 440.2227 m/z

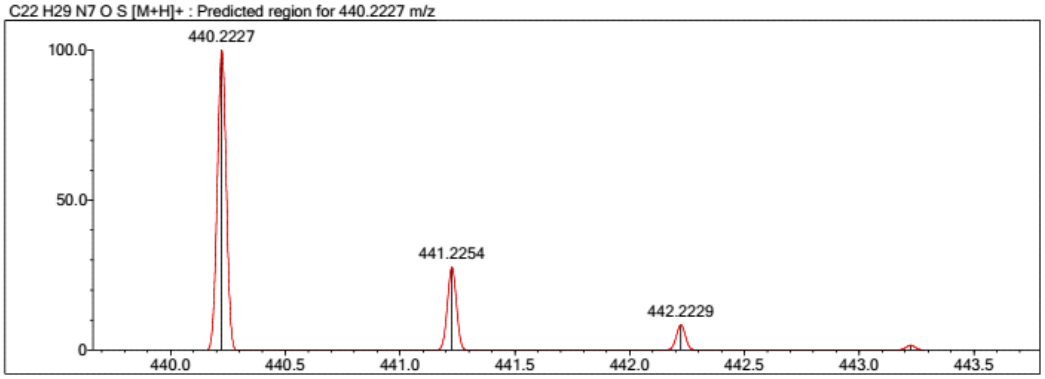

Rank	Score	Formula (M)	Ion	Meas. m/z	Pred. m/z	Df. (mDa)	Df. (ppm)	Iso	DBE
1	67.47	C22 H29 N7 O S	[M+H]+	440.2209	440.2227	-1.8	-4.09	73.12	12.0

Figure 5.9. *HR-MS of compound **3a***

5.1.4.2. N-(5-(Adamantan-1-yl)-1,3,4-thiadiazol-2-yl)-2-(4-(pyridin-2-yl)piperazin-1-yl)acetamide (3b)

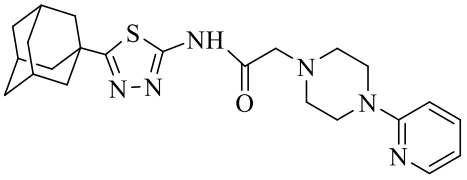

Figure 5.10. *Molecular structure of compound* ***(3b)***

It was synthesized according to method D. Yield: 81 %. Physical appearance: light creamy powder. Experimental m.p.: 172-173 ˚C.

IR (ATR) υ_{max} (cm^{-1}): 3151 (N-H stretching), 2927-2845 (sp^3 C-H stretching), 1701 (C=O stretching), 1591-1436 (aromatic C=C and C=N stretching), 1244 (C-N stretching).

^{1}H-NMR (300 MHz) (DMSO-*d*$_6$) δ (ppm): 1.73 (6H, s, adamantane-H), 1.99 (6H, s, adamantane-H), 2.04 (3H, s, adamantane-H), 2.59 (4H, br-s, piperazine's $H_{2,6}$), 3.37 (2H, s, CO-$\underline{CH_2}$), 3.5 (4H, br-s, piperazine's $H_{3,5}$), 6.62 (1H, t, *J*= 6.48 Hz, pyridine's H_5), 6.8 (1H, d, *J*= 8.58 Hz, pyridine's H_3), 7.51 (1H, t, *J*= 7.8 Hz, pyridine's H_4), 8.09 (1H, d, *J*= 4.77 Hz, pyridine's H_6), 11.25 (H, br-s, $\underline{N\text{-}H}$).

^{13}C-NMR (75 MHz) (DMSO-*d*$_6$) δ (ppm): 28.3 (adamantane), 36.28 (adamantane), 37.66 (adamantane), 43.12 (adamantane), 45.01 (piperazine), 52.64 (piperazine), 60.51 (CO-$\underline{C}H_2$-), 107.54 (pyridine's $\underline{C_3}$), 113.42 (pyridine's $\underline{C_5}$), 137.95 (pyridine's $\underline{C_4}$), 148 (pyridine's $\underline{C_6}$), 157.7 (thiadiazole), 159.41 (pyridine's $\underline{C_2}$), 168.86 (thiadiazole), 174.11 (CO).

HRMS (ESI) (m/z) $[M+1]^+$: for $C_{23}H_{30}N_6OS$ calculated: 439.2275; found: 439.2263.

DOPNALAB

	Item	Value
	Acquired Date&Time	9.06.2022 13:44:01
	Acquired by	System Administrator
	Filename	C:\Users\dopnalab\Desktop\MASAÜSTÜ\LEYLA YURTDAŞ\AYL-A-B\AYL-A2.3.ispd
	Spectrum name	AYL-A2.3
	Sample name	AYL-A2
	Sample ID	
	Option	
	Comment	
	No. of Scans	15
	Resolution	4 [cm-1]
	Apodization	Happ-Genzel

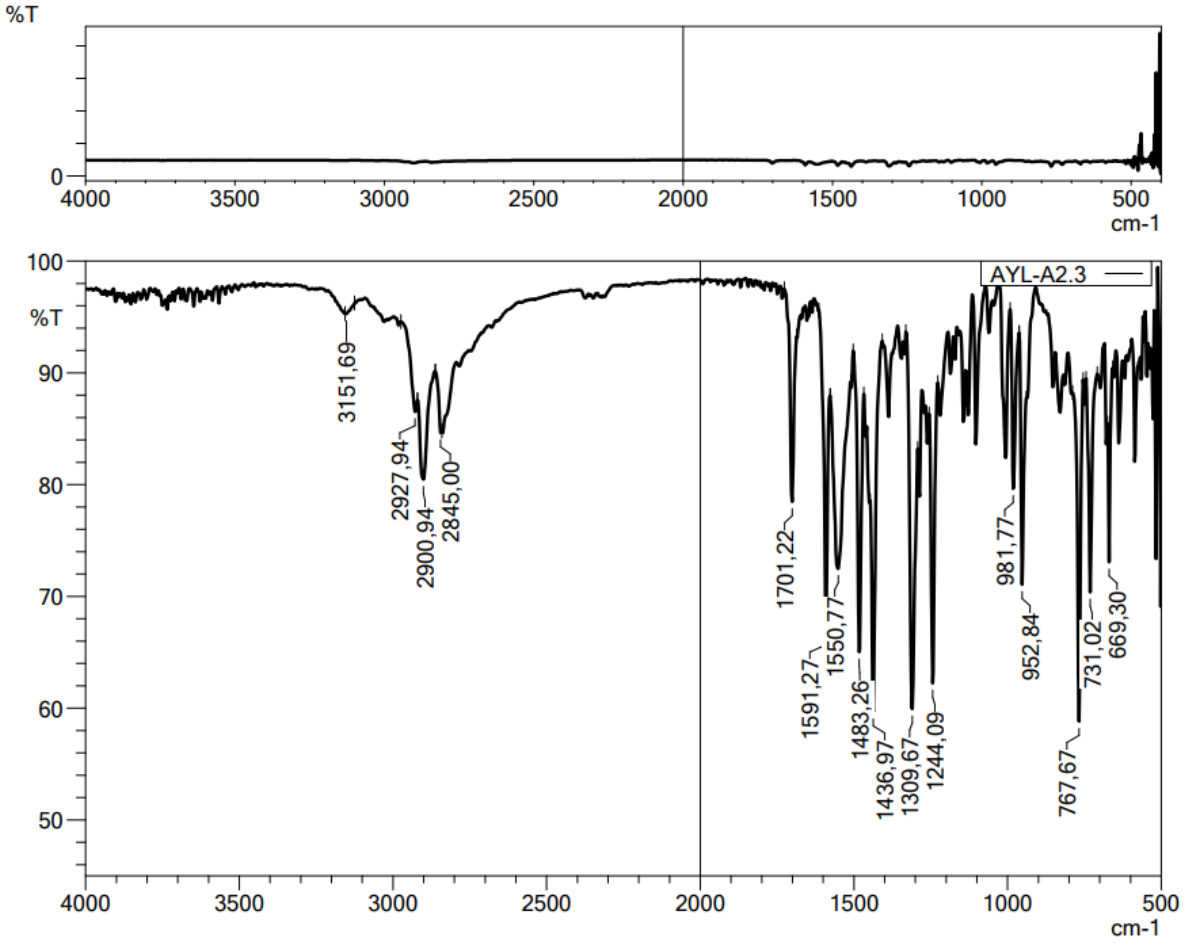

Figure 5.11. *IR spectrum of compound* **3b**

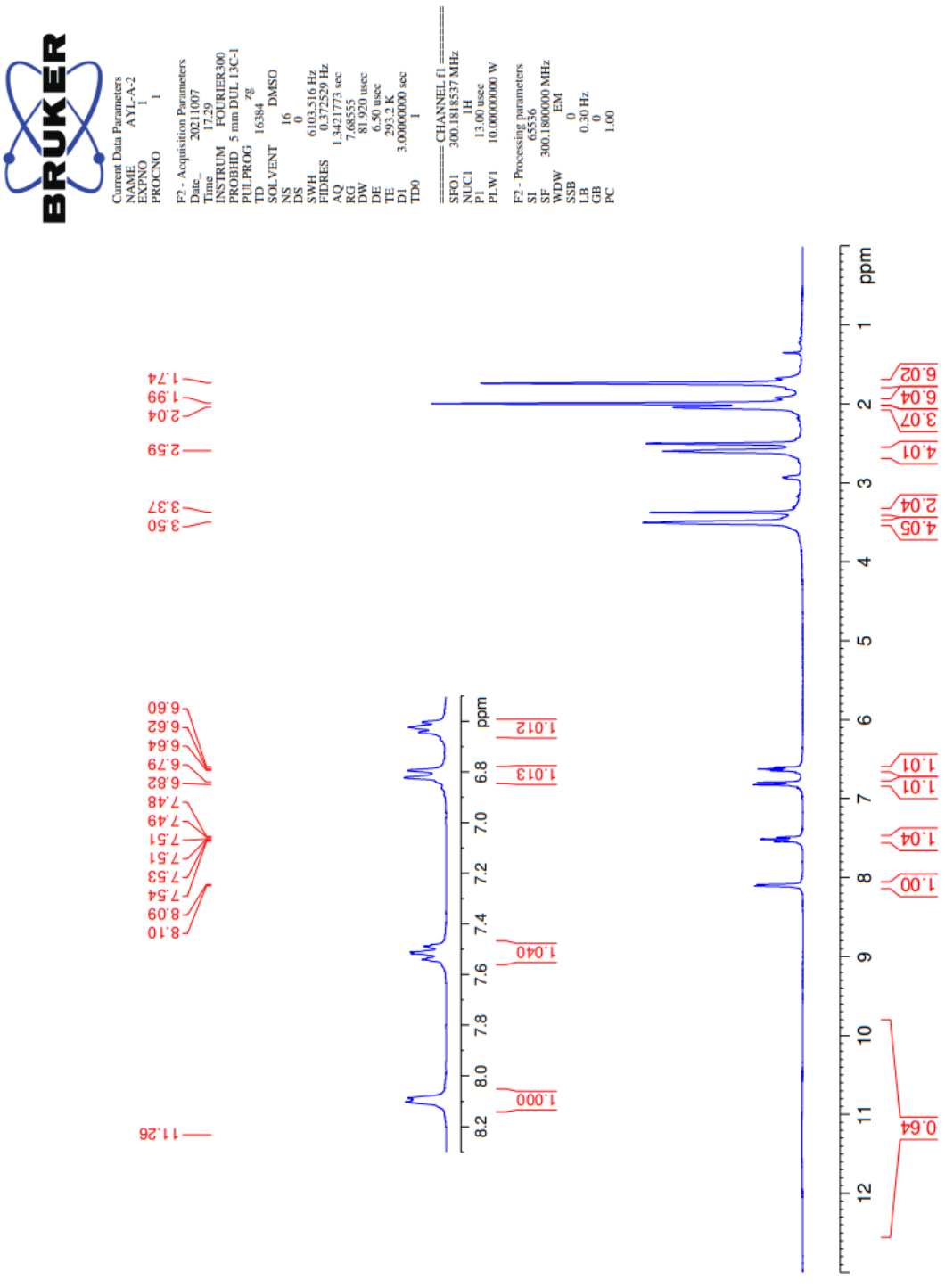

Figure 5.12. *^{1}H-NMR spectrum of compound **3b***

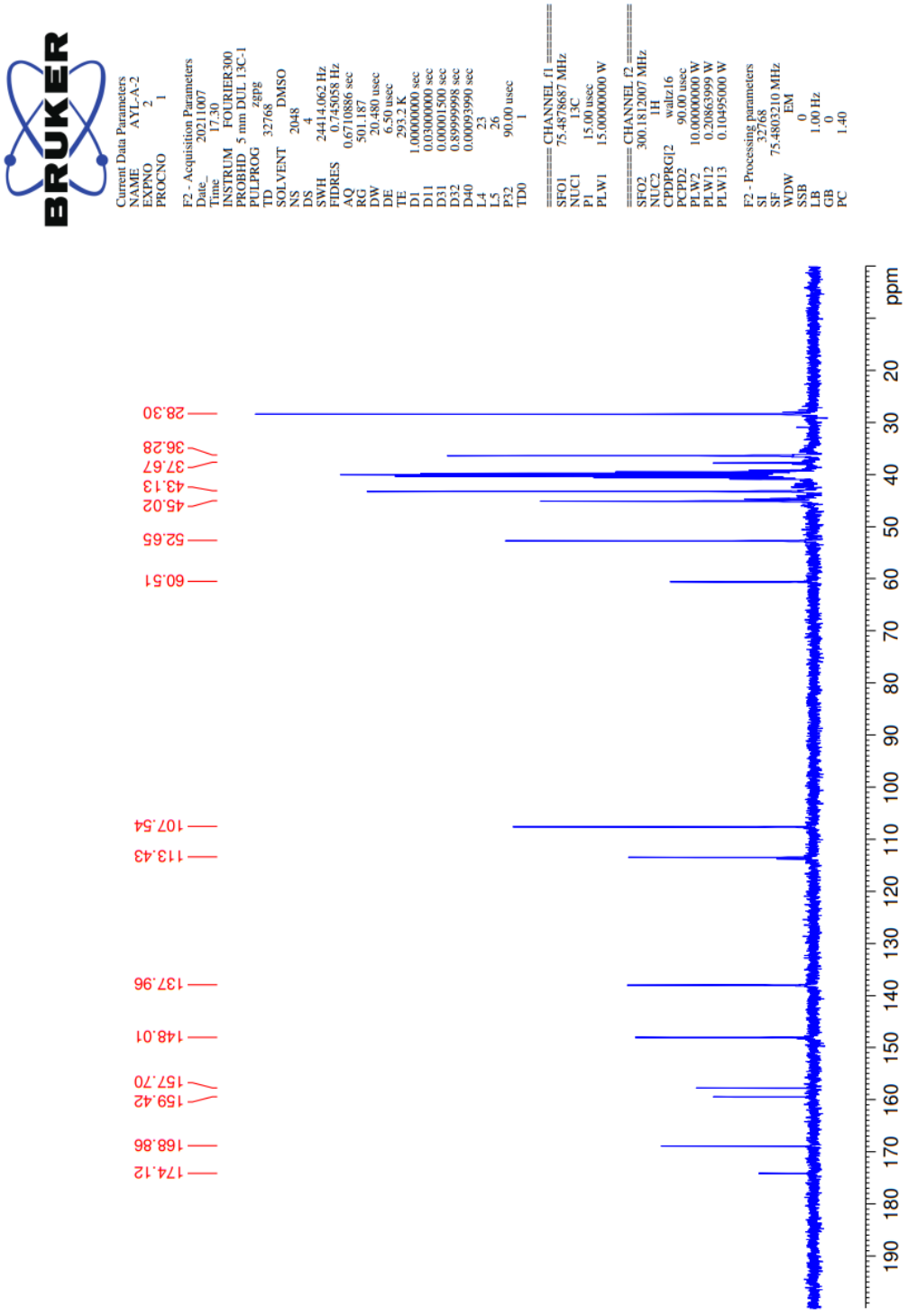

Figure 5.13. *^{13}C-NMR spectrum of compound **3b***

Elmt	Val.	Min	Max	Elmt	Val.	Min	Max	Elmt	Val.	Min	Max	Elmt	Val.	Min	Max	Use Adduct
H	1	10	40	O	2	0	4	S	2	1	1	Ru	2	0	0	H
C	4	9	40	F	1	0	0	Cl	1	0	1	Pd	2	0	0	
N	3	2	10	P	3	0	0	Br	1	0	0	I	3	0	0	

Error Margin (ppm): 5
HC Ratio: unlimited
Max Isotopes: 3
MSn Iso RI (%): 10.00

DBE Range: 5.0 - 25.0
Apply N Rule: yes
Isotope RI (%): 1.00
MSn Logic Mode: AND

Electron Ions: both
Use MSn Info: yes
Isotope Res: 9000
Max Results: 150

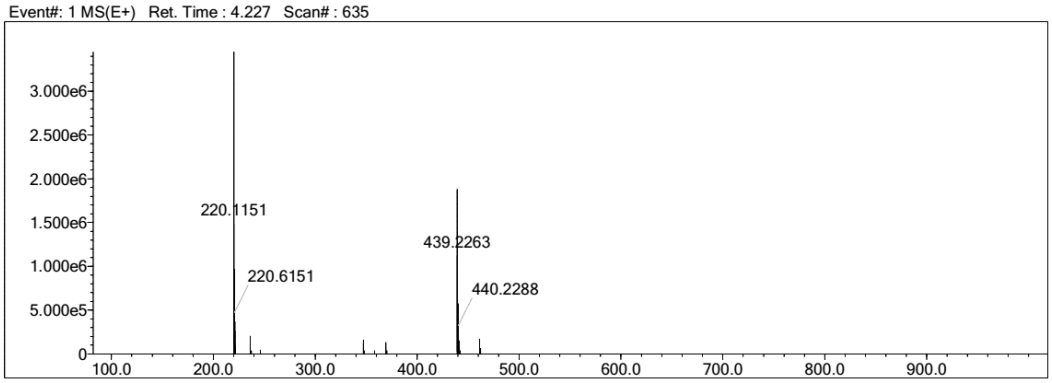

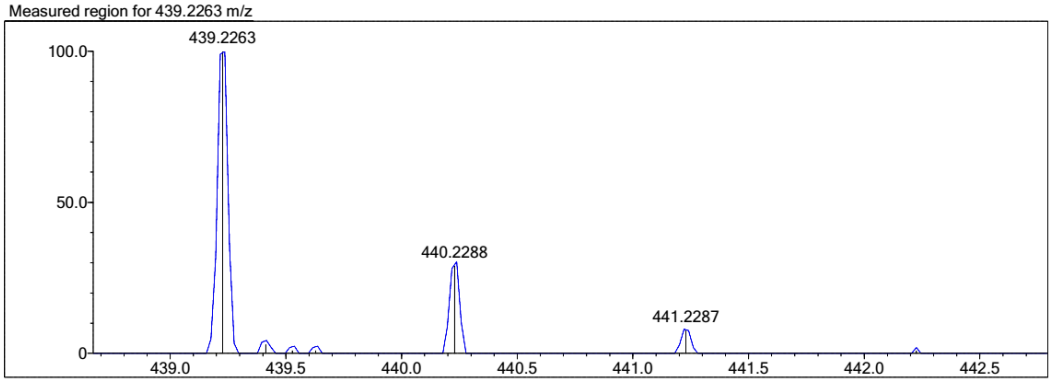

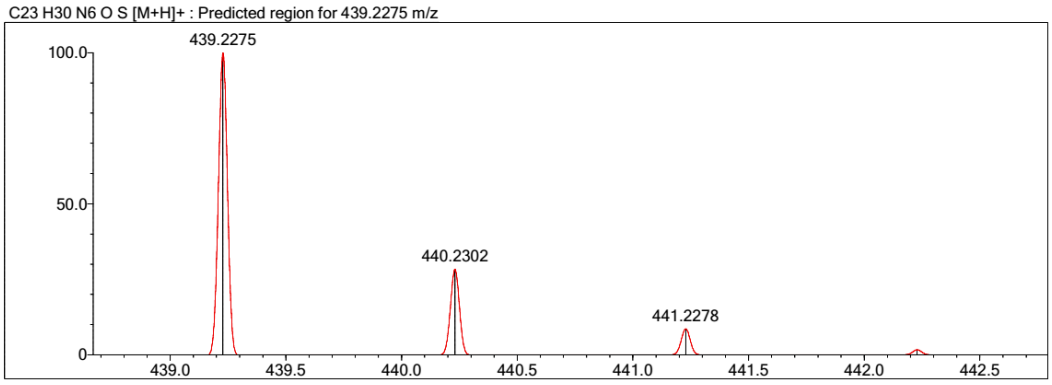

Rank	Score	Formula (M)	Ion	Meas. m/z	Pred. m/z	Df. (mDa)	Df. (ppm)	Iso	DBE
1	95.67	C23 H30 N6 O S	[M+H]+	439.2263	439.2275	-1.2	-2.73	100.00	12.0

Figure 5.14. *HR-MS of compound **3b***

5.1.4.3. N-(5-(Adamantan-1-yl)-1,3,4-thiadiazol-2-yl)-2-(4-phenylpiperazin-1-yl)acetamide (3c)

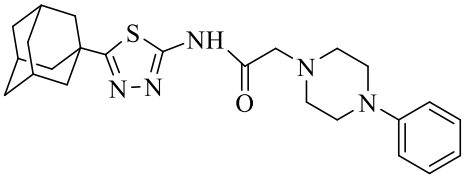

Figure 5.15. *Molecular structure of compound **(3c)***

It was synthesized according to method D. Yield: 94 %. Physical appearance: light yellow powder. Experimental m.p.: 172-173 ˚C.

IR (ATR) υ_{max} (cm^{-1}): 3142 (N-H stretching), 3022 (Aromatic sp^2 C-H stretching), 2904-2848 (sp^3 C-H stretching), 1687 (C=O stretching), 1597-1448 (aromatic C=C and C=N stretching), 1284 (C-N stretching).

^{1}H-NMR (300 MHz) (DMSO-*d*$_6$) δ (ppm): 1.73 (6H, s, adamantane-H), 1.98 (6H, s, adamantane-H), 2.03 (3H, s, adamantane-H), 2.65 (4H, br-s, piperazine's $H_{2,6}$), 3.14 (4H, br-s, piperazine's $H_{3,5}$), 3.37 (2H, s, CO-$\underline{CH_2}$), 6.76 (1H, t, *J*= 7.11 Hz, phenyl H_4), 6.91 (2H, d, *J*= 8.1 Hz, phenyl $_{2,6}$) 7.19 (2H, t, *J*= 7.23 Hz, phenyl $H_{3,5}$), 11.6 (H, br-s, $\underline{N\text{-}H}$).

^{13}C-NMR (75 MHz) (DMSO-*d*$_6$) δ (ppm): 28.31 (adamantane), 36.29 (adamantane), 37.66 (adamantane), 43.13 (adamantane), 48.61 (piperazine), 52.85 (piperazine), 60.46 (CO-$\underline{C}H_2$), 115.88 (phenyl), 119.27 (phenyl), 129.36 (phenyl), 151.43 (phenyl's C_1), 157.71 (thiadiazole), 168.82 (thiadiazole), 174.09 ($\underline{C}O$).

HRMS (ESI) (m/z) $[M+1]^+$: for $C_{24}H_{31}N_5OS$ calculated: 438.2322; found: 438.2306.

DOPNALAB

	Item	Value
	Acquired Date&Time	9.06.2022 14:06:28
	Acquired by	System Administrator
	Filename	C:\Users\dopnalab\Desktop\MASAÜSTÜ\LEYLA YURTDAŞ\AYL-A-B\AYL-A8.1.ispd
	Spectrum name	AYL-A8.1
	Sample name	AYL-A8
	Sample ID	
	Option	
	Comment	
	No. of Scans	15
	Resolution	4 [cm-1]
	Apodization	Happ-Genzel

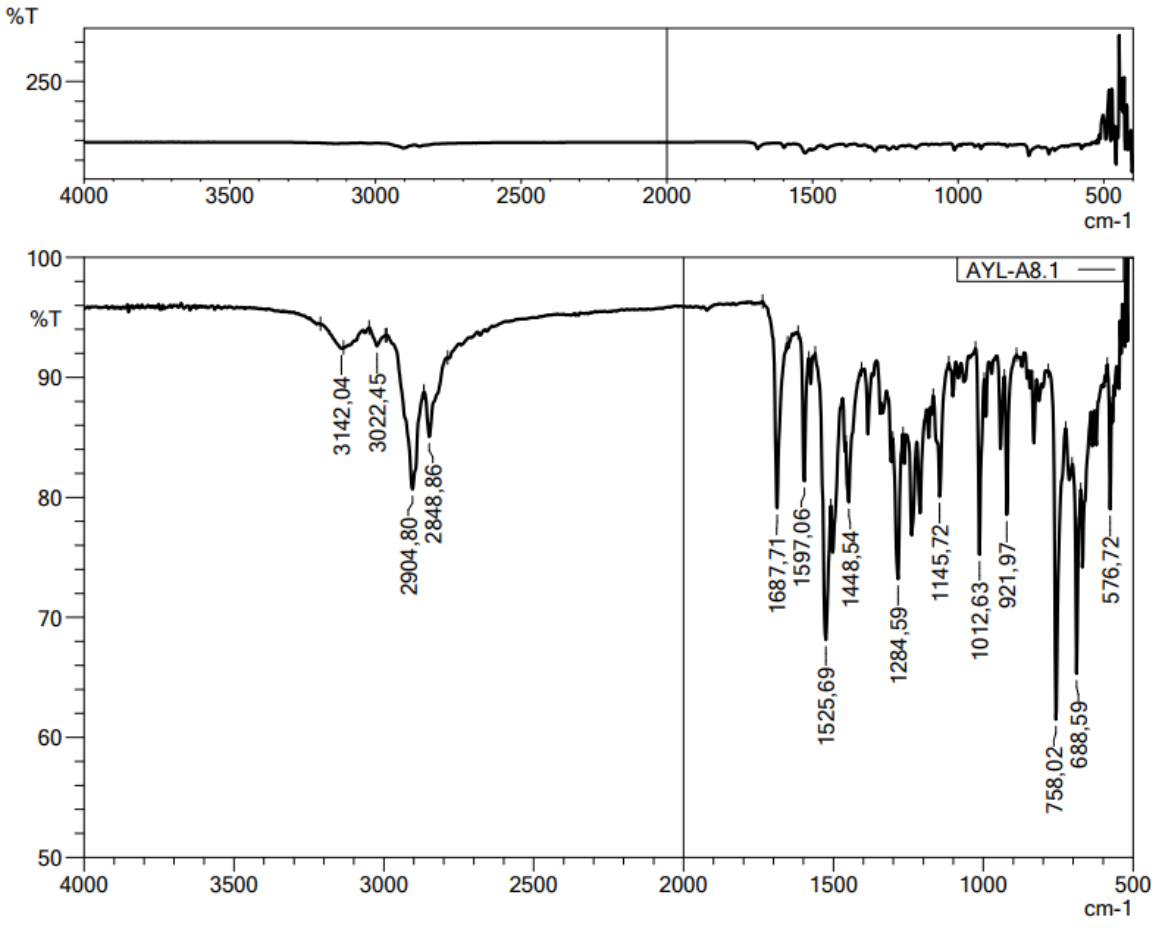

Figure 5.16. *IR spectrum of compound* ***3c***

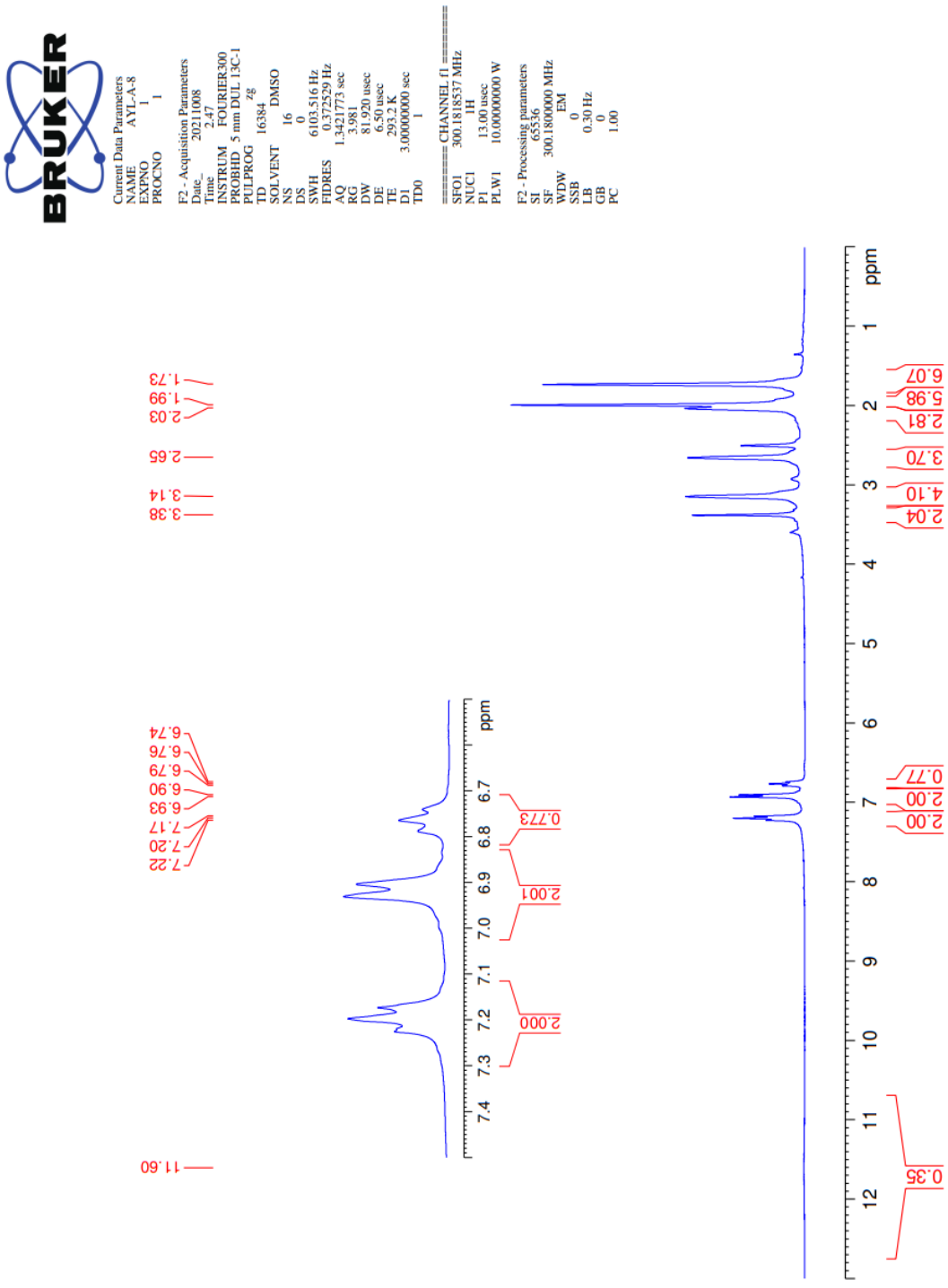

Figure 5.17. *^{1}H-NMR spectrum of compound **3c***

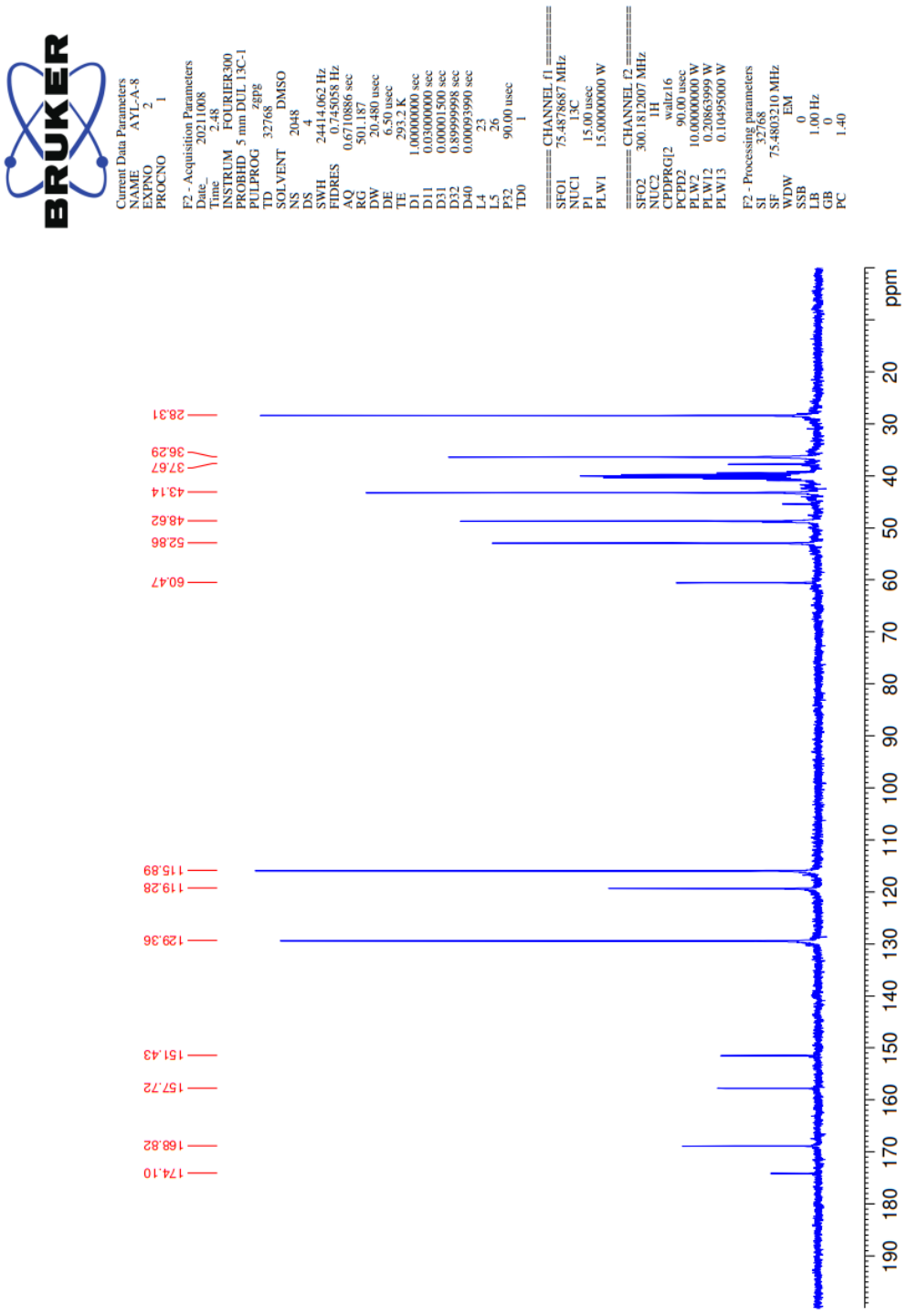

Figure 5.18. *^{13}C-NMR spectrum of compound **3c***

Elmt	Val.	Min	Max	Elmt	Val.	Min	Max	Elmt	Val.	Min	Max	Elmt	Val.	Min	Max	Use Adduct
H	1	10	40	O	2	0	4	S	2	1	1	Ru	2	0	0	H
C	4	9	40	F	1	0	0	Cl	1	0	1	Pd	2	0	0	
N	3	2	10	P	3	0	0	Br	1	0	0	I	3	0	0	

Error Margin (ppm): 5
HC Ratio: unlimited
Max Isotopes: 3
MSn Iso RI (%): 10.00

DBE Range: 5.0 - 25.0
Apply N Rule: yes
Isotope RI (%): 1.00
MSn Logic Mode: AND

Electron Ions: both
Use MSn Info: yes
Isotope Res: 9000
Max Results: 150

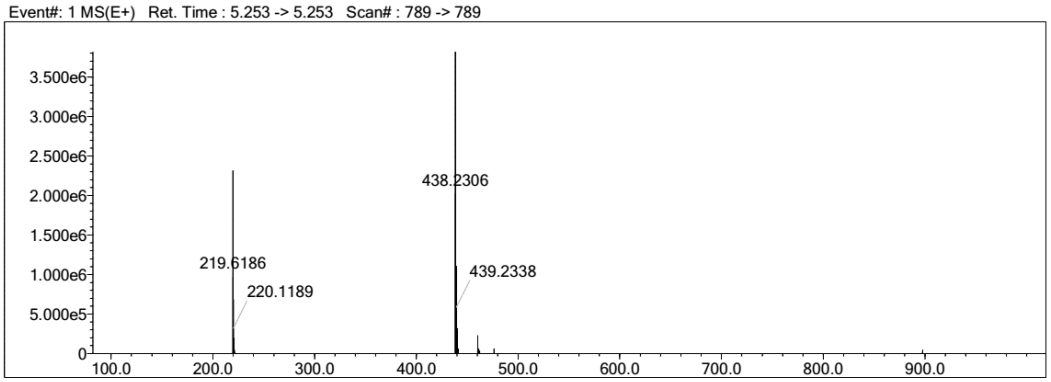

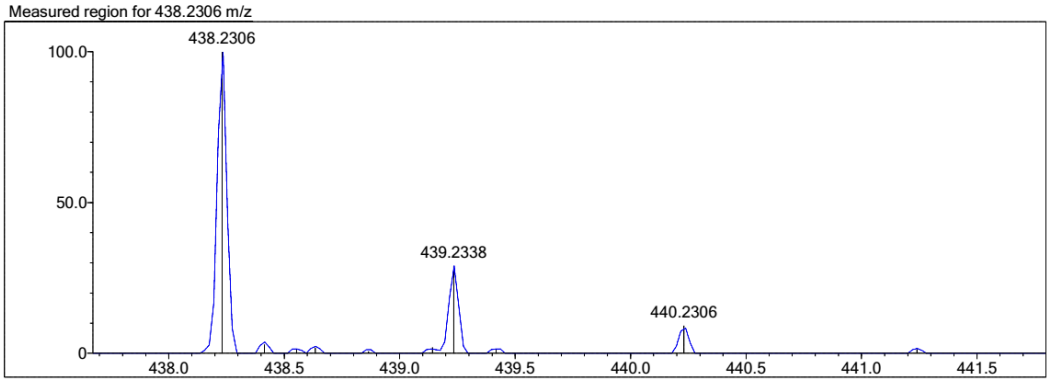

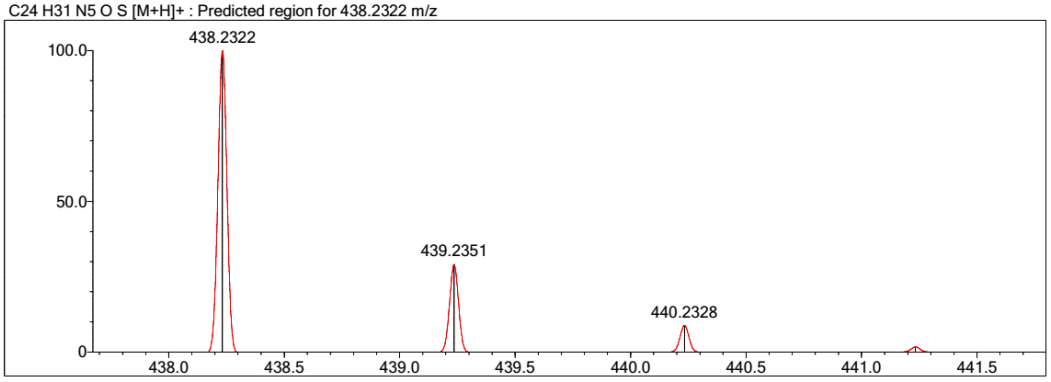

Rank	Score	Formula (M)	Ion	Meas. m/z	Pred. m/z	Df. (mDa)	Df. (ppm)	Iso	DBE
1	83.83	C24 H31 N5 O S	[M+H]+	438.2306	438.2322	-1.6	-3.65	89.77	12.0

Figure 5.19. *HR-MS of compound **3c***

5.1.4.4. N-(5-(Adamantan-1-yl)-1,3,4-thiadiazol-2-yl)-2-(4-(furan-2-carbonyl) piperazin-1-yl)acetamide (3d)

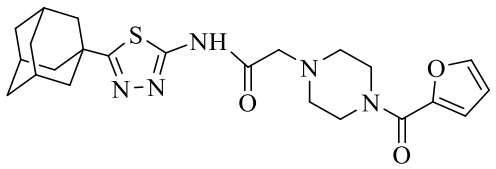

Figure 5.20. *Molecular structure of compound* ***(3d)***

It was synthesized according to method D. Yield: 75 %. Physical appearance: white powder. Experimental m.p.: 206-207 ˚C.

IR (ATR) υ_{max} (cm^{-1}): 3136 (N-H stretching), 3116 (Aromatic sp^2 C-H stretching), 2933-2843 (sp^3 C-H stretching), 1701 (C=O stretching), 1620 (C=O stretching), 1556-1436 (aromatic C=C and C=N stretching), 1300- 1280 (Aromatic C-O stretching), 1134 (C-N stretching).

^{1}H-NMR (300 MHz) (DMSO-*d_6*) δ (ppm): 1.73 (6H, s, adamantane's H), 1.98 (6H, s, adamantane- H), 2.03 (3H, s, adamantane-H), 2.57 (4H, br-s, piperazine's $H_{2,6}$), 3.38 (2H, s, CO-$\underline{CH_2}$), 3.67 (4H, br-s, piperazine's $H_{3,5}$), 6.6 (H, t, *J*= 1.52 Hz, furan-H_4), 6.97 (H, d, *J*= 2.68 Hz, furan-H_3), 7.82 (H, s, furan-H_5), 12.3 (H, br-s, $\underline{N\text{-}H}$).

^{13}C-NMR (75 MHz) (DMSO-*d_6*) δ (ppm): 28.29 (adamantane), 36.28 (adamantane), 37.66 (adamantane), 43.12 (adamantane), 52.84 (piperazine), 60.12 (CO-$\underline{C}H_2$-), 111.74 (furan), 116.01 (furan), 145.17 (furan), 147.4 (furan), 157.67 (thiadiazole), 158.7 (piperazine-$\underline{CO}$-furan), 168.8 (thiadiazole), 174.12 (NH-$\underline{CO}$-CH_2).

HRMS (ESI) (m/z) $[M+1]^+$: for $C_{23}H_{29}N_5O_3S$ calculated: 456.2064; found: 456.2054.

DOPNALAB

	Item	Value
	Acquired Date&Time	9.06.2022 14:00:56
	Acquired by	System Administrator
	Filename	C:\Users\dopnalab\Desktop\MASAÜSTÜ\LEYLA YURTDAŞ\AYL-A-B\AYL-A7.1.ispd
	Spectrum name	AYL-A7.1
	Sample name	AYL-A7
	Sample ID	
	Option	
	Comment	
	No. of Scans	15
	Resolution	4 [cm-1]
	Apodization	Happ-Genzel

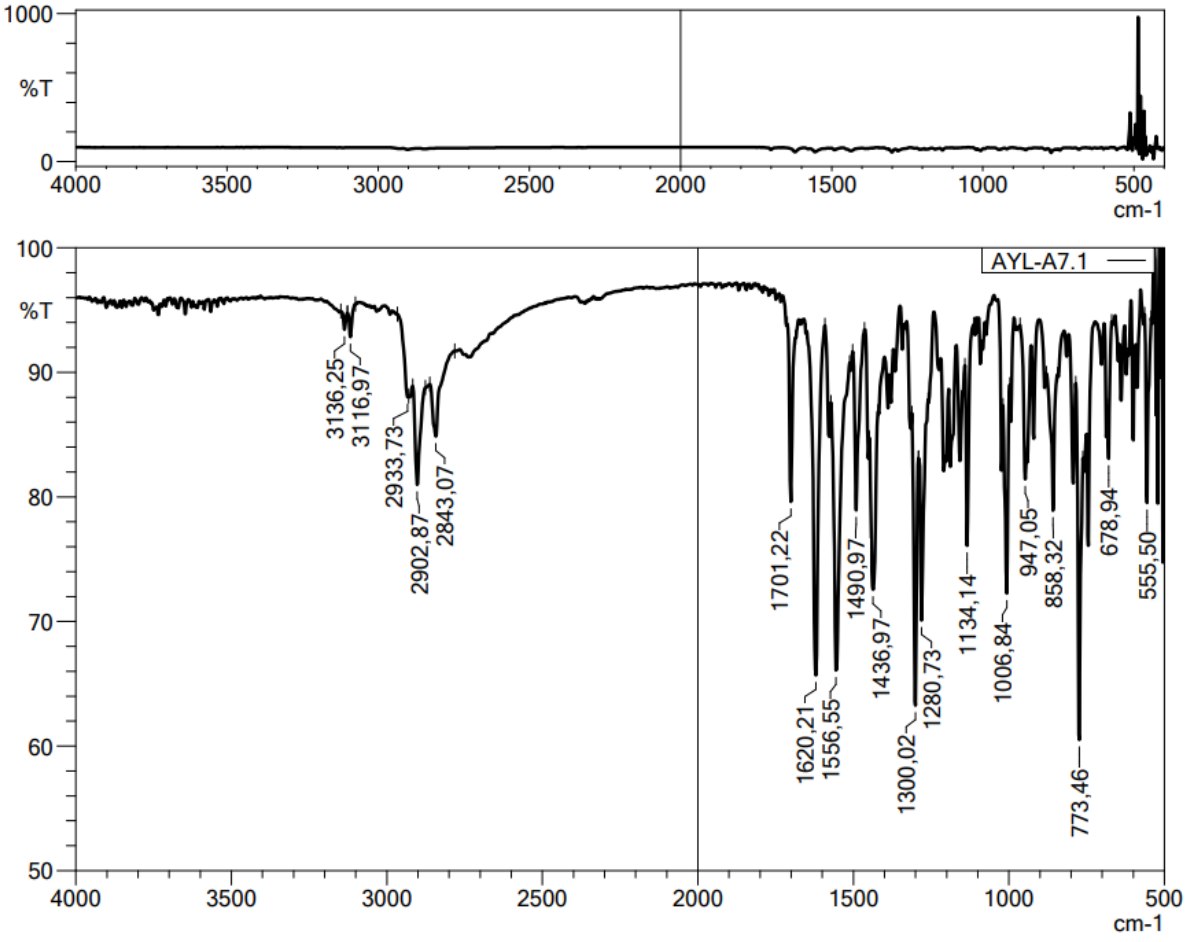

Figure 5.21. *IR spectrum of compound* ***3d***

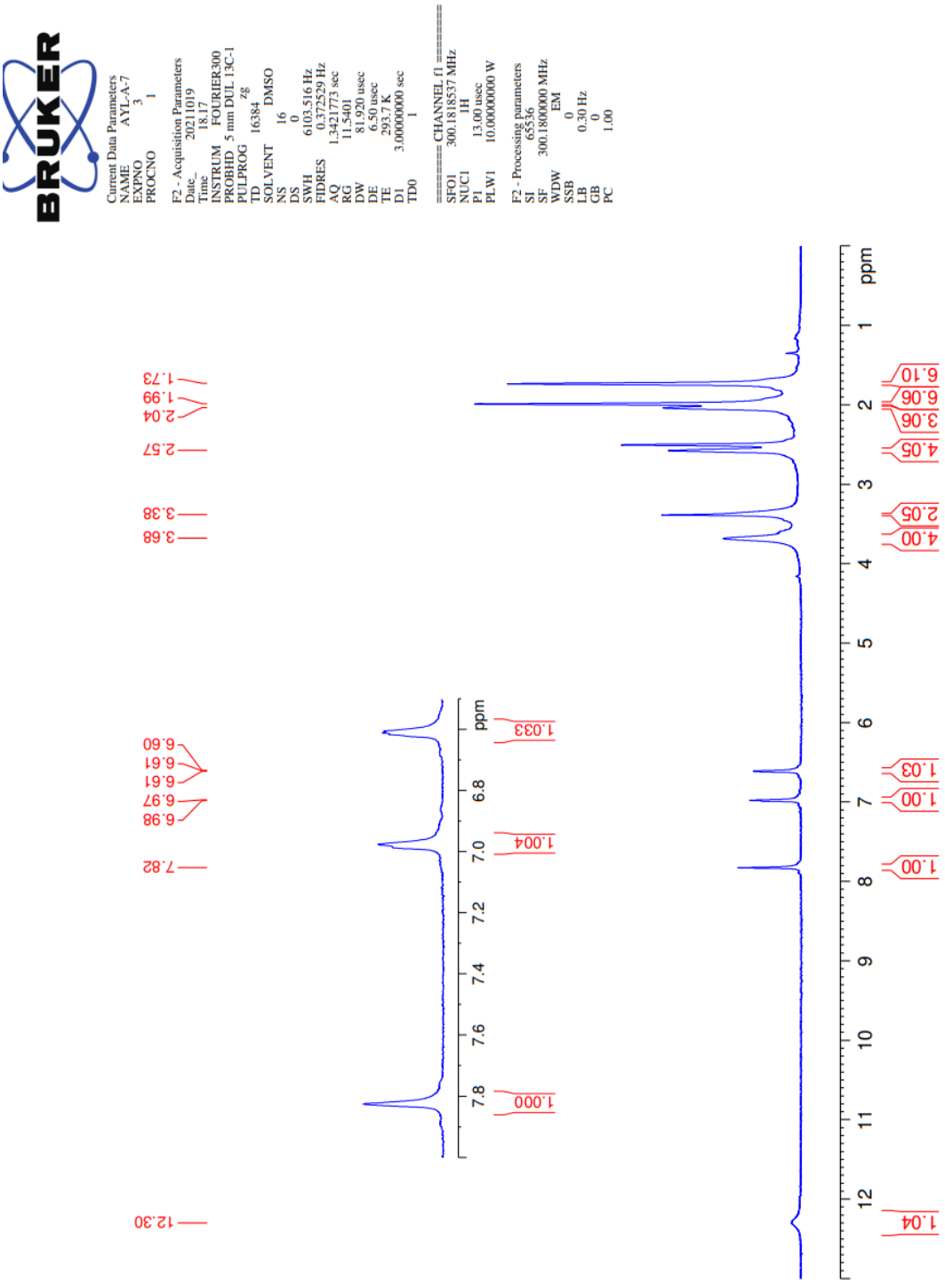

Figure 5.22. *^{1}H-NMR spectrum of compound **3d***

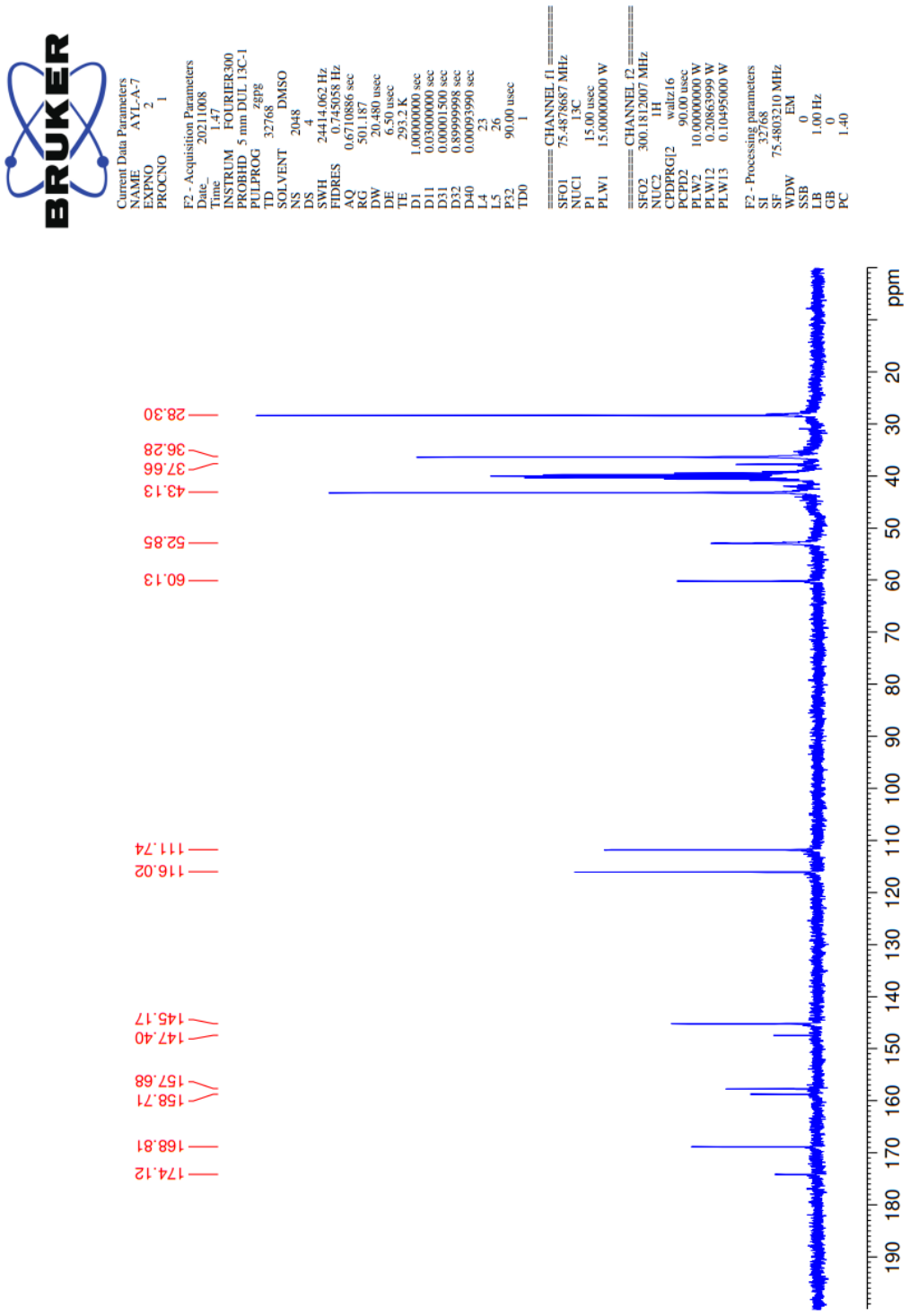

Figure 5.23. *^{13}C-NMR spectrum of compound **3d***

Elmt	Val.	Min	Max	Elmt	Val.	Min	Max	Elmt	Val.	Min	Max	Elmt	Val.	Min	Max	Use Adduct
H	1	10	40	O	2	0	4	S	2	1	1	Ru	2	0	0	H
C	4	9	40	F	1	0	0	Cl	1	0	1	Pd	2	0	0	
N	3	2	10	P	3	0	0	Br	1	0	0	I	3	0	0	

Error Margin (ppm): 5
HC Ratio: unlimited
Max Isotopes: 3
MSn Iso RI (%): 10.00

DBE Range: 5.0 - 25.0
Apply N Rule: yes
Isotope RI (%): 1.00
MSn Logic Mode: AND

Electron Ions: both
Use MSn Info: yes
Isotope Res: 9000
Max Results: 150

Event#: 1 MS(E+) Ret. Time : 4.507 -> 4.507 - 4.307 -> 4.311 Scan# : 677 -> 677 - 647 -> 647

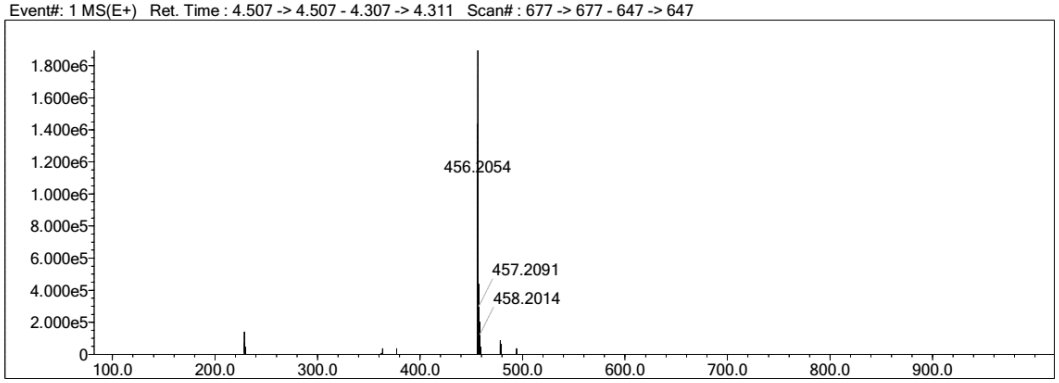

Measured region for 456.2054 m/z

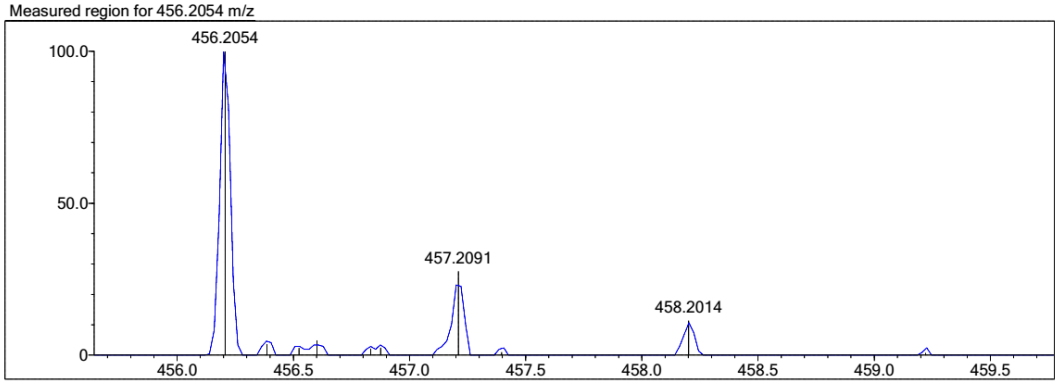

C23 H29 N5 O3 S [M+H]+ : Predicted region for 456.2064 m/z

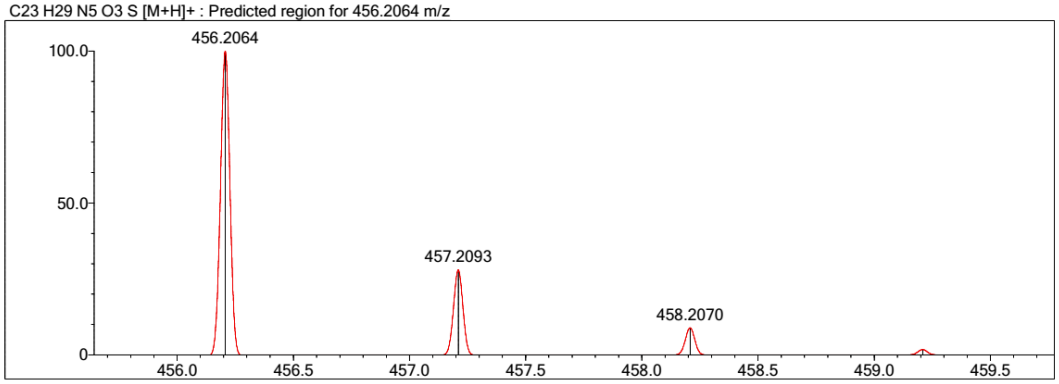

Rank	Score	Formula (M)	Ion	Meas. m/z	Pred. m/z	Df. (mDa)	Df. (ppm)	Iso	DBE
1	57.94	C23 H29 N5 O3 S	[M+H]+	456.2054	456.2064	-1.0	-2.19	59.72	12.0

Figure 5.24. *HR-MS of compound **3d***

5.1.4.5. N-(5-(Adamantan-1-yl)-1,3,4-thiadiazol-2-yl)-2-(4-ethylpiperazin-1-yl)acetamide (3e)

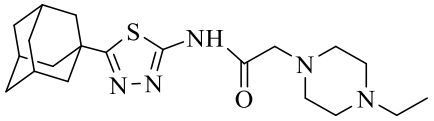

Figure 5.25. *Molecular structure of compound* ***(3e)***

It was synthesized according to method D. Yield: 58 %. Physical appearance: white powder. Experimental m.p.: 152-153 ˚C.

IR (ATR) υ_{max} (cm^{-1}): 3140 (N-H stretching), 2966-2806 (sp^3 C-H stretching), 1701 (C=O stretching), 1564-1438 (aromatic C=N stretching), 1172 (C-N stretching).

^{1}H-NMR (300 MHz) ($CDCl_3$) δ (ppm): 1.10 (3H, t, *J*= 7.23 Hz, CH_2 - $\underline{CH_3}$), 1.80 (6H, s, adamantane-H), 2.10 (9H, s, adamantane-H), 2.46 (2H, q, J_1= 7.23 Hz, J_2= 14.41 Hz, $\underline{CH_2}$ - CH_3), 2.55 (4H, br-s, piperazine's $H_{3,5}$), 2.67 (4H, t, *J*= 3.98 Hz, piperazine's $H_{2,6}$), 3.28 (2H, s, CO-$\underline{CH_2}$),10.55 (H, br-s, $\underline{N\text{-}H}$).

^{13}C-NMR (75 MHz) ($CDCl_3$) δ (ppm): 11.96 (CH_2-$\underline{CH_3}$) 28.41 (adamantane), 36.39 (adamantane), 37.88 (adamantane), 43.22 (adamantane), 52.16 ($\underline{CH_2}$-CH_3), 52.49 (piperazine), 53.65 (piperazine), 60.01 (CO-$\underline{C}H_2$-), 157.21 (thiadiazole), 168.5 (thiadiazole), 175.98 (CO).

HRMS (ESI) (m/z) $[M+1]^+$: for $C_{20}H_{31}N_5OS$ calculated: 390.2322; found: 390.2304.

DOPNALAB

	Item	Value
	Acquired Date&Time	9.06.2022 13:51:20
	Acquired by	System Administrator
	Filename	C:\Users\dopnalab\Desktop\MASAÜSTÜ\LEYLA YURTDAŞ\AYL-A-B\AYL-A3.1.ispd
	Spectrum name	AYL-A3.1
	Sample name	AYL-A3
	Sample ID	
	Option	
	Comment	
	No. of Scans	15
	Resolution	4 [cm-1]
	Apodization	Happ-Genzel

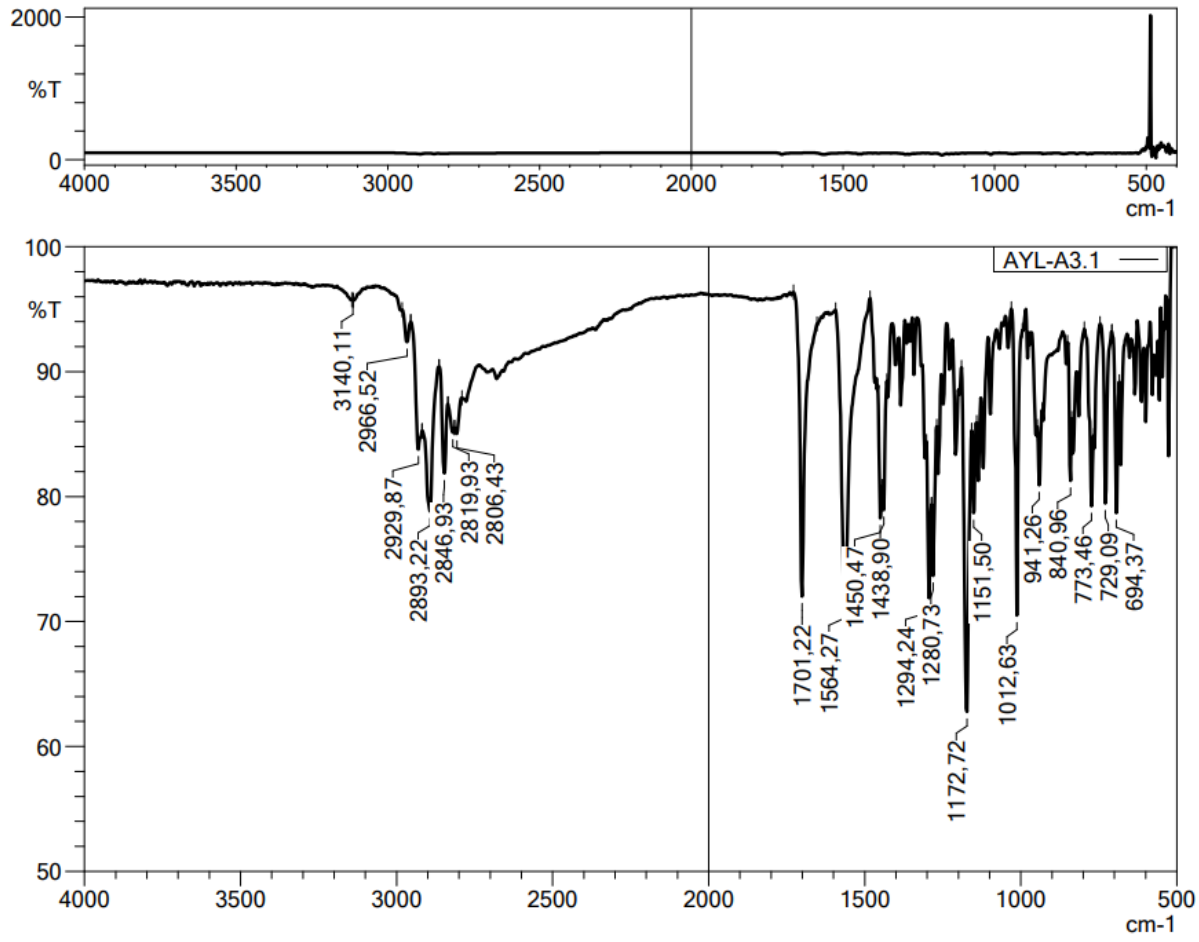

Figure 5.26. *IR spectrum of compound* ***3e***

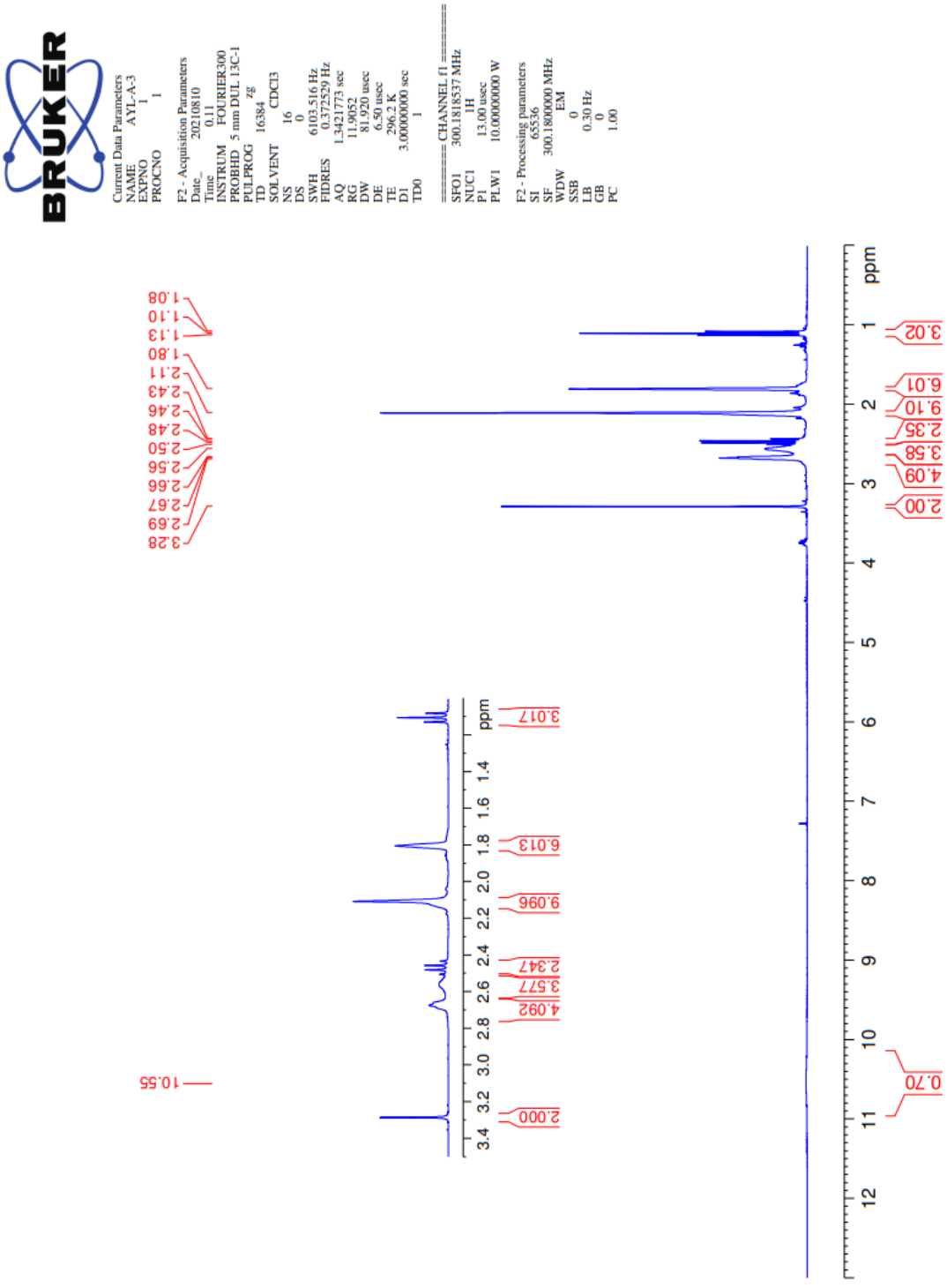

Figure 5.27. *[1]H-NMR spectrum of compound **3e***

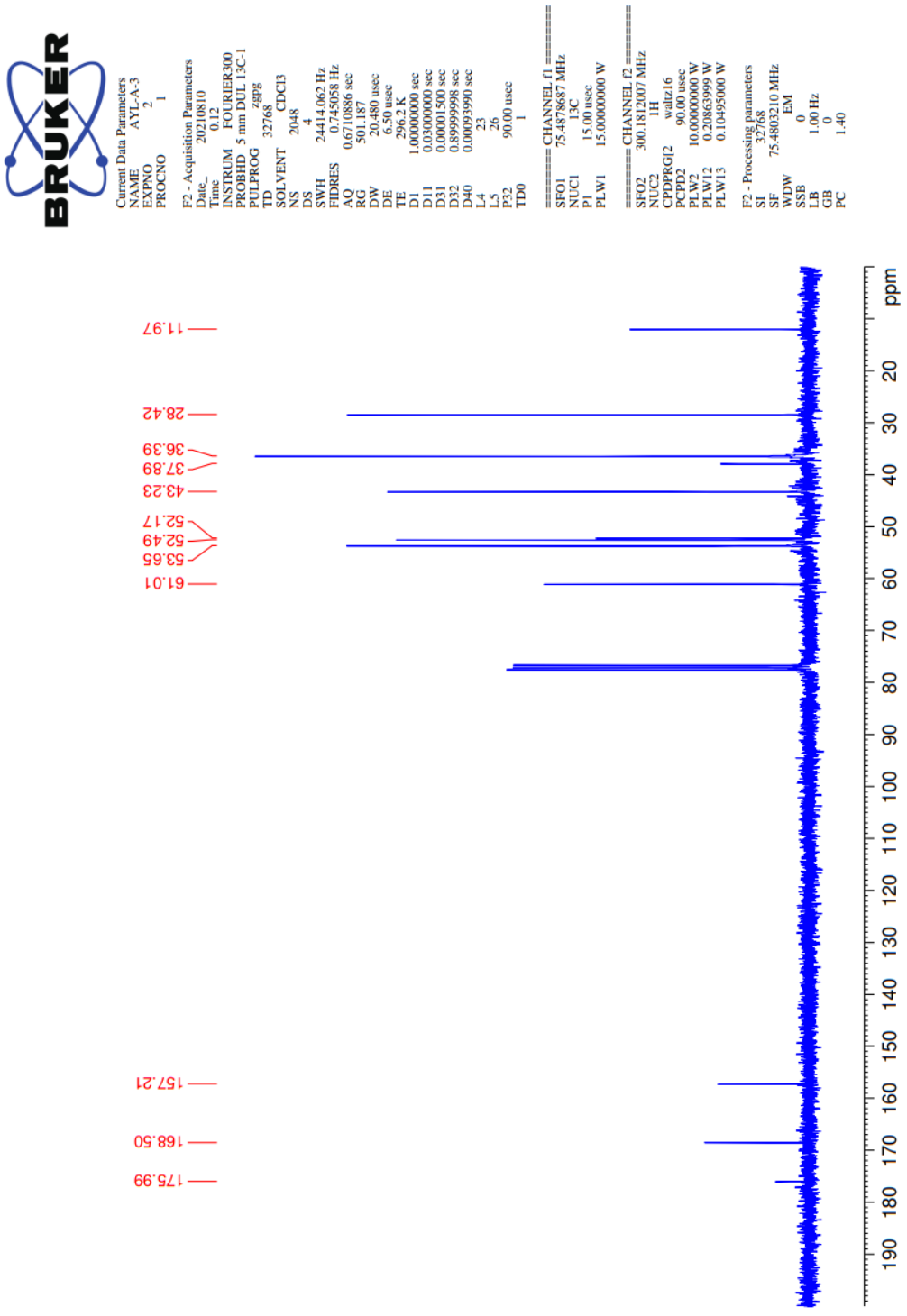

Figure 5.28. *^{13}C-NMR spectrum of compound **3e***

Elmt	Val.	Min	Max	Elmt	Val.	Min	Max	Elmt	Val.	Min	Max	Elmt	Val.	Min	Max	Use Adduct
H	1	10	40	O	2	0	4	S	2	1	1	Ru	2	0	0	H
C	4	9	40	F	1	0	0	Cl	1	0	1	Pd	2	0	0	
N	3	2	10	P	3	0	0	Br	1	0	0	I	3	0	0	

Error Margin (ppm): 5
HC Ratio: unlimited
Max Isotopes: 3
MSn Iso RI (%): 10.00

DBE Range: 5.0 - 25.0
Apply N Rule: yes
Isotope RI (%): 1.00
MSn Logic Mode: AND

Electron Ions: both
Use MSn Info: yes
Isotope Res: 9000
Max Results: 150

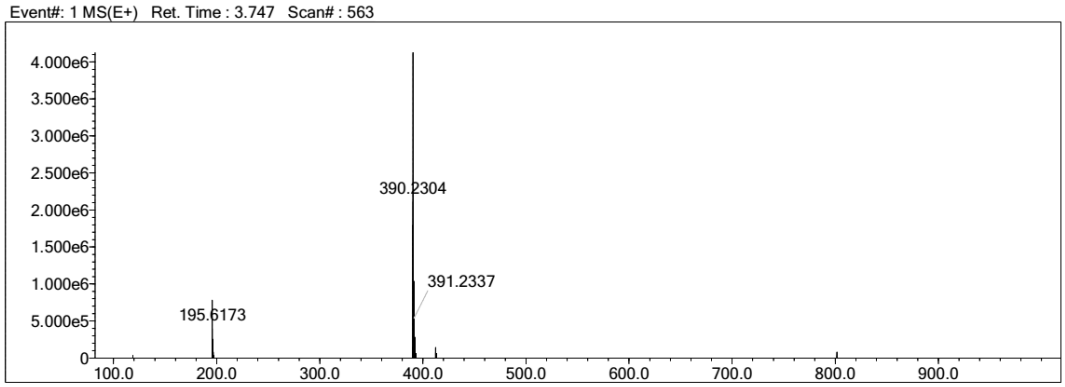

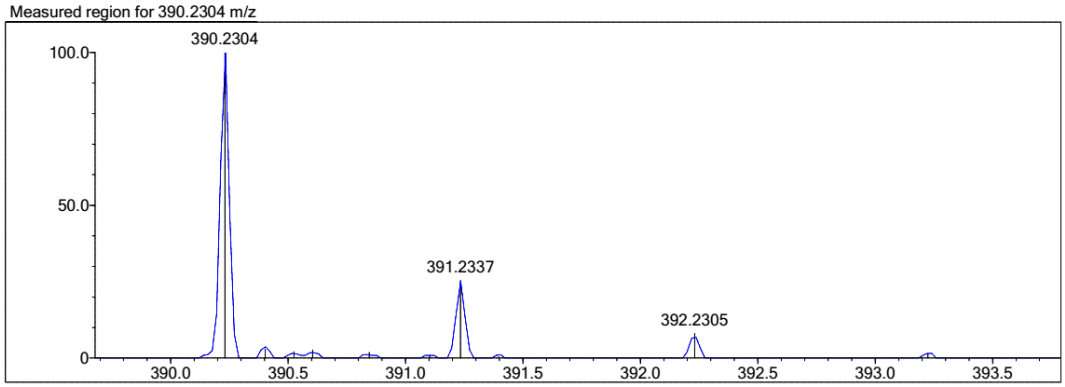

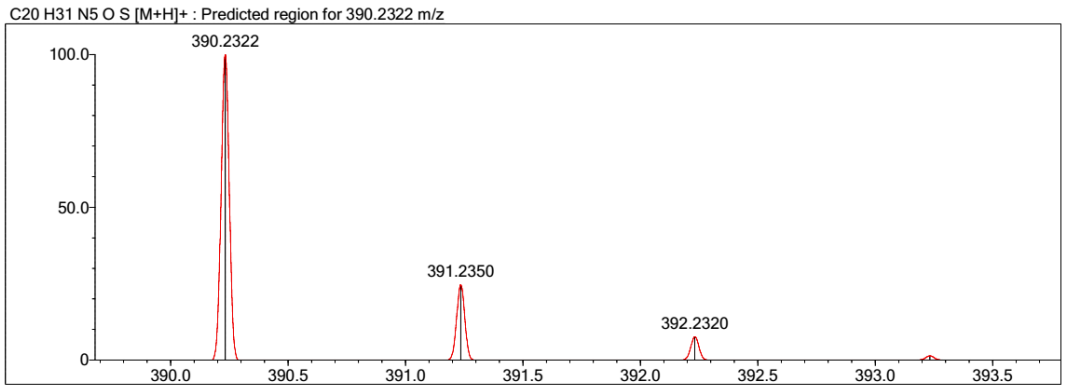

Rank	Score	Formula (M)	Ion	Meas. m/z	Pred. m/z	Df. (mDa)	Df. (ppm)	Iso	DBE
1	76.87	C20 H31 N5 O S	[M+H]+	390.2304	390.2322	-1.8	-4.61	84.50	8.0

Figure 5.29. *HR-MS of compound **3e***

5.1.4.6. N-(5-(Adamantan-1-yl)-1,3,4-thiadiazol-2-yl)-2-(4-methylpiperazin-1-yl)acetamide (3f)

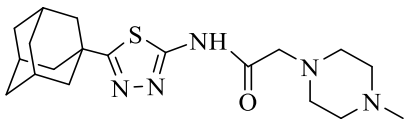

Figure 5.30. *Molecular structure of compound **(3f)***

It was synthesized according to method D. Yield: 55 %. Physical appearance: white powder. Experimental m.p.: 170-171 ˚C.

IR (ATR) υ_{max} (cm^{-1}): 3153 (N-H stretching), 2929-2777 (sp^3 C-H stretching), 1705 (C=O stretching), 1571-1438 (aromatic C=N stretching), 1172 (C-N stretching).

^{1}H-NMR (300 MHz) (DMSO-*d*$_6$) δ (ppm): 1.73 (6H, s, adamantane- H), 1.98 (6H, s, adamantane-H), 2.03 (3H, s, adamantane-H), 2.14 (3H, s, -CH_3), 2.31 (4H, br-s, piperazine's H), 2.49 (4H, t, *J*= 1.68 Hz, piperazine's H), 3.28 (2H, s, CO-CH_2),12.03 (H, br-s, N-H).

^{13}C-NMR (75 MHz) (DMSO-*d*$_6$) δ (ppm): 28.3 (adamantane), 36.29 (adamantane), 37.65 (adamantane), 43.12 (adamantane), 46.21 (CH_3), 52.83 (piperazine), 55.01 (piperazine), 60.5 (CO-CH_2-), 157.67 (thiadiazole), 168.87 (thiadiazole), 174.05 (CO).

HRMS (ESI) (m/z) $[M+1]^+$: for $C_{19}H_{29}N_5OS$ calculated: 376.2166; found: 376.2156.

DOPNALAB

	Item	Value
	Acquired Date&Time	9.06.2022 13:55:39
	Acquired by	System Administrator
	Filename	C:\Users\dopnalab\Desktop\MASAÜSTÜ\LEYLA YURTDAŞ\AYL-A-B\AYL-A4.1.ispd
	Spectrum name	AYL-A4.1
	Sample name	AYL-A4
	Sample ID	
	Option	
	Comment	
	No. of Scans	15
	Resolution	4 [cm-1]
	Apodization	Happ-Genzel

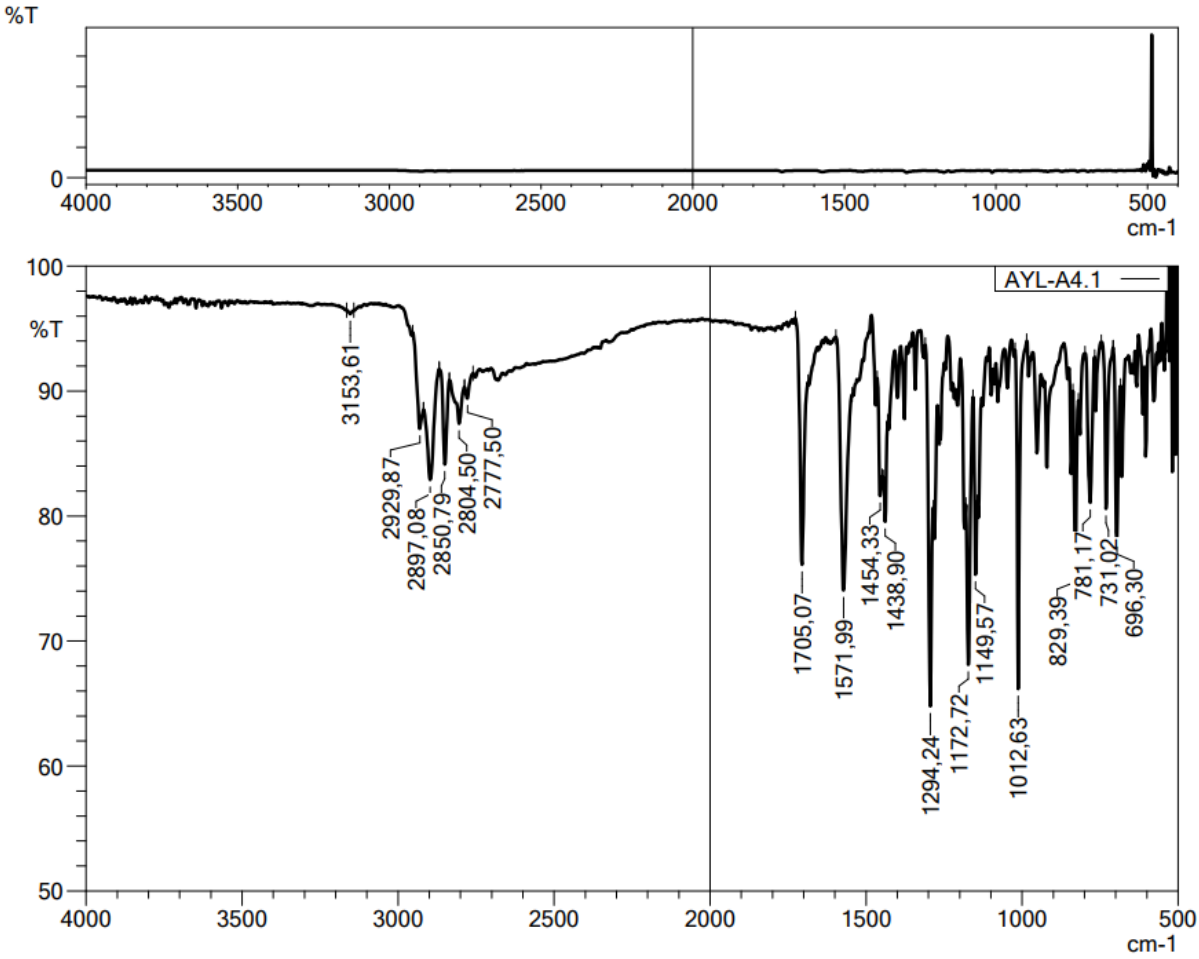

Figure 5.31. *IR spectrum of compound **3f***

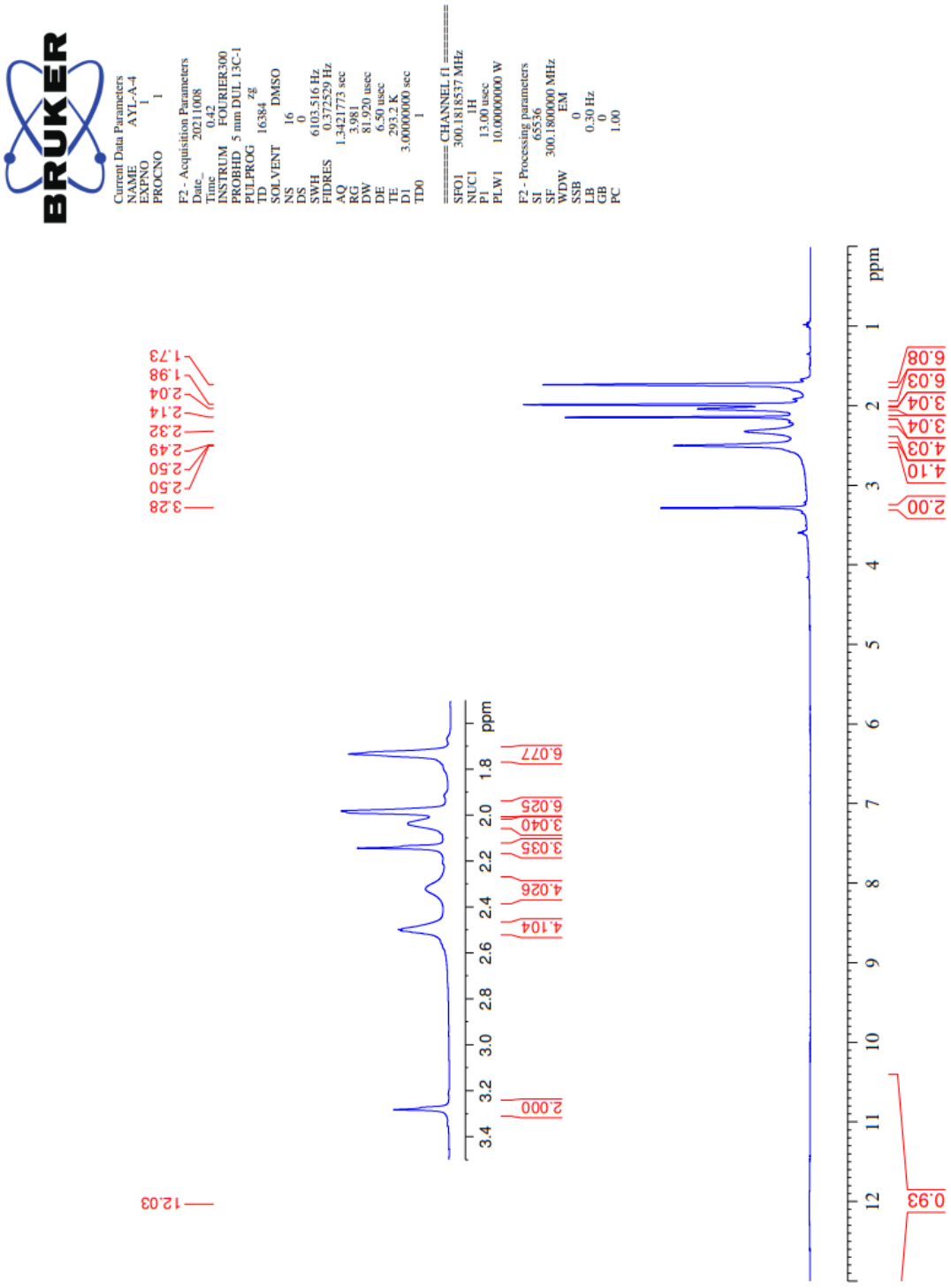

Figure 5.32. *^{1}H-NMR spectrum of compound **3f***

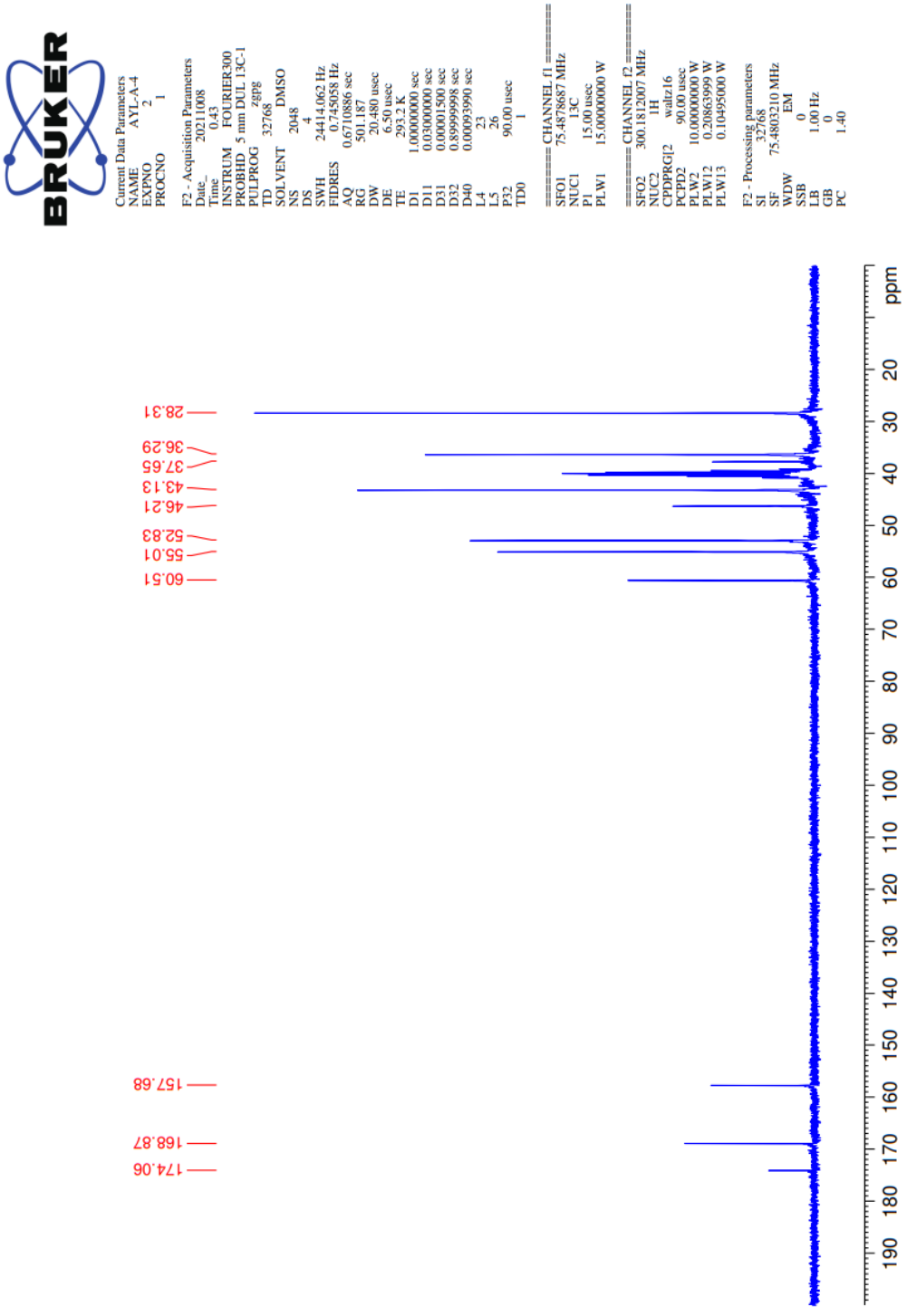

Figure 5.33. *^{13}C-NMR spectrum of compound **3f***

Elmt	Val.	Min	Max	Elmt	Val.	Min	Max	Elmt	Val.	Min	Max	Elmt	Val.	Min	Max	Use Adduct
H	1	10	40	O	2	0	4	S	2	1	1	Ru	2	0	0	H
C	4	9	40	F	1	0	0	Cl	1	0	1	Pd	2	0	0	
N	3	2	10	P	3	0	0	Br	1	0	0	I	3	0	0	

Error Margin (ppm): 5
HC Ratio: unlimited
Max Isotopes: 3
MSn Iso RI (%): 10.00

DBE Range: 5.0 - 25.0
Apply N Rule: yes
Isotope RI (%): 1.00
MSn Logic Mode: AND

Electron Ions: both
Use MSn Info: yes
Isotope Res: 9000
Max Results: 150

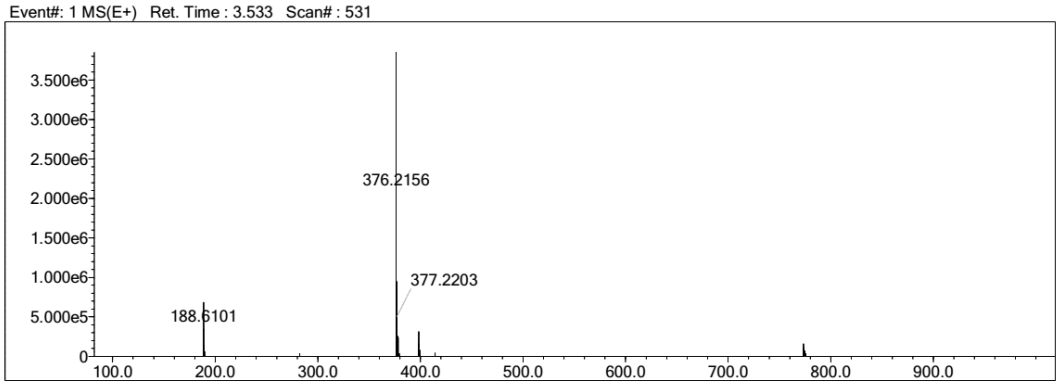

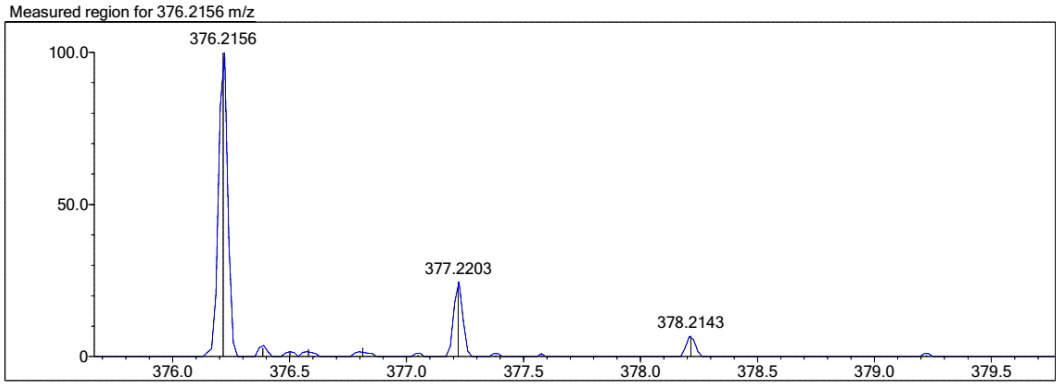

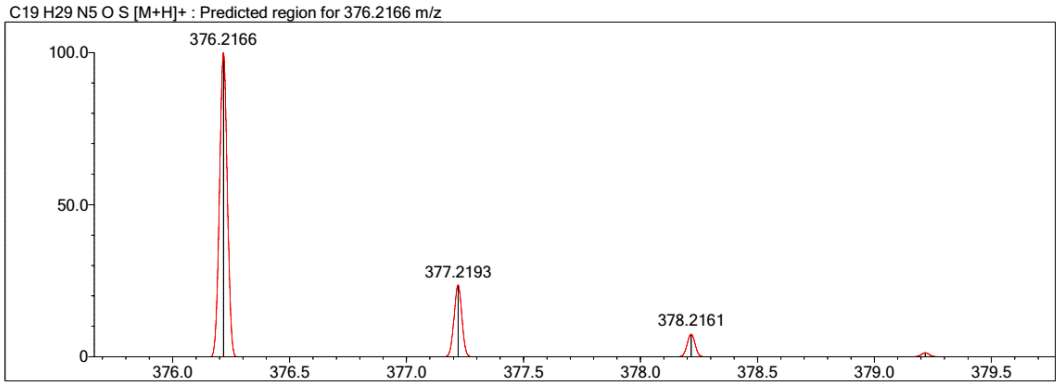

Rank	Score	Formula (M)	Ion	Meas. m/z	Pred. m/z	Df. (mDa)	Df. (ppm)	Iso	DBE
1	84.67	C19 H29 N5 O S	[M+H]+	376.2156	376.2166	-1.0	-2.66	88.34	8.0

Figure 5.34. *HR-MS of compound **3f***

5.1.4.7. N-(5-(Adamantan-1-yl)-1,3,4-thiadiazol-2-yl)-2-(pyrrolidin-1-yl)acetamide (3g)

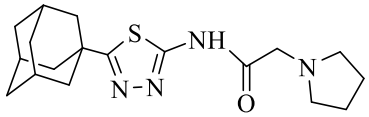

Figure 5.35. *Molecular structure of compound* ***(3g)***

It was synthesized according to method D. Yield: 84 %. Physical appearance: light brown powder. Experimental m.p.: 160-161 ˚C.

IR (ATR) υ_{max} (cm^{-1}): 3159 (N-H stretching), 2926-2794 (sp^3 C-H stretching), 1703 (C=O stretching), 1556-1448 (aromatic C=N stretching), 1301 (C-N stretching).

^{1}H-NMR (300 MHz) (DMSO-*d*$_6$) δ (ppm): 1.68- 1.74 (10H, m, adamantane-H and pyrrolidine's $H_{3,4}$), 1.98 (6H, s, adamantane-H), 2.03 (3H, s, adamantane-H), 2.57 (4H, br-s, pyrrolidine's $H_{2,5}$), 3.41 (2H,s, CO-$\underline{CH_2}$), 11.4 (H, br-s, $\underline{N\text{-}H}$).

^{13}C-NMR (75 MHz) (DMSO-*d*$_6$) δ (ppm): 23.85 (pyrrolidine's $\underline{C_{3,4}}$), 28.31(adamantane), 36.29 (adamantane), 37.64 (adamantane), 43.13 (adamantane), 53.81 (pyrrolidine's $\underline{C_{2,5}}$), 57.94 (CO-$\underline{CH_2}$), 157.91(thiadiazole), 169.29 (thiadiazole), 173.94 (CO).

HRMS (ESI) (m/z) $[M+1]^+$: for $C_{18}H_{26}N_4OS$ calculated: 347.1900; found: 347.1887.

DOPNALAB

	Item	Value
	Acquired Date&Time	9.06.2022 14:12:47
	Acquired by	System Administrator
	Filename	C:\Users\dopnalab\Desktop\MASAÜSTÜ\LEYLA YURTDAŞ\AYL-A-B\AYL-A12.1.ispd
	Spectrum name	AYL-A12.1
	Sample name	AYL-A12
	Sample ID	
	Option	
	Comment	
	No. of Scans	15
	Resolution	4 [cm-1]
	Apodization	Happ-Genzel

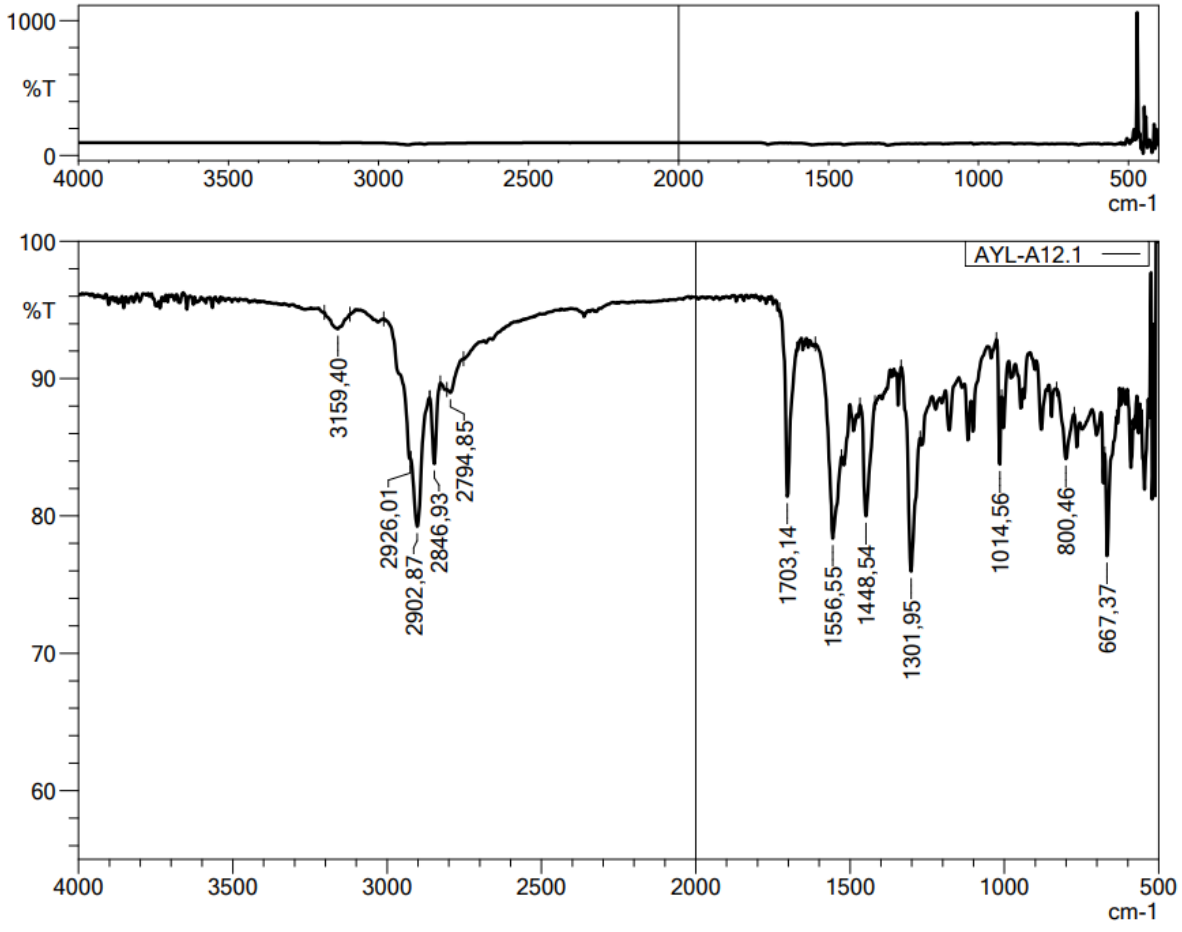

Figure 5.36. *IR spectrum of compound* ***3g***

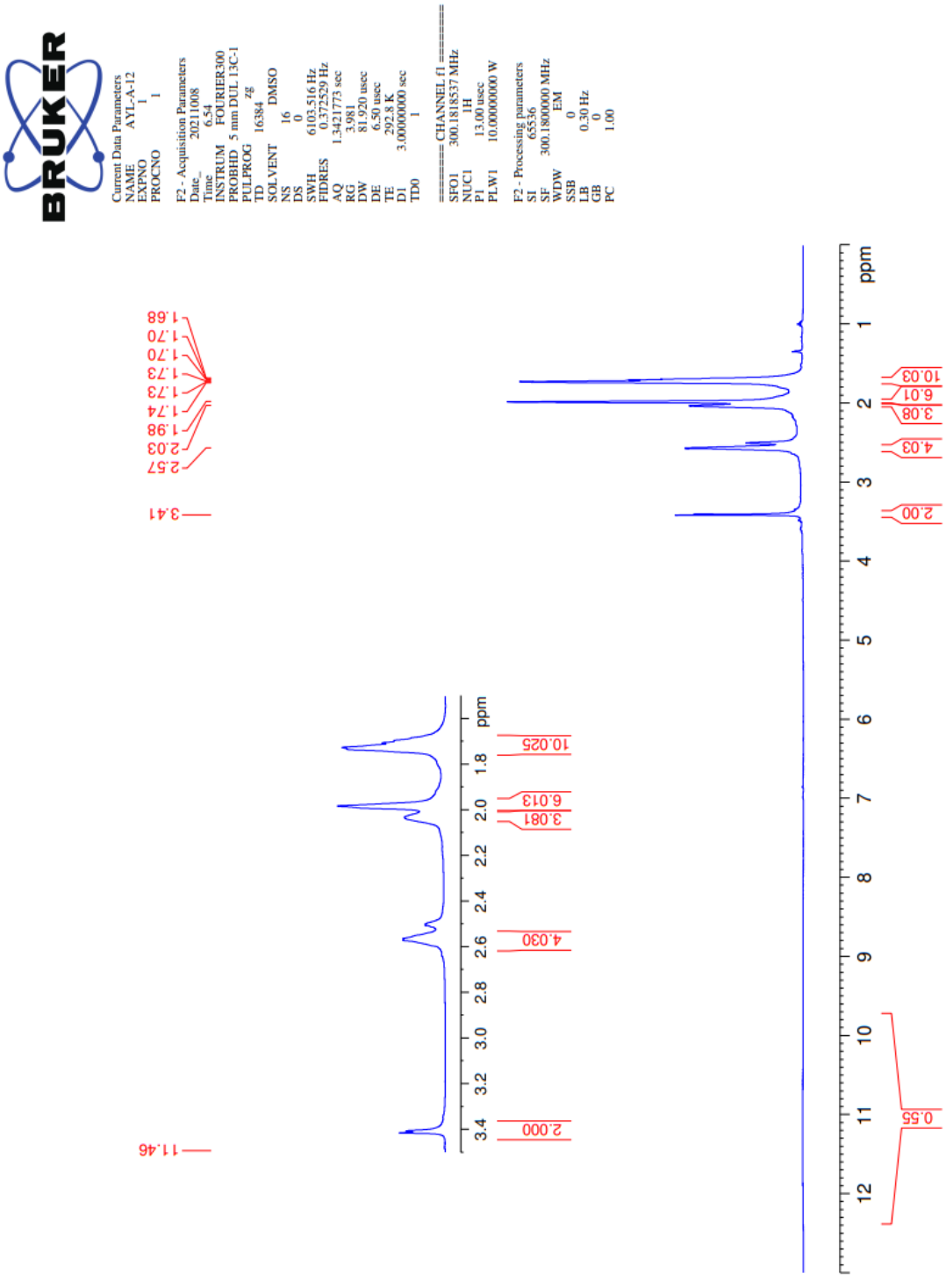

Figure 5.37. *[1]H-NMR spectrum of compound **3g***

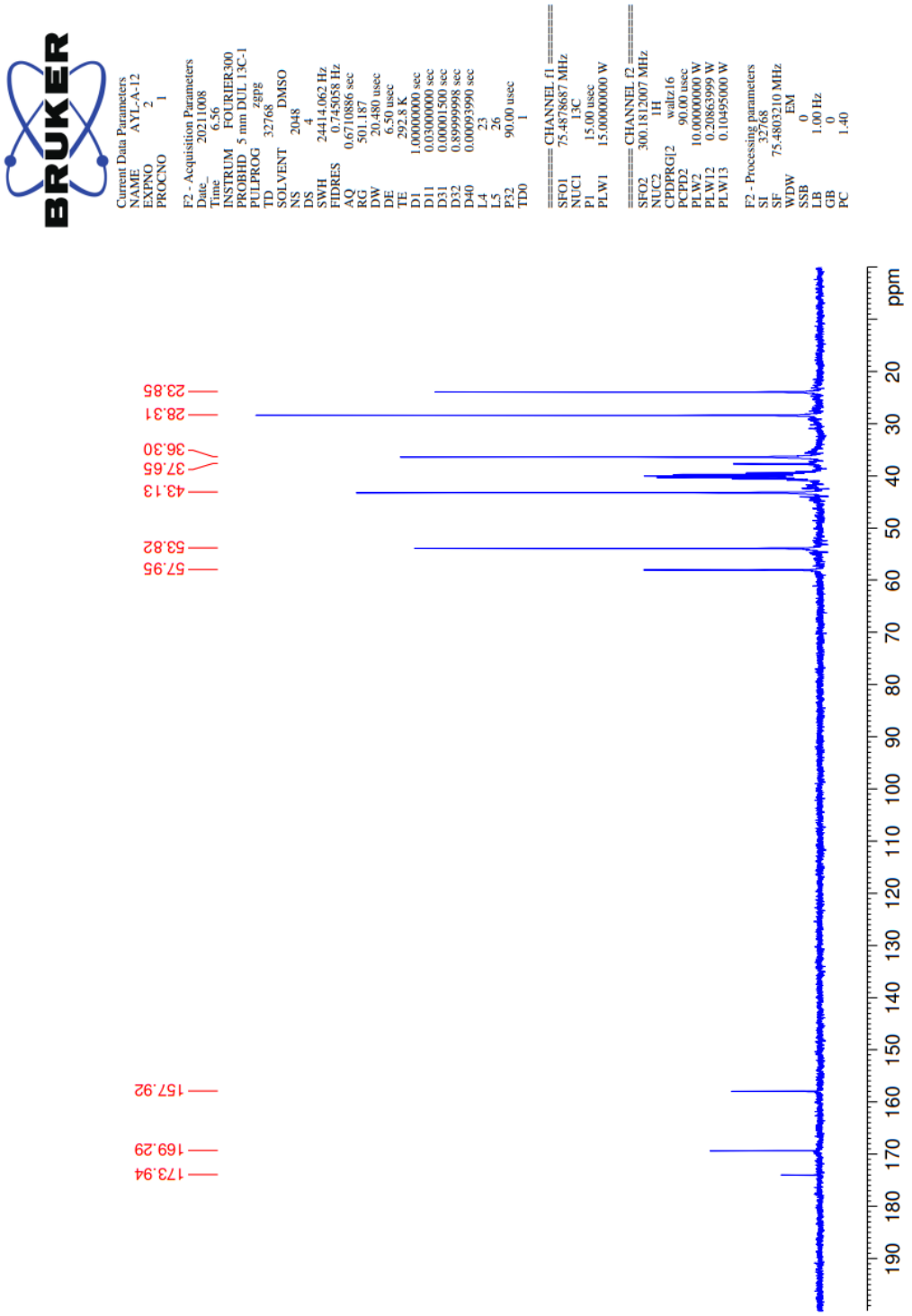

Figure 5.38. *^{13}C-NMR spectrum of compound **3g***

Elmt	Val.	Min	Max	Elmt	Val.	Min	Max	Elmt	Val.	Min	Max	Elmt	Val.	Min	Max	Use Adduct
H	1	10	40	O	2	0	5	S	2	0	1	Ru	2	0	0	H
C	4	9	40	F	1	0	0	Cl	1	0	1	Pd	2	0	0	
N	3	0	10	P	3	0	0	Br	1	0	0	I	3	0	0	

Error Margin (ppm): 5
HC Ratio: unlimited
Max Isotopes: 3
MSn Iso RI (%): 10.00

DBE Range: 5.0 - 25.0
Apply N Rule: yes
Isotope RI (%): 1.00
MSn Logic Mode: AND

Electron Ions: both
Use MSn Info: yes
Isotope Res: 9000
Max Results: 150

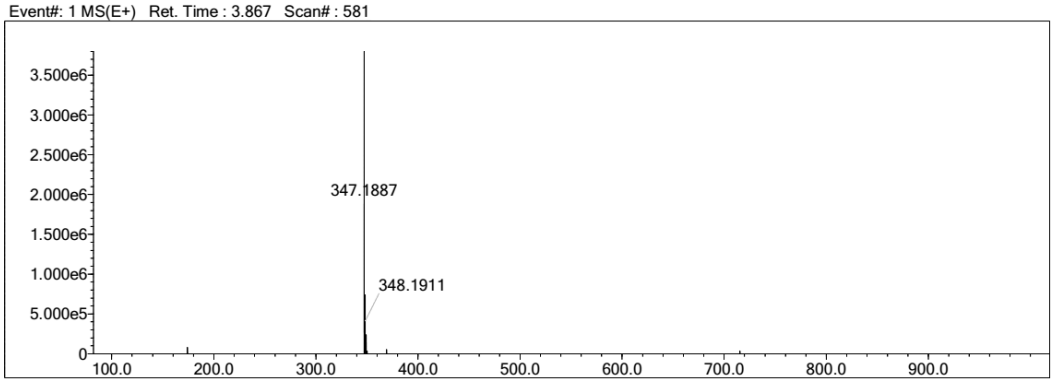

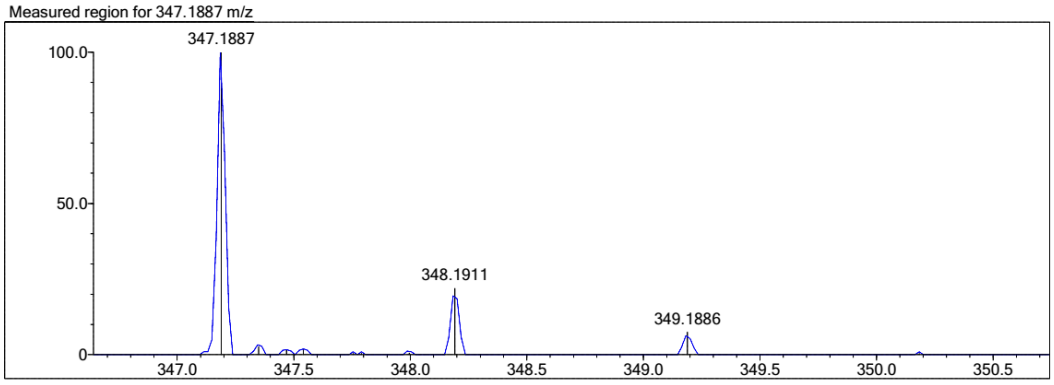

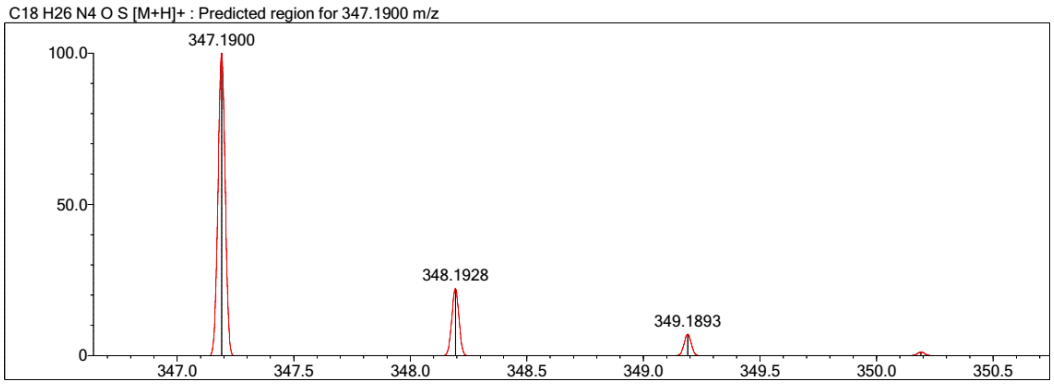

Rank	Score	Formula (M)	Ion	Meas. m/z	Pred. m/z	Df. (mDa)	Df. (ppm)	Iso	DBE
2	56.73	C18 H26 N4 O S	[M+H]+	347.1887	347.1900	-1.3	-3.74	60.91	8.0

Figure 5.39. *HR-MS of compound **3g***

5.1.4.8. N-(5-(Adamantan-1-yl)-1,3,4-thiadiazol-2-yl)-2-(piperidin-1-yl)acetamide (3h)

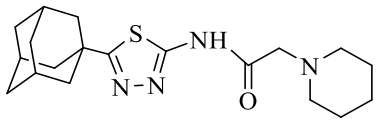

Figure 5.40. *Molecular structure of compound* ***(3h)***

It was synthesized according to method D. Yield: 88 %. Physical appearance: light yellow crystals. Experimental m.p.: 169-170 ˚C. Literature m.p.: 200-202 ˚C [114].

IR (ATR) υ_{max} (cm^{-1}): 3145 (N-H stretching), 2937-2845 (sp^3 C-H stretching), 1699 (C=O stretching), 1548-1438 (aromatic C=N stretching), 1305 (C-N stretching).

^{1}H-NMR (300 MHz) (DMSO-*d*$_6$) δ (ppm): 1.33-1.39 (2H, m, piperidine's H_4), 1.46-1.54 (4H, m, piperidine's $H_{3,5}$), 1.73 (6H, s, adamantane-H), 1.98 (6H, s, adamantane-H), 2.04 (3H, s, adamantane-H), 2.44 (4H, t, *J*= 4.68 Hz, piperidine's $H_{2,6}$), 3.24 (2H, s, CO-$\underline{CH_2}$), 11.83 (H, br-s, $\underline{N\text{-}H}$).

^{13}C-NMR (75 MHz) (DMSO-*d*$_6$) δ (ppm): 23.96 (piperidine's $\underline{C_4}$), 25.91 (piperidine's $\underline{C_{3,5}}$), 28.3 (adamantane), 36.29 (adamantane), 37.65 (adamantane), 43.13 (adamantane), 54.16 (piperidine's $\underline{C_{2,6}}$), 61.39 (CO-$\underline{CH_2}$), 157.74 (thiadiazole), 169.16 (thiadiazole), 174.03 (CO).

HRMS (ESI) (m/z) $[M+1]^+$: for $C_{19}H_{28}N_4OS$ calculated: 361.2057; found: 361.2036.

DOPNALAB

	Item	Value
	Acquired Date&Time	9.06.2022 14:17:15
	Acquired by	System Administrator
	Filename	C:\Users\dopnalab\Desktop\MASAÜSTÜ\LEYLA YURTDAŞ\AYL-A-B\AYL-A13.1.ispd
	Spectrum name	AYL-A13.1
	Sample name	AYL-A13
	Sample ID	
	Option	
	Comment	
	No. of Scans	15
	Resolution	4 [cm-1]
	Apodization	Happ-Genzel

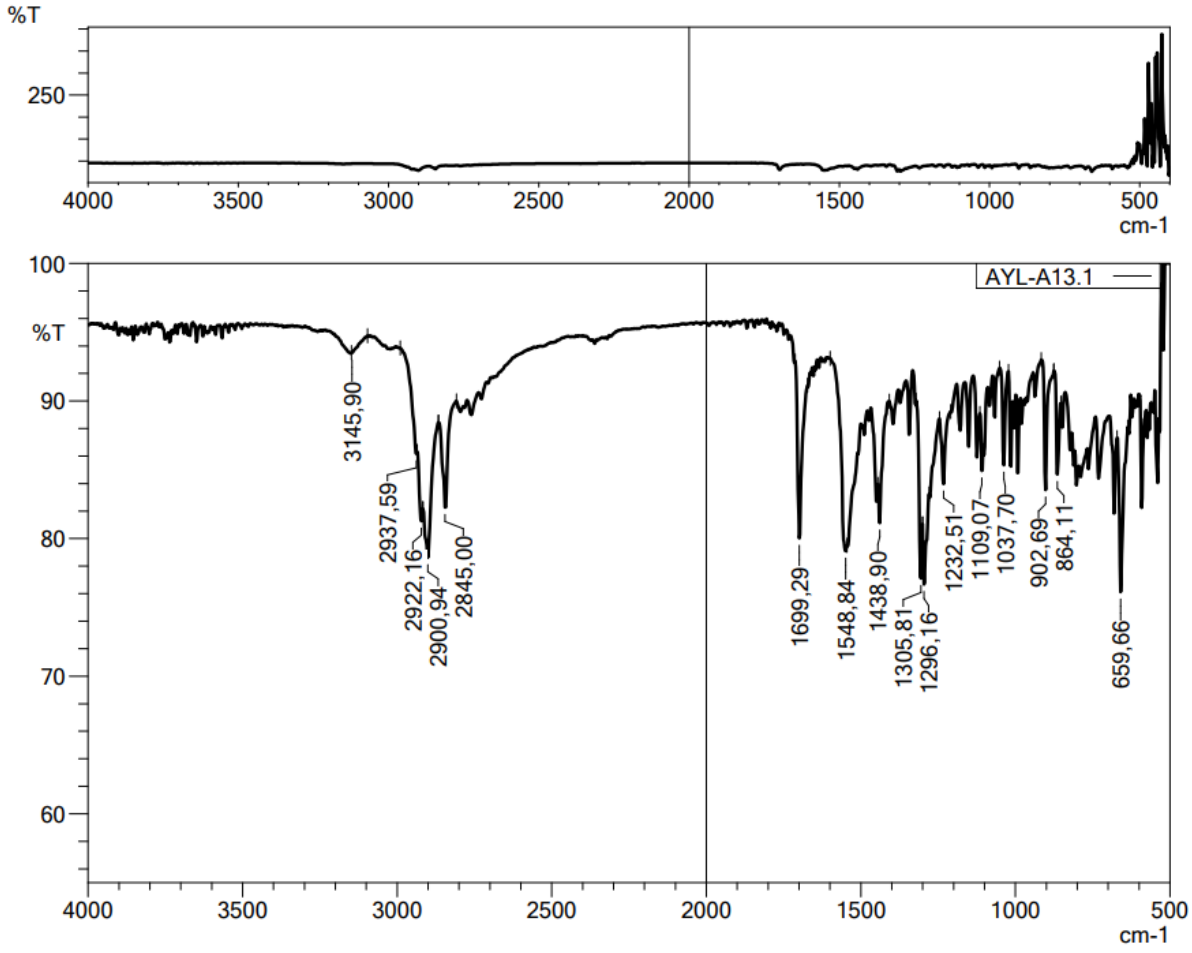

Figure 5.41. *IR spectrum of compound* ***3h***

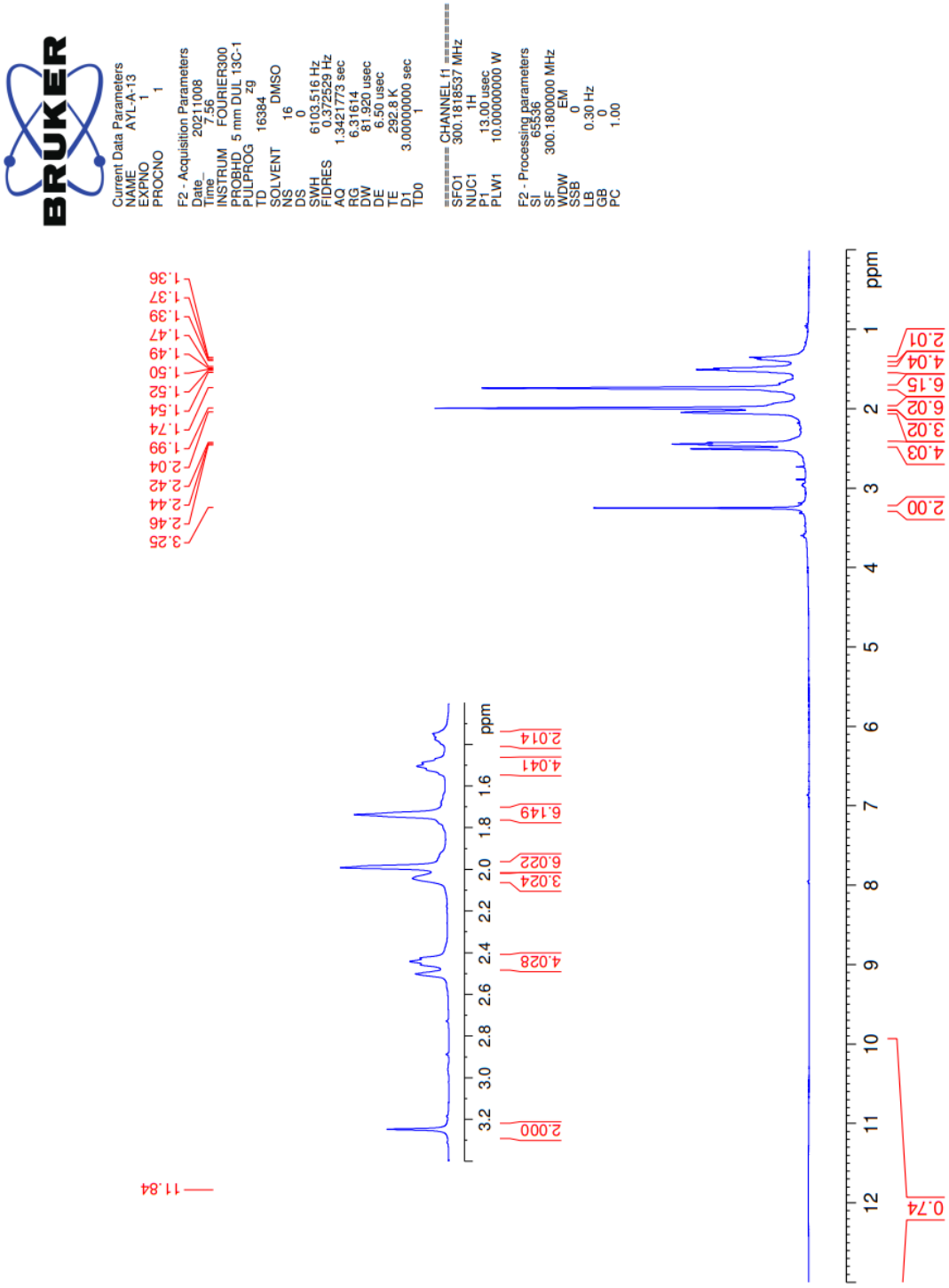

Figure 5.42. *^{1}H-NMR spectrum of compound **3h***

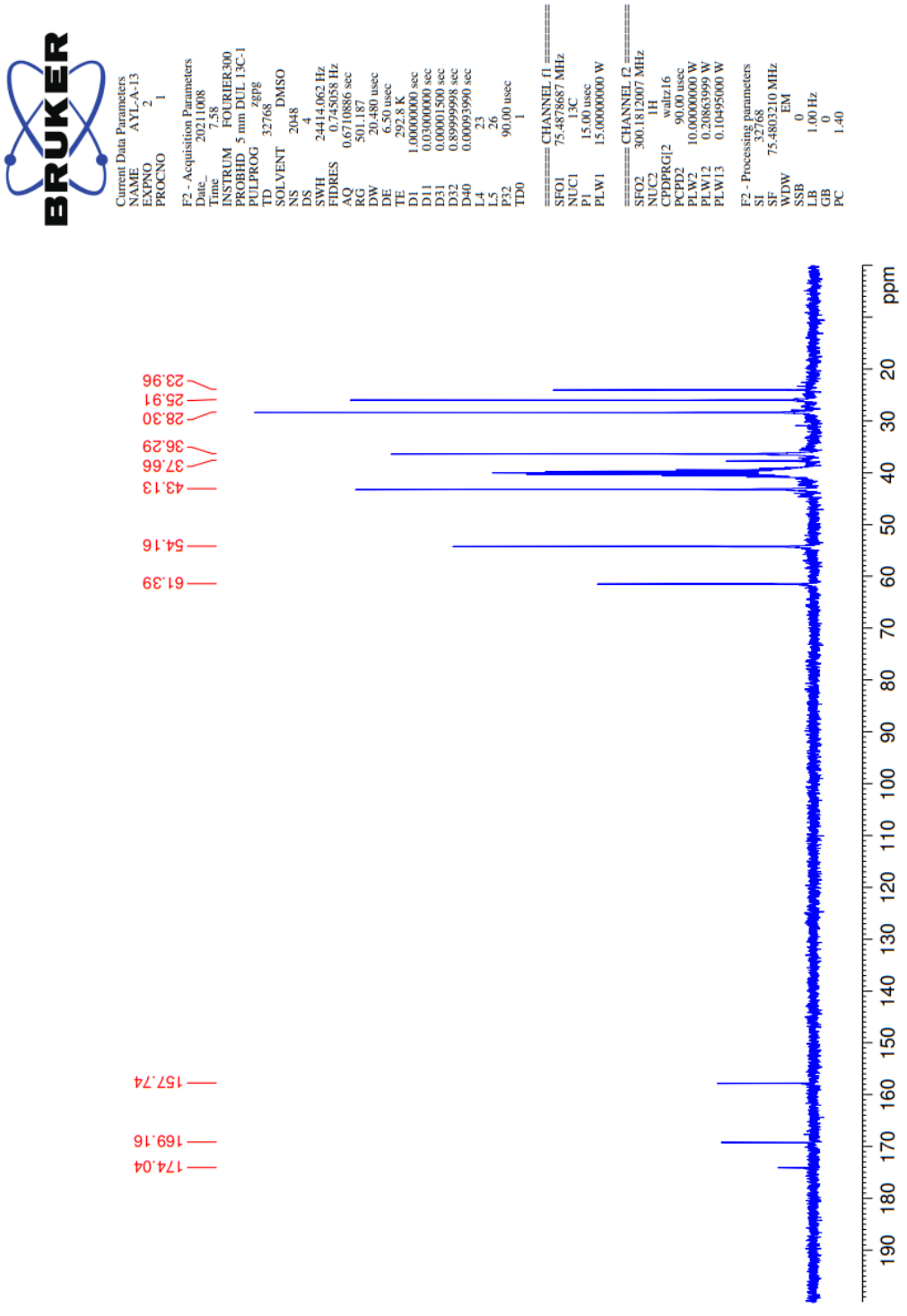

Figure 5.43. *^{13}C-NMR spectrum of compound **3h***

Elmt	Val.	Min	Max	Elmt	Val.	Min	Max	Elmt	Val.	Min	Max	Elmt	Val.	Min	Max	Use Adduct
H	1	10	40	O	2	0	5	S	2	1	1	Ru	2	0	0	H
C	4	9	40	F	1	0	0	Cl	1	0	1	Pd	2	0	0	
N	3	0	10	P	3	0	0	Br	1	0	0	I	3	0	0	

Error Margin (ppm): 6
HC Ratio: unlimited
Max Isotopes: 3
MSn Iso RI (%): 10.00

DBE Range: 5.0 - 25.0
Apply N Rule: yes
Isotope RI (%): 1.00
MSn Logic Mode: AND

Electron Ions: both
Use MSn Info: yes
Isotope Res: 9000
Max Results: 150

Event#: 1 MS(E+) Ret. Time : 3.720 Scan# : 559

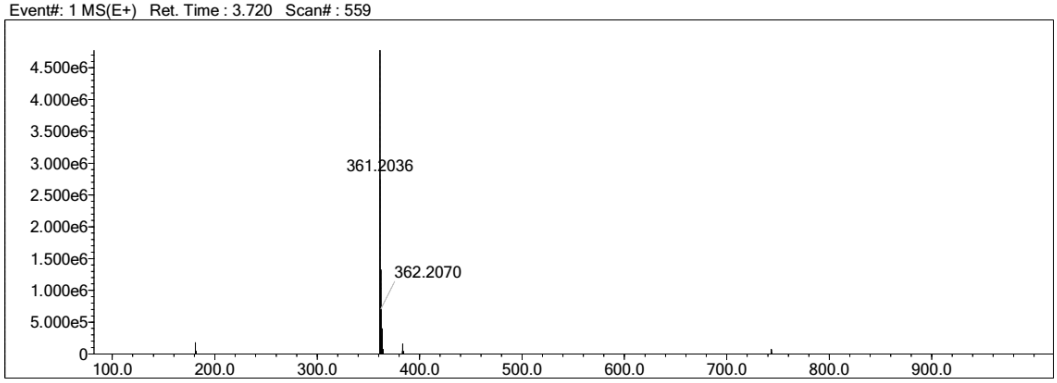

Measured region for 361.2036 m/z

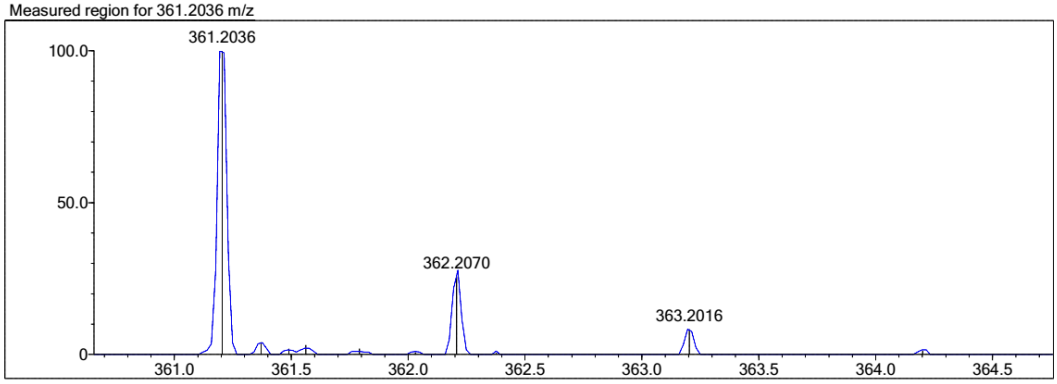

C19 H28 N4 O S [M+H]+ : Predicted region for 361.2057 m/z

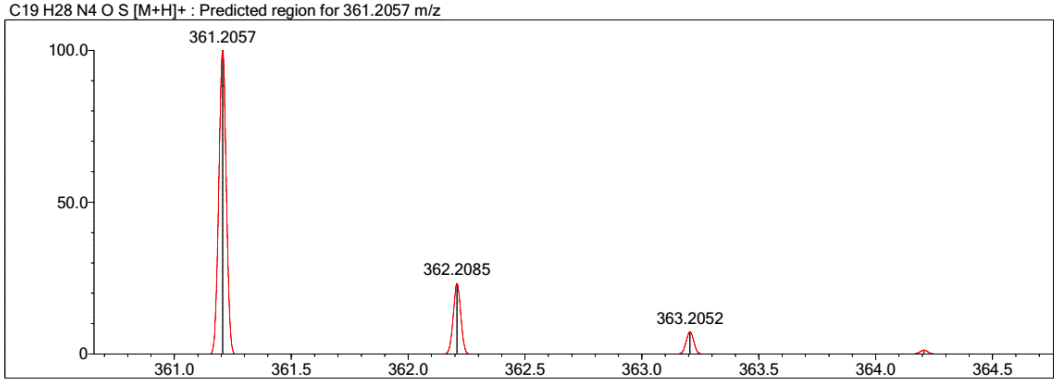

Rank	Score	Formula (M)	Ion	Meas. m/z	Pred. m/z	Df. (mDa)	Df. (ppm)	Iso	DBE
1	72.23	C19 H28 N4 O S	[M+H]+	361.2036	361.2057	-2.1	-5.81	88.19	8.0

Figure 5.44. *HR-MS of compound **3h***

5.1.4.9. N-(5-(Adamantan-1-yl)-1,3,4-thiadiazol-2-yl)-2-morpholinoacetamide (3i)

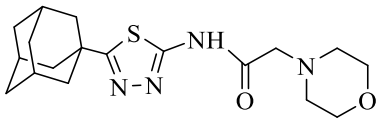

Figure 5.45. *Molecular structure of compound* ***(3i)***

It was synthesized according to method D. Yield: 89 %. Physical appearance: light yellow. Experimental m.p.: 206-207 ˚C.

IR (ATR) υ_{max} (cm^{-1}): 3163 (N-H stretching), 2900-2845 (sp^3 C-H stretching), 1705 (C=O stretching), 1548-1444 (aromatic C=N stretching), 1301 (C-N stretching), 1112 (C-O stretching).

^{1}H-NMR (300 MHz) (DMSO-*d*$_6$) δ (ppm): 1.72 (6H, s, adamantane-H), 1.97 (6H, s, adamantane-H), 2.01 (3H, s, adamantane-H), 2.49 (4H, br-s, morpholine's $H_{3,5}$), 3.30 (2H, s, CO-$\underline{CH_2}$), 3.57 (4H, br-s, morpholine's $H_{2,6}$), 12.00 (1H, br-s, $\underline{N\text{-}H}$).

^{13}C-NMR (75 MHz) (DMSO-*d*$_6$) δ (ppm): 28.3 (adamantane), 36.28 (adamantane), 37.63 (adamantane), 43.12 (adamantane), 53.3 (morpholine's $\underline{C_{3,5}}$), 60.75 (CO-$\underline{CH_2}$), 66.55 (morpholine's $\underline{C_{2,6}}$), 157.66 (thiadiazole), 168.71 (thiadiazole), 174.04 (CO).

HRMS (ESI) (m/z) $[M+1]^+$: for $C_{18}H_{26}N_4O_2S$ calculated: 363.1849; found: 363.1831.

DOPNALAB

	Item	Value
	Acquired Date&Time	9.06.2022 14:23:16
	Acquired by	System Administrator
	Filename	C:\Users\dopnalab\Desktop\MASAÜSTÜ\LEYLA YURTDAŞ\AYL-A-B\AYL-A15.1.ispd
	Spectrum name	AYL-A15.1
	Sample name	AYL-A15
	Sample ID	
	Option	
	Comment	
	No. of Scans	15
	Resolution	4 [cm-1]
	Apodization	Happ-Genzel

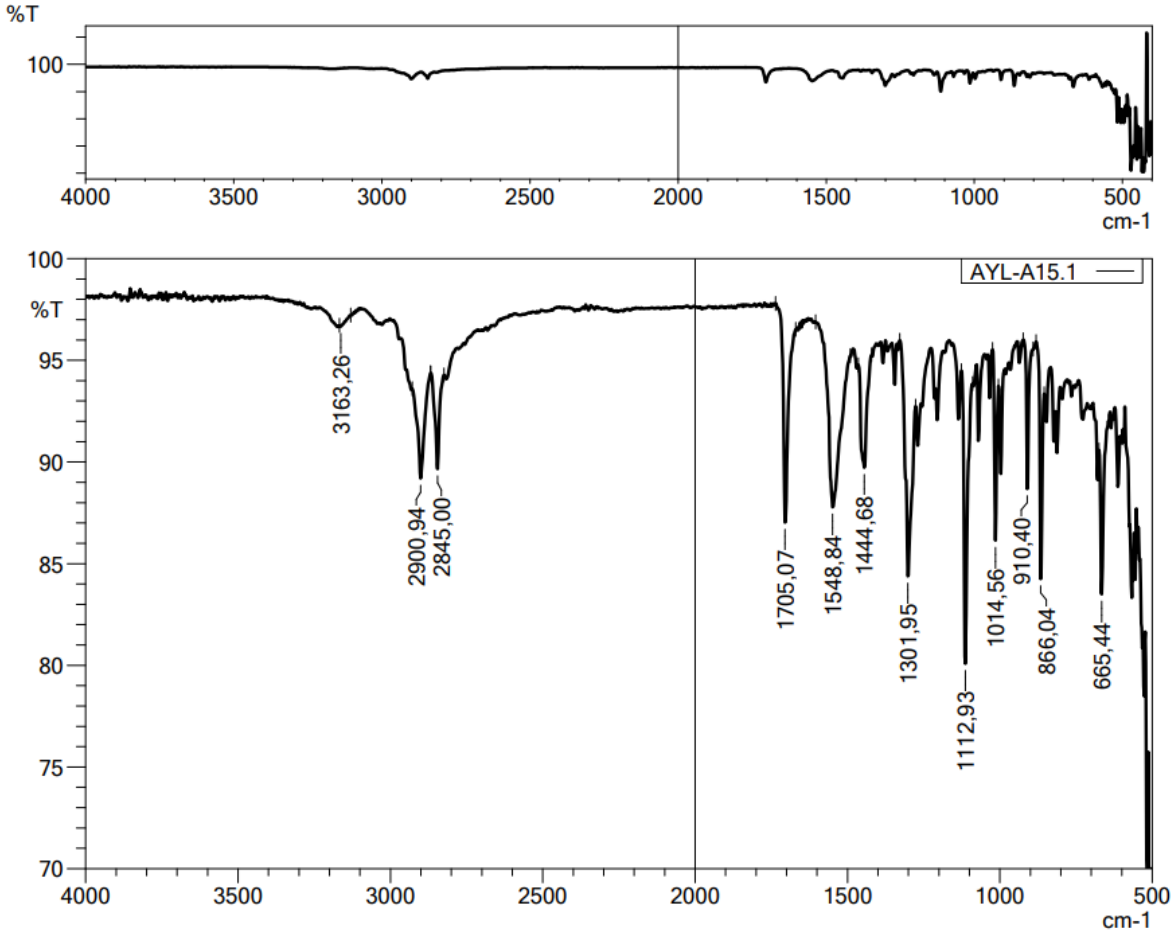

Figure 5.46. *IR spectrum of compound* ***3i***

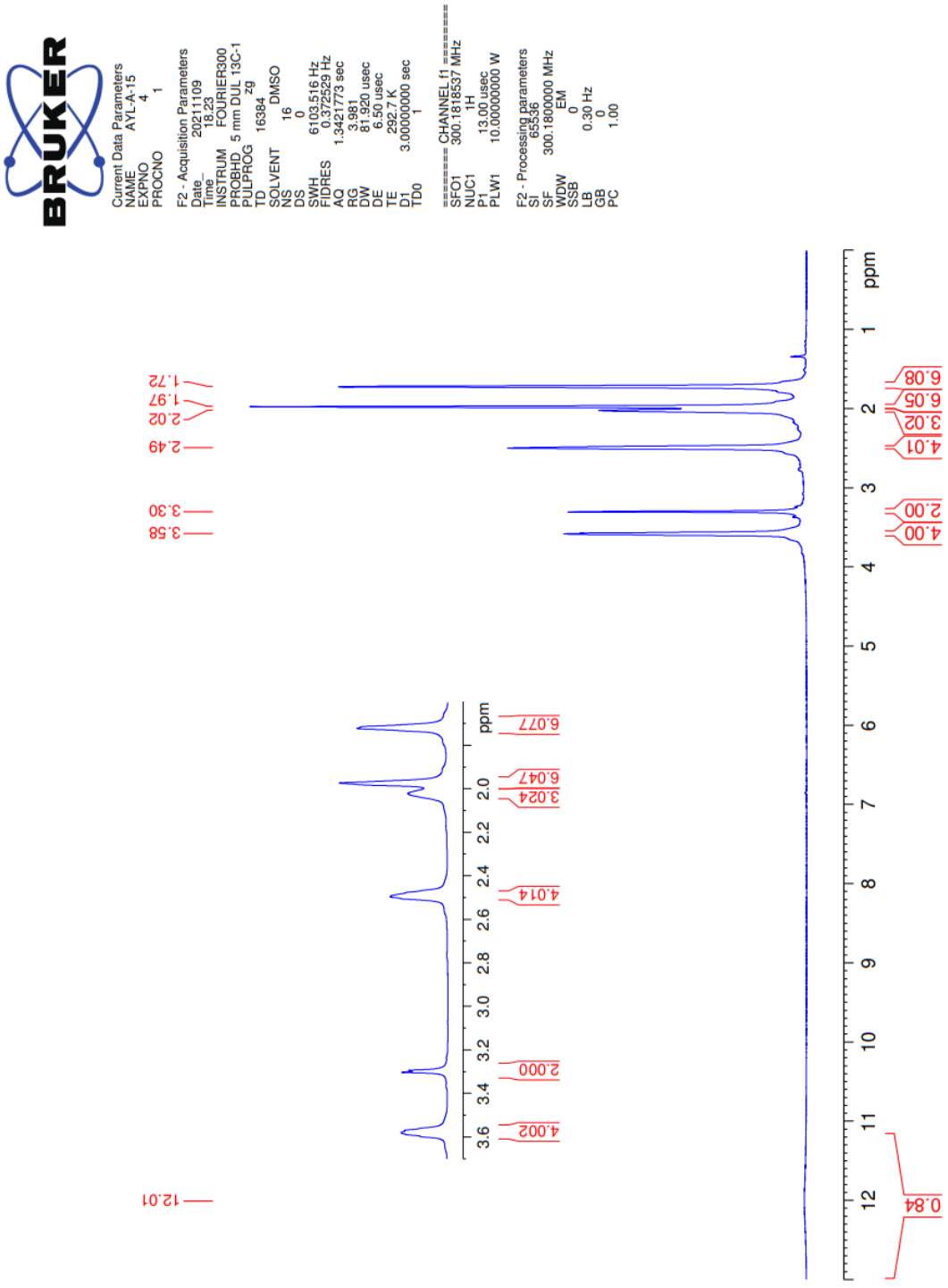

Figure 5.47. *[1]H-NMR spectrum of compound **3i***

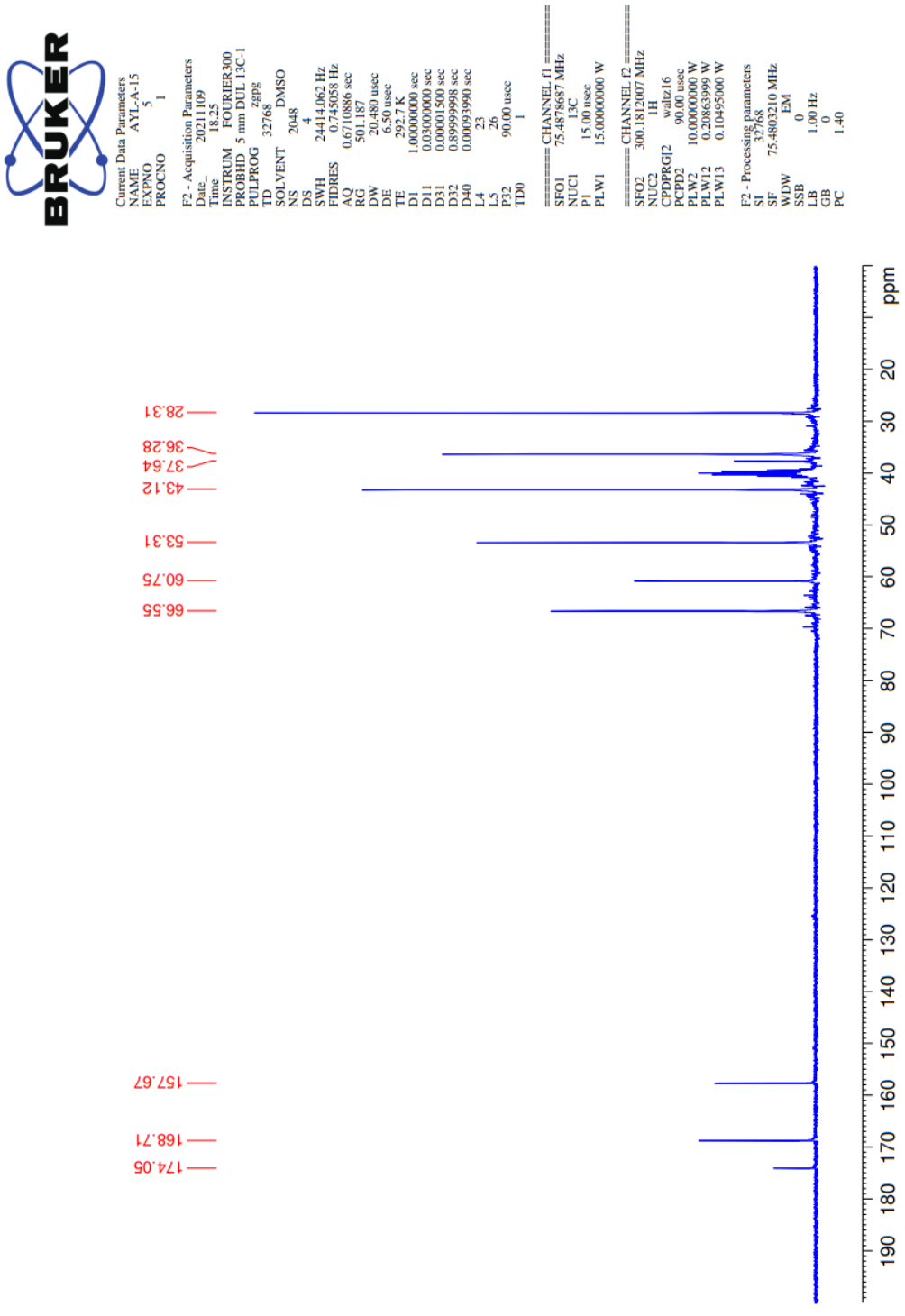

Figure 5.48. *^{13}C-NMR spectrum of compound **3i***

Elmt	Val.	Min	Max	Elmt	Val.	Min	Max	Elmt	Val.	Min	Max	Elmt	Val.	Min	Max	Use Adduct
H	1	10	40	O	2	0	5	S	2	1	1	Ru	2	0	0	H
C	4	9	40	F	1	0	0	Cl	1	0	1	Pd	2	0	0	
N	3	0	10	P	3	0	0	Br	1	0	0	I	3	0	0	

Error Margin (ppm): 6
HC Ratio: unlimited
Max Isotopes: 3
MSn Iso RI (%): 10.00

DBE Range: 5.0 - 25.0
Apply N Rule: yes
Isotope RI (%): 1.00
MSn Logic Mode: AND

Electron Ions: both
Use MSn Info: yes
Isotope Res: 9000
Max Results: 150

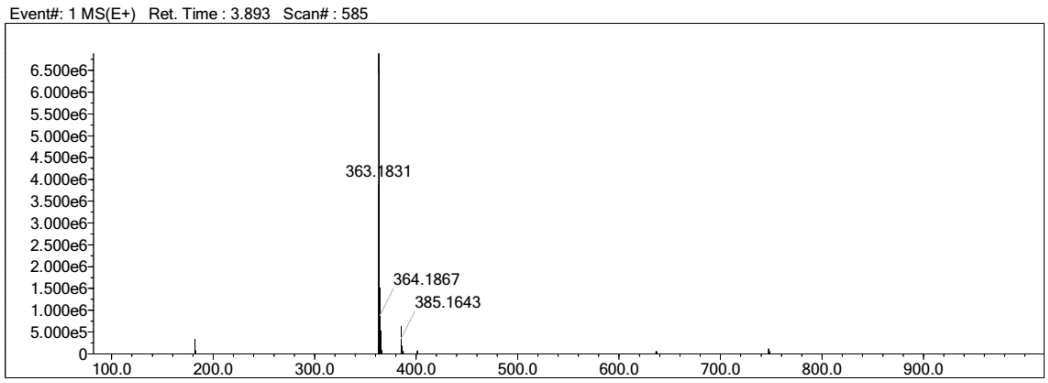

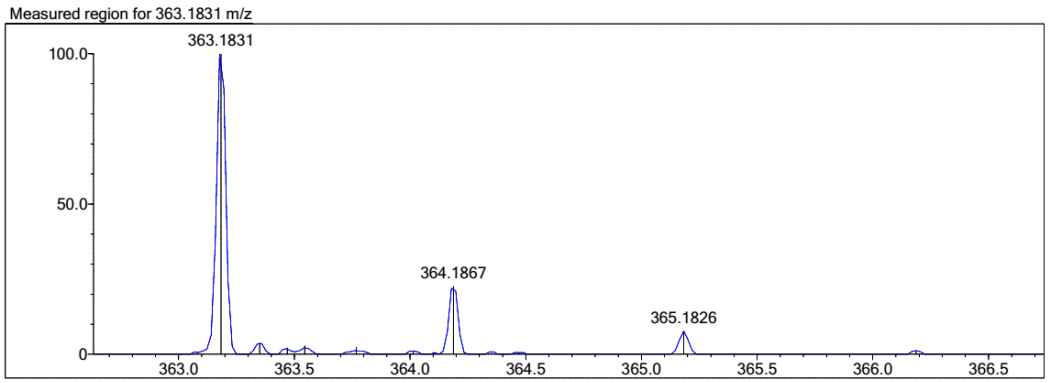

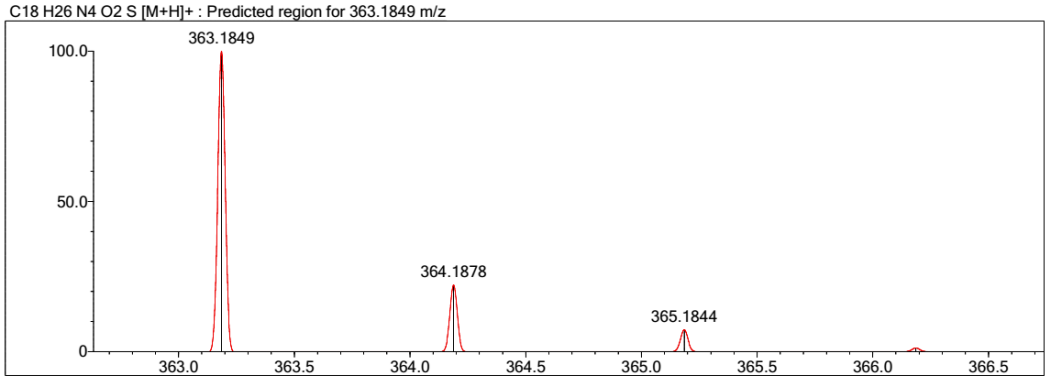

Rank	Score	Formula (M)	Ion	Meas. m/z	Pred. m/z	Df. (mDa)	Df. (ppm)	Iso	DBE
2	85.08	C18 H26 N4 O2 S	[M+H]+	363.1831	363.1849	-1.8	-4.96	94.43	8.0

Figure 5.49. *HR-MS of compound **3i***

5.1.4.10. N-(5-(Adamantan-1-yl)-1,3,4-thiadiazol-2-yl)-2-thiomorpholinoacetamide (3j)

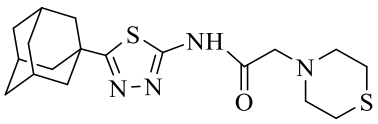

Figure 5.50. *Molecular structure of compound **(3j)***

It was synthesized according to method D. Yield: 89 %. Physical appearance: light brown. Experimental m.p.: 196-197 ˚C.

IR (ATR) υ_{max} (cm^{-1}): 3172 (N-H stretching), 2931-2846 (sp^3 C-H stretching), 1703 (C=O stretching), 1517-1452 (aromatic C=N stretching), 1300-1286 (C-N stretching).

^{1}H-NMR (300 MHz) (DMSO-*d*$_6$) δ (ppm): 1.72 (6H, s, adamantane's $H_{6,8,9}$), 1.97 (6H, s, adamantane- H), 2.02 (3H, s, adamantane-H), 2.60 (4H, br-s, thiomorpholine-$H_{2,6}$), 2.73 (4H, br-s, thiomorpholine- $H_{3,5}$), 3.32 (2H, s, CO-$\underline{CH_2}$), 11.88 (H, br-s, $\underline{N\text{-}H}$).

^{13}C-NMR (75 MHz) (DMSO-*d*$_6$) δ (ppm): 27.95 (thiomorpholine's $\underline{C_{2,6}}$), 28.7 (adamantane), 36.69 (adamantane), 38.07 (adamantane), 43.53 (adamantane), 54.95 (thiomorpholine's $\underline{C_{3,5}}$), 61.61 (CO-$\underline{CH_2}$), 158.06 (thiadiazole), 169.53 (thiadiazole), 174.51 (CO).

HRMS (ESI) (m/z) $[M+1]^+$: for $C_{18}H_{26}N_4OS_2$ calculated: 379.1621; found: 379.1611.

DOPNALAB

	Item	Value
	Acquired Date&Time	9.06.2022 14:29:13
	Acquired by	System Administrator
	Filename	C:\Users\dopnalab\Desktop\MASAÜSTÜ\LEYLA YURTDAŞ\AYL-A-B\AYL-A16.1.ispd
	Spectrum name	AYL-A16.1
	Sample name	AYL-A16
	Sample ID	
	Option	
	Comment	
	No. of Scans	15
	Resolution	4 [cm-1]
	Apodization	Happ-Genzel

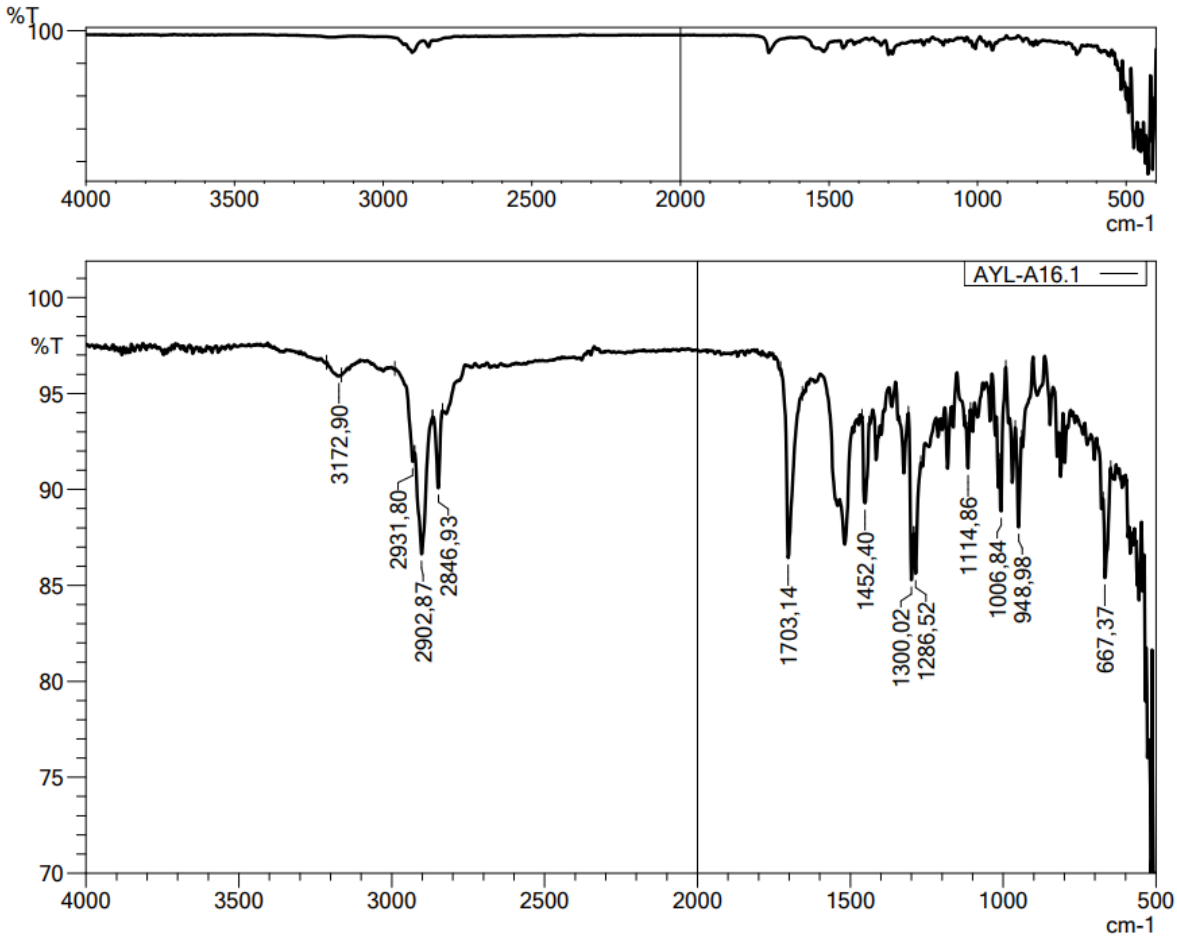

Figure 5.51. *IR spectrum of compound* ***3j***

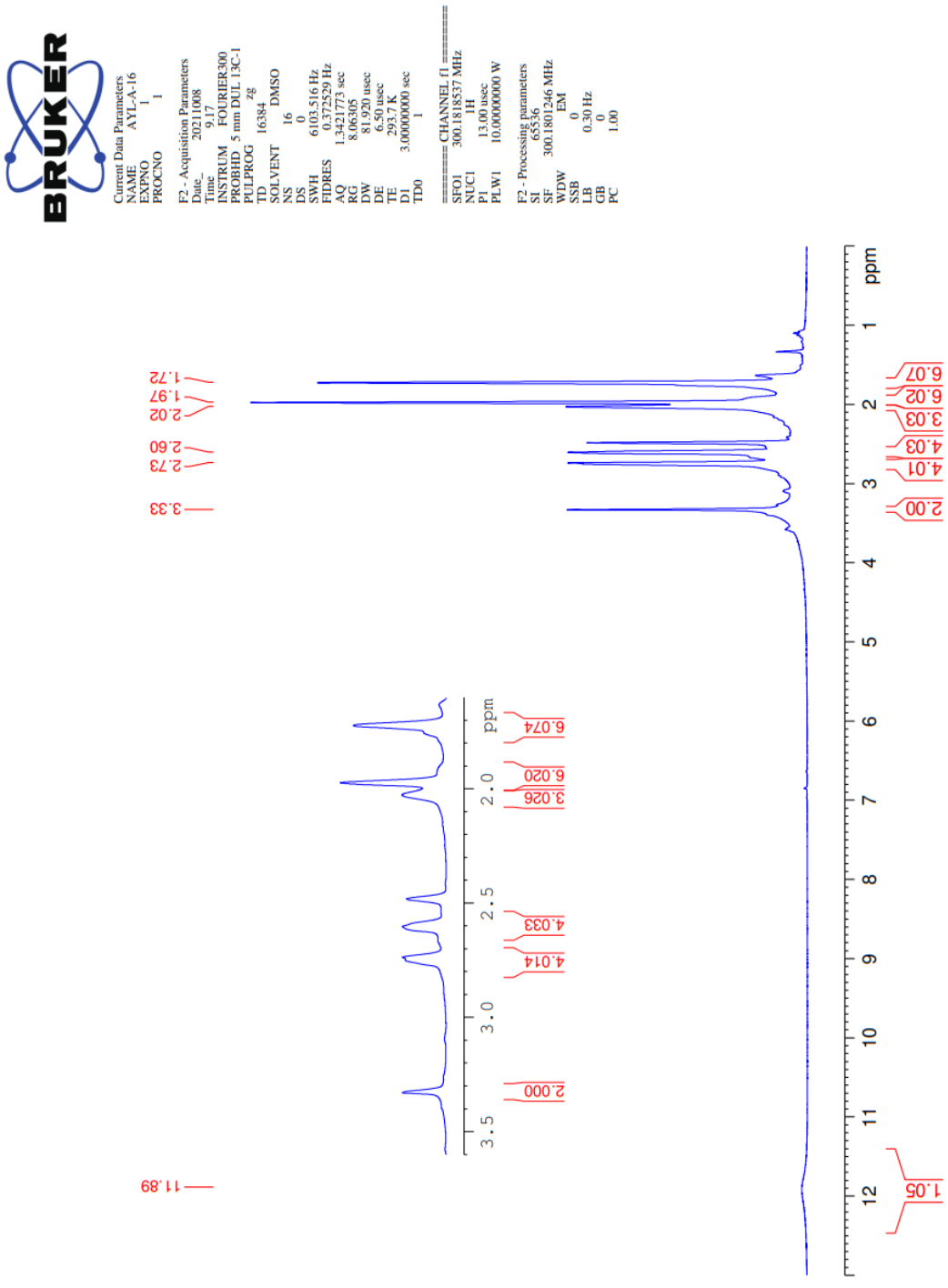

Figure 5.52. *[1]H-NMR spectrum of compound **3j***

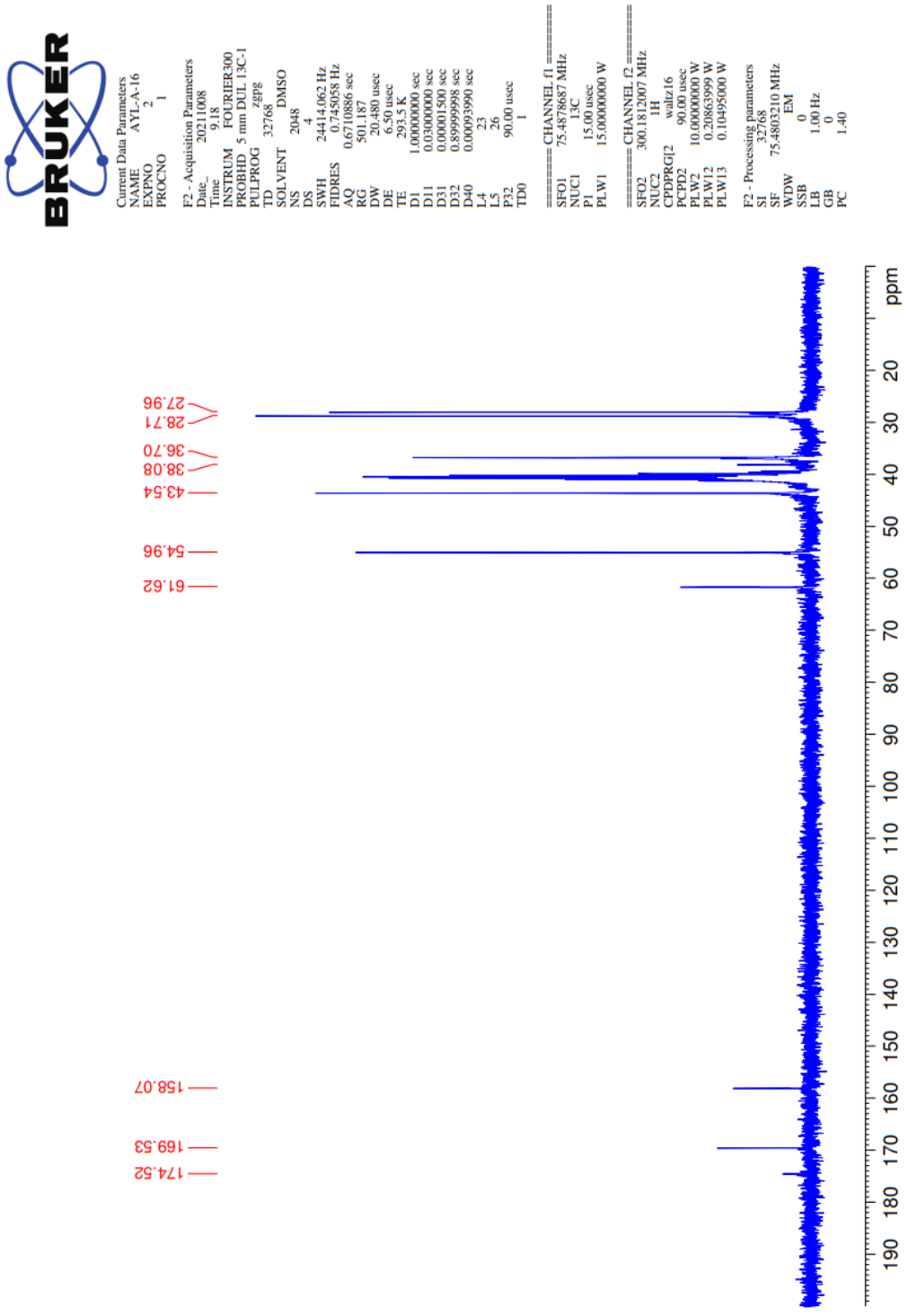

Figure 5.53. *^{13}C-NMR spectrum of compound **3j***

Elmt	Val.	Min	Max	Elmt	Val.	Min	Max	Elmt	Val.	Min	Max	Elmt	Val.	Min	Max	Use Adduct
H	1	10	40	O	2	0	5	S	2	1	2	Ru	2	0	0	H
C	4	9	40	F	1	0	0	Cl	1	0	1	Pd	2	0	0	
N	3	0	10	P	3	0	0	Br	1	0	0	I	3	0	0	

Error Margin (ppm): 5
HC Ratio: unlimited
Max Isotopes: 3
MSn Iso RI (%): 10.00

DBE Range: 5.0 - 25.0
Apply N Rule: yes
Isotope RI (%): 1.00
MSn Logic Mode: AND

Electron Ions: both
Use MSn Info: yes
Isotope Res: 9000
Max Results: 150

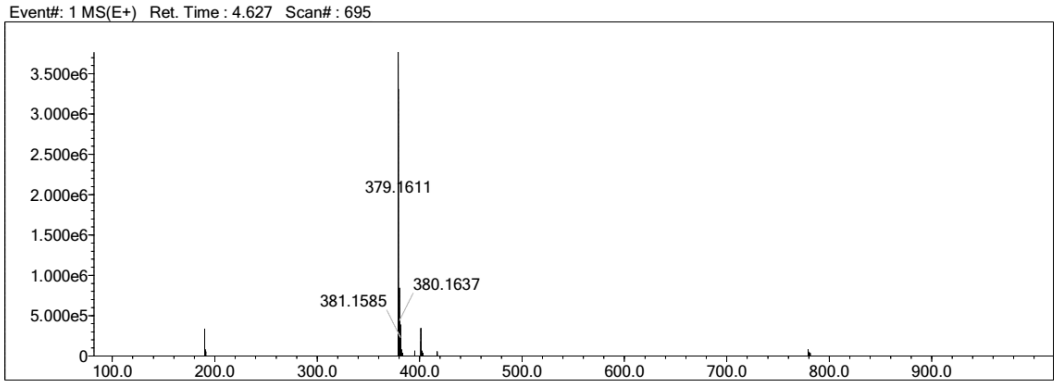

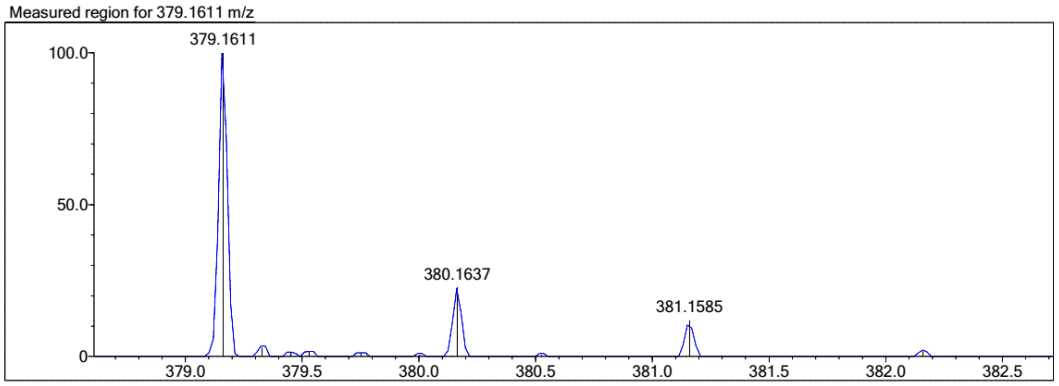

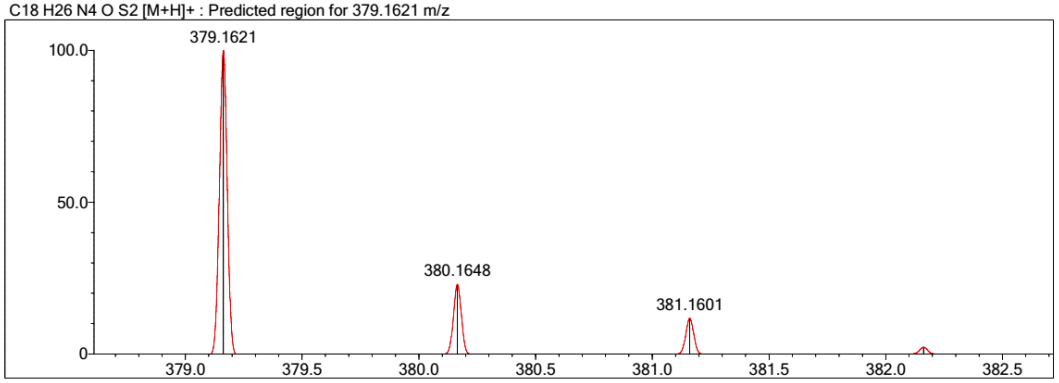

Rank	Score	Formula (M)	Ion	Meas. m/z	Pred. m/z	Df. (mDa)	Df. (ppm)	Iso	DBE
1	79.66	C18 H26 N4 O S2	[M+H]+	379.1611	379.1621	-1.0	-2.64	83.06	8.0

Figure 5.54. *HR-MS of compound **3j***

5.1.5. Synthesis of *N*-(5-(adamantan-1-yl)-1,3,4-thiadiazol-2-yl)-2-substituted-propanamide derivatives (4a-4g)

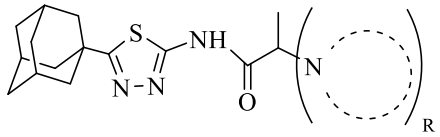

Figure 5.55. *General molecular structure of derivatives (**4a-4g**)*

5.1.5.1. N-(5-(Adamantan-1-yl)-1,3,4-thiadiazol-2-yl)-2-(4-(pyrimidin-2-yl)piperazin-1-yl)propanamide (4a)

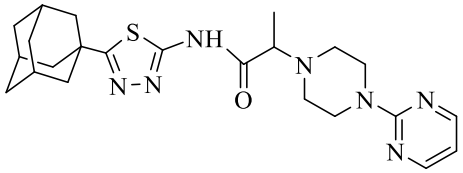

Figure 5.56. *Molecular structure of compound* ***(4a)***

It was synthesized according to method E. Yield: 67 %. Physical appearance: white powder. Experimental m.p.: 115-116 ˚C.

IR (ATR) υ_{max} (cm^{-1}): 3149 (N-H stretching), 2902- 2848 (sp^3 C-H stretching), 1695 (C=O stretching), 1585-1446 (aromatic C=C and C=N stretching), 1163 (C-N stretching).

^{1}H-NMR (300 MHz) (DMSO-*d*$_6$) δ (ppm): 1.20 (3H, br-s, CH-$\underline{CH_3}$), 1.71 (6H, s, adamantane-H), 1.97 (6H, adamantane-H), 2.01 (3H, s, adamantane-H), 2.55 (4H, br-s, piperazine's $H_{2,6}$), 3.56 (1H, q, J_1= 5.41 Hz, J_2= 10.56 Hz, $\underline{CH}$-CH_3), 3.72 (4H,s, piperazine-$H_{3,5}$), 6.59 (1H, t, J= 4.05 Hz, pyrimidine's H_5), 8.31 (2H, br-s, pyrimidine's $H_{4,6}$), 12.64 (H, br-s, $\underline{N\text{-}H}$).

^{13}C-NMR (75 MHz) (DMSO-*d*$_6$) δ (ppm): 13.83 (CH-$\underline{CH_3}$), 28.74 (adamantane), 36.74 (adamantane), 38.07 (adamantane), 43.57 (adamantane), 44.43 (piperazine), 49.57 (piperazine), 62.73 (CO-$\underline{CH}$), 110.91 (pyrimidine), 158.35 (thiadiazole), 158.78 (pyrimidine), 161.98 (pyrimidine), 171.93 (thiadiazole), 174.45 (CO).

HRMS (ESI) (m/z) $[M+1]^+$: for $C_{23}H_{31}N_7OS$ calculated: 454.2384; found: 454.2362.

DOPNALAB

	Item	Value
	Acquired Date&Time	8.06.2022 13:45:22
	Acquired by	System Administrator
	Filename	C:\Users\dopnalab\Desktop\MASAÜSTÜ\LEYLA YURTDAŞ\AYL-A-B\AYL-B1.1.ispd
	Spectrum name	AYL-B1.1
	Sample name	AYL-B1
	Sample ID	
	Option	
	Comment	
	No. of Scans	15
	Resolution	4 [cm-1]
	Apodization	Happ-Genzel

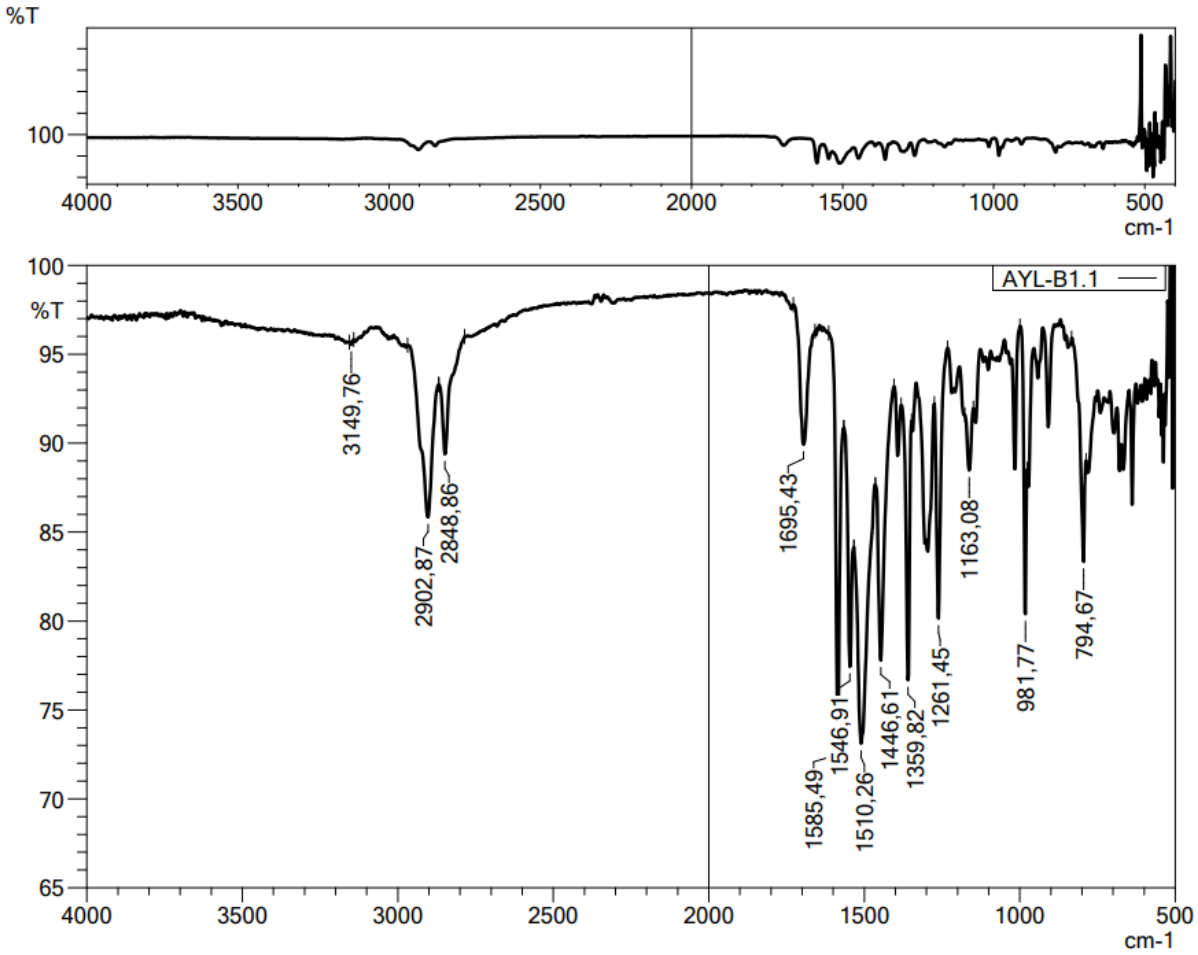

Figure 5.57. *IR spectrum of compound* ***4a***

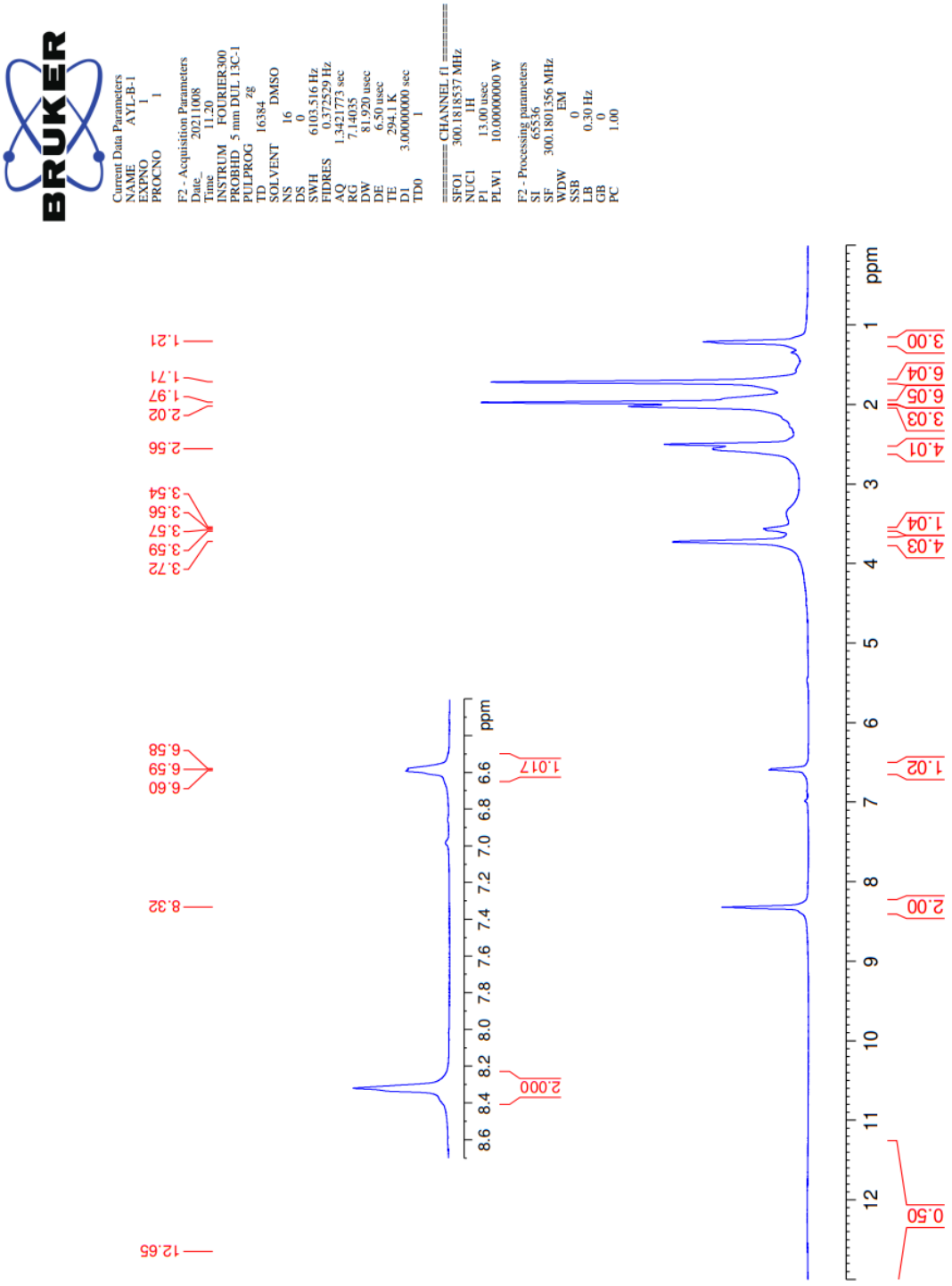

Figure 5.58. *[1]H-NMR spectrum of compound **4a***

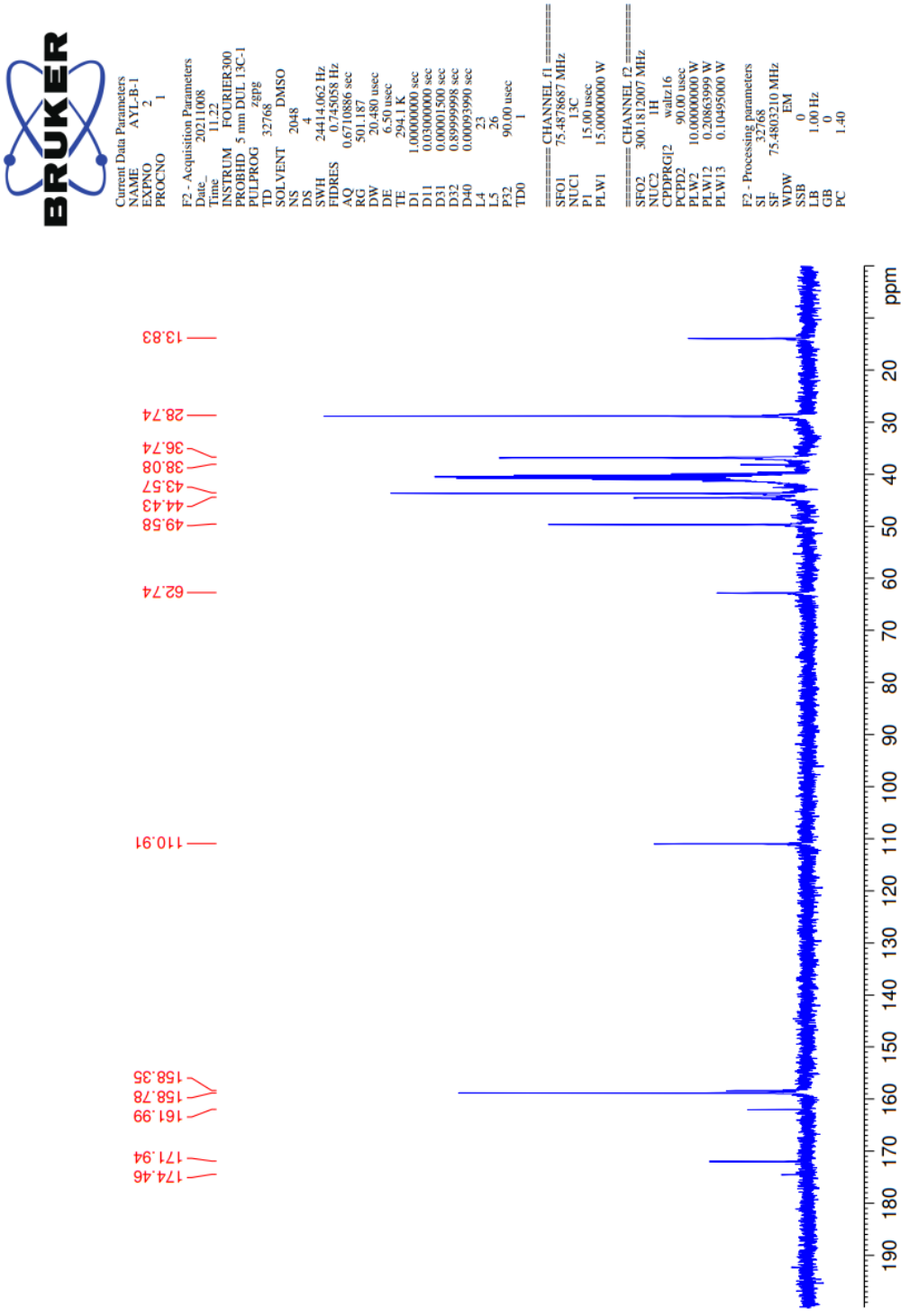

Figure 5.59. *^{13}C-NMR spectrum of compound **4a***

Elmt	Val.	Min	Max	Elmt	Val.	Min	Max	Elmt	Val.	Min	Max	Elmt	Val.	Min	Max	Use Adduct
H	1	10	40	O	2	0	5	S	2	1	1	Ru	2	0	0	H
C	4	9	40	F	1	0	0	Cl	1	0	1	Pd	2	0	0	
N	3	0	10	P	3	0	0	Br	1	0	0	I	3	0	0	

Error Margin (ppm): 5
HC Ratio: unlimited
Max Isotopes: 3
MSn Iso RI (%): 10.00

DBE Range: 5.0 - 25.0
Apply N Rule: yes
Isotope RI (%): 1.00
MSn Logic Mode: AND

Electron Ions: both
Use MSn Info: yes
Isotope Res: 9000
Max Results: 150

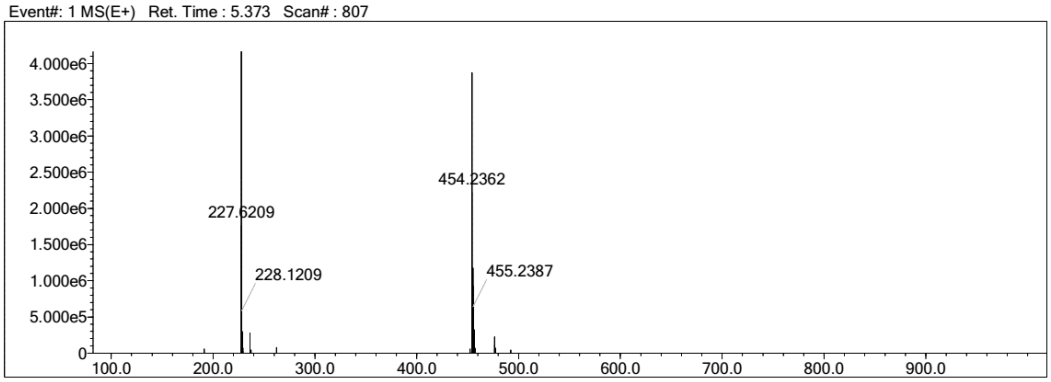

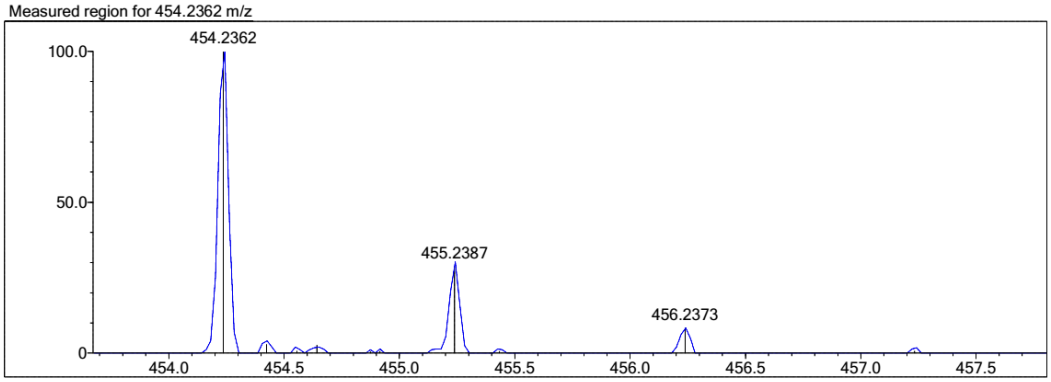

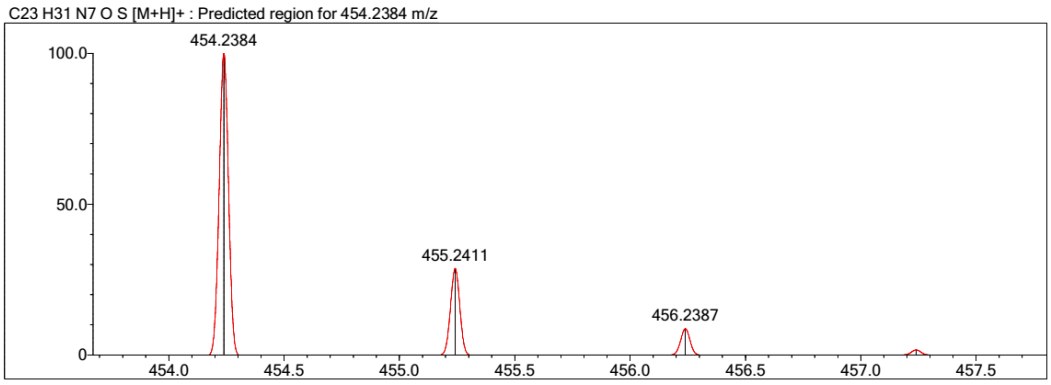

Rank	Score	Formula (M)	Ion	Meas. m/z	Pred. m/z	Df. (mDa)	Df. (ppm)	Iso	DBE
2	80.85	C23 H31 N7 O S	[M+H]+	454.2362	454.2384	-2.2	-4.84	89.44	12.0

Figure 5.60. *HR-MS of compound* ***4a***

5.1.5.2. N-(5-(Adamantan-1-yl)-1,3,4-thiadiazol-2-yl)-2-(4-(pyridin-2-yl)piperazin-1-yl)propanamide (4b)

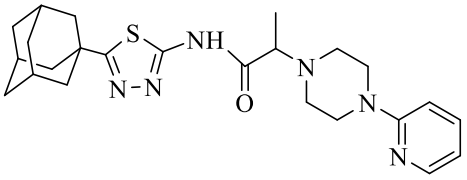

Figure 5.61. *Molecular structure of compound* ***(4b)***

It was synthesized according to method E. Yield: 72 %. Physical appearance: white powder. Experimental m.p.: 240-241 ˚C.

IR (ATR) υ_{max} (cm^{-1}): 3001 (N-H stretching), 2902-2821 (sp^3 C-H stretching), 1697 or 1591 (C=O stretching), 1554 -1435 (aromatic C=C and C=N stretching), 1242 (C-N stretching).

^{1}H-NMR (300 MHz) (DMSO-*d*$_6$) δ (ppm): 1.18 (3H, d, *J*= 6.73 Hz, -CH-$\underline{CH_3}$), 1.72 (6H, s, adamantane-H), 1.95 (6H, s, adamantane-H), 2.01 (3H, s, adamantane-H), 2.58 (4H, t, *J*= 6.15 Hz, piperazine's $H_{2,6}$), 3.30 (1H, q, J_1= 6.59 Hz, J_2= 14.38Hz, $\underline{CH}$-CH_3), 3.43 (4H, s, piperazine's $H_{3,5}$), 6.59 (H, t, *J*= 5.87 Hz, pyridine's H_5), 6.77 (H, d, *J*= 8.56 Hz, , pyridine's H_3), 7.48 (H, t, *J*= 6.91 Hz, pyridine's H_4), 8.07 (H, d, *J*= 4.53 Hz, pyridine's H_6).

^{13}C-NMR (75 MHz) (DMSO-*d*$_6$) δ (ppm): 15.02 (CH-$\underline{CH_3}$), 28.41 (adamantane), 36.53 (adamantane), 37.5 (adamantane), 43.31 (adamantane), 45.45 (piperazine), 49.47 (piperazine), 64.62 (CO-$\underline{CH}$), 107.42 (pyridine), 113.21 (pyridine), 137.86 (pyridine), 147.98 (pyridine), 159.53 (thiadiazole), 163.48 (pyridine), 171.37 (thiadiazole), 174.3 (CO).

HRMS (ESI) (m/z) $[M+1]^+$: for $C_{24}H_{32}N_6OS$ calculated: 453.2431; found: 453.2417.

DOPNALAB

	Item	Value
	Acquired Date&Time	8.06.2022 13:51:14
	Acquired by	System Administrator
	Filename	C:\Users\dopnalab\Desktop\MASAÜSTÜ\LEYLA YURTDAŞ\AYL-A-B\AYL-B2.1.ispd
	Spectrum name	AYL-B2.1
	Sample name	AYL-B2
	Sample ID	
	Option	
	Comment	
	No. of Scans	15
	Resolution	4 [cm-1]
	Apodization	Happ-Genzel

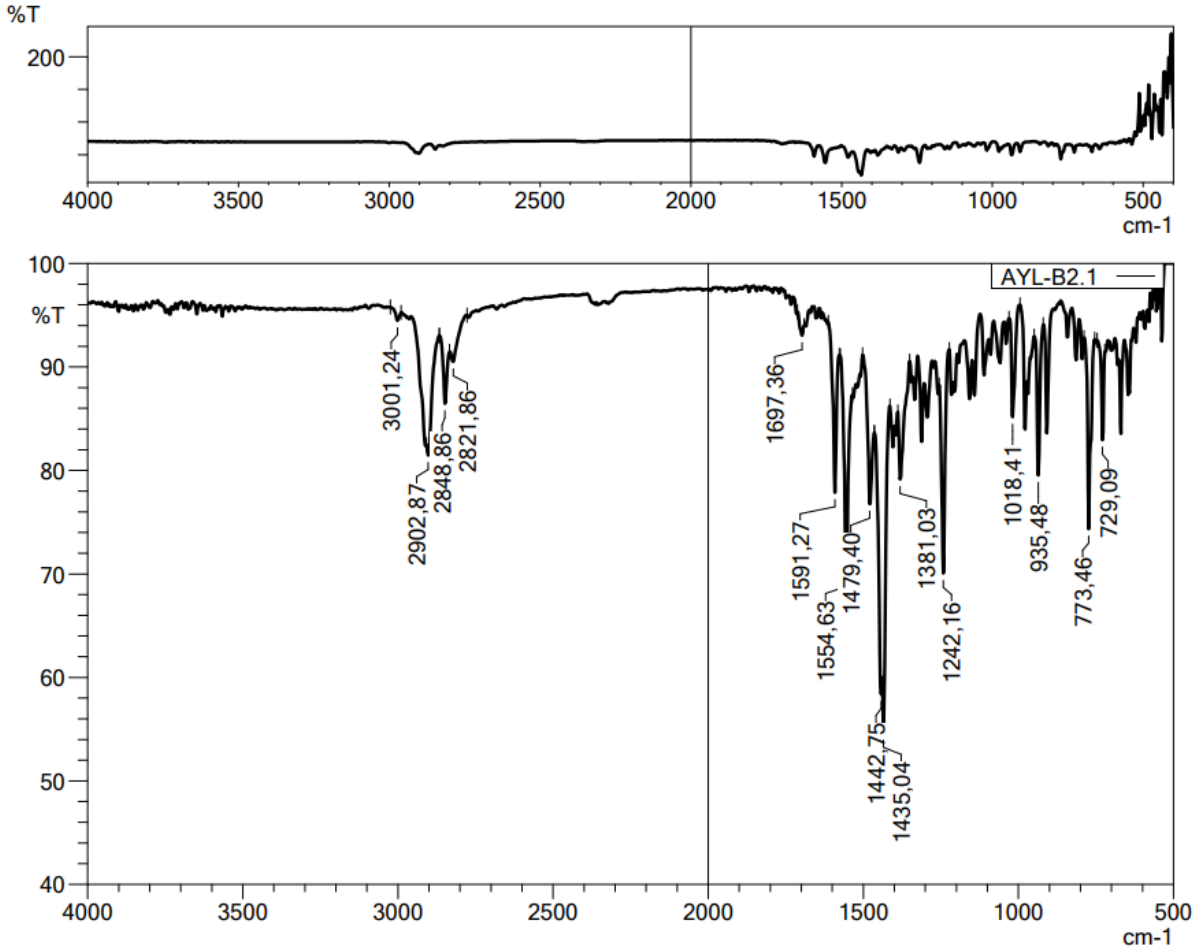

Figure 5.62. *IR spectrum of compound* ***4b***

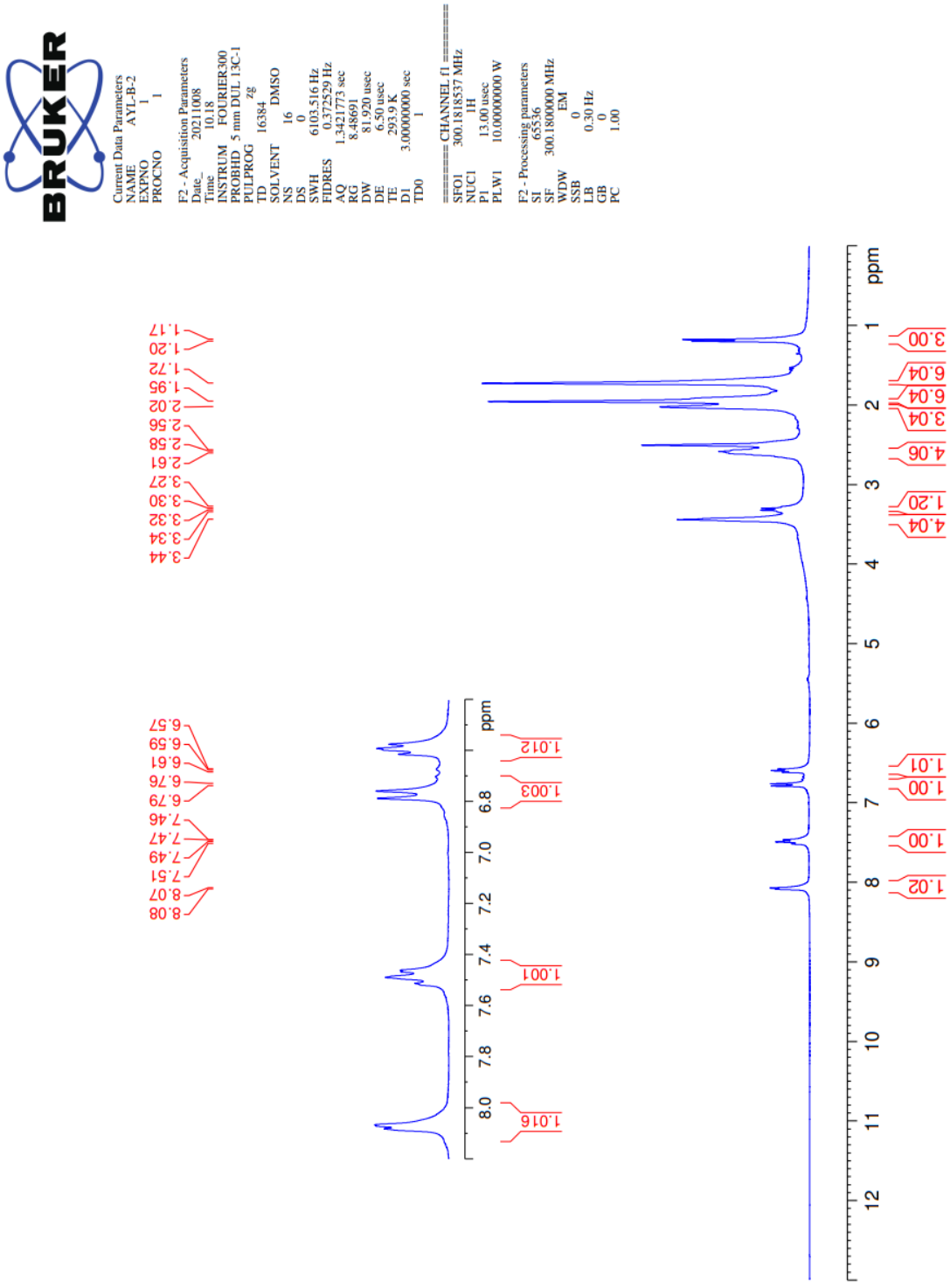

Figure 5.63. *[1]H-NMR spectrum of compound **4b***

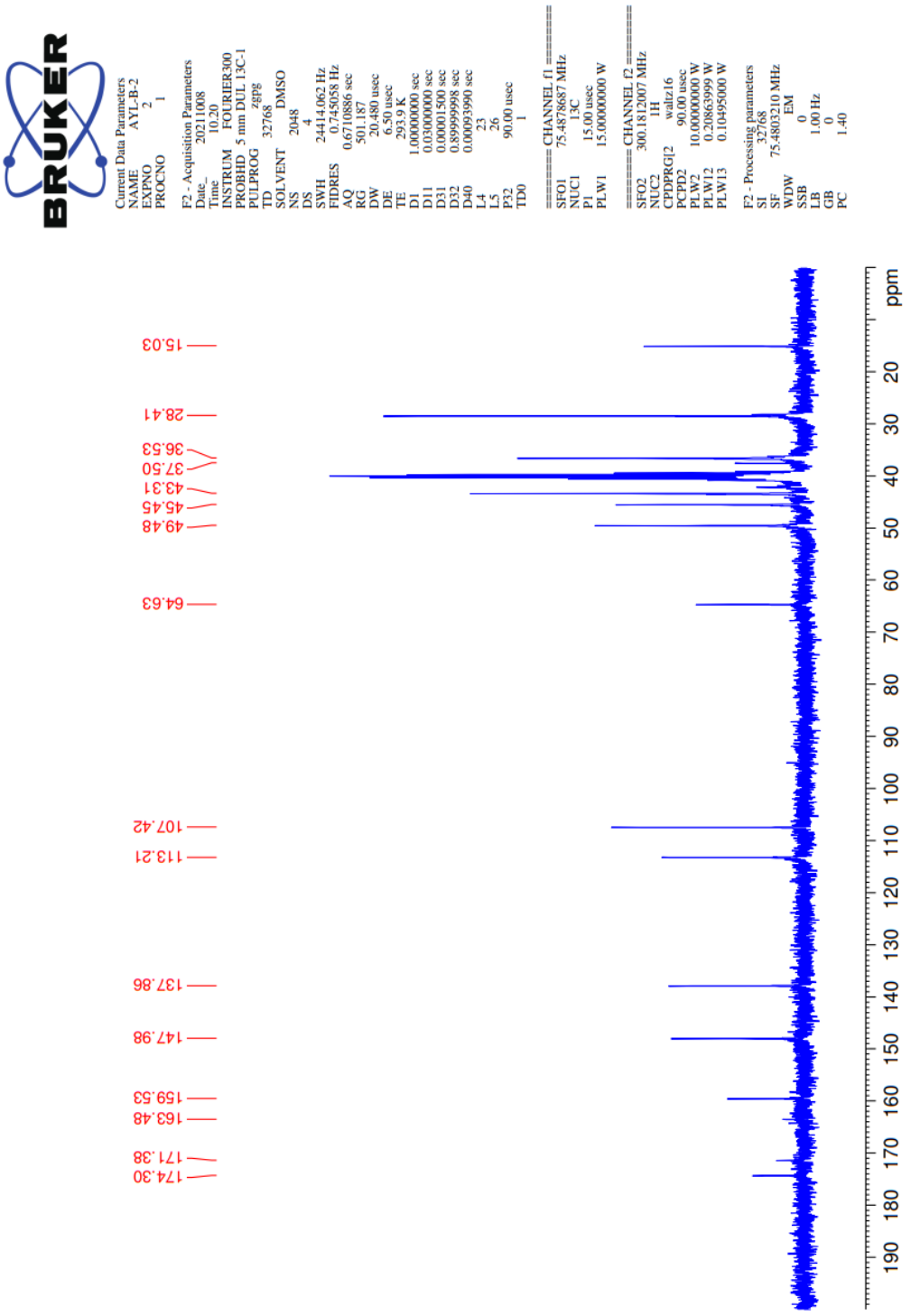

Figure 5.64. *^{13}C-NMR spectrum of compound **4b***

Elmt	Val.	Min	Max	Elmt	Val.	Min	Max	Elmt	Val.	Min	Max	Elmt	Val.	Min	Max	Use Adduct
H	1	10	40	O	2	0	5	S	2	1	1	Ru	2	0	0	H
C	4	9	40	F	1	0	0	Cl	1	0	1	Pd	2	0	0	
N	3	0	10	P	3	0	0	Br	1	0	0	I	3	0	0	

Error Margin (ppm): 5
HC Ratio: unlimited
Max Isotopes: 3
MSn Iso RI (%): 10.00

DBE Range: 5.0 - 25.0
Apply N Rule: yes
Isotope RI (%): 1.00
MSn Logic Mode: AND

Electron Ions: both
Use MSn Info: yes
Isotope Res: 9000
Max Results: 150

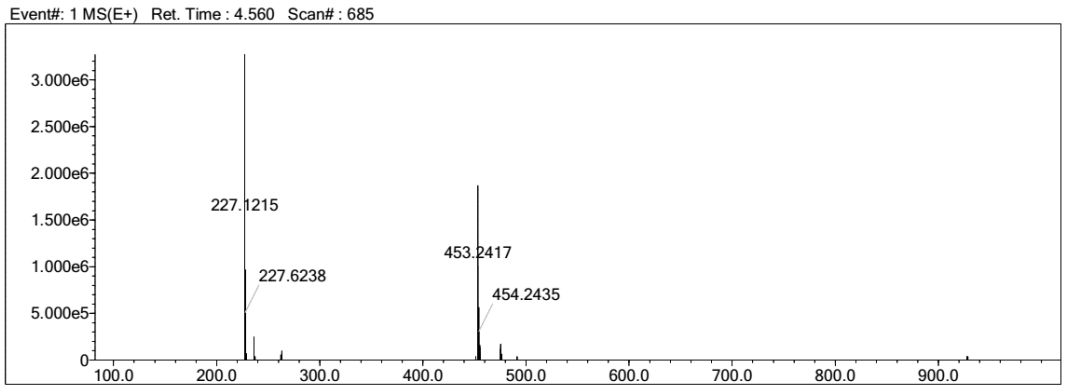

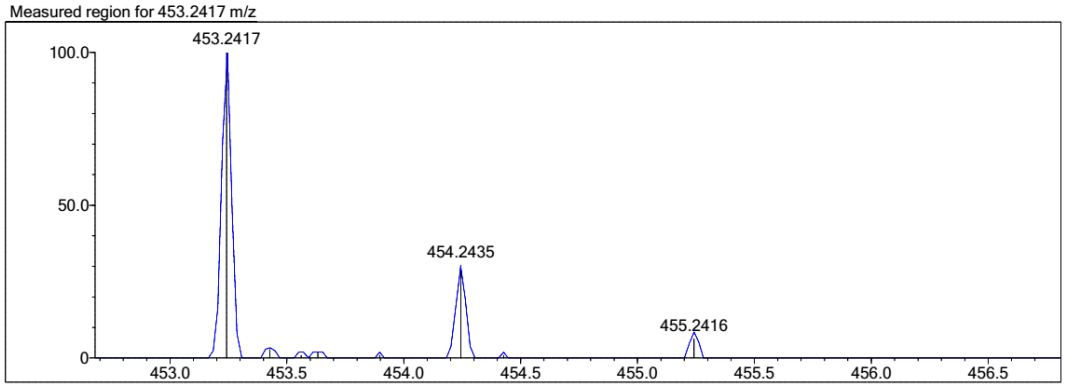

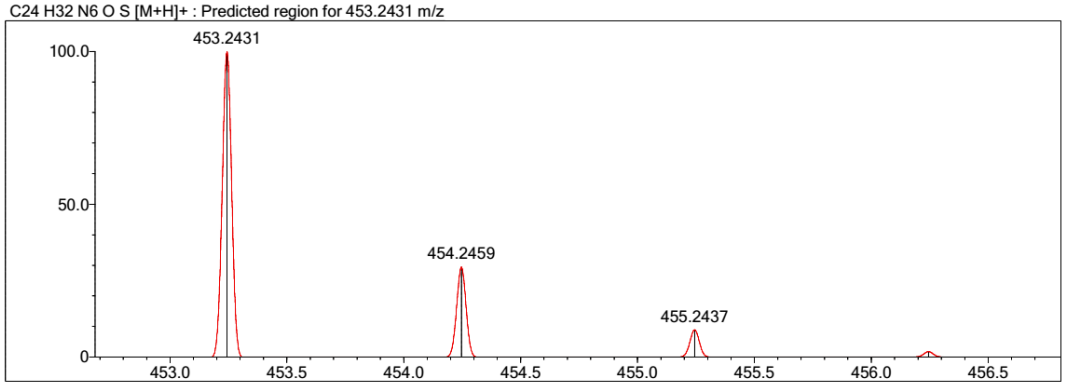

Rank	Score	Formula (M)	Ion	Meas. m/z	Pred. m/z	Df. (mDa)	Df. (ppm)	Iso	DBE
1	92.06	C24 H32 N6 O S	[M+H]+	453.2417	453.2431	-1.4	-3.09	97.13	12.0

Figure 5.65. *HR-MS of compound* ***4b***

5.1.5.3. N-(5-(Adamantan-1-yl)-1,3,4-thiadiazol-2-yl)-2-(4-phenylpiperazin-1-yl) propanamide (4c)

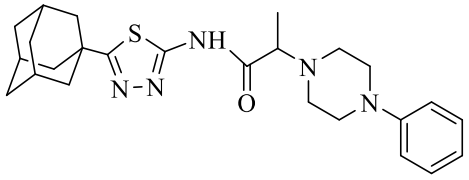

Figure 5.66. *Molecular structure of compound **(4c)***

It was synthesized according to method E. Yield: 74 %. Physical appearance: light creamy powder. Experimental m.p.: 241-242 ˚C.

IR (ATR) υ_{max} (cm^{-1}): 3061 (N-H stretching), 2904-2848 (sp^3 C-H stretching), 1697 (C=O stretching), 1552-1504 (aromatic C=C and C=N stretching), 1282 (C-N stretching).

^{1}H-NMR (400 MHz) ($CDCl_3$) δ (ppm): 1.40 (3H, d, *J*= 6.98 Hz, COCH-$\underline{CH_3}$), 1.81 (6H, s, adamantane-$H_)$, 2.12 (9H, s, adamantane-H), 2.71- 2.83 (4H, m, piperazine-H), 3.05 and 3.16 (2H, 2t, *J*= 4.77 Hz and *J*= 4.69 Hz, piperazine-H), 3.28 (2H, br-s, piperazine-H), 3.48 (1H, q, J_1= 6.98 Hz, J_2= 13.98 Hz, CO$\underline{CH}$-CH_3), 6.89 (1H, t, *J*= 6.04 Hz, phenyl's H_4), 6.95 (2H, d, *J*= 8.13 Hz, phenyl's $H_{2,6}$), 7.29 (2H, t, *J*= 7.72 Hz, phenyl's $H_{3,5}$).

^{13}C-NMR (100 MHz) ($CDCl_3$) δ (ppm): 10.97 (COCH-$\underline{CH_3)}$, 28.43 (adamantane), 36.41 (adamantane), 37.89 (adamantane), 43.24 (adamantane), 49.49 (piperazine), 49.79 (piperazine), 63.71 (CO-$\underline{CH}$), 116.41 (phenyl), 120.24 (phenyl), 129.20 (phenyl), 150.98 (phenyl), 157.57 (thiadiazole), 171.73 (thiadiazole), 175.87 (CO).

HRMS (ESI) (m/z) $[M+1]^+$: for $C_{25}H_{33}N_5OS$ calculated: 452.2479; found: 452.2462.

DOPNALAB

	Item	Value
	Acquired Date&Time	8.06.2022 14:10:23
	Acquired by	System Administrator
	Filename	C:\Users\dopnalab\Desktop\MASAÜSTÜ\LEYLA YURTDAŞ\AYL-A-B\AYL-B8.1.ispd
	Spectrum name	AYL-B8.1
	Sample name	AYL-B8
	Sample ID	
	Option	
	Comment	
	No. of Scans	15
	Resolution	4 [cm-1]
	Apodization	Happ-Genzel

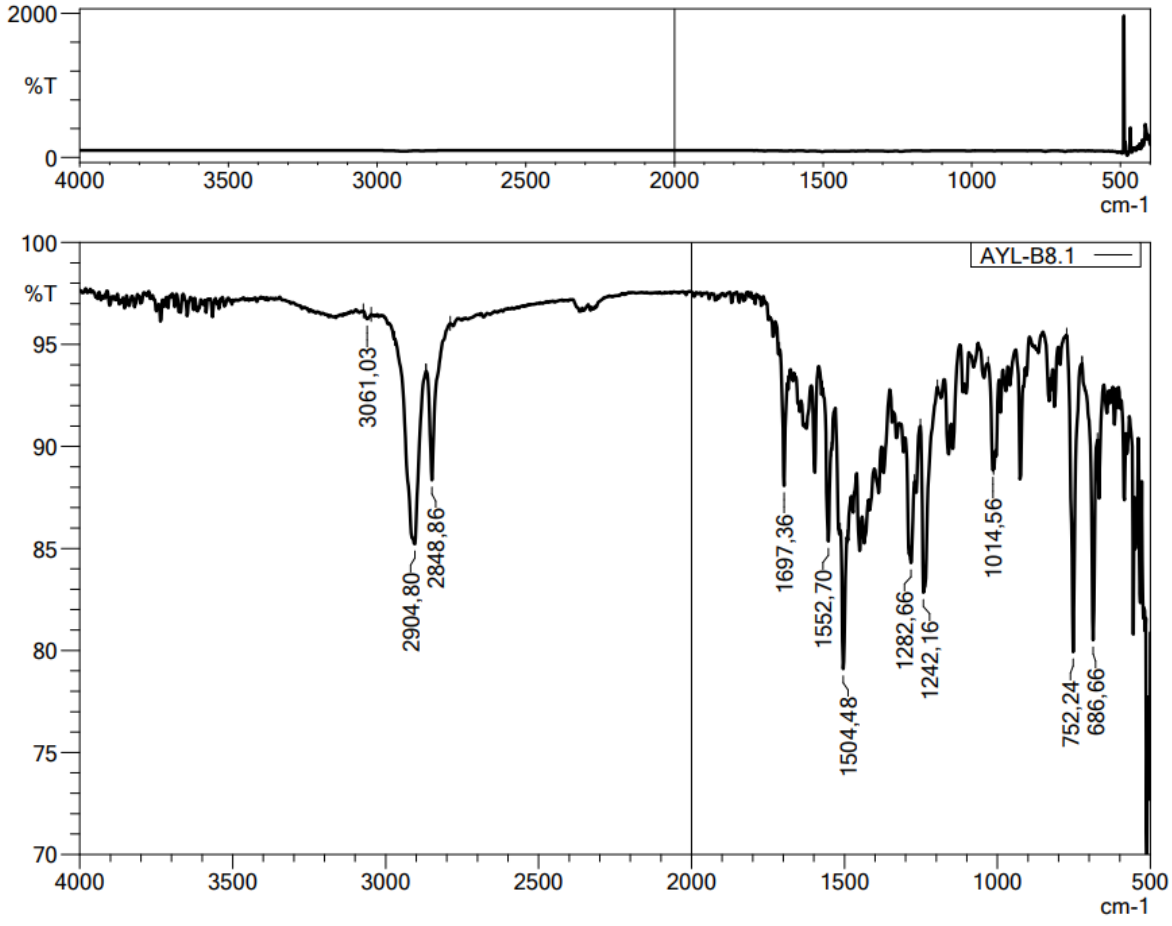

Figure 5.67. *IR spectrum of compound* ***4c***

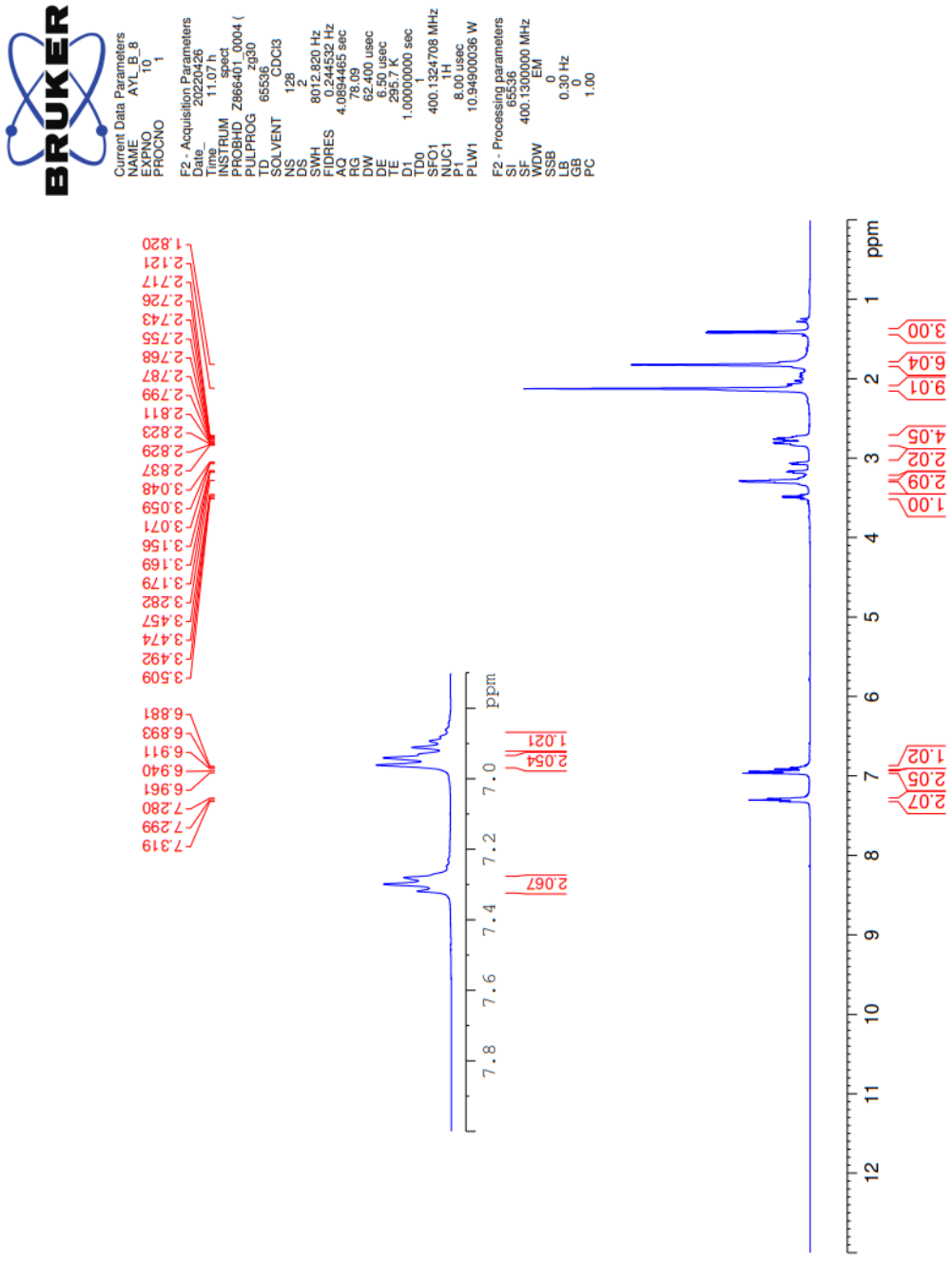

Figure 5.68. *^{1}H-NMR spectrum of compound* ***4c***

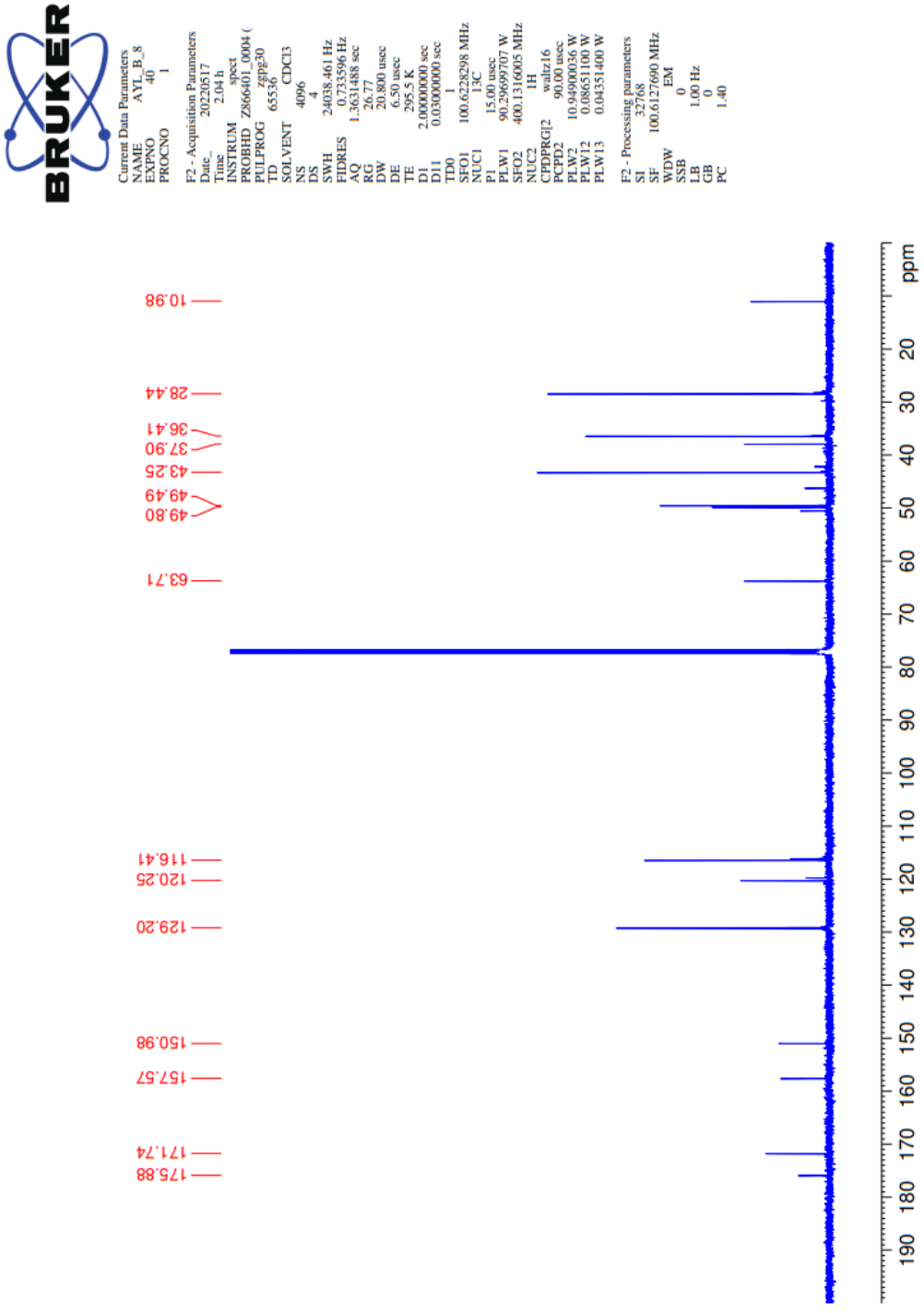

Figure 5.69. *^{13}C-NMR spectrum of compound **4c***

Elmt	Val.	Min	Max	Elmt	Val.	Min	Max	Elmt	Val.	Min	Max	Elmt	Val.	Min	Max	Use Adduct
H	1	10	40	O	2	0	6	S	2	1	1	Ru	2	0	0	H
C	4	10	40	F	1	0	0	Cl	1	0	0	Pd	2	0	0	
N	3	0	7	P	3	0	0	Br	1	0	0	I	3	0	0	

Error Margin (ppm): 5
HC Ratio: unlimited
Max Isotopes: 3
MSn Iso RI (%): 10.00

DBE Range: 5.0 - 25.0
Apply N Rule: yes
Isotope RI (%): 1.00
MSn Logic Mode: AND

Electron Ions: both
Use MSn Info: yes
Isotope Res: 9000
Max Results: 150

Event#: 1 MS(E+) Ret. Time : 4.000 Scan# : 601

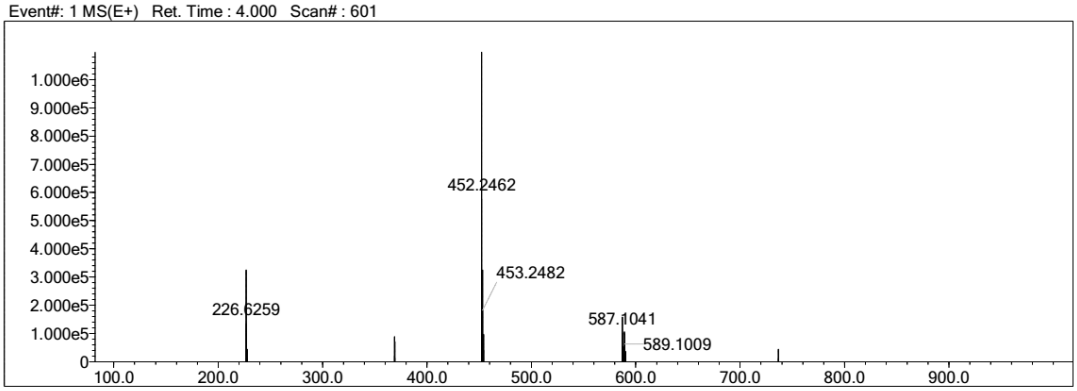

Measured region for 452.2462 m/z

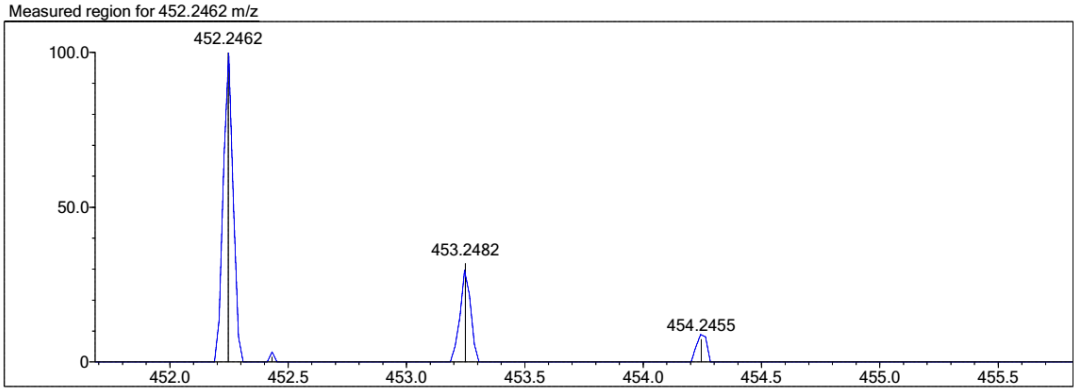

C25 H33 N5 O S [M+H]+ : Predicted region for 452.2479 m/z

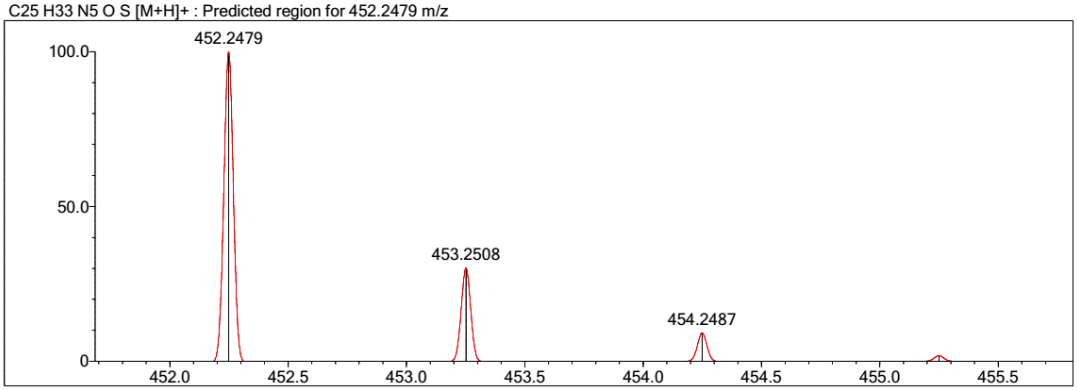

Rank	Score	Formula (M)	Ion	Meas. m/z	Pred. m/z	Df. (mDa)	Df. (ppm)	Iso	DBE
2	87.56	C25 H33 N5 O S	[M+H]+	452.2462	452.2479	-1.7	-3.76	94.05	12.0

Figure 5.70. *HR-MS of compound* ***4c***

5.1.5.4. N-(5-(Adamantan-1-yl)-1,3,4-thiadiazol-2-yl)-2-(4-ethylpiperazin-1-yl) propanamide (4d)

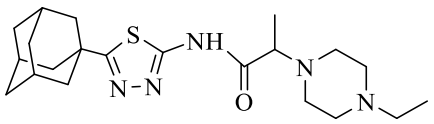

Figure 5.71. *Molecular structure of compound* ***(4d)***

It was synthesized according to method E. Yield: 50 %. Physical appearance: white powder. Experimental m.p.: 99-100 ˚C.

IR (ATR) υ_{max} (cm^{-1}): 3157 (N-H stretching), 2904-2819 (sp^3 C-H stretching), 1699 (C=O stretching), 1508-1450 (aromatic C=N stretching), 1170 (C-N stretching).

^{1}H-NMR (300 MHz) (DMSO-*d*$_6$) δ (ppm): 0.94 (3H, t, *J*= 7.02 Hz, N-CH_2<u>CH_3</u>), 1.17 (3H, d, *J*= 6.71 Hz, CO-CH-<u>CH_3</u>), 1.73 (6H, s, adamantane-H), 1.98 (6H, s, adamantane-H), 2.03 (3H, s, adamantane-H), 2.22-2.33 (10H, m, piperazine's H and N-<u>CH_2</u>-CH_3), 3.47 (1H, q, J_1= 6.58 Hz, J_2= 13.29 Hz, <u>CH</u>-CH_3), 12.06 (1H, br-s, N-H).

^{13}C-NMR (75 MHz) (DMSO-*d*$_6$) δ (ppm): 12.49 (N-CH_2<u>CH_3</u>), 13.33 (CO-CH-<u>CH_3</u>), 28.29 (adamantane), 36.29 (adamantane), 37.64 (adamantane), 43.13 (adamantane), 49.19 (N-<u>CH_2</u>CH_3), 52.04 (piperazine), 53.06 (piperazine), 62.14 (CO-<u>CH</u>), 157.71(thiadiazole), 171.42 (thiadiazole), 174.06 (CO).

HRMS (ESI) (m/z) $[M+1]^+$: for $C_{21}H_{33}N_5OS$ calculated: 404.2479; found: 404.2467.

DOPNALAB

	Item	Value
	Acquired Date&Time	8.06.2022 13:55:47
	Acquired by	System Administrator
	Filename	C:\Users\dopnalab\Desktop\MASAÜSTÜ\LEYLA YURTDAŞ\AYL-A-B\AYL-B3.1.ispd
	Spectrum name	AYL-B3.1
	Sample name	AYL-B3
	Sample ID	
	Option	
	Comment	
	No. of Scans	15
	Resolution	4 [cm-1]
	Apodization	Happ-Genzel

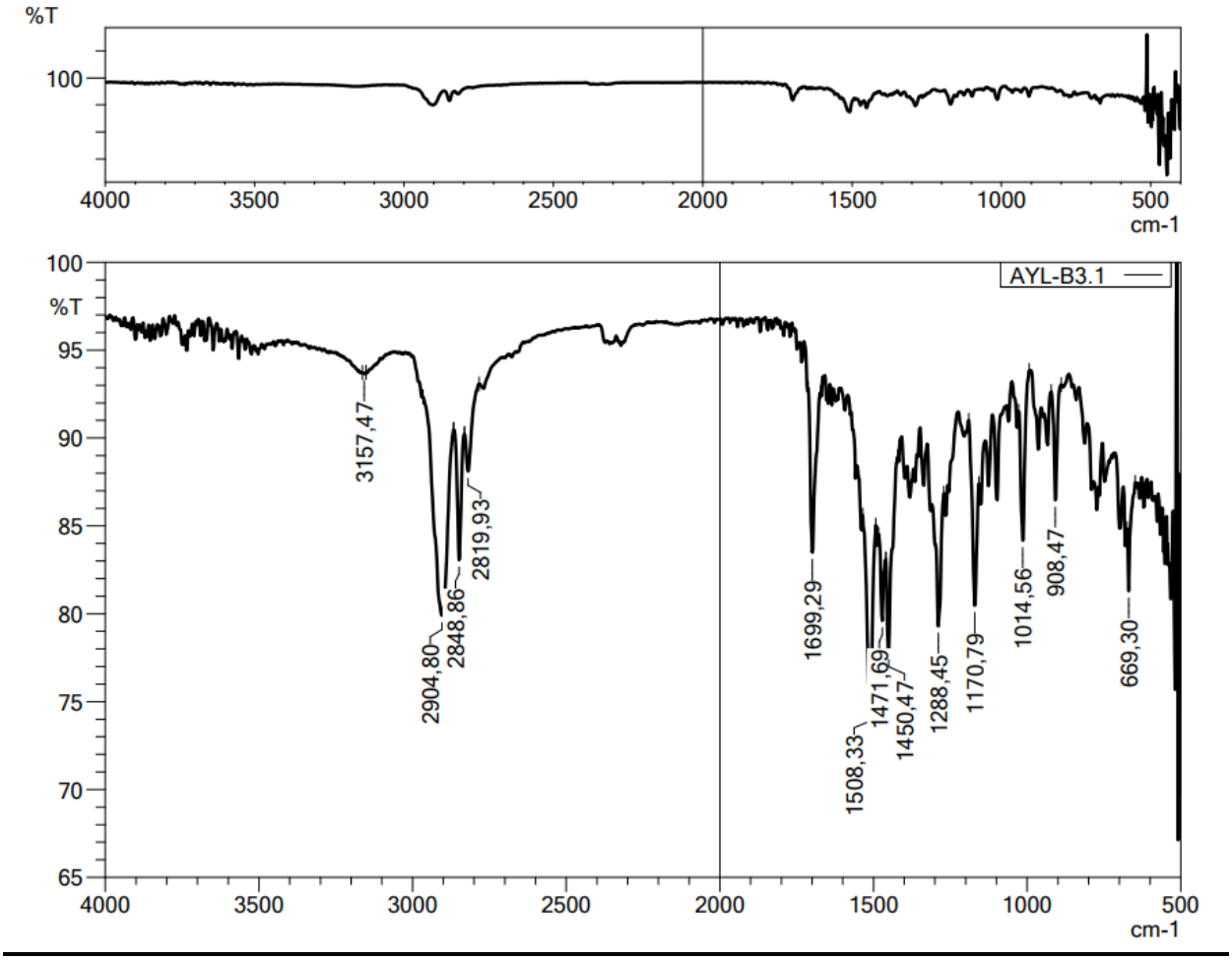

Figure 5.72. *IR spectrum of compound* ***4d***

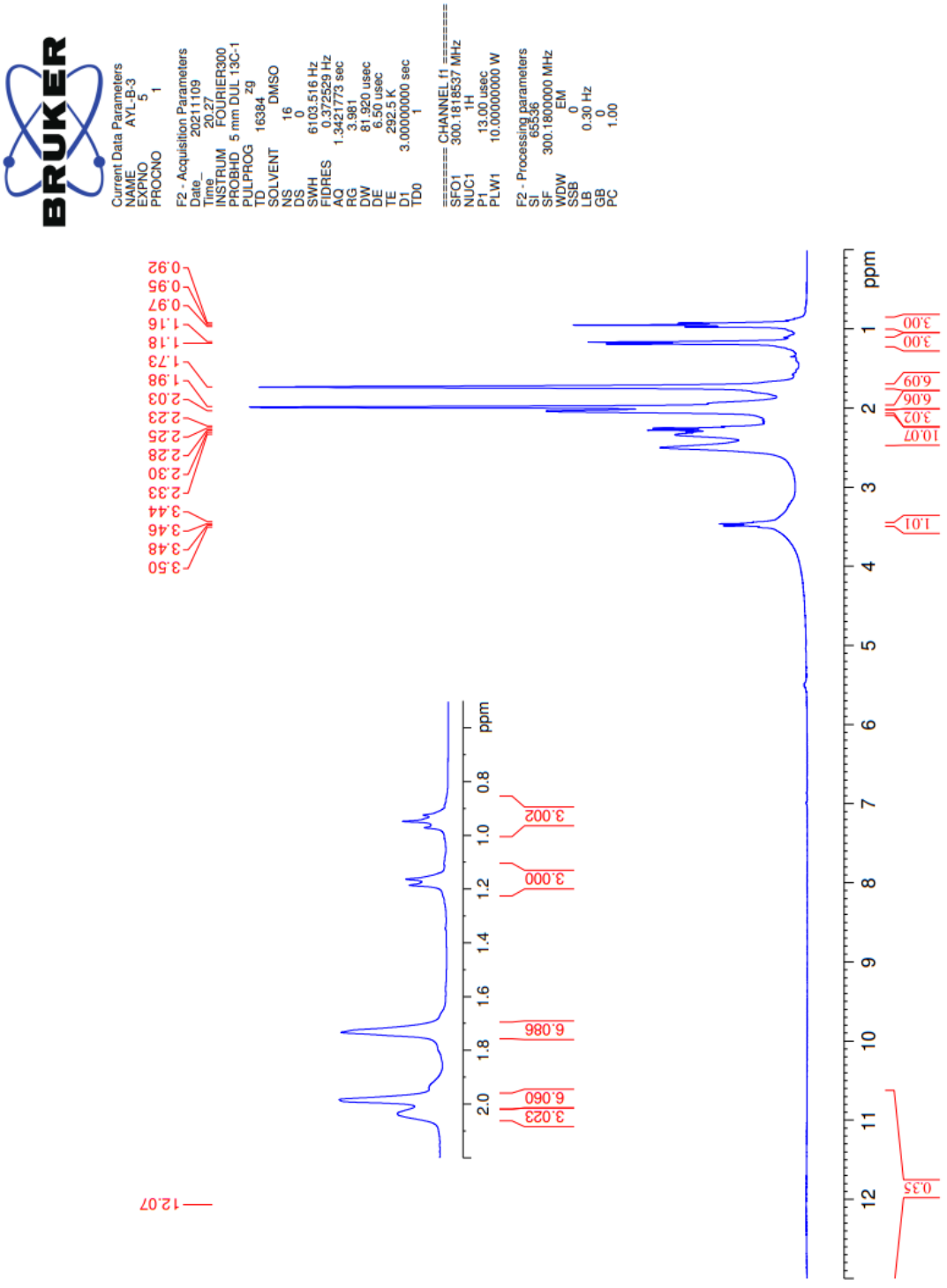

Figure 5.73. *[1]H-NMR spectrum of compound **4d***

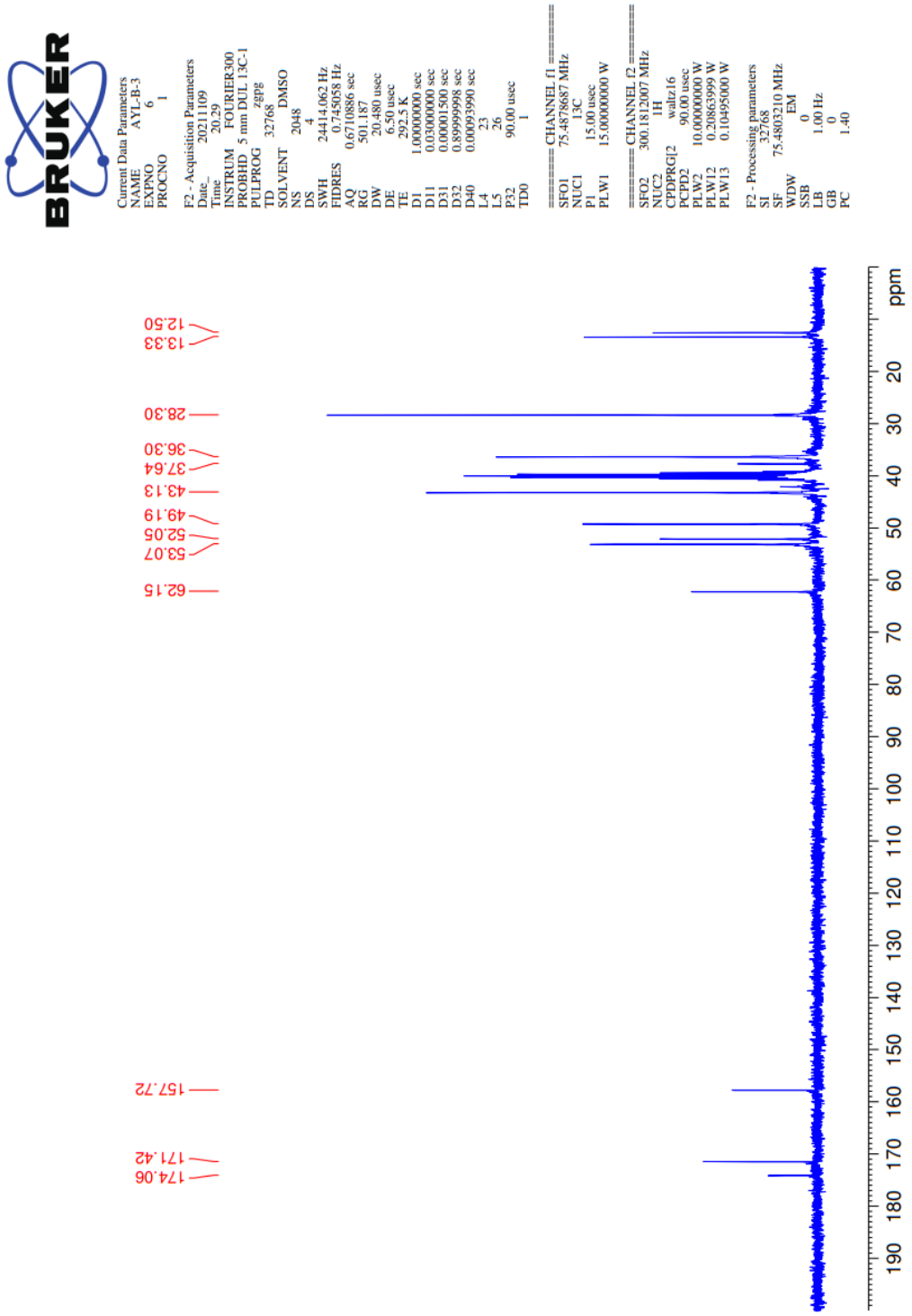

Figure 5.74. *^{13}C-NMR spectrum of compound **4d***

Elmt	Val.	Min	Max	Elmt	Val.	Min	Max	Elmt	Val.	Min	Max	Elmt	Val.	Min	Max	Use Adduct
H	1	10	40	O	2	0	6	S	2	1	1	Ru	2	0	0	H
C	4	10	40	F	1	0	0	Cl	1	0	0	Pd	2	0	0	
N	3	0	7	P	3	0	0	Br	1	0	0	I	3	0	0	

Error Margin (ppm): 5
HC Ratio: unlimited
Max Isotopes: 3
MSn Iso RI (%): 10.00

DBE Range: 5.0 - 25.0
Apply N Rule: yes
Isotope RI (%): 1.00
MSn Logic Mode: AND

Electron Ions: both
Use MSn Info: yes
Isotope Res: 9000
Max Results: 150

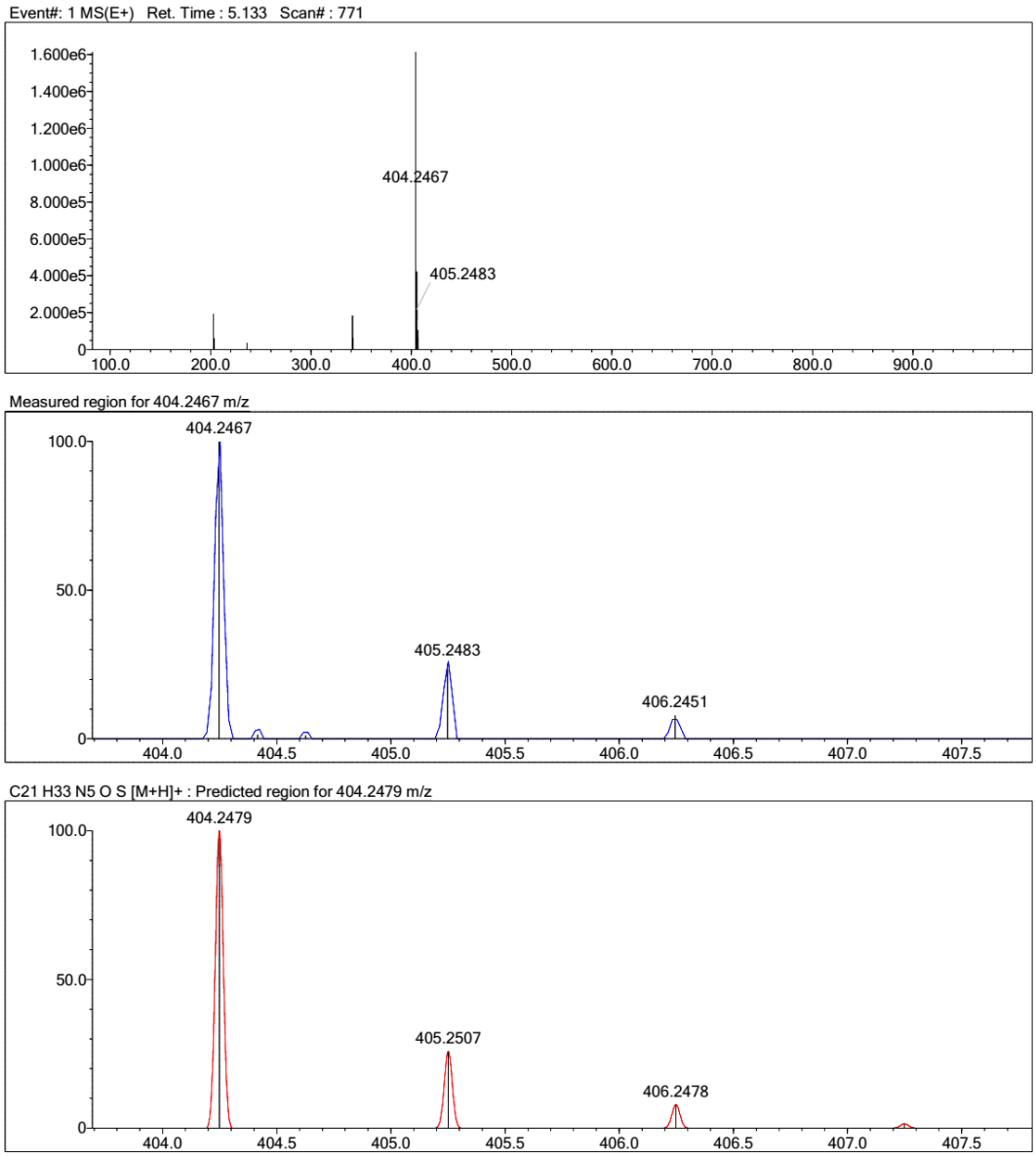

Rank	Score	Formula (M)	Ion	Meas. m/z	Pred. m/z	Df. (mDa)	Df. (ppm)	Iso	DBE
1	78.29	C21 H33 N5 O S	[M+H]+	404.2467	404.2479	-1.2	-2.97	82.35	8.0

Figure 5.75. *HR-MS of compound* ***4d***

5.1.5.5. N-(5-(Adamantan-1-yl)-1,3,4-thiadiazol-2-yl)-2-(4-(2-(dimethylamino)ethyl) piperazin-1-yl)propanamide (4e)

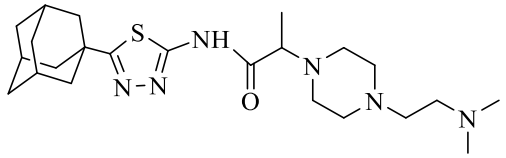

Figure 5.76. *Molecular structure of compound* ***(4e)***

It was synthesized according to method E. Yield: 73 %. Physical appearance: light yellow liquid.

IR (ATR) υ_{max} (cm^{-1}): 3145 (N-H stretching), 2900-2816 (sp^3 C-H stretching), 1693 (C=O stretching), 1514-1290 (aromatic C=N stretching), 1165-1014 (C-N stretching).

^{1}H-NMR (300 MHz) (DMSO-*d*$_6$) δ (ppm): 1.14-1.20 (3H, m, COCH-$\underline{CH_3}$), 1.74 (6H, s, adamantane-H), 1.99 (6H, adamantane-H), 2.04 (3H, s, adamantane-H), 2.12 (6H, s, N-($\underline{CH_3}$)$_2$), 2.32 (4H, br-s, piperazine- H), 2.38 (4H, br-s, piperazine-H), 2.95-3.35 (2H, m, N-$\underline{CH_2}$), 3.47 (2H,q, J_1= 6.72 Hz, J_2= 13.53 Hz, N-$\underline{CH_2}$), 4.03 (1H,q, J_1= 7.11Hz, J_2= 14.25 Hz, CO-$\underline{CH}$-CH_3).

^{13}C-NMR (75 MHz) (DMSO-*d*$_6$) δ (ppm): 13.34 (COCH-$\underline{CH_3}$), 28.29 (adamantane), 36.29 (adamantane), 37.64 (adamantane), 43.12 (adamantane), 45.92 (N-($\underline{CH_3}$)$_2$), 49.18 (piperazine), 53.78 (piperazine), 56.23 (piperazine- ($\underline{CH_2}$)$_2$-N), 56.94 (piperazine- ($\underline{CH_2}$)$_2$-N), 62.09 (CO-$\underline{CH}$), 157.66 (thiadiazole), 171.37 (thiadiazole), 174.08 (CO).

HRMS (ESI) (m/z) $[M+1]^+$: For $C_{23}H_{38}N_6OS$ calculated: 447.2901; found: 447.2880.

DOPNALAB

	Item	Value
	Acquired Date&Time	8.06.2022 14:02:02
	Acquired by	System Administrator
	Filename	C:\Users\dopnalab\Desktop\MASAÜSTÜ\LEYLA YURTDAŞ\AYL-A-B\AYL-B5.1.ispd
	Spectrum name	AYL-B5.1
	Sample name	AYL-B5
	Sample ID	
	Option	
	Comment	
	No. of Scans	15
	Resolution	4 [cm-1]
	Apodization	Happ-Genzel

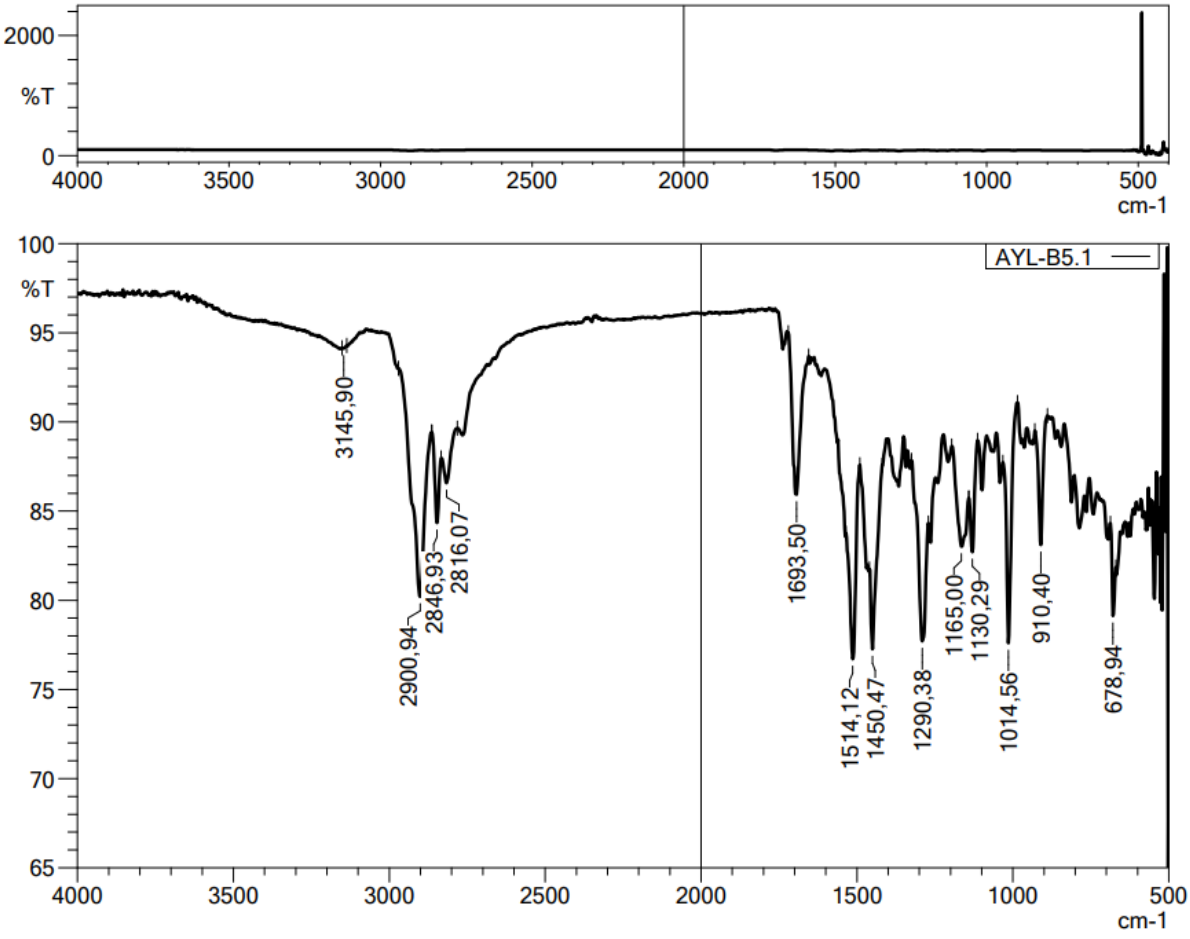

Figure 5.77. *IR spectrum of compound* ***4e***

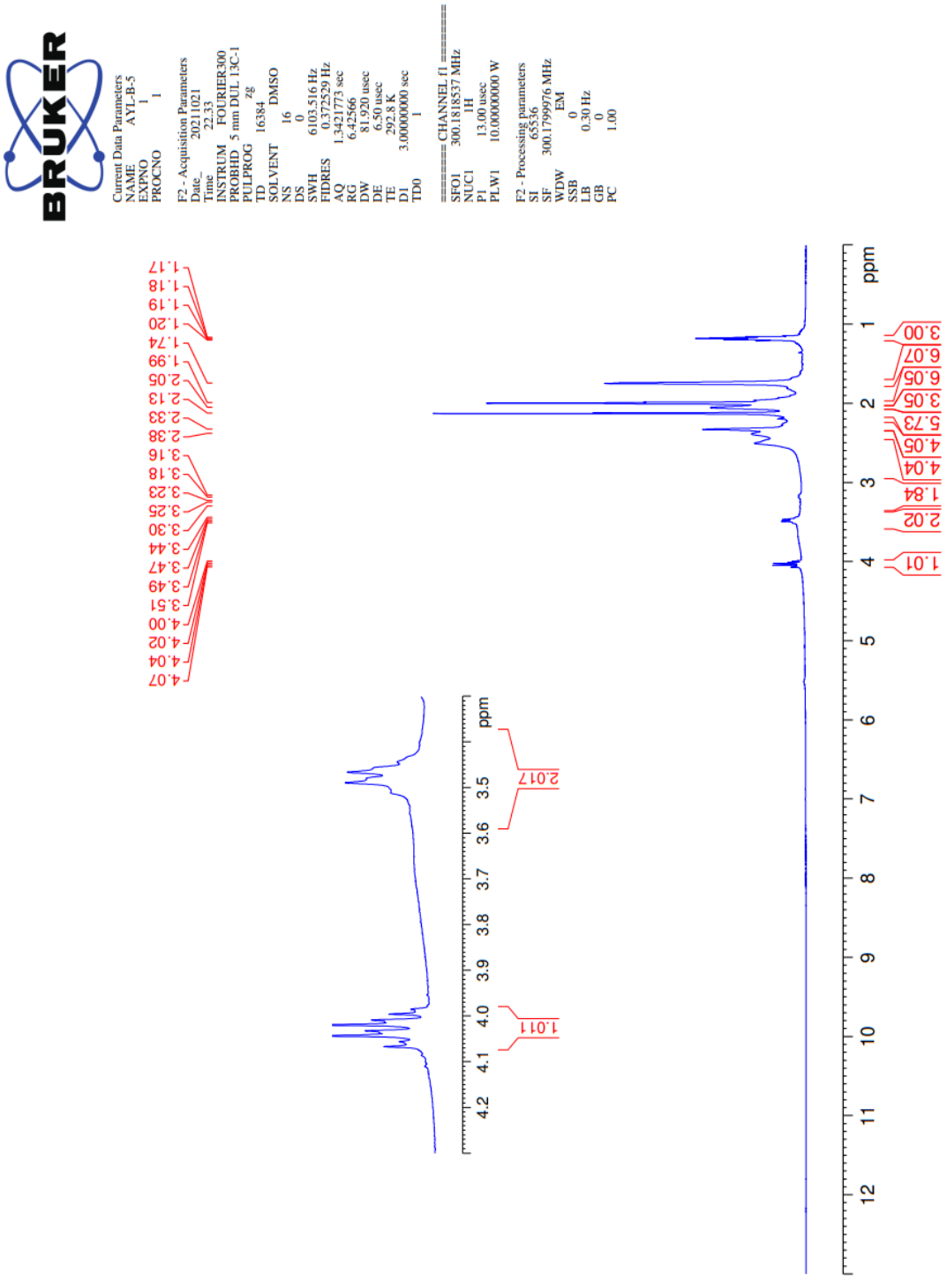

Figure 5.78. *[1]H-NMR spectrum of compound* ***4e***

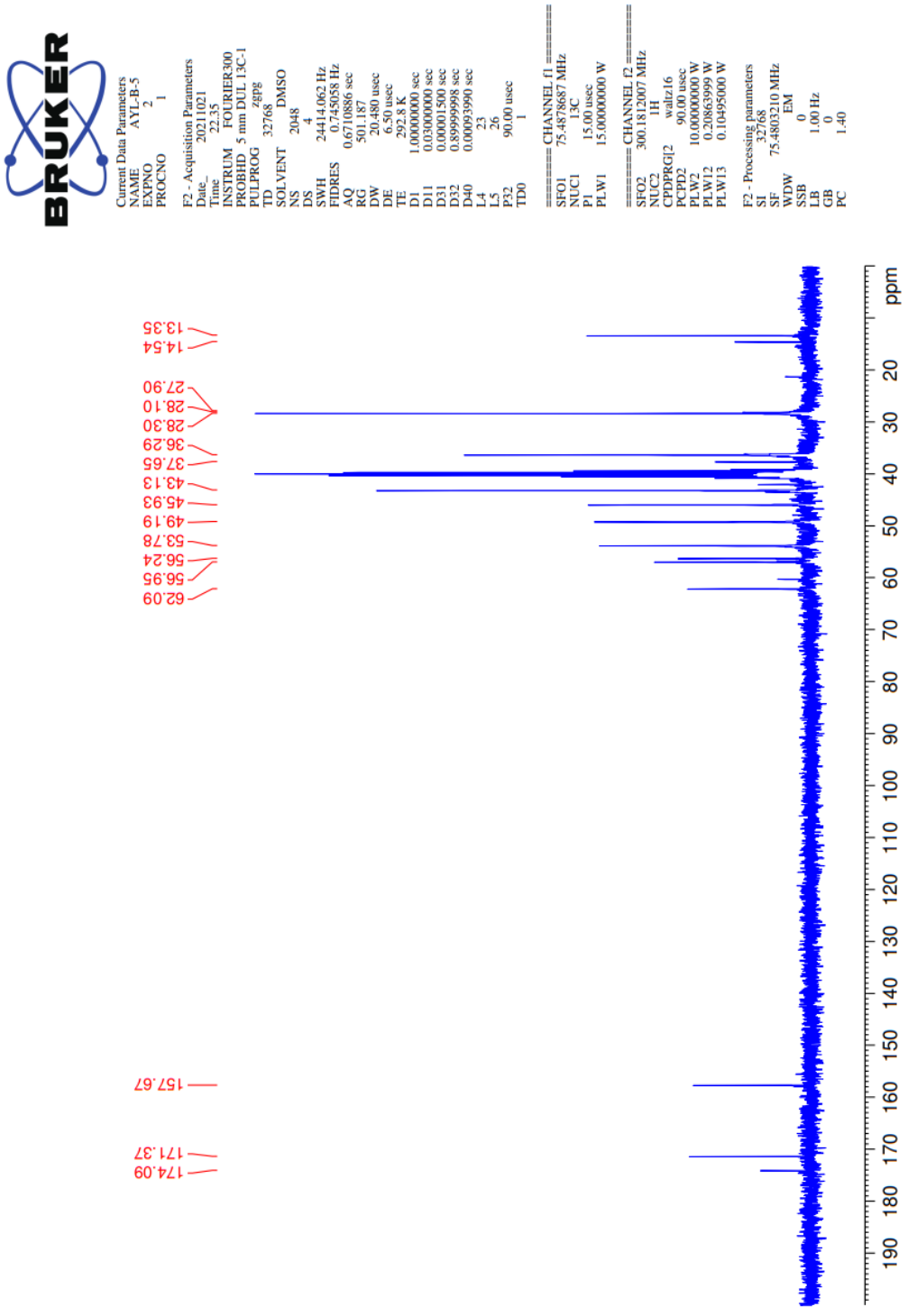

Figure 5.79. *^{13}C-NMR spectrum of compound **4e***

Elmt	Val.	Min	Max	Elmt	Val.	Min	Max	Elmt	Val.	Min	Max	Elmt	Val.	Min	Max	Use Adduct
H	1	10	40	O	2	0	6	S	2	1	1	Ru	2	0	0	H
C	4	10	40	F	1	0	0	Cl	1	0	0	Pd	2	0	0	
N	3	0	7	P	3	0	0	Br	1	0	0	I	3	0	0	

Error Margin (ppm): 5
HC Ratio: unlimited
Max Isotopes: 3
MSn Iso RI (%): 10.00

DBE Range: 5.0 - 25.0
Apply N Rule: yes
Isotope RI (%): 1.00
MSn Logic Mode: AND

Electron Ions: both
Use MSn Info: yes
Isotope Res: 9000
Max Results: 150

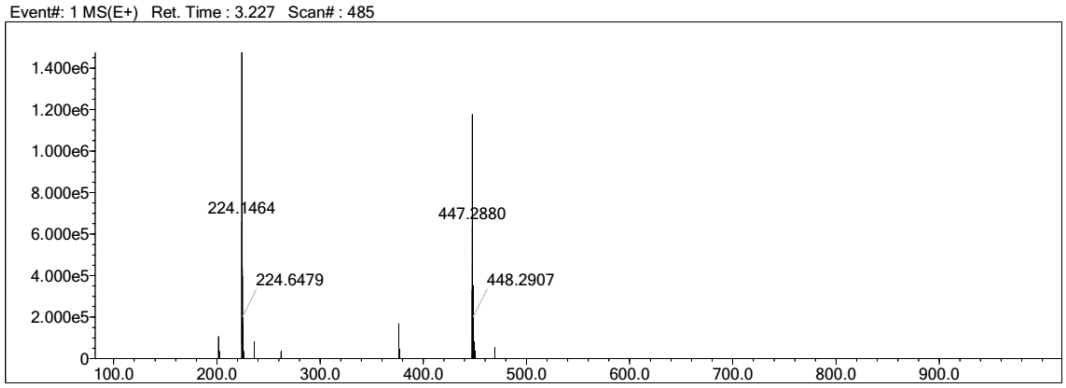

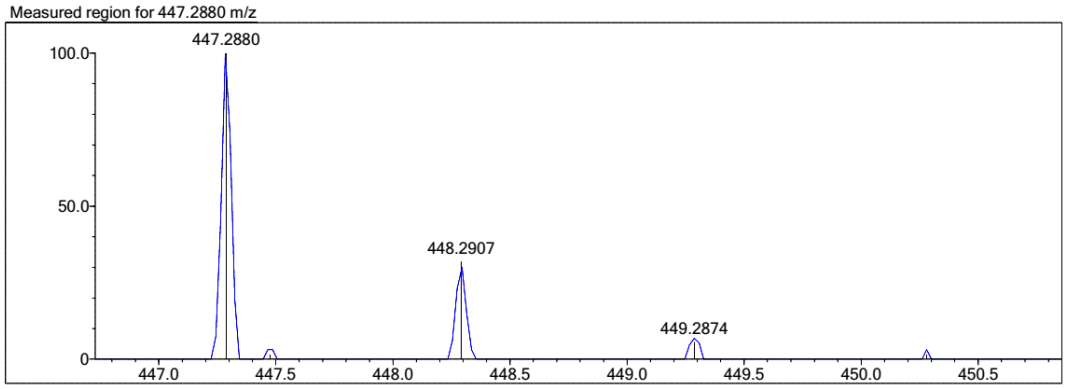

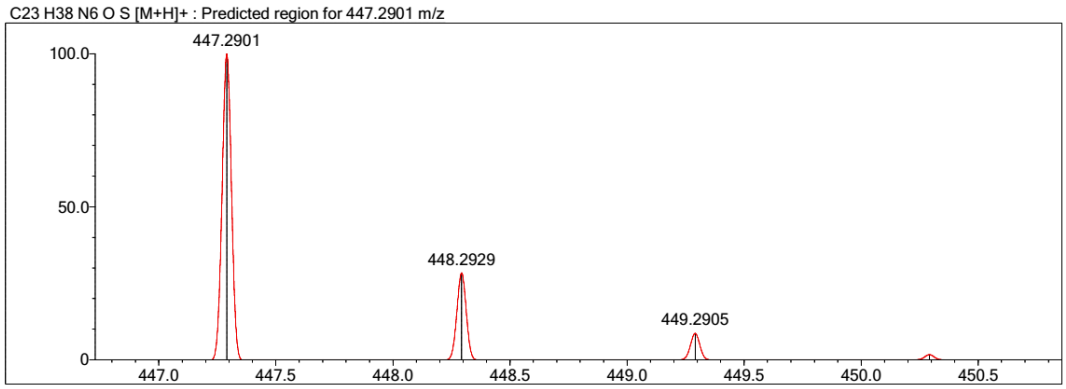

Rank	Score	Formula (M)	Ion	Meas. m/z	Pred. m/z	Df. (mDa)	Df. (ppm)	Iso	DBE
1	56.70	C23 H38 N6 O S	[M+H]+	447.2880	447.2901	-2.1	-4.69	62.46	8.0

Figure 5.80. *HR-MS of compound* ***4e***

5.1.5.6. N-(5-(Adamantan-1-yl)-1,3,4-thiadiazol-2-yl)-2-(pyrrolidin-1-yl)propanamide (4f)

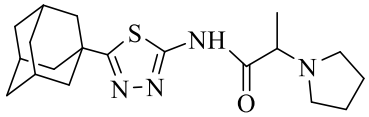

Figure 5.81. *Molecular structure of compound* ***(4f)***

It was synthesized according to method E. Yield: 70 %. Physical appearance: white powder. Experimental m.p.: 158-159 ˚C.

IR (ATR) υ_{max} (cm^{-1}): 3134 (N-H stretching), 2974-2794 (sp^3 C-H stretching), 1691 (C=O stretching), 1537-1450 (aromatic C=N stretching), 1294 (C-N stretching).

^{1}H-NMR (400 MHz) ($CDCl_3$) δ (ppm): 1.39 (3H, d, *J*= 7.01 Hz, COCH-$\underline{CH_3}$), 1.80 (6H, s, adamantane-H), 1.83-1.88 (4H, m, pyrrolidine's $H_{3,4}$), 2.11 (9H, s, adamantane-H), 2.60- 2.69 (4H, m, pyrrolidine's $H_{2,5}$), 3.30 (1H, q, J_1= 6.99 Hz, J_2= 13.98 Hz, CO$\underline{CH}$-CH_3).

^{13}C-NMR (100 MHz) ($CDCl_3$) δ (ppm): 15.40 (COCH-$\underline{CH_3}$), 23.47 (pyrrolidine's $\underline{C_{3,4}}$), 28.44 (adamantane), 36.41 (adamantane), 37.86 (adamantane), 43.23 (adamantane), 50.88 (pyrrolidine's $\underline{C_{2,5}}$), 62.43 (CO-$\underline{CH}$), 157.6 (thiadiazole), 172.86 (thiadiazole), 175.77 (CO).

HRMS (ESI) (m/z) $[M+1]^+$: for $C_{19}H_{28}N_4OS$ calculated: 361.2057; found: 361.2042

DOPNALAB

	Item	Value
	Acquired Date&Time	8.06.2022 14:18:50
	Acquired by	System Administrator
	Filename	C:\Users\dopnalab\Desktop\MASAÜSTÜ\LEYLA YURTDAŞ\AYL-A-B\AYL-B12.1.ispd
	Spectrum name	AYL-B12.1
	Sample name	AYL-B12
	Sample ID	
	Option	
	Comment	
	No. of Scans	15
	Resolution	4 [cm-1]
	Apodization	Happ-Genzel

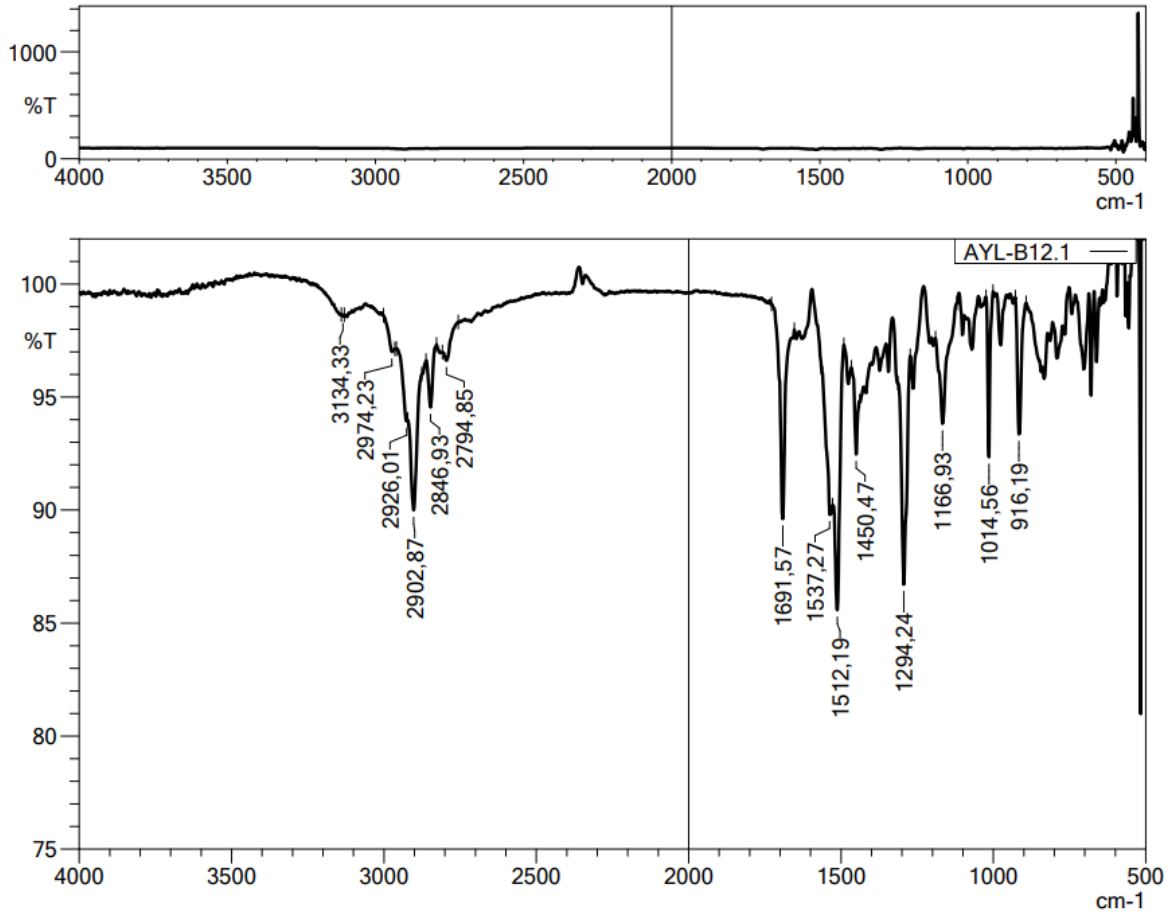

Figure 5.82. *IR spectrum of compound* ***4f***

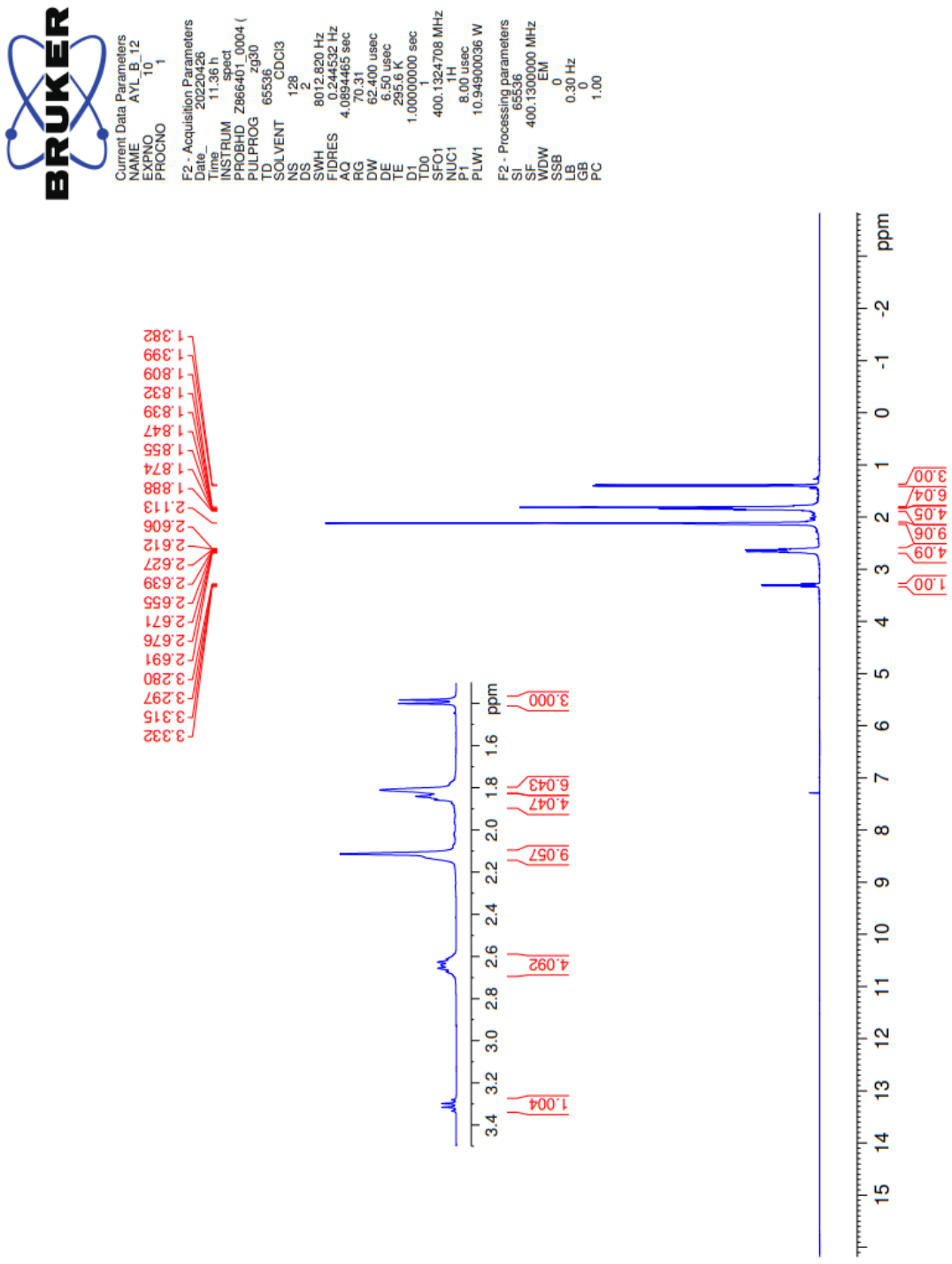

Figure 5.83. *[1]H-NMR spectrum of compound* ***4f***

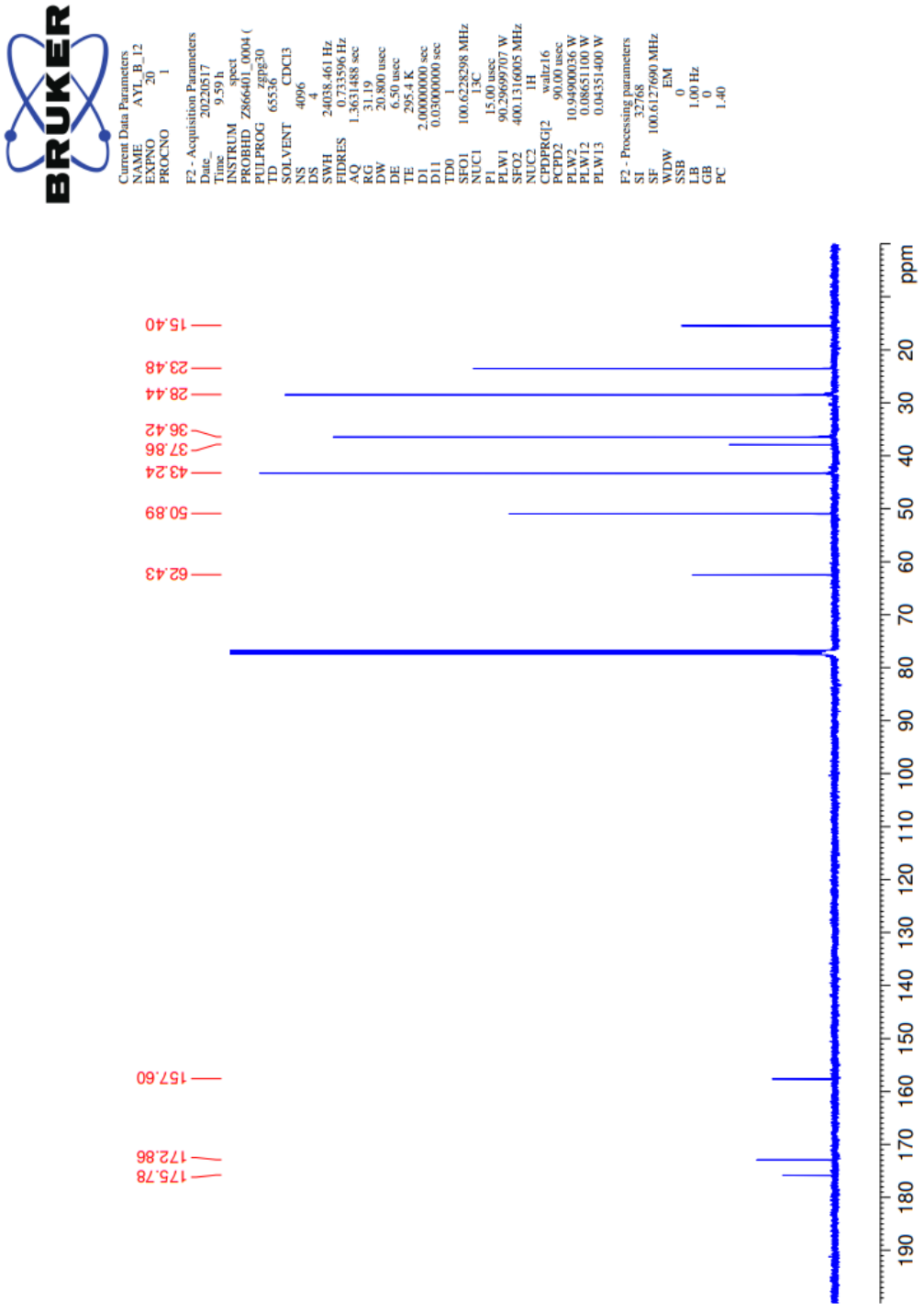

Figure 5.84. *^{13}C-NMR spectrum of compound **4f***

Elmt	Val.	Min	Max	Elmt	Val.	Min	Max	Elmt	Val.	Min	Max	Elmt	Val.	Min	Max	Use Adduct
H	1	10	40	O	2	0	1	S	2	1	1	Ru	2	0	0	H
C	4	10	40	F	1	0	0	Cl	1	0	0	Pd	2	0	0	
N	3	0	4	P	3	0	0	Br	1	0	0	I	3	0	0	

Error Margin (ppm): 50
HC Ratio: unlimited
Max Isotopes: 3
MSn Iso RI (%): 10.00

DBE Range: 5.0 - 20.0
Apply N Rule: yes
Isotope RI (%): 1.00
MSn Logic Mode: AND

Electron Ions: both
Use MSn Info: yes
Isotope Res: 9000
Max Results: 150

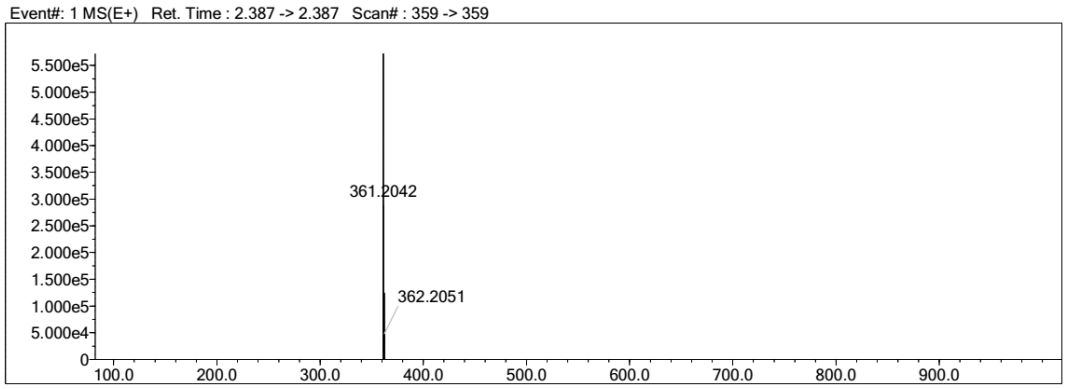

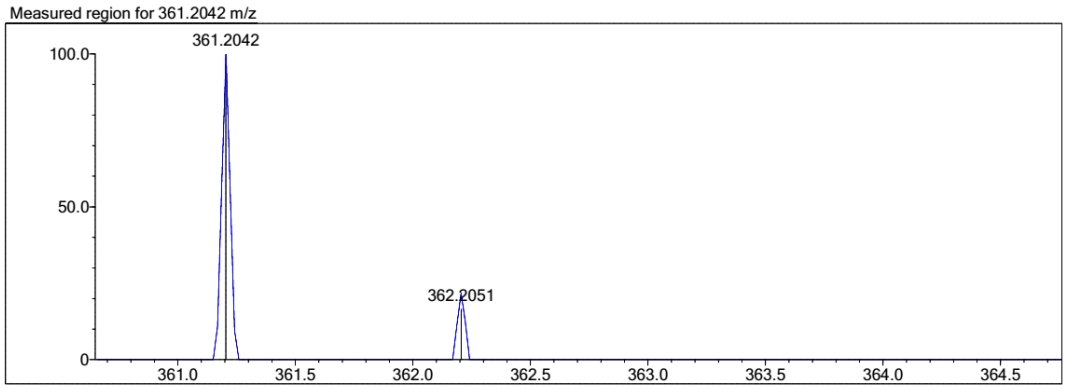

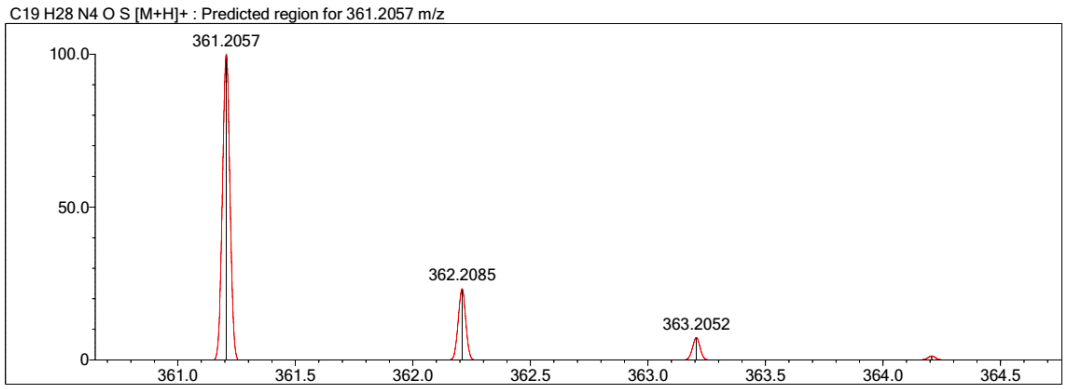

Rank	Score	Formula (M)	Ion	Meas. m/z	Pred. m/z	Df. (mDa)	Df. (ppm)	Iso	DBE
1	0.00	C19 H28 N4 O S	[M+H]+	361.2042	361.2057	-1.5	-4.15	0.00	8.0

Figure 5.85. *HR-MS of compound* ***4f***

5.1.5.7. N-(5-(Adamantan-1-yl)-1,3,4-thiadiazol-2-yl)-2-morpholinopropanamide (4g)

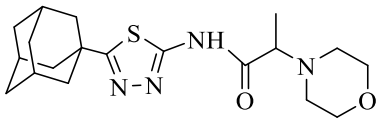

Figure 5.86. *Molecular structure of compound* ***(4g)***

It was synthesized according to method E. Yield: 63 %. Physical appearance: white powder. Experimental m.p.: 195-196 ˚C.

IR (ATR) υ_{max} (cm^{-1}): 3161 (N-H stretching), 2927-2852 (sp^3 C-H stretching), 1734 (C=O stretching), 1541-1448 (aromatic C=N stretching), 1296 (C-N stretching), 1116 (C-O stretching).

^{1}H-NMR (300 MHz) (DMSO-*d*$_6$) δ (ppm): 1.19 (3H, d, *J*= 6.81Hz, COCH-$\underline{CH_3}$), 1.74 (6H, s, adamantane-H), 1.99 (6H, s, adamantane-H), 2.04 (3H, s, adamantane-H), 2.43-2.55 (4H, m, morpholine's $H_{3,5}$), 3.48 (1H, q, J_1= 6.87 Hz, J_2= 13.75 Hz, CO-$\underline{CH}$), 3.57 (4H, s, morpholine's $H_{2,6}$), 12.17 (1H, br-s, N-H).

^{13}C-NMR (75 MHz) (DMSO-*d6*) δ (ppm): 13.29 (COCH-$\underline{CH_3}$), 28.29 (adamantane), 36.29 (adamantane), 37.64 (adamantane), 43.12 (adamantane), 49.8 (morpholine $C_{3,5}$), 62.4 (morpholine $C_{2,6}$), 66.85 (CO-$\underline{CH}$), 157.67 (thiadiazole), 171.34 (thiadiazole), 174.13 (CO).

HRMS (ESI) (m/z) $[M+1]^+$: for $C_{19}H_{28}N_4O_2S$ calculated: 337.2006; found: 337.1987.

DOPNALAB

	Item	Value
	Acquired Date&Time	8.06.2022 14:23:17
	Acquired by	System Administrator
	Filename	C:\Users\dopnalab\Desktop\MASAÜSTÜ\LEYLA YURTDAŞ\AYL-A-B\AYL-B15.1.ispd
	Spectrum name	AYL-B15.1
	Sample name	AYL-B15
	Sample ID	
	Option	
	Comment	
	No. of Scans	15
	Resolution	4 [cm-1]
	Apodization	Happ-Genzel

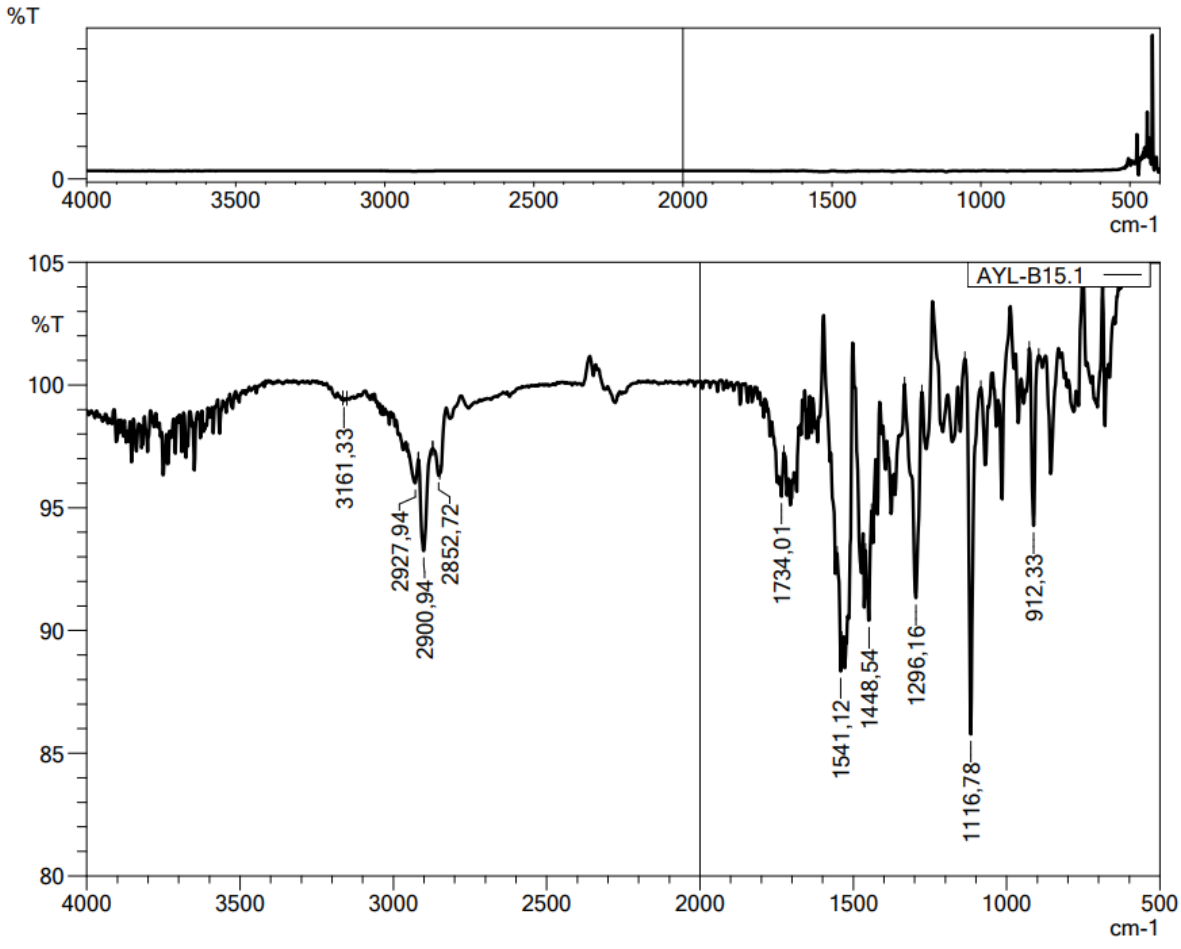

Figure 5.87. *IR spectrum of compound* ***4g***

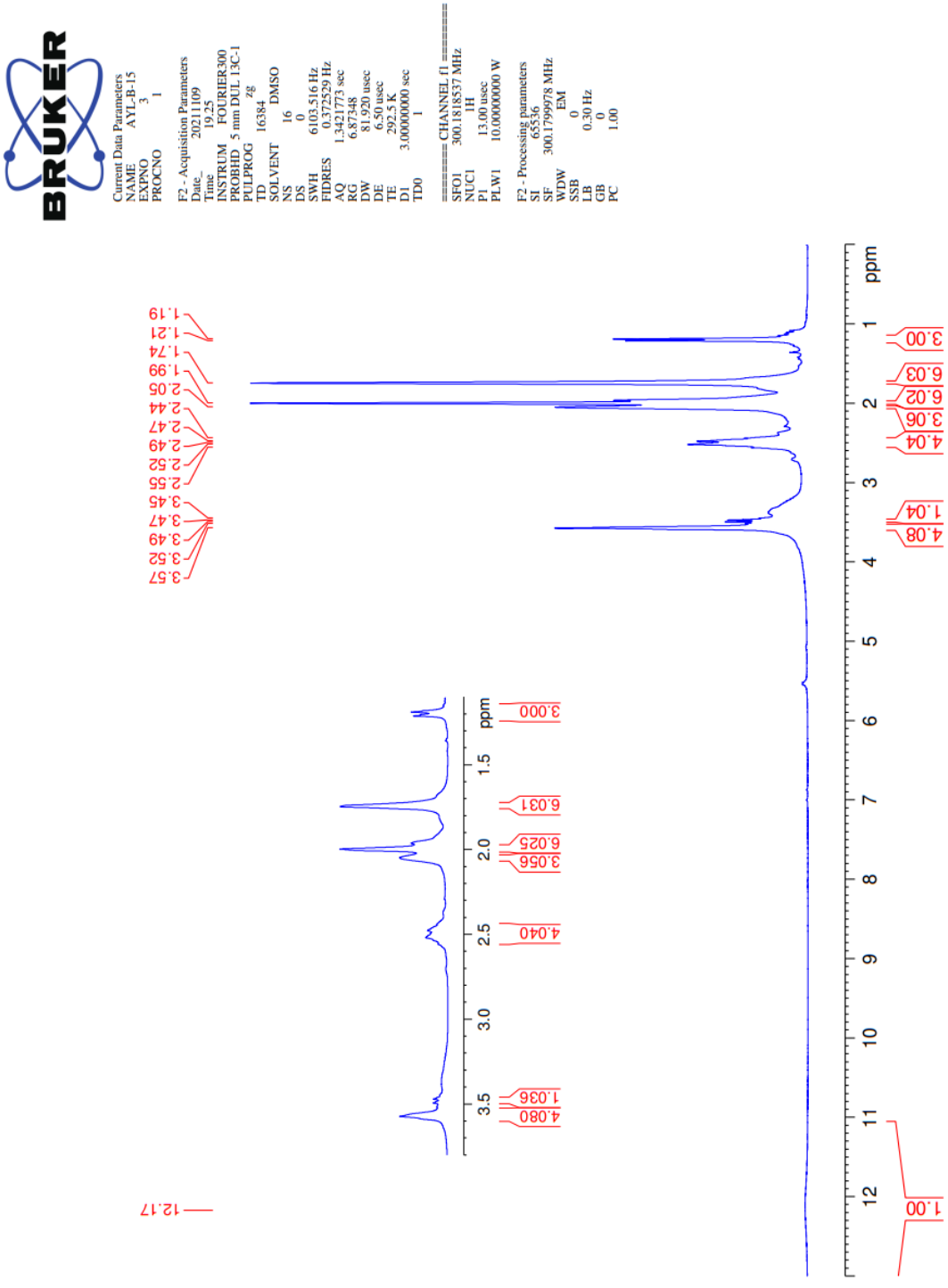

Figure 5.88. *^{1}H-NMR spectrum of compound **4g***

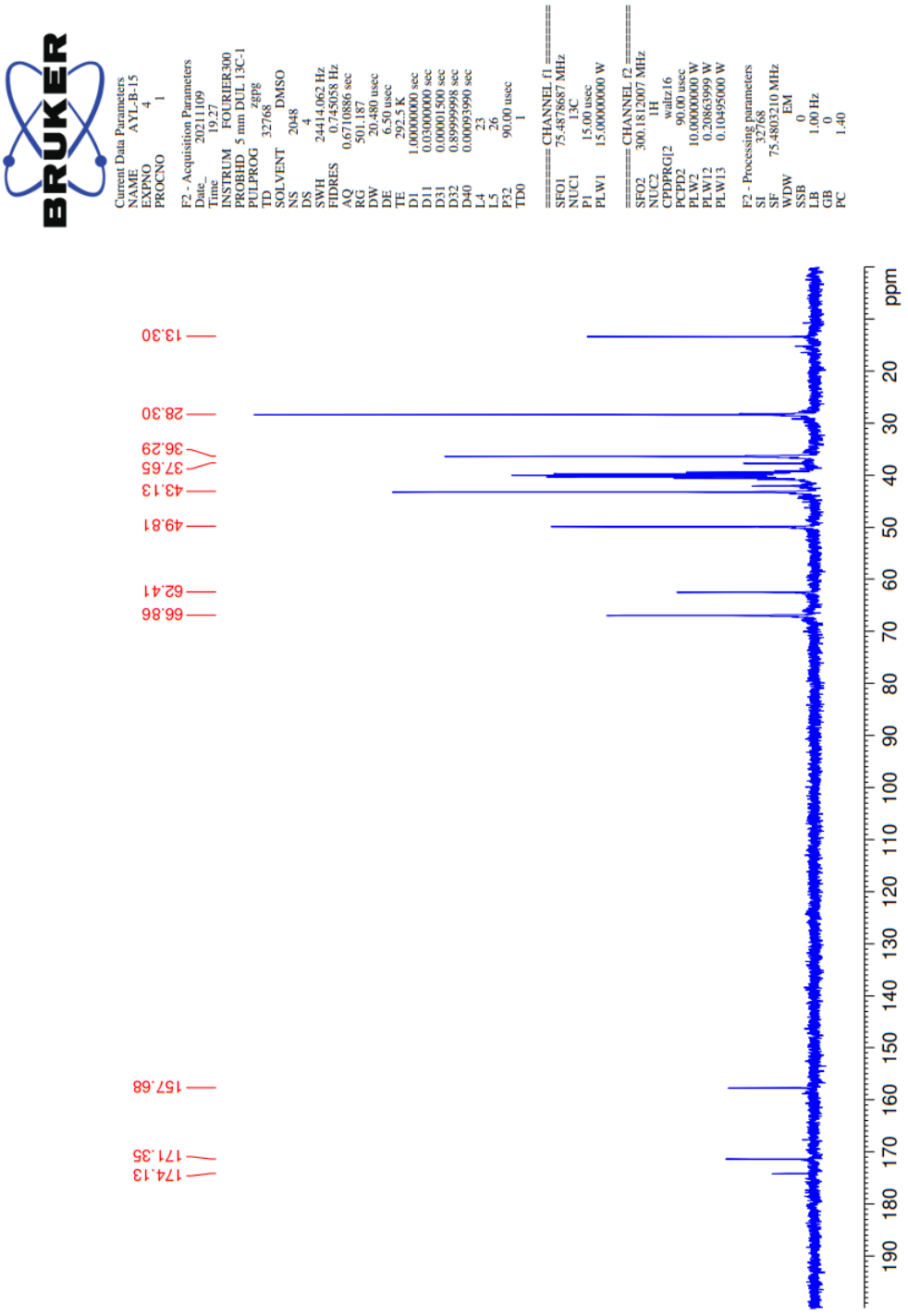

Figure 5.89. *^{13}C-NMR spectrum of compound **4g***

Elmt	Val.	Min	Max	Elmt	Val.	Min	Max	Elmt	Val.	Min	Max	Elmt	Val.	Min	Max	Use Adduct
H	1	10	40	O	2	0	6	S	2	1	1	Ru	2	0	0	H
C	4	10	40	F	1	0	0	Cl	1	0	0	Pd	2	0	0	
N	3	0	7	P	3	0	0	Br	1	0	0	I	3	0	0	

Error Margin (ppm): 5
HC Ratio: unlimited
Max Isotopes: 3
MSn Iso RI (%): 10.00

DBE Range: 5.0 - 25.0
Apply N Rule: yes
Isotope RI (%): 1.00
MSn Logic Mode: AND

Electron Ions: both
Use MSn Info: yes
Isotope Res: 9000
Max Results: 150

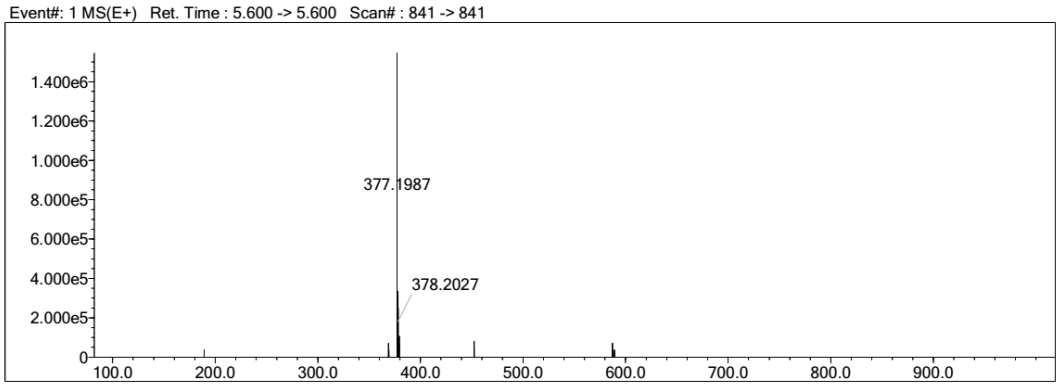

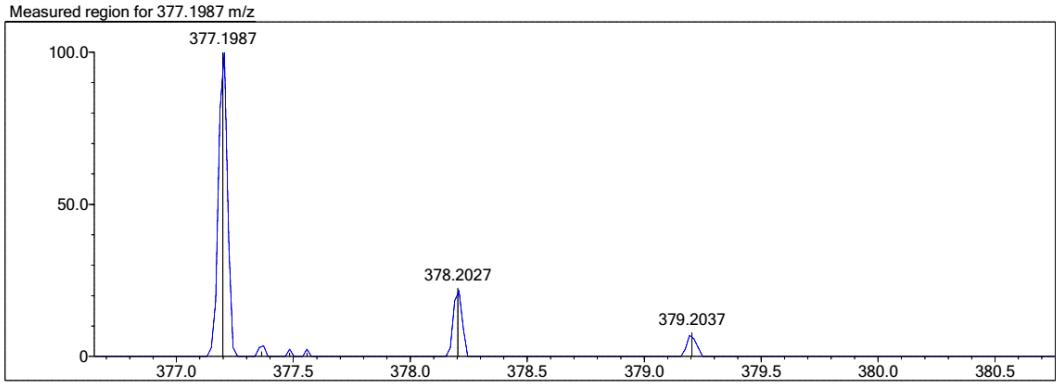

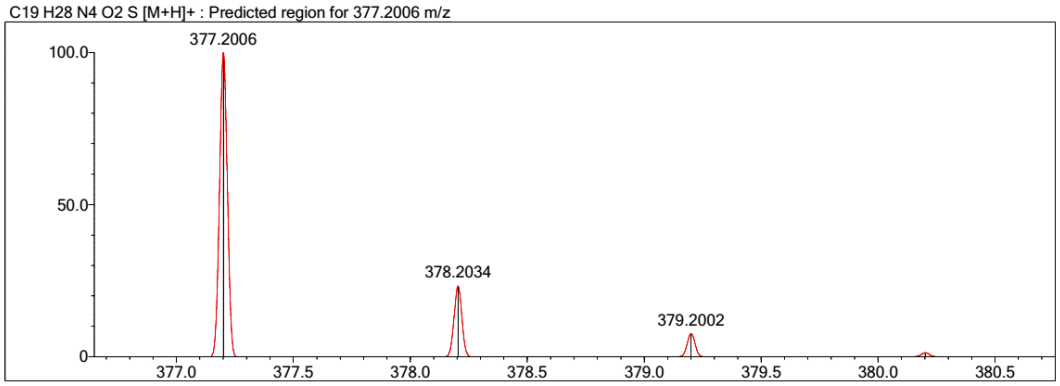

Rank	Score	Formula (M)	Ion	Meas. m/z	Pred. m/z	Df. (mDa)	Df. (ppm)	Iso	DBE
1	77.49	C19 H28 N4 O2 S	[M+H]+	377.1987	377.2006	-1.9	-5.04	86.49	8.0

Figure 5.90. *HR-MS of compound* ***4g***

5.2. Evaluation of Synthetic Methods

Two pathways each with three-step synthetic methods in the order of (A →B →D) and (A →C→E) were followed to obtain the derivatives **(3a-3j)** and **(4a-4g)**, respectively as illustrated in **Figure 5.91**. These two pathways share the first step of the synthetic method (A); however, the latter two steps are different in terms of the nature of the acetylating reactant (B versus C) and in terms of the reaction conditions (D versus E).

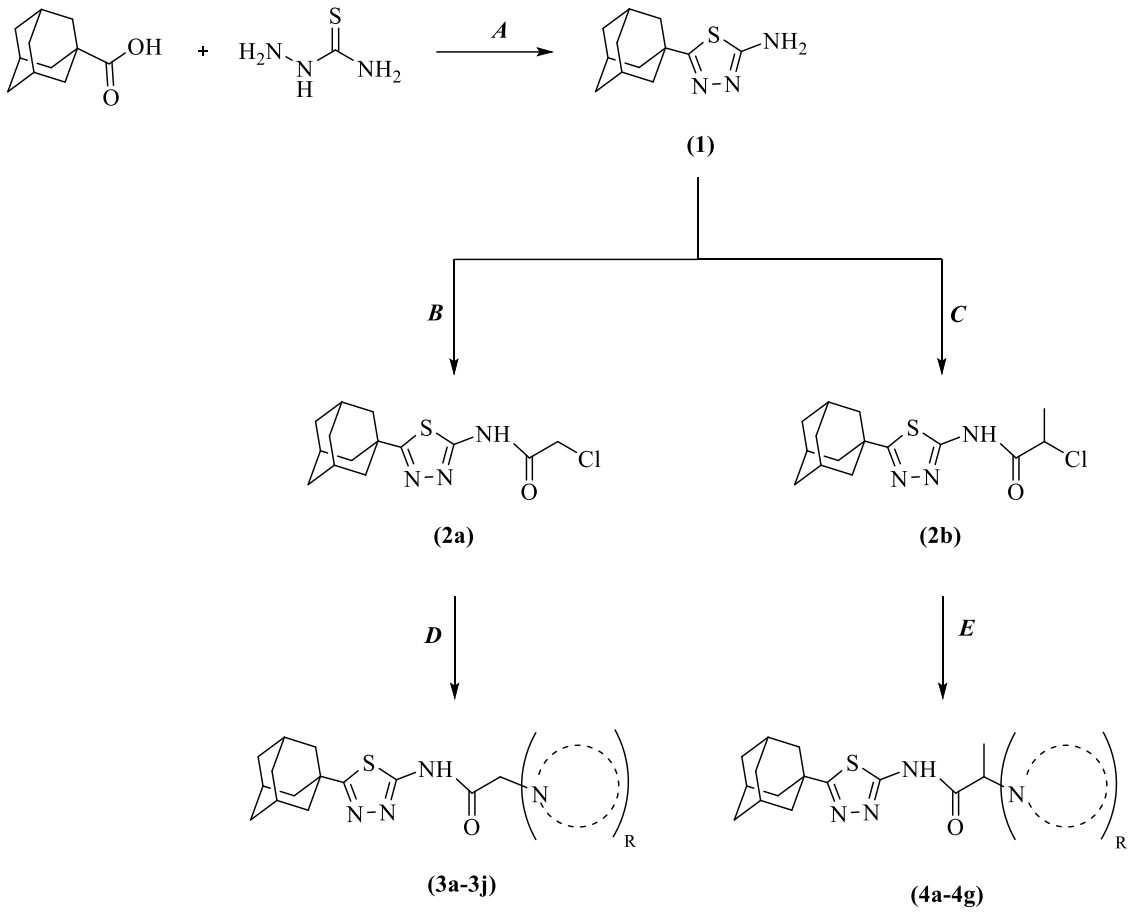

Figure 5.91. *General synthesis of the compounds (Methods A-E)*

In the first step synthetic method (A) that is the same in both pathways, 5-(adamantan-1-yl)-1,3,4-thiadiazol-2-amine **(1)** was cyclized upon a one-pot synthesis method that involves the interaction of 1-adamantane carboxylic acid and thiosemicarbazide in the presence of $POCl_3$. The reaction mechanism suggested for the cyclodehydration synthesis of 5-(adamantan-1-yl)-1,3,4-thiadiazol-2-amine **(1)** is presented in **Figure 5.92**.

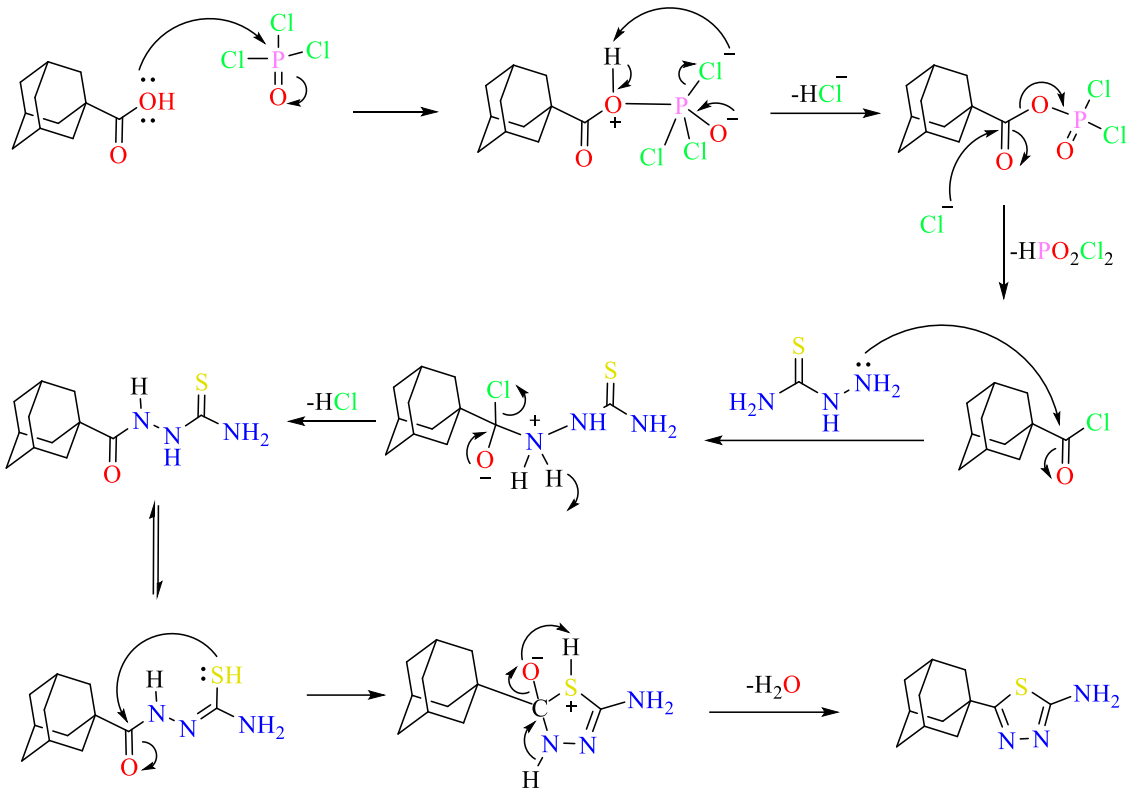

Figure 5.92. *Mechanism of cyclization of 5-(adamantan-1-yl)-1,3,4-thiadiazol-2-amine*

In the second step synthetic method in the two pathways (B and C), 5-(adamantan-1-yl)-1,3,4-thiadiazol-2-amine **(1)** in TEA/THF solution was reacted with chloroacetyl chloride in B procedure and with 2-chloropropionyl chloride in C procedure to produce *N*-(5-(adamantan-1-yl)-1,3,4-thiadiazol-2-yl)-2-chloroacetamide **(2a)** and *N*-(5-(adamantan-1-yl)-1,3,4-thiadiazol-2-yl)-2-chloropropanamide **(2b)**, respectively. The suggested reaction mechanism is presented in **Figure 5.93**.

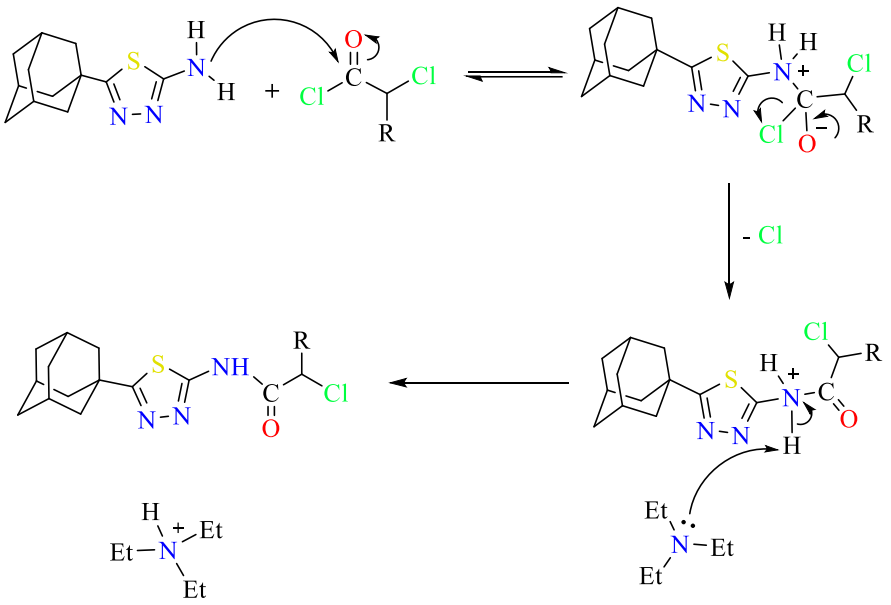

R: -H in method B, -CH_3 in method D

Figure 5.93. *Mechanism of the synthesis of N-(5-(adamantan-1-yl)-1,3,4-thiadiazol-2-yl)-2-chloroacetamide (Method B) and N-(5-(adamantan-1-yl)-1,3,4-thiadiazol-2-yl)-2-chloropropanamide (Method C)*

In the third step synthetic method (D) within the first pathway, *N*-(5-(adamantan-1-yl)-1,3,4-thiadiazol-2-yl)-2-substituted-acetamide derivatives **(3a-3j)** were obtained from the treatment of *N*-(5-(adamantan-1-yl)-1,3,4-thiadiazol-2-yl)-2-chloroacetamide **(2a)** with an appropriate cyclic secondary amine derivative in THF in the presence of TEA as a basic catalyst. The suggested mechanism for the reaction is presented in **Figure 5.94**.

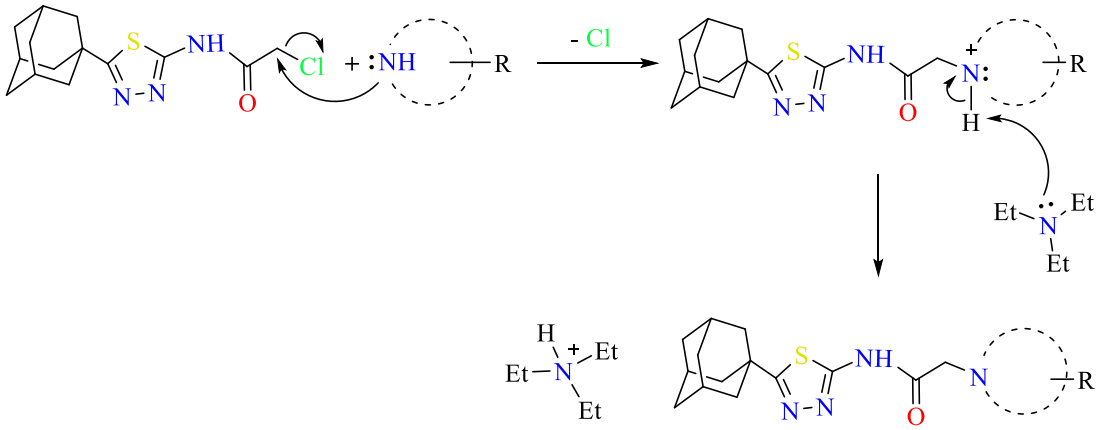

Figure 5.94. *Mechanism of the synthesis of N-(5-(adamantan-1-yl)-1,3,4-thiadiazol-2-yl)-2-substituted-acetamide derivatives (**3a-3j**)*

In the third step synthetic method (E) within the second pathway, *N*-(5-(adamantan-1-yl)-1,3,4-thiadiazol-2-yl)-2-substituted-propanamide derivatives **(4a-4g)** were obtained from the treatment of *N*-(5-(adamantan-1-yl)-1,3,4-thiadiazol-2-yl)-2-chloropropanamide **(2b)** with an appropriate cyclic secondary amine derivative in ACN in the presence of K_2CO_3 as a basic catalyst at 80-100 ˚C. The suggested mechanism for the reaction is presented in **Figure 5.95**.

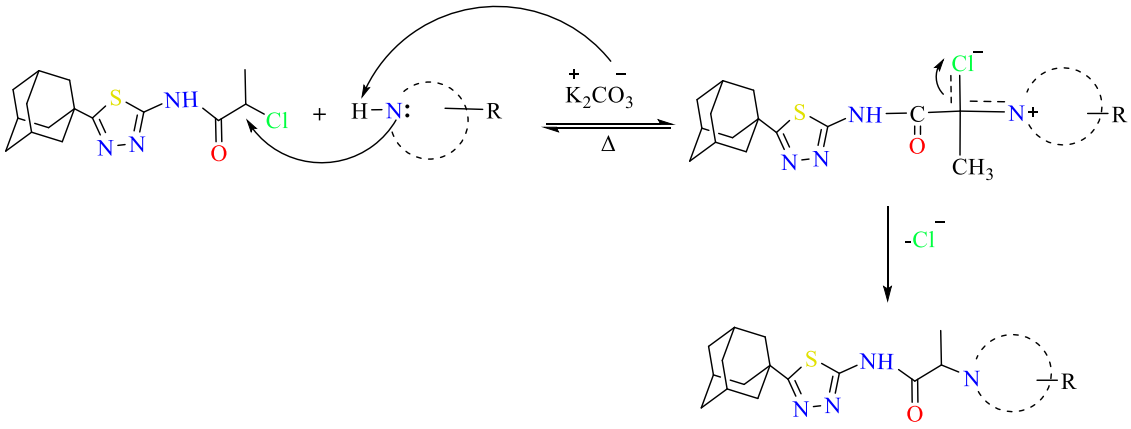

Figure 5.95. *Mechanism of the synthesis of N-(5-(adamantan-1-yl)-1,3,4-thiadiazol-2-yl)-2-substituted-propanamide derivatives (**4a-4g**)*

All final synthesized compounds are original derivatives except for the **3h** derivative which was synthesized previously by Wassel *et al.* [114]. The yield range of the final compounds was between 55-96% for **3a-3j** derivatives while it was between 50-74% for **4a-4g** derivatives. The purity and chemical structure of all final targeted compounds were approved using chemical spectral analysis including IR, ^{1}H-NMR, ^{13}C-NMR and HR-MS as shown in **subsection 5.1.**

5.3. Evaluation of Chemical Spectral Data

5.3.1. Evaluation of IR spectra

The main functional groups that are common between final synthesized compounds were confirmed using IR spectrometry. The N-H stretching of the amidic functional groups was seen above 3000 cm^{-1}. In the general range of 2974- 2777 cm^{-1}, the stretching of sp^3 C-H was observed. The C=O of the amidic functional group was noticed in the range of 1687- 1734 cm^{-1}. The stretching of the aromatic C=C and C=N were seen at 1597- 1290 cm^{-1} while the C-N stretching was at 1305- 1014 cm^{-1}.

5.3.2. Evaluation of ^{1}H-NMR spectra

All synthesized compounds contain an adamantane ring as a common scaffold in their basic skeleton. According to the obtained ^{1}H-NMR spectra, protons of the adamantyl moiety were observed to have three signals in the range of 1.68- 1.74 ppm, 1.95- 1.99 ppm and 2.01- 2.04 ppm in all compounds except in compounds **3e**, **4c** and **4f** which have two signals within the same general chemical shift range at around 1.80 ppm and 2.10 ppm. This could be due to the instrument's applied magnetic power that does not allow for an optimum resolution of these compounds, however both cases of the adamantyl moiety's spectra either as three signals [102] or as two signals [115] agree with the literature data. These signals were all noticed as singlets except for the first adamantane's signal within compound **3g** which appears as a multiplet because it was partially mixed with the signal of pyrrolidine's protons.

The signal of the amidic proton which is also a common scaffold was observed as a broad singlet peak in most derivatives in the range of 10.53- 12.64 ppm.

The protons of the carbon located between the amidic carbonyl carbon and the cyclic secondary amine derivatives that present as a methylene group in compounds **3a**-**3j** and a methine group in compounds **4a**-**4g** were observed to have a signal in the general range of 3.24- 4.03 ppm. As expected, the splitting of this signal was quartet for the methine group while it was singlet for the methylene group, however methylene group showed a doublet peak in compounds **3g** and **3i** probably due to the magnetic anisotropy.

In derivatives **4a-4g**, protons of -CH_3 within the propanamide group have a signal with chemical shift values in the range of 1.14-1.40 ppm. As expected, this signal has a doublet splitting in all compounds except in compound **4a** and compound **4e** the signal was noticed as a broad singlet peak due to the non-optimal resolution conditions and multiplet, respectively. The ^{1}H-NMR values of these common scaffolds are summarized in **Figure 5.96**.

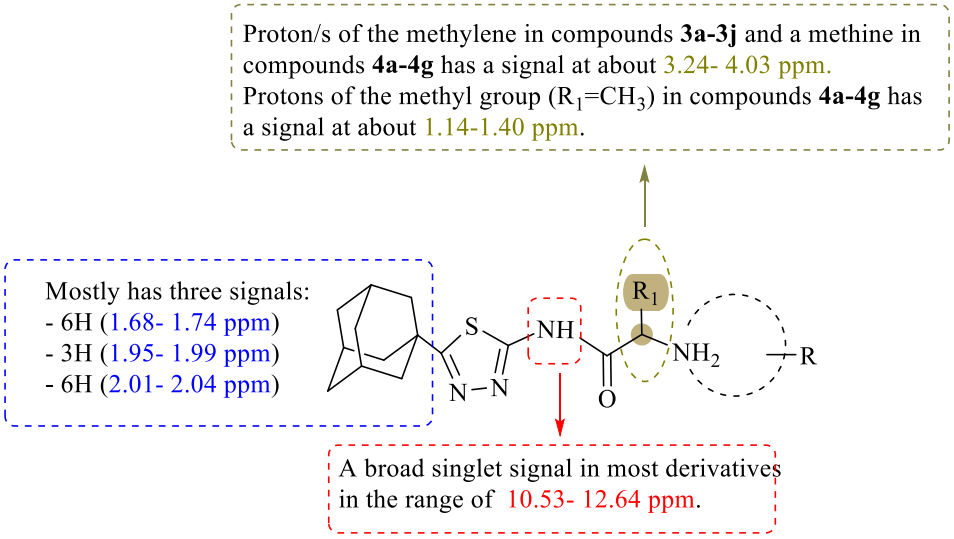

Figure 5.96. *The ^{1}H-NMR values of the common scaffolds in targeted compounds*

For the secondary cyclic amine substituents, protons of the piperazine ring were found to have chemical shift values in the range of 2.22- 3.75 ppm. The protons of pyrrolidine's methylene groups in compounds **3g** and **4f** were noticed as two signals, the first signal with multiplet peaks corresponds to protons at C_3 and C_4 in the general range of 1.68-1.84 ppm while the second signal corresponds to protons at C_2 and C_5 in the general range of 2.57-2.69 ppm with splitting either as a broad singlet peak because of the non-optimal resolution conditions in compound **3g** or as a multiplet peak in compound **4f**. The protons of the methylene groups within the piperidine ring in compound **3h** were observed as three signals, the first has multiplet peaks at 1.33-1.39 ppm corresponding to protons at C_4, the second has also multiplet peaks at 1.46-1.54 ppm corresponding to protons at C_3 and C_5 and the third has triplet peaks at 2.44 ppm corresponding to protons at C_2 and C_6. Two signals were assigned to morpholine's methylene groups, these signals appeared either as broad singlets peak because of the non-optimal resolution conditions or as multiplet peaks. The first signal has a broad singlet peak at 2.49 ppm and multiplet peaks at 2.43 -2.55 ppm in compounds **3i** and **4g**, respectively while the second signal was a broad singlet peak at 3.57 ppm in both compounds. The variation in the chemical shift values of the two signals of morpholine is caused by the difference in the electronegativity between nitrogen and oxygen atoms as methylene groups next to the nitrogen atom appear at lower chemical shift values than those next to the oxygen atom. In a similar pattern to morpholine's protons, protons of thiomorpholine's methylene groups were noticed to appear as two broad singlet signals. The first was at 2.6 ppm and

the second at 2.73 ppm in compound **3j** as the effect of electronegativity makes methylene's protons that are adjacent to the nitrogen atom shift to a higher chemical shift value than those adjacent to the sulfur atom.

Finally, protons of the substituents attached to the fourth position of piperazine showed consistent spectral results. Aromatic protons of the pyrimidinyl moiety in compounds **3a** and **4a** were noticed to have two signals, the first is a triplet peak at around 6.59-6.60 ppm while the second at around 8.31-8.34 ppm either as a doublet peak such as in compound **3a** or as broad singlet peak due to the insufficient resolution such as in compound **4a**. Four signals were related to the four aromatic protons of the pyridinyl moiety in compounds **3b** and **4b** ordered from the most shielded to the least shielded as follows, a triplet signal at around 6.59-6.62 ppm, a doublet signal at around 6.77-6.80 ppm, a triplet signal at around 7.48- 7.51 ppm and a doublet signal at around 8.07-8.09 ppm. The aromatic protons of the phenyl ring were assigned to three signals, the first has triplet peaks at 6.67 and 6.86 ppm, the second has doublet peaks at 6.91 and 6.95 ppm and the third has triplet peaks at 7.19 and 7.29 ppm in compounds **3c** and **4c**, respectively. Three signals were assigned to the aromatic furoyl substituent in compounds **3d** ordered from the lower to the higher chemical shift as follows, a triplet signal at 6.6 ppm, a doublet signal at 6.97 ppm and a singlet signal due to the insufficient resolution at 7.82 ppm.

Protons of the aliphatic ethyl groups have two signals, the first with triplet peaks relating to the -CH_3 at around 0.94 and 1.10 ppm while the second signal relating to the -CH_2- at around 2.22 and 2.46 ppm in compounds **3e** and **4d**, respectively. The aliphatic methyl group in compound **3f** showed a singlet signal at 2.14 ppm. For the aliphatic *N, N*-dimethylaminoethyl moiety in compound **4e**, the two methyl groups appeared as a singlet signal at around 2.12 ppm while the protons of the aminoethyl showed in the range of 2.95- 3.47 ppm.

5.3.3. Evaluation of ^{13}C-NMR spectra

Based on the obtained ^{13}C-NMR spectra of synthesized compounds, signals were detected as expected and in agreement with literature data. Carbons of the first common scaffold in all synthesized compounds, adamantane, were seen upfilded to the right of the spectra with four signals ranging from the most shielded to the least shielded as follows, (28.29- 28.74 ppm), (36.28- 36.74 ppm), (37.5- 38.07 ppm) and (43.12- 43.57 ppm) [94, 102]. In contrast, the two carbons of the second common aromatic scaffold, 1,3,4-thiadiazole, were observed downfield to the left of the spectra with two signals, the first of which ranges from 157.21 to 159-53 ppm while the second ranges from 168.5 to 172.86 ppm [102, 114]. The carbonyl carbon of the amide functional group which is the third common moiety in all compounds ranged between 173.94 to 175.98 ppm as the most deshielded signal downfield the spectra [114]. The carbon adjacent to the amidic carbonyl carbon which exists as a methylene group in compounds **3a-3j** and a methine group in compounds **4a-4g** has a signal in the range of 57.94- 61.61 ppm and 62.09- 66.85 ppm, respectively. For compounds **4a-4g**, the -CH_3 within the propanamide group was noticed in the range of 10.97- 15.40 ppm in the expected aliphatic region. The ^{13}C-NMR values of these common scaffolds are summarized in **Figure 5.97**.

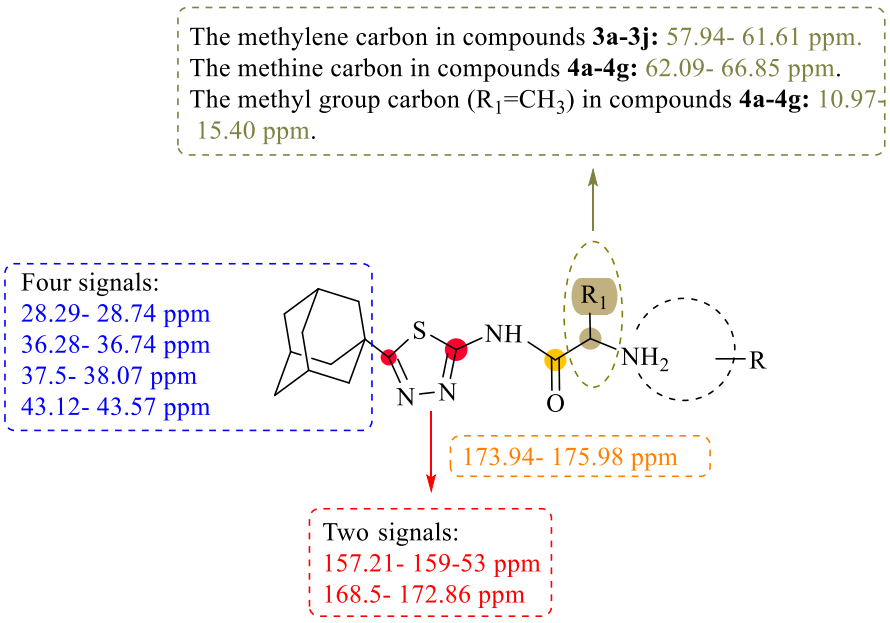

Figure 5.97. *The ^{13}C-NMR values of the common scaffolds in targeted compounds*

For the secondary cyclic amine substituents, carbons were observed in the general range of 23.47-66.55 ppm upfield to the right of the spectra. Piperazine moiety was observed to have two signals in the range of 43.66- 55.01 ppm in all synthesized compounds containing it except for compound **3d** which has one signal at 52.84 ppm. Two signals were assigned to the pyrrolidine moiety, the first of which was at 23.85 ppm and 23.47 ppm while the second was at 53.81 ppm and 50.88 ppm in compounds **3g** and **4f,** respectively. The piperidine moiety in compound **3h** was observed to have three signals, the first at 23.96 ppm, the second at 25.91 ppm and the third at 54.16 ppm. Morpholine moiety was also observed to have two signals, however their chemical shifts were observed at larger values due to the presence of an extra more electronegative oxygen atom. The first signal was at 53.3 ppm and 49.8 ppm while the second was at 66.55 ppm and 62.4 ppm for compounds **3i** and **4g**, respectively. Thiomorpholine moiety in compound **3j** displayed two signals as expected, the first at 27.95 ppm while the second at 54.95 ppm.

For substituents attached to the fourth position of piperazine moiety, the chemical shift values of their carbons differ depending on the nature of these substituents. Generally, aromatic substituents were noticed in the range of 107.42- 163.48 ppm while aliphatic substituents were noticed in the range of 11.96- 56.94 ppm. In addition to that, the carbonyl group that links piperazine and furan rings in compound **3d** was observed to have its signal at 158.7 ppm.

5.3.4. Evaluation of HR-MS spectra

The mass spectra of all final synthesized compounds were determined by LCMS-IT-TOF using the electrospray ionization- positive ion mode technique (ESI+). When samples are injected, they first passed through liquid chromatography to detect any impurities before their mass is analyzed by the mass spectrometer unit of the instrument.

According to the obtained results, no impurities were observed in the chromatogram. In addition to that, the [M+1] peaks in the mass spectra of all final synthesized compounds matched their expected molecular weights.

5.4. Evaluation of Acetylcholinesterase Inhibitory Activity of Targeted Compounds

All synthesized compounds were screened for their *in vitro* inhibitory activity against both AChE and BChE using donepezil and tacrine as the reference drugs against

AChE and BChE, respectively by using Elman modified method as explained in **subsection 4.5**. The % of inhibition at concentrations of 10^{-3} M and 10^{-4} M was first determined for all compounds and compounds that displayed higher than 50% inhibition activity at both concentrations were further investigated at additional lower concentrations from 10^{-5} to 10^{-9} M to determine their IC_{50} values and the obtained results are presented in **Table 5.1**.

Generally, compounds were inactive against BChE with % inhibition in the range of 24.663- 38.267 % and 20.262- 28.247 % at concentrations 10^{-3} M and 10^{-4} M, respectively. In contrast, compounds showed more inhibition efficacy toward AChE with % inhibition in the range of 42.827 -94.239 % and 34.424- 92.787 % at concentrations 10^{-3} M and 10^{-4} M, respectively.

While most of the compounds were able to inhibit more than 50% of AChEs at the concentration of 10^{-3} M, five compounds ordered in terms of activity as follows, **4a**, **4b**, **3a**, **3d** and **3b** were able to maintain their % of inhibition above 50 at the concentration of 10^{-4} M and showed inhibition activity at lower concentrations with significant IC_{50} values.

Notably, among other cyclic secondary amine derivatives present within the structures of synthesized compounds, the piperazine ring was the one present in all active compounds. This observation proposes many reasons including the fact that the piperazine ring can serve as a bio-isostere of the piperidine ring of donepezil [116, 117], as well as the presence of an additional nitrogen atom with acceptable electronegativity between the electronegativity of oxygen and sulfur in morpholine and thiomorpholine rings, respectively that can participate in compound's stabilization and binding within the active site. On the other hand, the piperazine ring within the most active compounds was linked at the fourth nitrogen atom to one of the heterocyclic aromatic substituents pyrimidinyl (**3a** and **4a**) or pyridinyl (**3b** and **4b**) or furoyl (**3d**), however the only difference between these compounds (**3a**, **3b** and **3d**) vs. (**4a**, **4b)** is an extra methyl group that firstly introduces a stereogenic center and secondly increases the hydrophobic character within the structures of the latter group.

Among these five active compounds, compound **4a** which has a pyrimidinyl moiety was the most potent AChEI with remarkable IC_{50} values of 0.036 μM. The substitution of pyrimidinyl moiety in compound **4a** for pyridinyl moiety in compound **4b** decreased the activity by nearly 1.4 times with an IC_{50} value of 0.052 μM. Despite the high structural

similarities between **4a** and **3a**, the absence of the methyl group, consequently the stereogenic center in compound **3a** was noticed to negatively affect the inhibition activity of this compound with an IC_{50} value of 0.067 μM that is nearly 1.8 times lower potent than compound **4a**, which highlight the importance of this methyl group in either introducing a special spatial arrangement for atoms or increasing the hydrophobic character within the active site. Compared to compound **3a**, the inhibition activity was decreased by nearly 4.3 times and 2.4 times for compounds **3b** and **3d**, respectively when the pyrimidinyl moiety in compound **3a** was replaced by either pyridinyl moiety in **3b** or fuoryl moiety in **3d**.

In summary, considering the structure-activity relationship of synthesized compounds, the presence of both the methyl group and the heterocyclic aromatic pyrimidinyl moiety attached to the nitrogen atom at the fourth position of the piperazine ring are the major factors that positively affect the inhibition activity of the synthesized compounds, however other possible factors are presented in **Figure 5.98**.

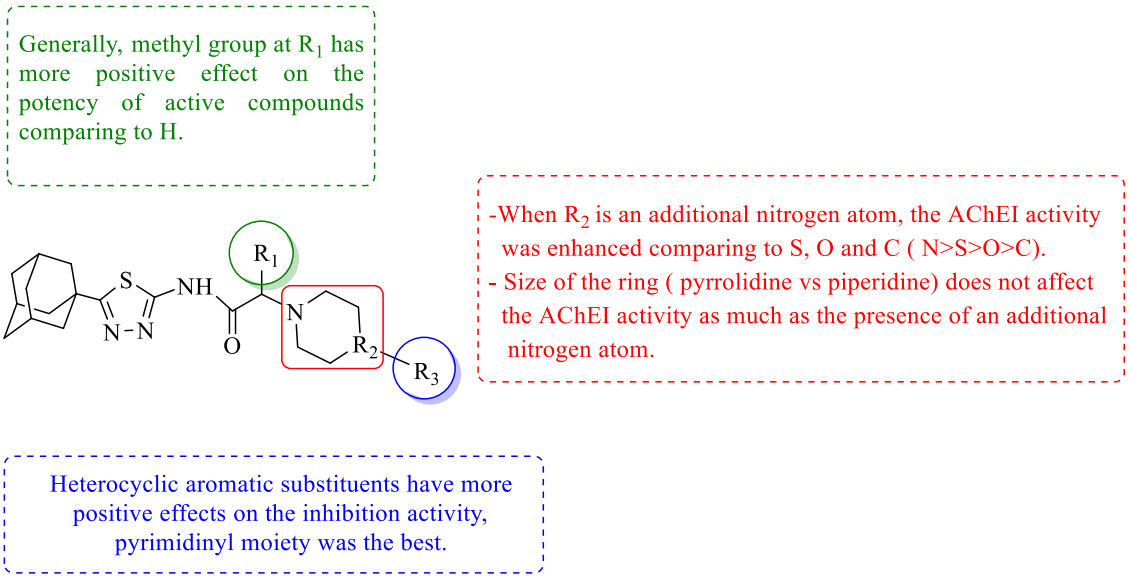

Figure 5.98. *General structural-activity relationship of the synthesized compounds*

Table 5.1. *% Inhibition at 10^{-3} and 10^{-4} M concentrations and IC_{50} (μM) values of the synthesized compounds, donepezil and tacrine against AChE and BChE.*

Compound	AChE % İnhibition		AChE IC_{50} (μM)	BChE % İnhibition		BChE IC_{50} (μM)
	10^{-3} M	10^{-4} M		10^{-3} M	10^{-4} M	
3a	**92.152 ±2.422**	**87.676 ±1.703**	**0.067 ±0.003**	31.521 ±0.832	27.608 ±0.751	>1000
3b	**86.759 ±1.069**	**81.334 ±0.964**	**0.288 ±0.011**	28.236 ±0.958	22.132 ±0.809	>1000
3c	**67.647 ±1.833**	39.086 ±0.897	>100	32.320 ±1.063	24.761 ±0.822	>1000
3d	**90.182 ±1.933**	**84.567 ±2.254**	**0.159 ±0.006**	27.608 ±0.847	21.459 ±0.885	>1000
3e	**79.432 ±2.197**	41.362 ±0.922	>100	36.747 ±1.055	23.841 ±0.947	>1000
3f	**82.595 ±1.958**	48.814 ±1.257	>100	31.089 ±1.157	20.262 ±0.844	>1000
3g	49.346 ±0.957	40.134 ±0.951	>1000	29.834 ±0.974	23.075 ±0.775	>1000
3h	43.487 ±1.084	34.424 ±0.729	>1000	34.959 ±1.162	26.966 ±0.875	>1000
3i	48.090 ±0.862	36.797 ±0.874	>1000	38.267 ±1.285	23.620 ±0.896	>1000
3j	**53.741 ±0.731**	42.551 ±0.933	>100	30.059 ±0.957	20.448 ±0.964	>1000
4a	**94.239 ±2.356**	**92.787 ±2.150**	**0.036 ±0.001**	27.111 ±0.850	22.195 ±0.917	>1000
4b	**92.848 ±1.957**	**89.561 ±1.824**	**0.052 ±0.002**	28.457 ±1.011	21.011 ±0.823	>1000
4c	46.637 ±1.041	35.364 ±0.889	>1000	32.962 ±1.389	27.336 ±0.970	>1000
4d	**79.723 ±2.374**	48.215 ±1.002	>100	24.663 ±0.959	20.547 ±0.830	>1000
4e	48.190 ±1.421	40.658 ±1.097	>1000	32.549 ±1.089	20.652 ±0.851	>1000
4f	**81.525 ±1.727**	39.438 ±0.944	>100	34.174 ±0.867	24.112 ±0.958	>1000
4g	42.827 ±0.879	38.790 ±0.985	>1000	33.464 ±0.966	28.247 ±0.958	>1000
Donepezil	99.156 ±1.302	97.395 ±1.255	0.0201 ±0.0010	-	-	-
Tacrine	-	-	-	99.827 ±1.378	98.675 ±1.450	0.0064 ±0.0002

5.5. Evaluation of Monoamine Oxidases Inhibitory Activity of Targeted Compounds

The *in vitro* inhibition activity of all synthesized compounds was tested also against MAO-A and MAO-B while moclobemide and selegiline were used as the reference drugs against MAO-A and MAO-B, respectively by using the fluorometric method as explained in **subsection 4.6**. The % of inhibition at concentrations of 10^{-3} M and 10^{-4} M was initially measured for all compounds, and those with more than 50% inhibitory activity at both concentrations were subsequently studied at lower concentrations ranging from 10^{-5} to 10^{-9} M to determine their IC_{50} values.

According to the obtained results in **Table 5.2**, compounds had no significant activity against MAO-A with % inhibition in the range of 25.134- 47.318 % at both 10^{-3} and 10^{-4} M concentrations. However, synthesized compounds were prominently more active against MAO-B with % inhibition in the range of 28.651- 93.471 % at the initial concentrations 10^{-3} and 10^{-4} M.

While most of the compounds showed over 50% inhibition against MAO-B at the initial concentration of 10^{-3} M, three compounds that are **3a, 4a** and **4b** retained their inhibition activity at the lower concentration of 10^{-4} M and were further investigated to calculate their IC_{50} values. Despite the finding that compounds were generally more potent toward AChE than MAO-B, they showed consistent activity results with the same three active compounds arranged as following **4a**, **4b** and **3a** in terms of activity against both enzymes. Among the three compounds, compound **4a** was also the most significant inhibitor against MAO-B with an IC_{50} of 0.054 μM, making it a remarkable dual inhibitor against both AChE and MAO-B enzymes. In addition to that, compounds **4b** and **3a** were moderately effective against MAO-B.

Table 5.2. *% Inhibition at 10^{-3} and 10^{-4} M concentrations and IC_{50} (μM) values of the synthesized compounds, moclobemide and selegiline against MAO-A and MAO-B.*

Compound	MAO-A % İnhibition		MAO-A IC_{50} (μM)	MAO-B % İnhibition		MAO-B IC_{50} (μM)
	10^{-3} M	10^{-4} M		10^{-3} M	10^{-4} M	
3a	39.166 ±1.321	31.059 ±0.959	>1000	**85.667 ±1.927**	**82.385 ±2.144**	**0.402 ±0.018**
3b	37.648 ±0.966	26.684 ±0.832	>1000	**72.142 ±2.052**	42.366 ±0.892	>100
3c	41.377 ±1.395	34.651 ±1.197	>1000	41.585 ±1.068	36.274 ±0.857	>1000
3d	36.289 ±0.922	27.469 ±0.874	>1000	46.752 ±0.866	28.651 ±0.721	>1000
3e	40.760 ±1.558	30.324 ±1.047	>1000	**68.823 ±1.833**	40.536 ±1.090	>100
3f	42.417 ±1.751	28.131 ±0.875	>1000	44.654 ±0.928	39.614 ±0.957	>1000
3g	43.668 ±1.907	30.866 ±0.920	>1000	48.890 ±0.974	40.159 ±0.962	>1000
3h	37.923 ±1.155	32.526 ±0.963	>1000	45.961 ±0.811	37.421 ±0.833	>1000
3i	34.439 ±0.947	27.941 ±0.885	>1000	**62.422 ±1.658**	42.744 ±1.108	>100
3j	38.121 ±1.223	25.134 ±0.874	>1000	**68.241 ±1.921**	46.864 ±0.857	>100
4a	40.048 ±1.675	33.259 ±1.097	>1000	**93.471 ±2.436**	**89.286 ±1.923**	**0.054 ±0.002**
4b	42.555 ±1.035	38.047 ±0.929	>1000	**91.552 ±1.866**	**88.679 ±2.144**	**0.141 ±0.006**
4c	39.699 ±0.984	31.697 ±0.752	>1000	**56.109 ±1.174**	41.666 ±0.721	>100
4d	46.862 ±1.427	32.586 ±0.961	>1000	**74.663 ±1.336**	40.528 ±0.968	>100
4e	40.723 ±1.021	36.838 ±0.964	>1000	48.358 ±0.855	36.423 ±0.959	>1000
4f	47.318 ±0.839	32.122 ±0.874	>1000	**52.754 ±1.328**	32.241 ±0.836	>100
4g	46.864 ±1.636	32.657 ±1.057	>1000	**77.921 ±1.878**	39.070 ±0.836	>100
Moclobemide	94.121 ±2.760	82.143 ±2.691	6.0613 ±0.2625	-	-	-
Selegiline	-	-	-	98.589 ±2.055	94.850 ±1.114	0.0374 ±0.0016

5.6. Evaluation of the Pharmacokinetic Profile

Besides evaluating pharmacological activity, an early prediction of the pharmacokinetic profile for active drug candidates is a necessity during the drug development process to avoid expensive late-stage failures [118]. According to the *in silico* obtained data as shown in **Table 5.3**, all active derivatives obey Lipinski's rule by causing no violation with molecular weights less than 500, one hydrogen bond donor, 5 to 6 hydrogen bond acceptors and 1.65- 2.69 octanol/water partition coefficient (MLogP). Thus, all compounds can serve as orally active drugs as they adhere to Lipinski's rule which requires no more than one violation [119]. In terms of aqueous solubility (Log S), all compounds are considered moderately soluble with -5.08 to -4.35 ranging values. Additionally, all compounds are highly absorbed from the gastrointestinal system. As drugs for neurological disorders including AD need to cross the BBB to reach their targets, the BBB permeability scores for active compounds were estimated and values were ranging from 3.36 to 4.21 indicating that they are good BBB permeable drug candidates for AD. DLS values were between 1.30 and 1.71 scores. Based on all these data, all synthesized active compounds are proved to have favorable *in silico* pharmacokinetic profiles which further supports their pharmacological activity.

Table 5.3. *Pharmacokinetic parameters of the active compounds* ***3a, 3b, 3d, 4a*** *and* ***4b***

Cpd.	MW[a]	HBA[a]	HBD[a]	MLogP[a]	LogS[a]	BBB Score[b]	GIA[a]	DLS[b]	No.V[a]
3a	439.58	6	1	1.88	-4.35	3.82	High	1.49	0
3b	438.59	5	1	2.48	-4.75	4.21	High	1.35	0
3d	455.57	6	1	1.65	-4.42	3.36	High	1.30	0
4a	453.6	6	1	2.09	-4.68	3.79	High	1.71	0
4b	452.62	5	1	2.69	-5.08	4.17	High	1.46	0
Donepezil	379.49	4	0	3.06	-4.81	5.29	High	1.56	0
Selegiline	187.28	1	0	3.25	-2.88	4.89	High	0.85	0

Cpd.: compound**, MW:** molecular weight (g/mol), **HBA:** number of hydrogen bond acceptors, **HBD:** number of hydrogen bond donors, **MLog P:** octanol/water partition coefficient, **Log S:** aqueous solubility (highly soluble > 0 > very soluble > −2 > soluble > −4 > moderately soluble > −6 > poorly soluble > −10 > insoluble), **BBB score:** blood-brain barrier score ranges from the lowest 0 to the highest 6 penetration, **GIA:** gastrointestinal absorption, **DLS:** drug-likeness score (0-2) and **No.V:** number of Lipinski's rule Violation. [a]: calculated using SwissADME software [109]. [b]: calculated using Molsoft software [111].

5.7. Evaluation of Molecular Docking

5.7.1. Docking within the active site of acetylcholinesterase enzyme.

Since synthesized compounds were more effective against AChE, molecular docking was applied to assess the possible binding interactions of the novel most active compounds **4a, 4b** and **3a** within the active site of AChE.

AChEs have a prominent narrow ≈ 20 Å long deep gorge that penetrates the middle of their structures and widens at the bottom leading to the central active site which is ≈ 4 Å away from the bottom [120]. Binding active sites within AChEs can be classified into two sites that are the central catalytic anionic site (CAS) and the peripheral anionic site (PAS). The CAS contains further four subunits that are esteratic subsite, anionic subsite, acyl pocket and oxyanion subsite. The esteratic subsite which contains the known catalytic triad amino acids Ser203, His447 and Glu334 is mainly responsible for the hydrolysis of the ester bond of ACh. The anionic subsite which contains Trp86, Tyr130, Tyr133, Tyr337 and Phe338 amino acids is important for the proper alignment of substrates and the stabilization of the substrate's positive charge by the formation of π-cation interactions. The acyl pocket which includes Phe295 and Phe297 amino acids binds to the acetyl group of ACh while the oxyanion subsite which includes the hydrogen bond donor residues Gly121, Gly122, and Ala204 binds to the carbonyl oxygen by hydrogen bond interactions which helps to stabilize the tetrahedral enzyme-substrate complex [116, 121-123].

In contrast, PAS locates on the surface of ChEs near the gorge entrance and containing Tyr72, Asp74, Tyr124, Tyr341 and Trp286 amino acid residues. It does not play a role itself in ACh hydrolysis, however, it can work as an allosteric modulator for the CAS. In addition, PAS was found to interact with the fibrils of Aβ peptides forming stable AChE- Aβ complexes which lead to significant increases in the neurotoxic Aβ aggregates formation in AD [124-127].

While AChEIs differ in their binding modes to either CAS or PAS or both simultaneously, the used reference within this study donepezil was found to be acting as dual binding sites inhibitor binding to both CAS and PAS. According to the crystal structure of the *h*AChE- donepezil complex reported by Cheung *et al.* in 2012, the indole rings of Trp86 in CAS and Trp286 in PAS form two important stacking π-π interactions with the benzyl and indanone rings of donepezil, respectively. Regarding the piperidine structural moiety, nitrogen can form water-mediated hydrogen bond interactions with

Tyr341 at the PAS and Tyr337 at the CAS that are permitted by ≈ 142˚ piperidine ring flipping, however, carbons at one side are packed tightly against the hydrophobic sides of Tyr337, Phe338 and His447 at CAS while carbons at the other side are oriented toward the negatively charged and hydrophilic sides of Asp74, Tyr124 at PAS [128]. Additional important binding interactions of donepezil were also reported using molecular modeling approaches including the π-cation interactions of the positive charged piperidine's nitrogen with the phenyl groups of Tyr341 [69], Tyr337 and Trp86 [129], the electrostatic interaction of the positive charged piperidine nitrogen with the negatively charged carboxylate group of Asp74 [130].

Lu *et al.* in their *in-silico* study which was published in 2011 emphasized that π-π stacking interactions with residues in the anionic subsite (Trp86, Tyr334 and Phe331) and in the PAS (Trp286), besides hydrogen bond interactions with residues at the bottom of the gorge are among the crucial binding interactions for potent AChEIs [131]. Additionally, the hydrogen bond interaction of Phe295, the π-π interaction of His447 [132] and the hydrogen bond interaction of Glu202 [123] have also been reported as crucial binding interactions for the inhibition of AChE.

Analysis of the two-dimensional (2D) and three-dimensional (3D) docking poses of the most active novel synthesized compounds **4a**, **4b** and **3a** which are displayed in **Figures 5.99**- **Figure 5.105** revealed that all these compounds can bind to both CAS and PAS, hence similarly to donepezil they are considered dual binding site inhibitors.

Each of the active compounds **4a**, **4b** and **3a** bind to AChE with a total of seven binding interactions, two of them at the PAS while the other five are at the CAS (**Figure 5.99**). The two binding interactions at the PAS are common in all three compounds involving a π-π stacking interaction between 1,3,4-thiadiazole ring moiety and Trp286 residue and another π-cation interaction between the positive ionized piperazine's nitrogen and Tyr341 residue. At the CAS, three common interactions are involved in the binding of these compounds to AChE, namely a π-cation interaction between Tyr337 in the anionic subsite and the positive ionized piperazine's nitrogen, a hydrogen bond interaction between Phe295 and N_3 of the 1,3,4-thiadiazole ring moiety and an aromatic hydrogen bond interaction (Ar H-bond) between the hydrogen at C_5 of the aromatic pyrimidine (**4a** and **3a**) or the hydrogen at C_4 of the aromatic pyridine (**4b**) and the carbonyl oxygen of Glh202 as shown in the 3D poses.

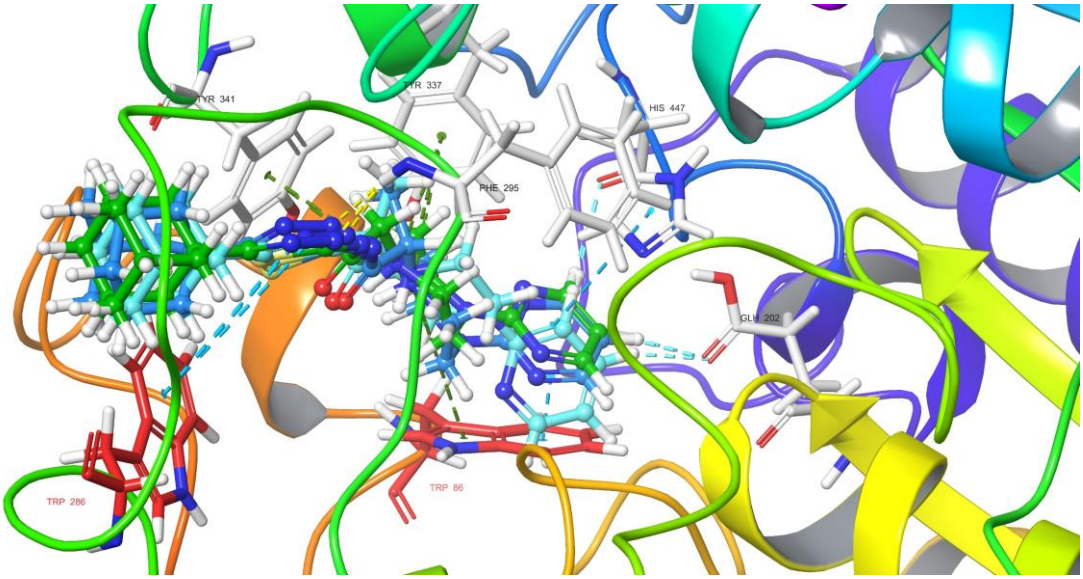

Figure 5.99. *3D Overlay of the three most active compounds (**3a**, **4a** and **4b**) in the active site of AChE*

Compound **4a** binds to AChE by additional two bonds, one involves the π-cation interaction of the indole ring of Trp86 with the positive ionized piperazine's nitrogen. The other one is an Ar H-bond interaction between the hydrogen at C_4 of the aromatic pyrimidine moiety with the carbonyl oxygen of His447 residue as shown in the 3D pose (**Figure 5.101**).

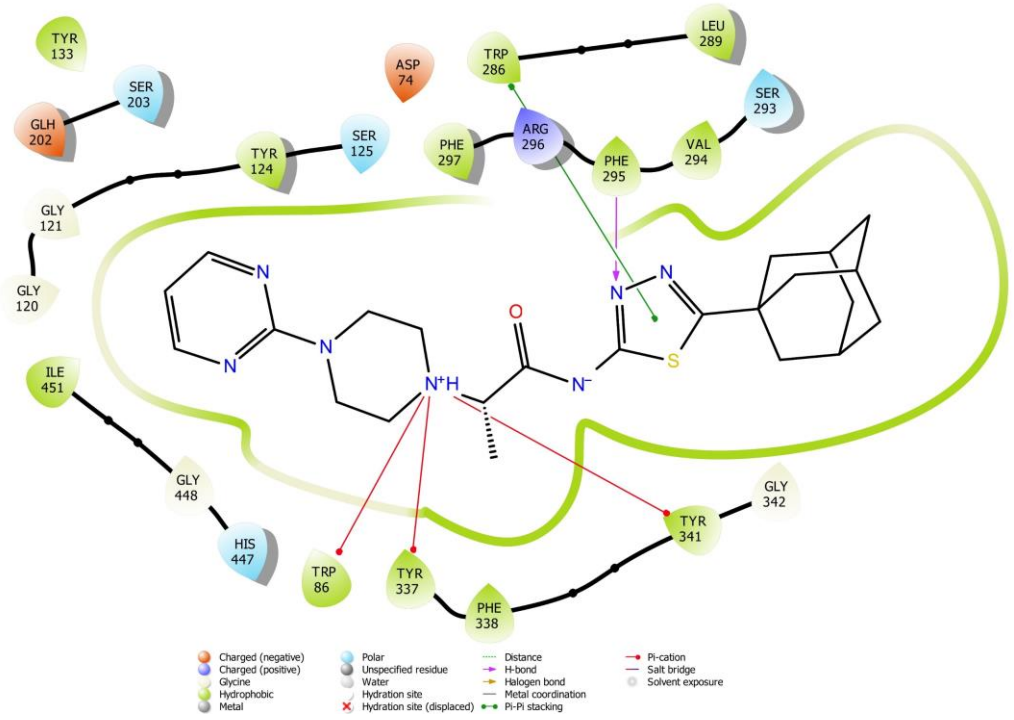

Figure 5.100. *2D Pose of the interaction of compound **4a** with AChE*

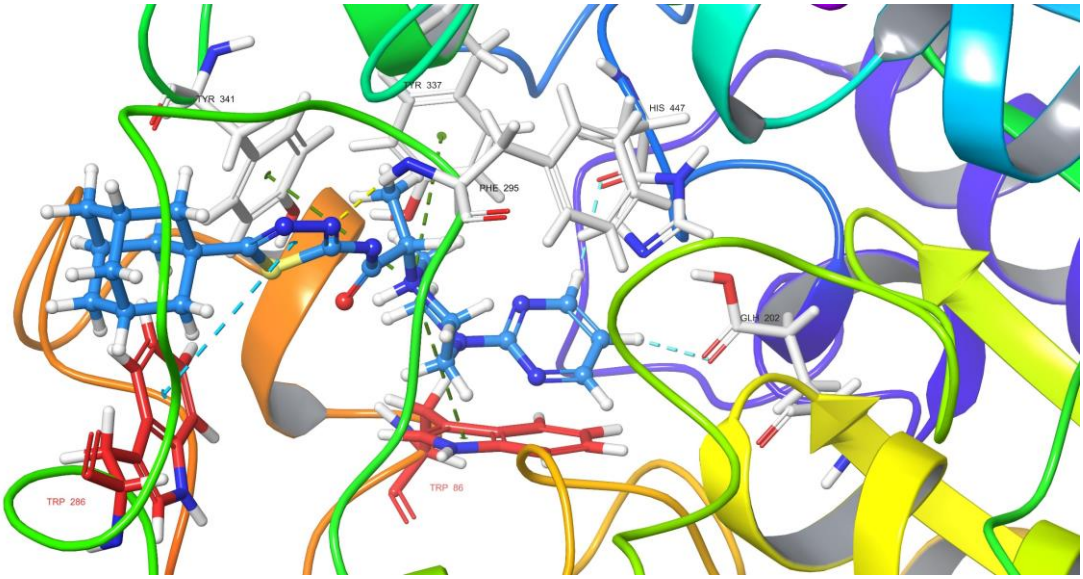

Figure 5.101. *3D Pose of the interaction of compound **4a** with AChE*

The indole ring of Trp86 was found to bind to compound **4b** by additional two bonds. One of which is a stacking π-π interaction with the pyridine moiety, similarly to donepezil. The other one is a π-cation interaction with the positive ionized piperazine's nitrogen, similarly to compound **4a**.

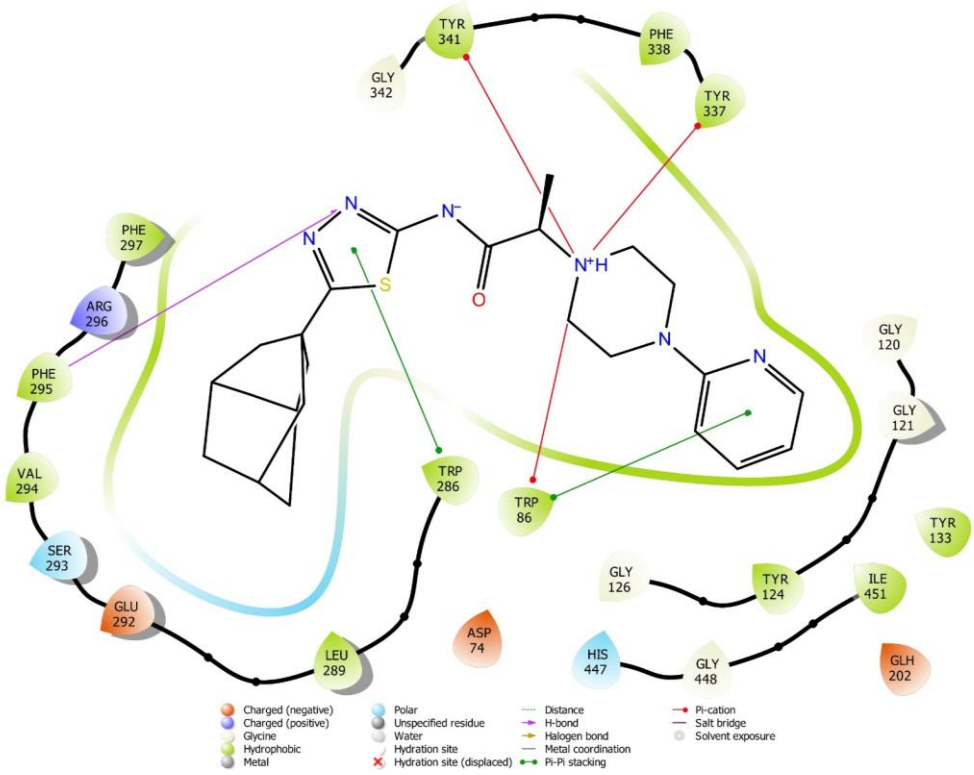

Figure 5.102. *2D Pose of the interaction of compound **4b** with AChE*

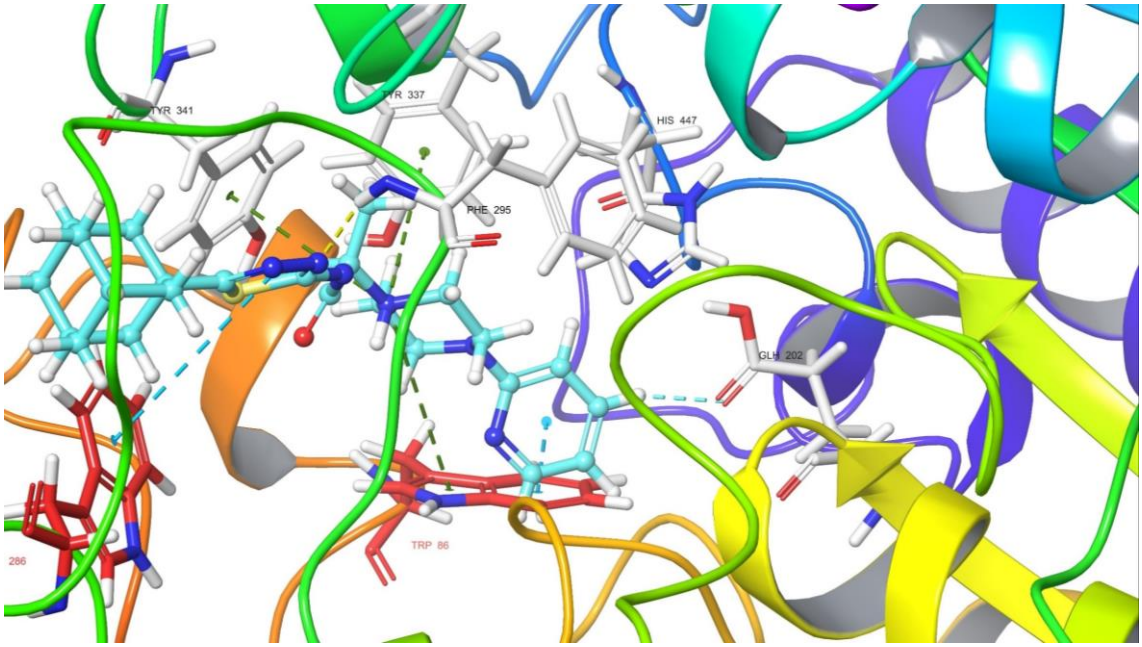

Figure 5.103. *3D Pose of the interaction of compound **4b** with AChE*

For compound **3a**, two additional binding interactions were also noticed, one is a π-π stacking interaction between the aromatic pyrimidine ring and His447 and the other is an Ar H-bond interaction as shown in the 3D pose (**Figure 5.105**) between the hydrogen at C_4 of the aromatic pyrimidine moiety with the carbonyl oxygen of His447 residue, similarly to compound **4a**. However, Trp86 was not found to participate in the binding interaction with the enzyme.

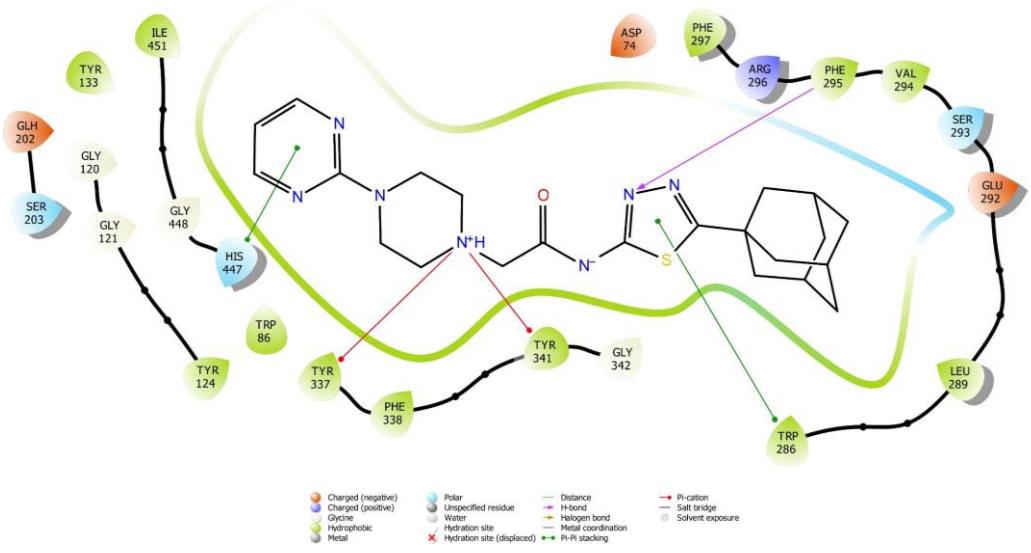

Figure 5.104. *2D Pose of the interaction of compound **3a** with AChE*

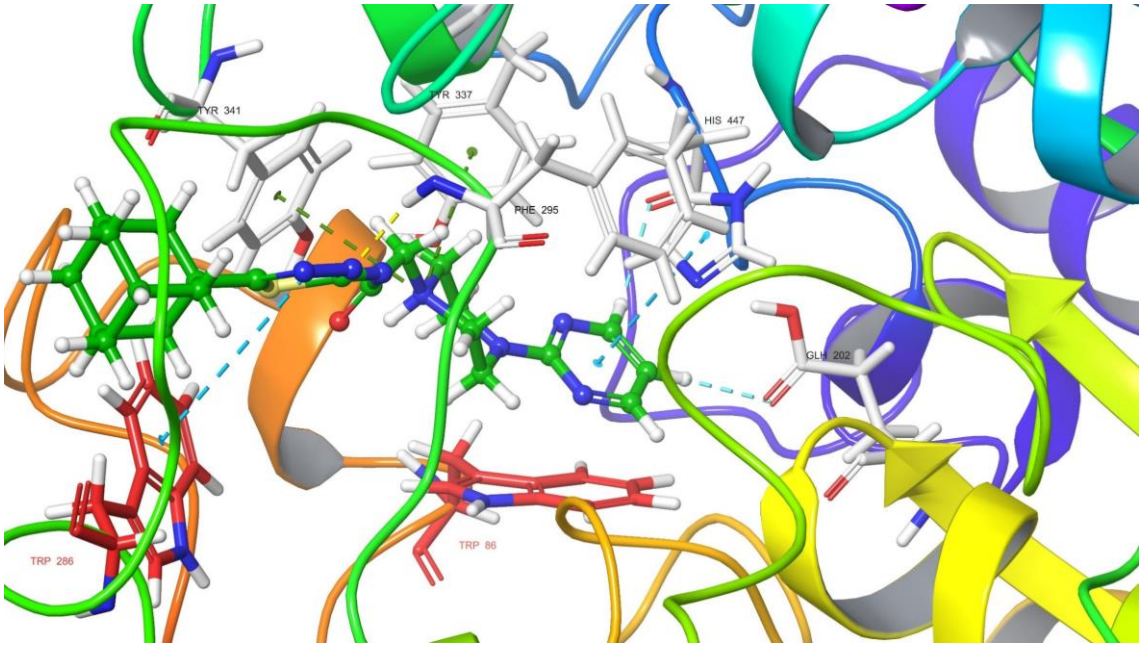

Figure 5.105. *3D Pose of the interaction of compound **3a** with AChE*

When the results of the *in vitro* inhibition activity against AChE and the results of the *in silico* docking studies were analyzed, it was noticed that compound **4a** which had the most potent activity among the three compounds comes in the middle between **3a** and **4b** in terms of the binding interaction pattern as one of the two additional interactions is in common with **3a** while the other is in common with **4b** as summarized in **Table 5.4**.

Overall, it can be concluded that besides the other important common interactions of the three compounds, maintaining balanced binding interactions with both residues Trp86 and His447 has the most positive effect on the activity as observed in compound **4a**. However, the absence of binding interaction with Trp86 as in compound **3a** decreases the activity more than the absence of binding interaction with His447 as in compound **4b** which emphasizes further the importance of the binding interaction with Trp86 in boosting the activity of potent AChEIs.

Table 5.4. *Summary of the binding interactions of the most active compounds with AChE*

	PAS		**CAS**						
	Tyr341 π-cation	Trp286 π-π	Tyr337 π-cation	Phe295 H-bond	GlH202 ArH-bond	His447 Ar H-bond	His447 π-π	Trp86 π-cation	Trp86 π-π
3a	✓	✓	✓	✓	✓	✓	✓		
4a	✓	✓	✓	✓	✓	✓		✓	
4b	✓	✓	✓	✓	✓			✓	✓

5.7.2. Docking within the active site of monoamine oxidase-B enzyme.

According to the crystal structure of *h*MAO-B, it has a dimeric structure with two cavities that are linked by gating residues Tyr326 and ILE199. The first one is a smaller hydrophobic entrance cavity whereas the second one is a larger hydrophobic substrate cavity where the substrate binding site and the FAD coenzyme are located. The FAD at the bottom of the substrate cavity, along with the two neighboring Tyr398 and Tyr435, form an aromatic cage that is responsible for amine recognition [133, 134].

Among the amino acid residues lining the active site of MAO, Tyr435 is considered a crucial one for potent substrate's activity while Tyr326 has also a positive effect on the activity. Additionally, lipophilicity and binding interactions with Gln206 appeared to play a beneficial role in substrate selectivity for MAO-B [134, 135].

Analysis of the 2D pose (**Figure 5.106**) and 3D pose (**Figure 5.107**) of the molecular docking study for the most active compound **4a** against *h*MAO-B enzyme showed that the compound fitted well inside the active site and is quite close to the FAD cofactor with a total of seven binding interactions. Interestingly, four of these bonds involve the heterocyclic pyrimidinyl moiety of the compound. Among these four bonds, one was a π–π stacking interaction with the phenyl group of Tyr435 which is a crucial amino acid residue for the binding interaction of many potent compounds. The other three bonds of pyrimidinyl moiety were aromatic H-bond interactions, two are between the hydrogens at C_4 and C_5 and the carbonyl oxygen of Tyr434 while the last is between the hydrogen at C_6 and Cys172 residue as shown in the 3D pose. The 1,3,4-thiadiazole moiety was found to participate in an additional π–π stacking interaction, similar to its interaction with AChE, but this time with the phenyl group of Tyr326 amino acid residue, which at the same time interact with the amidic carbonyl oxygen through aromatic H-bond interaction as shown in the 3D pose. Additionally, a hydrogen bond interaction was found between the ionized positive nitrogen atom of the piperazine ring and the carbonyl oxygen of Gln 206 which is a relevant residue for MAO-B selectivity.[134, 135].

Overall, the *in silico* docking result of compound **4a** was in harmony with the *in vitro* inhibition activity evaluation against *h*MAO-B.

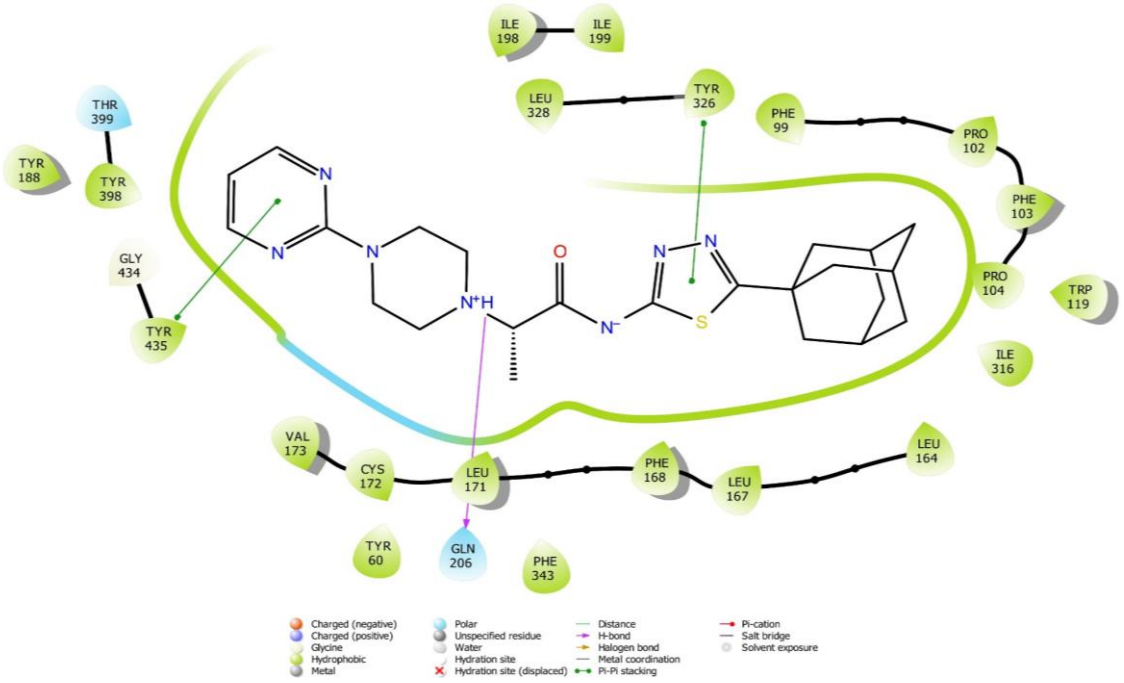

Figure 5.106. *2D Pose of the interaction of compound **4a** with hMAO-B*

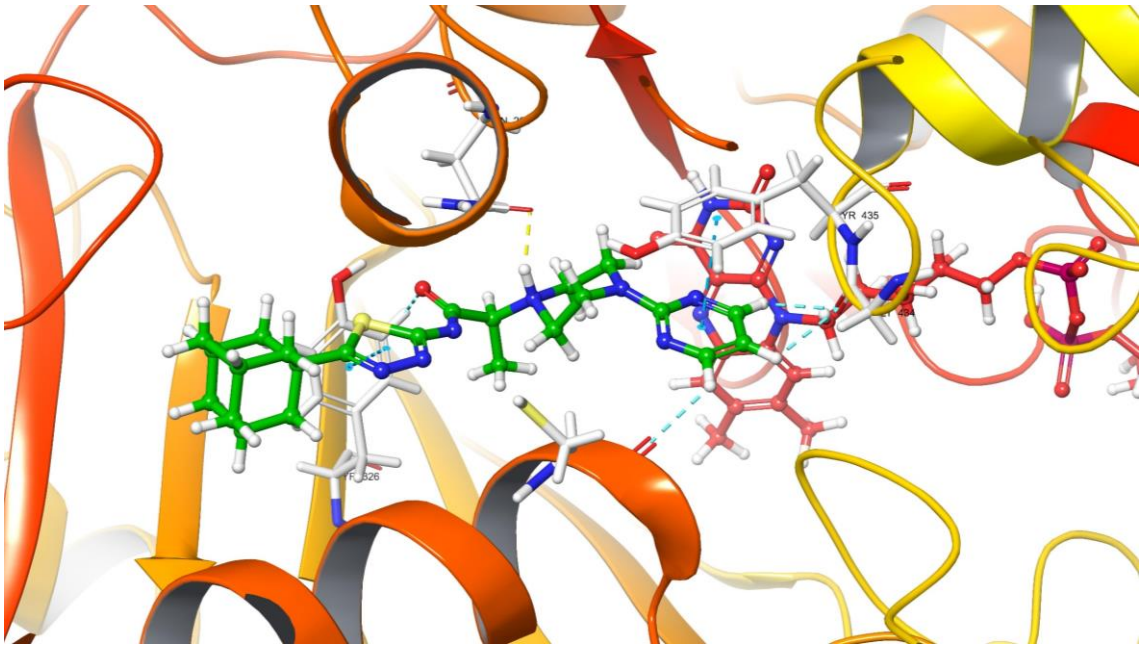

Figure 5.107. *3D Pose of the interaction of compound **4a** with hMAO-B*

6. CONCLUSION AND FURTHER RECOMMENDATIONS

Due to the complex nature of AD and the insufficient efficacy of the clinically used single-targeted drugs, researchers have turned their focus to the design and development of MTDs that interact with many targets involved in the disease's pathogenetic pathways. In the present work, the wide biological profile, improved lipophilicity, and metabolic stability of the 1,3,4-thiadiazole ring, as well as the characteristic properties of the bulky lipophilic adamantane structure, were used in the design and synthesis of novels *N*-(5-(adamantan-1-yl)-1,3,4-thiadiazol-2-yl)-2-(4-un/substituted) cyclic secondary amino-acetamide/propanamide derivatives that were further evaluated against both ChEs and MAOs which contribute negatively to AD pathogenesis.

According to the biological evaluation results, compounds showed more activity toward ChEs than MAOs. In terms of the activity against ChEs, compounds were significantly more active toward AChEs than BChs with compounds **3a, 3b, 3d, 4a** and **4b** possessing considerable inhibition activity against AChEs, however compounds **4a, 4b** and **3a** were the most active, respectively with binding ability to both CAS and PAS within AChE active site. Thus, they have a secondary non-cholinergic function associated with their ability to bind PAS and prevent the formation of the neurotoxic AChE- Aβ complexes. In terms of the activity against MAOs, compounds were more active toward MAO-B than MAO-A with compounds **3a**, **4a** and **4b** showing considerable inhibition activity against MAO-B, however compound **4a** was the most active. Overall, compounds **3a**, **4a**, and **4b** have dual inhibitory activity against AChE and MAO-B, with compound **4a** being the most active and a viable dual inhibitor candidate with a competent *in silico* pharmacokinetic profile.

In the light of all findings, additional structural modifications, additional biological assessments against other AD-associated pathological targets, *in vivo* cytotoxicity studies and *in-vivo* investigation of the pharmacokinetic profile of the most active compounds are all suggested for future studies.

REFERENCES

[1] World Health Organization (2021): Dementia. WHO.

[2] Serge Gauthier, P.R.-N., José A. Morais, Claire Webster (2021): World Alzheimer Report 2021: Journey through the diagnosis of dementia. London, England.

[3] Abeysinghe, A., Deshapriya, R., Udawatte, C. (2020). Alzheimer's disease; a review of the pathophysiological basis and therapeutic interventions. *Life Sci.*, 256, 117996.

[4] Kumar, N., Kumar, V., Anand, P., Kumar, V., Ranjan Dwivedi, A., Kumar, V. (2022). Advancements in the development of multi-target directed ligands for the treatment of Alzheimer's disease. *Bioorg. Med. Chem.*, 61, 116742.

[5] Bartus, R.T., Dean, R.L., 3rd, Beer, B., Lippa, A.S. (1982). The cholinergic hypothesis of geriatric memory dysfunction. *Science*, 217 (4558), 408-414.

[6] Guo, J., Mi, Z., Jiang, X., Zhang, C., Guo, Z., Li, L., Gu, J., Zhou, T., Bai, R., Xie, Y. (2021). Design, synthesis and biological evaluation of potential anti-AD hybrids with monoamine oxidase B inhibitory and iron-chelating effects. *Bioorg. Chem.*, 108, 104564.

[7] Manzoor, S., Hoda, N. (2020). A comprehensive review of monoamine oxidase inhibitors as Anti-Alzheimer's disease agents: A review. *Eur. J. Med. Chem.*, 206, 112787.

[8] Marucci, G., Buccioni, M., Ben, D.D., Lambertucci, C., Volpini, R., Amenta, F. (2021). Efficacy of acetylcholinesterase inhibitors in Alzheimer's disease. *Neuropharmacology*, 190, 108352.

[9] Sharma, K. (2019). Cholinesterase inhibitors as Alzheimer's therapeutics (Review). *Mol. Med. Rep.*, 20 (2), 1479-1487.

[10] Ferris, S.H. (2003). Evaluation of memantine for the treatment of Alzheimer's disease. *Expert Opin. Pharmacother.*, 4 (12), 2305-2313.

[11] Schmitt, F., Ryan, M., Cooper, G. (2007). A brief review of the pharmacologic and therapeutic aspects of memantine in Alzheimer's disease. *Expert Opin. Drug Metab. Toxicol.*, 3 (1), 135-141.

[12] Haddad, H.W., Malone, G.W., Comardelle, N.J., Degueure, A.E., Kaye, A.M., Kaye, A.D. (2022). Aducanumab, a novel anti-amyloid monoclonal antibody, for

the treatment of Alzheimer’s disease: A Comprehensive review. *J. Health Psychol. Res.*, 10 (1)

[13] Winslow, B.T., Onysko, M.K., Stob, C.M., Hazlewood, K.A. (2011). Treatment of Alzheimer disease. *Am. Fam. Physician.*, 83 (12), 1403-1412.

[14] Massoud, F., Leger, G.C. (2011). Pharmacological treatment of Alzheimer disease. *Can. J. Psychiatry*, 56 (10), 579-588.

[15] Agatonovic-Kustrin, S., Kettle, C., Morton, D.W. (2018). A molecular approach in drug development for Alzheimer's disease. *Biomed. Pharmacother.*, 106, 553-565.

[16] Revadigar, V., Ghalib, R.M., Murugaiyah, V., Embaby, M.A., Jawad, A., Mehdi, S.H., Hashim, R., Sulaiman, O. (2014). Enzyme inhibitors involved in the treatment of Alzheimer’s disease, In *Drug Design and Discovery in Alzheimer's Disease*, (p. 142-198).

[17] Saglik, B.N., Kaya Cavusoglu, B., Osmaniye, D., Levent, S., Acar Cevik, U., Ilgin, S., Ozkay, Y., Kaplancikli, Z.A., Ozturk, Y. (2019). In vitro and in silico evaluation of new thiazole compounds as monoamine oxidase inhibitors. *Bioorg. Chem.*, 85, 97-108.

[18] Guzior, N., Wieckowska, A., Panek, D., Malawska, B. (2015). Recent development of multifunctional agents as potential drug candidates for the treatment of Alzheimer's disease. *Curr. Med. Chem.*, 22 (3), 373-404.

[19] Hiremathad, A., Piemontese, L. (2017). Heterocyclic compounds as key structures for the interaction with old and new targets in Alzheimer's disease therapy. *Neural Regen. Res.*, 12 (8), 1256-1261.

[20] Martorana, A., Giacalone, V., Bonsignore, R., Pace, A., Gentile, C., Pibiri, I., Buscemi, S., Lauria, A., Piccionello, A.P. (2016). Heterocyclic scaffolds for the treatment of Alzheimer's disease. *Curr. Pharm. Des.*, 22 (26), 3971-3995.

[21] Haider, S., Alam, M.S., Hamid, H. (2015). 1,3,4-Thiadiazoles: a potent multi targeted pharmacological scaffold. *Eur. J. Med. Chem.*, 92, 156-177.

[22] Patani, G.A., LaVoie, E.J. (1996). Bioisosterism: A rational approach in drug design. *Chem. Rev.*, 96 (8), 3147-3176.

[23] Wishnok, J.S. (1973). Medicinal properties of adamantane derivatives. *J. Chem. Educ.*, 50 (11), 780-789.

[24] Lamoureux, G., Artavia, G. (2010). Use of the adamantane structure in medicinal chemistry. *Curr. Med. Chem.*, 17 (26), 2967-2978.

[25] Wanka, L., Iqbal, K., Schreiner, P.R. (2013). The lipophilic bullet hits the targets: medicinal chemistry of adamantane derivatives. *Chem. Rev.*, 113 (5), 3516-3604.

[26] Asif, M. (2016). Chemistry, synthesis and progress report on biological activities of thiadiazole compounds - a review. *Mediterr. J. Chem.*, 5 (5), 568-588.

[27] Sandström, J. (1968). Recent advances in the chemistry of 1,3,4-thiadiazoles, In *Advances in Heterocyclic Chemistry*, 9, (165-209).

[28] Chiacchio, U., Romeo, G. (2011). Thiadiazoles, In *Modern Heterocyclic Chemistry*, (p. 1253-1400).

[29] Kornis, G. (1984). 1,3,4-Thiadiazoles, In *Comprehensive Heterocyclic Chemistry*, (p. 545-577).

[30] Hu, Y., Li, C.Y., Wang, X.M., Yang, Y.H., Zhu, H.L. (2014). 1,3,4-Thiadiazole: synthesis, reactions, and applications in medicinal, agricultural, and materials chemistry. *Chem. Rev*, 114 (10), 5572-5610.

[31] Sainsbury, M. (1964). Five-membered heterocyclic compounds with three hetero-atoms in the ring, In *Rodd's Chemistry of Carbon Compounds*, (p. 1-209).

[32] Goerdeler, J., Ohm, J., Tegtmeyer, O. (2006). Darstellung und eigenschaften des 1.2.4- und des 1.3.4-thiodiazols. *Chem. Ber.*, 89 (6), 1534-1543.

[33] Fromm, E., Layer, E., Nerz, K. (1923). Abkömmlinge von thio-semicarbaziden und hydrazo-dithio-dicarbonamiden. *Justus Liebigs Ann. Chem.*, 433 (1), 1-17.

[34] Young, R.W., Wood, K.H. (2002). The cyclization of 3-acyldithiocarbazate esters1. *J. Am. Chem. Soc.*, 77 (2), 400-403.

[35] Foroumadi, A., Kiani, Z., Soltani, F. (2003). Antituberculosis agents VIII. Il *Farmaco*, 58 (11), 1073-1076.

[36] Hoggarth, E. (1949). 251. Compounds related to thiosemicarbazide. Part II. 1-Benzoylthiosemicarbazides. *J. Chem. Soc.(Resumed)*, 1163-1167.

[37] Whitehead, C.W., Traverso, J.J. (2002). Reactions of orthoesters with ureas. II. *J. Am. Chem. Soc.*, 77 (22), 5872-5877.

[38] Kurzer, F. (1961). 315. Thiadiazoles. Part XI. Synthesis and cyclisation of N-(thiobenzamido)guanidines and related compounds. *J. Chem. Soc. (Resumed)*, 1617-1625.

[39] Grigat, E., Pütter, R. (2006). Chemie der cyansäureester, IX: Umsetzung von cyansäureestern mit carbonsäuren und carbonsäurederivaten. *Chem. Ber.,* 98 (5), 1359-1364.

[40] Tsuji, T., Takenaka, K. (1982). Convenient synthesis of 2,7-disubstituted 5h-1,3,4-thiadiazolo[3,2-a]pyrimidin-5-ones and related compounds. *Bull. Chem. Soc. Jpn.,* 55 (2), 637-638.

[41] Thomsen, I., Pedersen, U., Rasmussen, P.B., Yde, B., Andersen, T.P., Lawesson, S.O. (1983). Novel and convenient methods for the preparation of substituted thiophenes, thiazoles, and 1,3,4-thiadiazole-2(3H)-thiones from bifunctional substrates. *Chem. Lett.,* 12 (6), 809-810.

[42] Chapleo, C.B., Myers, M., Myers, P.L., Saville, J.F., Smith, A.C., Stillings, M.R., Tulloch, I.F., Walter, D.S., Welbourn, A.P. (1986). Substituted 1,3,4-thiadiazoles with anticonvulsant activity. 1. Hydrazines. *J. Med. Chem.,* 29 (11), 2273-2280.

[43] Cho, N.S., Kim, G.N., Párkányi, C. (1993). Synthesis of 5-aroylamino-3H-1,3,4-thiadiazole-2-thiones and their tautomerism. *J. Heterocycl. Chem.,* 30 (2), 397-401.

[44] Kiryanov, A.A., Sampson, P., Seed, A.J. (2001). Synthesis of 2-alkoxy-substituted thiophenes, 1,3-thiazoles, and related S-heterocycles via Lawesson's reagent-mediated cyclization under microwave irradiation: applications for liquid crystal synthesis. *J. Org. Chem.,* 66 (23), 7925-7929.

[45] Niu, P., Kang, J., Tian, X., Song, L., Liu, H., Wu, J., Yu, W., Chang, J. (2015). Synthesis of 2-amino-1,3,4-oxadiazoles and 2-amino-1,3,4-thiadiazoles via sequential condensation and I_2-mediated oxidative C-O/C-S bond formation. *J. Org. Chem.,* 80 (2), 1018-1024.

[46] Jakovljević, K., Joksović, M.D., Botta, B., Jovanović, L.S., Avdović, E., Marković, Z., Mihailović, V., Andrić, M., Trifunović, S., Marković, V. (2019). Novel 1,3,4-thiadiazole conjugates derived from protocatechuic acid: Synthesis, antioxidant activity, and computational and electrochemical studies. *C. R. Chim.,* 22 (8), 585-598.

[47] Chandra Sekhar, D., Venkata Rao, D.V., Tejeswara Rao, A., Lav Kumar, U., Jha, A. (2019). Design and synthesis of 1,3,4-thiadiazole derivatives as novel anticancer and antitubercular agents. *Russ. J. Gen. Chem.,* 89 (4), 770-779.

[48] Xue, W., Li, X., Ma, G., Zhang, H., Chen, Y., Kirchmair, J., Xia, J., Wu, S. (2020). N-thiadiazole-4-hydroxy-2-quinolone-3-carboxamides bearing heteroaromatic rings as novel antibacterial agents: Design, synthesis, biological evaluation and target identification. *Eur. J. Med. Chem.,* 188, 112022.

[49] Mazzone, G., Puglisi, G., Marchetta, G., Corsaro, A. (1984). 2-pyridyl-5-alkyloxyphenyl-1,3,4-thiadiazoles by the action of sulfur on methylpyridines in the presence of alkyloxybenzoylhydrazines. *J. Heterocycl. Chem.,* 21 (1), 181-184.

[50] Mazzone, G., Puglisi, G., Bonina, F., Corsaro, A. (1983). A new synthesis of symmetrical 2,5-diaryl-1,3,4-thiadiazoles. *J. Heterocycl. Chem.,* 20 (5), 1399-1401.

[51] Lebrini, M., Bentiss, F., Lagrenée, M. (2005). Rapid synthesis of 2,5-disubtituted 1,3,4-thiadiazoles under microwave irradiation. *J. Heterocycl. Chem.,* 42 (5), 991-994.

[52] Linganna, N., LokanathaRai, K.M. (2006). Transformation of 1,3,4-oxadiazoles to 1,3,4-thiadiazoles using thiourea. *Synth. Commun.,* 28 (24), 4611-4617.

[53] Han, X., Yu, Y.L., Hu, Y.S., Liu, X.H. (2021). 1,3,4-Thiadiazole: A privileged scaffold for drug design and development. *Curr. Top. Med. Chem.,* 21 (28), 2546-2573.

[54] Hegab, M., Shamroukh, A. (2020). A Review on synthesis, therapeutic, and computational studies of substituted 1, 3, 4 thiadiazole derivatives. *Egypt J. Chem.,* 63 (11), 4387-4408.

[55] Jain, A.K., Sharma, S., Vaidya, A., Ravichandran, V., Agrawal, R.K. (2013). 1,3,4-Thiadiazole and its derivatives: A review on recent progress in biological activities. *Chem. Biol. Drug. Des.,* 81 (5), 557-576.

[56] Khalilullah, H., Khan, M.U., Mhmood, D., Akhtar, J., Osman, G. (2014). 1,3,4-Thiadiazole: A biologically active scaffold. *J. Pharm. Pharm. Sci.,* 6 (9), 8-15.

[57] Joseph, L., George, M., Mathews, P. (2015). A review on various biological activities of 1, 3, 4-thiadiazole derivatives. *J. Pharm. Chem. Biol. Sci.,* 3 (1), 329-345.

[58] Aliabadi, A. (2016). 1,3,4-Thiadiazole based anticancer agents. *Anticancer Agents Med. Chem.,* 16 (10), 1301-1314.

[59] Anthwal, T., Nain, S. (2021). 1,3,4-Thiadiazole scaffold: As anti-epileptic agents. *Front. Chem.*, 9, 671212.

[60] Li, Y., Geng, J., Liu, Y., Yu, S., Zhao, G. (2013). Thiadiazole-a promising structure in medicinal chemistry. *ChemMedChem*, 8 (1), 27-41.

[61] Dawood, K.M., Farghaly, T.A. (2017). Thiadiazole inhibitors: A patent review. *Expert Opin. Ther. Pat.*, 27 (4), 477-505.

[62] Gupta, A.K., Misra, H.K. (1980). Synthesis and evaluation of substituted quinazolone derivatives for antibacterial, antifungal, and antiacetylcholinesterase activities. *J. Pharm. Sci.*, 69 (11), 1313-1317.

[63] Altintop, M.D., Kaplancikli, Z.A., Ozdemir, A., Turan-Zitouni, G., Temel, H.E., Akalin, G. (2012). Synthesis and anticholinesterase activity and cytotoxicity of novel amide derivatives. *Arch. Pharm. (Weinheim)*, 345 (2), 112-116.

[64] Khan, I., Hanif, M., Hussain, M.T., Khan, A.A., Aslam, M.A.S., Rama, N.H., Iqbal, J. (2012). Synthesis, acetylcholinesterase and alkaline phosphatase inhibition of some new 1,2,4-triazole and 1,3,4-thiadiazole derivatives. *Aust. J. Chem.*, 65 (10).

[65] Skrzypek, A., Matysiak, J., Niewiadomy, A., Bajda, M., Szymanski, P. (2013). Synthesis and biological evaluation of 1,3,4-thiadiazole analogues as novel AChE and BuChE inhibitors. *Eur. J. Med. Chem.*, 62, 311-319.

[66] Skrzypek, A., Matysiak, J., Karpinska, M.M., Niewiadomy, A. (2013). Synthesis and anticholinesterase activities of novel 1,3,4-thiadiazole based compounds. *J Enzym. Inhib. Med. Chem.*, 28 (4), 816-823.

[67] Altintop, M., Ozdemir, A., Mohsen, U., Temel, H., Ciftci, G., Kaplancikli, Z. (2014). Synthesis and in vitro evaluation of thiadiazole derivatives as AChE, BuChE and LOX inhibitors. *Lett. Drug Des. Discov.*, 11 (9), 1062-1069.

[68] Xue, X.J., Wang, Y.B., Lu, P., Shang, H.F., She, J.X., Xia, L.X., Qian, H., Huang, W.L. (2014). Synthesis and in vitro evaluation of 1,3,4-thiadiazol-2-yl urea derivatives as novel AChE inhibitors. *Chem. Pharm. Bull. (Tokyo)*, 62 (6), 524-527.

[69] Liu, X.-J., Wang, L., Yin, L., Cheng, F.-C., Sun, H.-M., Liu, W.-W., Shi, D.-H., Cao, Z.-L. (2017). Synthesis and biological evaluation of novel glycosyl-containing 1,2,4-triazolo[3,4-b][1,3,4]thiadiazole derivatives as acetylcholinesterase inhibitors. *J. Chem. Res.*, 41 (10), 571-575.

[70] Uraz, M., Karakuş, S., Abu Mohsen, U., Kaplancıklı, Z.A., Rollas, S. (2016). The synthesis and evaluation of anti-acetylcholinesterase activity of some 4(3H)-quinazolinone derivatives bearing substituted 1,3,4- thiadiazole. *Marmara Pharm. J.*, 21 (24530), 96-101.

[71] Ujan, R., Saeed, A., Channar, P.A., Larik, F.A., Abbas, Q., Alajmi, M.F., El-Seedi, H.R., Rind, M.A., Hassan, M., Raza, H., Seo, S.Y. (2019). Drug-1,3,4-thiadiazole conjugates as novel mixed-type inhibitors of acetylcholinesterase: Synthesis, molecular docking, pharmacokinetics, and ADMET evaluation. *Molecules*, 24 (5).

[72] Acar Çevik, U., Sağlık, B.n. (2019). Synthesis, in vitro anticholinesterase and antimicrobial evaluation of new 1,3,4-thiadiazole-piperazine derivatives. *Bilecik Şeyh Edebali Üniversitesi Fen Bilimleri Dergisi*, 6 (2).

[73] Lotfi, S., Rahmani, T., Hatami, M., Pouramiri, B., Kermani, E.T., Rezvannejad, E., Mortazavi, M., Fathi Hafshejani, S., Askari, N., Pourjamali, N., Zahedifar, M. (2020). Design, synthesis and biological assessment of acridine derivatives containing 1,3,4-thiadiazole moiety as novel selective acetylcholinesterase inhibitors. *Bioorg. Chem.*, 105, 104457.

[74] Skrzypek, A., Matysiak, J., Karpinska, M., Czarnecka, K., Krecisz, P., Stary, D., Kukulowicz, J., Paw, B., Bajda, M., Szymanski, P., Niewiadomy, A. (2021). Biological evaluation and molecular docking of novel 1,3,4-thiadiazole-resorcinol conjugates as multifunctional cholinesterases inhibitors. *Bioorg. Chem.*, 107, 104617.

[75] Karcz, D., Starzak, K., Ciszkowicz, E., Lecka-Szlachta, K., Kaminski, D., Creaven, B., Jenkins, H., Radomski, P., Milos, A., Slusarczyk, L., Matwijczuk, A. (2021). Novel coumarin-thiadiazole hybrids and their Cu(II) and Zn(II) complexes as potential antimicrobial agents and acetylcholinesterase inhibitors. *Int. J.Mol. Sci.*, 22 (18).

[76] Abdelhafez, O.M., Amin, K.M., Ali, H.I., Abdalla, M.M., Batran, R.Z. (2012). Synthesis of new 7-oxycoumarin derivatives as potent and selective monoamine oxidase A inhibitors. *J. Med. Chem.*, 55 (23), 10424-10436.

[77] Wang, D., Hong, R.Y., Guo, M., Liu, Y., Chen, N., Li, X., Kong, D.X. (2019). Novel C7-substituted coumarins as selective monoamine oxidase inhibitors: Discovery, synthesis and theoretical simulation. *Molecules*, 24 (21).

[78] Saglik, B.N., Kaya Cavusoglu, B., Acar Cevik, U., Osmaniye, D., Levent, S., Ozkay, Y., Kaplancikli, Z.A. (2020). Novel 1,3,4-thiadiazole compounds as potential MAO-A inhibitors - design, synthesis, biological evaluation and molecular modelling. *RSC Med. Chem.*, 11 (9), 1063-1074.

[79] Bekircan, O., Danis, O., Sahin, M.E., Cetin, M. (2022). Monoamine oxidase A and B inhibitory activities of 3,5-diphenyl-1,2,4-triazole substituted [1,2,4]triazolo[3,4-b][1,3,4]thiadiazole derivatives. *Bioorg. Chem*., 118, 105493.

[80] Fort, R.C., Schleyer, P.v.R. (1964). Adamantane: Consequences of the Diamondoid Structure. *Chem. Rev.*, 64 (3), 277-300.

[81] Mansoori, G.A. (2008). Diamondoid molecules. Adv. Chem. Phys., 136, 207-258.

[82] Decker, H. (1924). 88. Versammlung deutscher naturforscher und ärzte. innsbruck, 21.–27. September 1924. *Angew. Chem. Int. Ed*., 37 (41), 781-822.

[83] Landa, S., Macháček, V. (1933). Sur l'adamantane, nouvel hydrocarbure extrait du naphte. *Collect. Czechoslov. Chem. Commun.*, 5, 1-5.

[84] Prelog, V., Seiwerth, R. (1941). Über die synthese des adamantans. *Ber. Dtsch. Chem. Ges. (A and B Series)*, 74 (10), 1644-1648.

[85] Prelog, V., Seiwerth, R. (1941). Über eine neue, ergiebigere darstellung des adamantans. *Ber. Dtsch. Chem. Ges. (A and B Series)*, 74 (11), 1769-1772.

[86] von R. Schleyer, P. (1957). A simple preparation of adamantane. *J. Am. Chem. Soc*., 79 (12), 3292-3292.

[87] Stockdale, T.P., Williams, C.M. (2015). Pharmaceuticals that contain polycyclic hydrocarbon scaffolds. *Chem. So.c Rev.*, 44 (21), 7737-7763.

[88] Spilovska, K., Zemek, F., Korabecny, J., Nepovimova, E., Soukup, O., Windisch, M., Kuca, K. (2016). Adamantane - A lead structure for drugs in clinical practice. *Curr. Med. Chem.*, 23 (29), 3245-3266.

[89] Spasov, A.A., Khamidova, T.V., Bugaeva, L.I., Morozov, I.S. (2000). Adamantane derivatives: Pharmacological and toxicological properties (review). *Pharm. Chem. J.*, 34 (1), 1-7.

[90] Sekutor, M., Mlinaric-Majerski, K., Hrenar, T., Tomic, S., Primozic, I. (2012). Adamantane-substituted guanylhydrazones: Novel inhibitors of butyrylcholinesterase. *Bioorg. Chem*, 41-42, 28-34.

[91] Simoni, E., Daniele, S., Bottegoni, G., Pizzirani, D., Trincavelli, M.L., Goldoni, L., Tarozzo, G., Reggiani, A., Martini, C., Piomelli, D., Melchiorre, C., Rosini,

M., Cavalli, A. (2012). Combining galantamine and memantine in multitargeted, new chemical entities potentially useful in Alzheimer's disease. *J. Med. Chem.*, 55 (22), 9708-9721.

[92] Al-Aboudi, A., Al-Qawasmeh, R.A., Shahwan, A., Mahmood, U., Khalid, A., Ul-Haq, Z. (2015). In-silico identification of the binding mode of synthesized adamantyl derivatives inside cholinesterase enzymes. *Acta Pharmacol. Sin.*, 36 (7), 879-886.

[93] Gazova, Z., Soukup, O., Sepsova, V., Siposova, K., Drtinova, L., Jost, P., Spilovska, K., Korabecny, J., Nepovimova, E., Fedunova, D., Horak, M., Kaniakova, M., Wang, Z.J., Hamouda, A.K., Kuca, K. (2017). Multi-target-directed therapeutic potential of 7-methoxytacrine-adamantylamine heterodimers in the Alzheimer's disease treatment. Biochim. Biophys. *Acta Mol. Basis Dis.*,1863 (2), 607-619.

[94] Kwong, H.C., Mah, S.H., Chia, T.S., Quah, C.K., Lim, G.K., Kumar, C.S.C. (2017). Cholinesterase inhibitory activities of adamantyl-based derivatives and their molecular docking studies. *Molecules*, 22 (6).

[95] Ocheretniuk, A.D., Kobzar, O.L., Kozachenko, O.P., Brovarets, V.S., Vovk, A.I. (2017). Synthesis and the activity assessment of adamantylcontaining thiazolium inhibitors of butyrylcholinesterase. *J. Org. Chem.*, 15 (4(60)), 48-55.

[96] Bachurin, S.O., Shevtsova, E.F., Makhaeva, G.F., Grigoriev, V.V., Boltneva, N.P., Kovaleva, N.V., Lushchekina, S.V., Shevtsov, P.N., Neganova, M.E., Redkozubova, O.M., Bovina, E.V., Gabrelyan, A.V., Fisenko, V.P., Sokolov, V.B., Aksinenko, A.Y., Echeverria, V., Barreto, G.E., Aliev, G. (2017). Novel conjugates of aminoadamantanes with carbazole derivatives as potential multitarget agents for AD treatment. *Sci. Rep.*, 7, 45627.

[97] Makhaeva, G.F., Shevtsova, E.F., Kovaleva, N.V., Rudakova, E.V., Neganova, M.E., Dubova, L.G., Shevtsov, P.N., Aksinenko, A.Y., Sokolov, V.B., Bachurin, S.O. (2018). Aminoadamantane conjugates with carbazole derivatives as potential multitarget agents for the treatment of Alzheimer’s disease. Effect of the spacer structure. *Russ. Chem. Bull.*, 67 (11), 2121-2126.

[98] Perez-Areales, F.J., Turcu, A.L., Barniol-Xicota, M., Pont, C., Pivetta, D., Espargaro, A., Bartolini, M., De Simone, A., Andrisano, V., Perez, B., Sabate, R., Sureda, F.X., Vazquez, S., Munoz-Torrero, D. (2019). A novel class of multitarget

anti-Alzheimer benzohomoadamantanechlorotacrine hybrids modulating cholinesterases and glutamate NMDA receptors. *Eur. J. Med. Chem.*, 180, 613-626.

[99] Bosak, A., Opsenica, D.M., Sinko, G., Zlatar, M., Kovarik, Z. (2019). Structural aspects of 4-aminoquinolines as reversible inhibitors of human acetylcholinesterase and butyrylcholinesterase. *Chem. Biol. Interact.*, 308, 101-109.

[100] Bachurin, S.O., Makhaeva, G.F., Shevtsova, E.F., Aksinenko, A.Y., Grigoriev, V.V., Shevtsov, P.N., Goreva, T.V., Epishina, T.A., Kovaleva, N.V., Pushkareva, E.A., Boltneva, N.P., Lushchekina, S.V., Gabrelyan, A.V., Zamoyski, V.L., Dubova, L.G., Rudakova, E.V., Fisenko, V.P., Bovina, E.V., Richardson, R.J. (2021). Conjugation of aminoadamantane and gamma-carboline pharmacophores gives rise to unexpected properties of multifunctional ligands. *Molecules*, 26 (18).

[101] Zindo, F.T., Barber, Q.R., Joubert, J., Bergh, J.J., Petzer, J.P., Malan, S.F. (2014). Polycyclic propargylamine and acetylene derivatives as multifunctional neuroprotective agents. *Eur. J. Med. Chem.*, 80, 122-134.

[102] Kadi, A.A., Al-Abdullah, E.S., Shehata, I.A., Habib, E.E., Ibrahim, T.M., El-Emam, A.A. (2010). Synthesis, antimicrobial and anti-inflammatory activities of novel 5-(1-adamantyl)-1,3,4-thiadiazole derivatives. *Eur. J. Med. Chem.*, 45 (11), 5006-5011.

[103] Yang, X.H., Xiang, L., Li, X., Zhao, T.T., Zhang, H., Zhou, W.P., Wang, X.M., Gong, H.B., Zhu, H.L. (2012). Synthesis, biological evaluation, and molecular docking studies of 1,3,4-thiadiazol-2-amide derivatives as novel anticancer agents. *Bioorg. Med. Chem.*, 20 (9), 2789-2795.

[104] Ellman, G.L., Courtney, K.D., Andres, V., Featherstone, R.M. (1961). A new and rapid colorimetric determination of acetylcholinesterase activity. *Biochemical Pharmacol.*, 7 (2), 88-95.

[105] Schrödinger (2020): Maestro,. 10.6 ed. Schrödinger LLC, New York,NY.

[106] Schrödinger (2020): LigPrep. 3.8 ed. Schrödinger, LLC, New York,NY.

[107] Schrödinger (2020): Glide. 7.1 ed. Schrödinger, LLC, New York,NY.

[108] Delaney, J.S. (2004). ESOL: Estimating aqueous solubility directly from molecular structure. *J. Chem. Inf. Comput. Sci.*, 44 (3), 1000-1005.

[109] SwissADME Web Tool. Swiss Institute of Bioinformatics.

[110] Daina, A., Michielin, O., Zoete, V. (2017). SwissADME: A free web tool to evaluate pharmacokinetics, drug-likeness and medicinal chemistry friendliness of small molecules. *Sci. Rep.*, 7, 42717.

[111] Drug-Likeness and molecular property prediction. Molsoft L.L.C.

[112] Narayanan, V.L., Bernstein, J. (1969): Adamantyl thiadiazoles. Google Patents.

[113] Fesatidou, M., Zagaliotis, P., Camoutsis, C., Petrou, A., Eleftheriou, P., Tratrat, C., Haroun, M., Geronikaki, A., Ciric, A., Sokovic, M. (2018). 5-Adamantan thiadiazole-based thiazolidinones as antimicrobial agents. Design, synthesis, molecular docking and evaluation. *Bioorg. Med. Chem*., 26 (16), 4664-4676.

[114] Wassel, M.M.S., Ammar, Y.A., Elhag Ali, G.A.M., Belal, A., Mehany, A.B.M., Ragab, A. (2021). Development of adamantane scaffold containing 1,3,4-thiadiazole derivatives: Design, synthesis, anti-proliferative activity and molecular docking study targeting EGFR. *Bioorg. Chem.*, 110, 104794.

[115] El-Emam, A., Lehmann, J. (1994). Adamantane derivatives IV: Unexpected debenzylation on ring closure of 1-(1-adamantylcarbonyl)-4-benzylthiosemicarbazide with sulphuric acid. *Monatsh. fur Chem.*, 125 (5), 587-591.

[116] Demir Ozkay, U., Can, O.D., Saglik, B.N., Acar Cevik, U., Levent, S., Ozkay, Y., Ilgin, S., Atli, O. (2016). Design, synthesis, and AChE inhibitory activity of new benzothiazole-piperazines. *Bioorg. Med. Chem. Lett.*, 26 (22), 5387-5394.

[117] Demirayak, Ş., Şahin, Z., Ertaş, M., Bülbül, E.F., Bender, C., Biltekin, S.N., Berk, B., Sağlık, B.N., Levent, S., Yurttaş, L. (2019). Novel thiazole-piperazine derivatives as potential cholinesterase inhibitors. *J. Heterocycl. Chem.*, 56 (12), 3370-3386.

[118] van de Waterbeemd, H., Gifford, E. (2003). ADMET in silico modelling: Towards prediction paradise? *Nat. Rev. Drug Discov.*, 2 (3), 192-204.

[119] Lipinski, C.A., Lombardo, F., Dominy, B.W., Feeney, P.J. (2001). Experimental and computational approaches to estimate solubility and permeability in drug discovery and development settings 1PII of original article: S0169-409X(96)00423-1. The article was originally published in Advanced Drug Delivery Reviews 23 (1997) 3–25. 1. *Adv. Drug Deliv. Rev.*, 46 (1-3), 3-26.

[120] Colovic, M.B., Krstic, D.Z., Lazarevic-Pasti, T.D., Bondzic, A.M., Vasic, V.M. (2013). Acetylcholinesterase inhibitors: pharmacology and toxicology. *Curr. Neuropharmacol.*, 11 (3), 315-335.

[121] Singh, H., Singh, J.V., Kaur, N., Sanduja, M., Singh, G., Bedi, P.M.S., Sharma, S. (2018). Rational approaches, design strategies, structure activity relationship and mechanistic insights for esterase inhibitors. *Mini Rev. Med. Chem.*, 18 (10), 837-894.

[122] Ordentlich, A., Barak, D., Kronman, C., Ariel, N., Segall, Y., Velan, B., Shafferman, A. (1998). Functional characteristics of the oxyanion hole in human acetylcholinesterase. *J. Biol. Chem.*, 273 (31), 19509-19517.

[123] Saglik, B.N., Ilgin, S., Ozkay, Y. (2016). Synthesis of new donepezil analogues and investigation of their effects on cholinesterase enzymes. *Eur. J. Med. Chem.*, 124, 1026-1040.

[124] Barak, D., Kronman, C., Ordentlich, A., Ariel, N., Bromberg, A., Marcus, D., Lazar, A., Velan, B., Shafferman, A. (1994). Acetylcholinesterase peripheral anionic site degeneracy conferred by amino acid arrays sharing a common core. *J. Biol. Chem.*, 269 (9), 6296-6305.

[125] Inestrosa, N.C., Alvarez, A., Pérez, C.A., Moreno, R.D., Vicente, M., Linker, C., Casanueva, O.I., Soto, C., Garrido, J. (1996). Acetylcholinesterase accelerates assembly of amyloid-β-peptides into Alzheimer's fibrils: Possible role of the peripheral site of the enzyme. *Neuron.*, 16 (4), 881-891.

[126] Rees, T. (2003). Acetylcholinesterase promotes beta-amyloid plaques in cerebral cortex. *Neurobiol. Aging*, 24 (6), 777-787.

[127] Alvarez, A., Opazo, C., Alarcon, R., Garrido, J., Inestrosa, N.C. (1997). Acetylcholinesterase promotes the aggregation of amyloid-beta-peptide fragments by forming a complex with the growing fibrils. *J. Mol. Biol.*, 272 (3), 348-361.

[128] Cheung, J., Rudolph, M.J., Burshteyn, F., Cassidy, M.S., Gary, E.N., Love, J., Franklin, M.C., Height, J.J. (2012). Structures of human acetylcholinesterase in complex with pharmacologically important ligands. *J. Med. Chem.*, 55 (22), 10282-10286.

[129] Singh, J.V., Thakur, S., Kumar, N., Singh, H., Mithu, V.S., Singh, H., Bhagat, K., Gulati, H.K., Sharma, A., Singh, H., Sharma, S., Bedi, P.M.S. (2022). Donepezil-

inspired multitargeting indanone derivatives as effective anti-Alzheimer's agents. *ACS Chem. Neurosci.*, 13 (6), 733-750.

[130] Saxena, A., Fedorko, J.M., Vinayaka, C.R., Medhekar, R., Radic, Z., Taylor, P., Lockridge, O., Doctor, B.P. (2003). Aromatic amino-acid residues at the active and peripheral anionic sites control the binding of E2020 (Aricept) to cholinesterases. *Eur. J. Biochem.*, 270 (22), 4447-4458.

[131] Lu, S.H., Wu, J.W., Liu, H.L., Zhao, J.H., Liu, K.T., Chuang, C.K., Lin, H.Y., Tsai, W.B., Ho, Y. (2011). The discovery of potential acetylcholinesterase inhibitors: A combination of pharmacophore modeling, virtual screening, and molecular docking studies. *J. Biomed. Sci.*, 18, 8.

[132] Choudhir, G., Sharma, S., Hariprasad, P. (2021). A combinatorial approach to screen structurally diverse acetylcholinesterase inhibitory plant secondary metabolites targeting Alzheimer's disease. *J. Biomol. Struct. Dyn.*, 1-14.

[133] Binda, C., Newton-Vinson, P., Hubalek, F., Edmondson, D.E., Mattevi, A. (2002). Structure of human monoamine oxidase B, a drug target for the treatment of neurological disorders. *Nat. Struct. Biol.*, 9 (1), 22-26.

[134] Can, O.D., Osmaniye, D., Demir Ozkay, U., Saglik, B.N., Levent, S., Ilgin, S., Baysal, M., Ozkay, Y., Kaplancikli, Z.A. (2017). MAO enzymes inhibitory activity of new benzimidazole derivatives including hydrazone and propargyl side chains. *Eur. J. Med. Chem.*, 131, 92-106.

[135] Evren, A.E., Nuha, D., Dawbaa, S., Saglik, B.N., Yurttas, L. (2022). Synthesis of novel thiazolyl hydrazone derivatives as potent dual monoamine oxidase-aromatase inhibitors. *Eur. J. Med. Chem.*, 229, 114097.